N° d'ordre : 000012 / 99

PhD Thesis presented for the obtention of the Degree of Docteur en Sciences de l'Université Nationale du Bénin

Option **Physique Théorique**

by

TITANTAH John Tatini

Title :

A QUANTUM STATISTICAL MODEL OF A THREE DIMENSIONAL LINEAR RIGID ROTATOR IN A BATH OF OSCILLATORS AND COMPUTER SIMULATION OF POLYMER SOLUTIONS

JURY :

Président : Prof. ASSIH (Université du Bénin, TOGO)

Referees : Prof. M. N. HOUNKONNOU (Université Nationale du Bénin, BENIN)
Prof. C. PIERLEONI (Universita 'Degli Studi Del L'Aquila, ITALIA)
Prof. J - P. RYCKAERT (Université Libre de Bruxelles BELGIQUE)

Examiner : Prof. TCHAKPELE (Université du Bénin ,TOGO)

Co-Supervisors : Prof. M. N. HOUNKONNOU
Prof. J - P. RYCKAERT

28 th APRIL 1999

Supported by a fellowship from the Belgian Government

Contents

Coupling Theory with Computer Simulations: Outlay of the thesis 6
0.1 Why couple theory with computer simulation? 6
0.2 Main results of the thesis 7

I A QUANTUM STATISTICAL MODEL OF A THREE DIMENSIONAL LINEAR RIGID ROTATOR IN A BATH OF OSCILLATORS 10

1 Generalities and the model 12
1.1 Generalities 12
1.2 The model 16
1.2.1 The system Hamiltonian 16
1.2.2 The Master Equation 17
1.3 The stability of the Master Equation 22

2 Electric birefringence induced by a constant field in relaxation regime 25
2.1 Introduction 25
2.2 The relaxation regime 25
2.3 The Kerr Effect Function 26
2.3.1 The master equations for the matrix elements 26
2.3.2 The classical Brownian limit 28
2.3.3 The rotating wave approximation (RWA) limit 32
2.4 Energy balance equation and Entropy Calculation 37

3 Dielectric property dynamics induced by a dc field 41
3.1 Introduction 41
3.2 The field dependent Master equation 42
3.3 The Master equations for matrix elements 43
3.4 The classical Brownian limit 48
3.4.1 The dc field susceptibility 49
3.4.2 The Kerr function 51
3.5 The rotating wave approximation (RWA) limit 53
3.5.1 The dc field susceptibility 55
3.5.2 The Kerr function 56

3.6 Discussions 61

4 steady state dielectric properties induced by ac and dc field coupling 66
4.1 Introduction 66
4.2 The electric susceptibility and the Kerr functions 67
4.2.1 The classical Brownian limit 67
4.2.2 The rotating wave approximation (RWA) limit 73
4.3 Discussions 75

Conclusions and Perspectives of Part I 83

Appendices 85

A 85
A.1 The initial condition on $\hat{\rho}_S(t)$ 85
A.2 Sample property proof 85
A.3 The initial condition on $\varphi_{l,l}(t)$ 86

B 87
B.1 Systems of hierarchies for $Y^m_{j,l}$ and $X_{j,l}$ 87
B.2 Expressions for $Y^0_{0,0}$, $Y^0_{0,1}$ and $Y^0_{0,2}$ 88
B.3 The dc, the ω and the 2ω components of the quantum Kerr function 90

II COMPUTER SIMULATION OF POLYMER SOLUTIONS 92

5 Simulation techniques 94
5.1 Introduction 94
5.2 Monte Carlo techniques 95
5.2.1 The Metropolis method 96
5.2.2 The periodic boundary conditions 97
5.2.3 The configurational biased Monte Carlo (CBMC) 98
5.3 Molecular Dynamics 99

6 On the stretched polymer statistical mechanics ensembles 103
6.1 Introduction 103
6.2 Single chain stretching domains 107
6.2.1 The linear regime 107
6.2.2 The Pincus blob regime 107
6.2.3 The finite extensibility regime 107
6.2.4 The N dependence of R_f at fixed-f 107
6.2.5 Typical force cross-over values in experimental set-ups 108
6.3 Fixed f and fixed-R ensembles for a single polymer chain 108
6.3.1 A reminder of textbook statistical mechanics 108
6.3.2 Elasticity laws in both stretched chain ensembles for specific models . . . 110
6.4 The connection formulae between fixed-f and fixed-R ensembles 112

6.4.1 General formalism . . . 113
6.4.2 Link between ensembles for specific chain models . . . 114
6.4.3 A second order approximation applied to the elasticity case . . . 117
6.4.4 Monte-Carlo calculations for the stretched hard-sphere necklace model . 119

7 Single polymer response to stretching forces 125
7.1 Introduction . . . 125
7.2 Models and Monte-Carlo (MC) program . . . 129
7.2.1 Models . . . 129
7.2.2 Monte-Carlo programs . . . 130
7.3 Bead rod excluded volume chain versus atomistic polyethylene . . . 132
7.3.1 Extension - force relationships . . . 132
7.3.2 The dependence of the gauche-trans populations on stretching . . . 137
7.3.3 The entropic and enthalpic forces in PE . . . 138
7.4 Residual dipole-dipole interaction of a stretched polymer . . . 142
7.4.1 Introduction . . . 142
7.4.2 $\langle P_2(\cos\alpha_{kk'})\rangle_f$ for a FJC . . . 144
7.4.3 Results . . . 145
7.4.4 Calculations of $P_2^{\parallel}(\eta)$ and $P_2^{\perp}(\eta)$ . . . 145
7.4.5 Domain of validity of the f^2 law . . . 147
7.4.6 Domain of validity of the r^2 law . . . 149
7.5 Static structure factor . . . 151
7.5.1 Some theoretical background . . . 153
7.5.2 $S_f(q)$ from the extension-force relationship . . . 155
7.5.3 Applications . . . 155

8 Effective potentials between two polymer segments in solution 161
8.1 Introduction . . . 161
8.2 The effective potential on a dimer . . . 163
8.3 Solvent effects on the properties of a system of two interacting pentamers . . . 166
8.3.1 Explicit solvent consideration . . . 167
8.3.2 The use of a realistic effective potential . . . 167
8.4 The smoothed density theory of intermolecular forces . . . 168
8.4.1 The Flory inter-penetrating uniform sphere theory . . . 171

Conclusions and Perspectives of Part II 174

Appendices 179

C 179
C.1 Proof of $(\partial f/\partial T)_r = -(\partial r/\partial T)_f/(\partial r/\partial f)_T$ . . . 179
C.2 Proof of the f^2 law for $\langle P_2(\alpha)\rangle_f$ . . . 179

D 181
D.1 The smoothed density theory on realistic segment distribution . . . 181

Dedication

To

My Beloved one

EKEME Lydia

Acknowledgements

I would like, first of all, to thank Professor M. N. Hounkonnou of the Institute de Mathématiques et Sciences Physiques (IMSP) and Professor J.-P. Ryckaert of the Unité de Physique de Polymère de L'Université Libre de Bruxelles (ULB)-Belgium for accepting to co-supervise this work. I will never forget their efforts and patience bestowed in proposing and following up the research topics and reading through the manuscripts. Most importantly, their fatherly loves in Benin and Belgium, respectively, rendered my stay in both countries quite enjoyable.

I am highly indebted to George Destrée of ULB for his great help in solving some of my computational problems. I benefited greatly from the rich discussions I had with Dr. C. Pierleoni of the Dipartimento di Fisica, Università 'Degli Studi Del L'Aquila-Italy during his brief stays in Brussels. I also enjoyed Professor M. Bauss's suggestions.

I acknowledge the great role played by Professor N. M. Kwato of the University of Yaounde I (Cameroon), for recommending me to IMSP and attaching an ever increasing interest in the evolution of my work.

I would like to thank the administration of IMSP for insuring a smooth evolution of the work. I salute the cordial relationship prevailing over the entire staff and student body of IMSP.

Henri and my colleagues Gianluigi, D. Monderen, Karim, Maud, Fouad all of the Unité de Physique de Polymère - ULB, you have left an indelible mark in my life.

My parents, your moral supports have urged me to look forward despite the numerous odds around and behind.

I heartily thank all those who have contributed, in one way or the other, to the realisation of this, rather brief but, promissing piece.

Coupling Theory with Computer Simulation: Main results of the thesis

0.1 Why couple theory with computer simulation?

From dilute gases through dilute solutions and colloidal particles in suspension to complex liquids like polymer solutions and surfactants, the science of materials is one of the most active scientific research domains whereby physicists, chemists and engineers have spent centuries and huge resources trying to disentangle the complexities surrounding nature. The issue of intermolecular forces, which often worried early scientists who believed that a universal intermolecular force law similar to that of Newton could be obtained that would explain the then mysteries like capillarity, the shape of macroscopic droplets of liquids etc, remains the central issue in modern scientific breakthroughs. Biological scientists are trailed into the dance of intermolecular interactions as it is discovered that the structure of biological molecules like DNA could be explained via intermolecular forces in a manner very similar to that used for day-to-day polymeric materials. In short, the domain of material science keeps widening as humanity maintains its quest to understand the subtilities underlying God's master-piece - nature.

The tools used in confronting the above tasks are three-fold. Engineers customarily will go the experimental way, the success of which depends on their capabilities to develop viable technical appareils. Theoreticians, armed with intuition and a high sense of imagination are often limited by the multidimensionality of nature and the nonlinearity surrounding dynamical systems. Today computer engineers have elaborated and brought up extra rapid-computing machines that are capable of solving, within minutes, well elaborated problems that bare pencil and paper wouldn't solve for decades. The phrase "well elaborated" must be underlined since the problem can only be adequately elaborated by someone armed with some theoretical background, mastering the computational procedures but lacking the rapidity required of a "robot" like a computer.

The agreements recorded between some experimentally observed properties of matter and those calculated computationally using a representative specimen of the matter comprising only some few hundreds or thousands of particles of the material has favoured the re-deployment of research resources. It is in this wise that a group of theoreticians have deemed necessary to exploit the growing computational skills at stages where pencil and paper cannot exceed, or to test the conclusions of the latter.

Today a material scientist (theoretician) who intends to prevail in his thread must boost, at least to some extent, of some mastery of both theoretical and numerical methods of tackling problems. The necessity is again greatly felt when the individual lives in a poor country where

basic experimental work cannot be afforded due to the costly nature of the tools needed, but can afford a hard disc, a keyboard and a screen.

The present thesis stands as an end product of a piece of work aimed, first of all, at widening the scope of vision of the student (and subsequently researcher) in the two complementary currents in material science. Secondly, it emerges as a research piece as it has permitted the elucidation of some essential but salient aspects of material science.

0.2 Main results of the thesis

The thesis is divided into two parts.

- In the first part we consider, theoretically, the dielectric properties (the electric susceptibility and the Kerr electric birefringence) of a system of optically active polar molecules (named rotators) embedded in a bath of noninteracting harmonic oscillators. The rotator-bath system is considered as a quantum mechanical system and new aspects capable of explaining spectral observations, especially those in the far infra red region of small polar molecules like HCl (in argon), are pointed out. We recover most results published in the literature on the classical aspects of the problem by simply taking the classical limits of our results. This part of the thesis has been earmarked by the following important results:

  1. We have brought out the relaxation mechanisms, both classically and quantum mechanically, governing the Kerr effect relaxation of the dielectric medium from a pre-established state of equilibrium in a constant electric field to the isotropic state in zero field [1].
  2. The susceptibility and the Kerr effect rise transients resulting from the sudden application of a constant electric field to the dielectric medium have been clarified with results capable of explaining observations over wide ranges of temperatures, frequencies and bath concentrations. A temperature-density (bath friction)-rotator inertia dependent cross-over is revealed over which a transition from classical to quantum aspects intervenes [2].
  3. The coupling of dc field and ac field (of frequency ω) on the dielectric medium has permitted us to show that highly polar but less polarisable molecules undergo lower frequency rotational transitions (transitions involving $l \rightarrow l \pm 1$) while highly polarisable molecules are dominated by transitions of the form $l \rightarrow l \pm 2$. It has also been shown that depending on the dominant harmonic (an ω or 2ω-harmonic) observed on the Kerr spectra of a liquid, the relative strengths of the permanent to induced dipole moments could be understood [3].
  4. The analysis of the quantum electrical susceptibility led us to elaborating master equations for appropriate transition matrix elements. The equations were quite general in field strength and could act as the basis for higher order field effects. Presently, we are using the master equations to consider nonlinear dielectric properties [4] .

- In the second part of the thesis we study the basic computational skills usually employed to compute the properties of condensed media. The methods range from the conventional

Monte-Carlo (MC) through the Configurational biased Monte-Carlo (CBMC) to Molecular Dynamics (MD). As a typical application of the CBMC technique for sampling the configurations of a macromolecule, we consider the elastic properties of two models of linear excluded volume polymer molecules. In the first model we assimilate a polymer molecule to a collection of $N+1$ hard spheres freely jointed together by N free rotating rigid bonds while in the second we consider a realistic polymer molecule, polyethylene (PE), characterised by restricted torsional and bending motions. Using these models,

1. we have pointed out the great difference that exists between the strain ensemble and stress ensemble elasticity laws of a polymer molecule characterised by the presence of excluded volume forces. An approximate theory, capable of accounting for this difference in some restricted length scale has been elaborated [5].
2. it has been possible to pin-point the force-extension laws in two types of solvent conditions for PE and the effect of stretching on some polymer structural properties like the relative populations of the gauche-trans conformations in PE, the static structure factor, the nuclear magnetic resonance dipolar residual interactions [6] and the relative importance of the entropic and enthalpic forces in a stretched PE molecule.
3. we have shown that the knowledge of the force-extension relationship of any linear polymer over all length scales can be used to deduce the neutron spectroscopic properties of the molecule over a wide range of scattering angles [7].

As a typical application of the Metropolis MC and MD methods, we investigated the the sensitive issue of the realities behind the ad hoc choices of intermolecular effective potentials for use in simulating the properties of a polymer solution in which solvent effect is accounted for by the so-called solvent mediated effective potentials. It is clearly pointed out that the realities of most widely used solvent mediated effective potentials should be limited by the thermodynamic state of the system under consideration [8].

Bibliography

[1] J. T. Titantah and M. N. Hounkonnou, *A quantum statistical mechanics Model of a Three dimensional linear rigid rotator in a bath of Oscillators: II- The Kerr effect relaxation.* J. Phys. A: Math. Gen. **30**: 6327-6346, 1997

[2] J. T. Titantah and M. N. Hounkonnou *A quantum statistical mechanics Model of a Three dimensional linear rigid rotator in a bath of Oscillators: III- dc field properties*, J. Phys. A: Math. Gen. **30**: 6347-6370, 1997

[3] J. T. Titantah and M. N. Hounkonnou, *quantum statistical mechanics Model of a Three dimensional linear rigid rotator in a bath of Oscillators: IV- dc and ac field coupling*, J. Phys. A: Math. Gen. **32**: 897-920, 1999

[4] J. T. Titantah and M. N. Hounkonnou, *A quantum statistical mechanics Model of a Three dimensional linear rigid rotator in a bath of Oscillators: V- Nonlinear susceptibility* (work in progress)

[5] J. T. Titantah, C. Pierleoni and J.-P. Ryckaert, *On the stretched polymer statistical mechanics ensembles* (submitted to Phys. Rev. E)

[6] J. T. Titantah, C. Pierleoni and J.-P. Ryckaert, *Single polymer response to stretching forces* (submitted to J. Chem. Phys.)

[7] J. T. Titantah and J.-P. Ryckaert, *The relationship between the free energy of a stretched chain and structure factor* (work in progress)

[8] J. T. Titantah and J.-P. Ryckaert, *Solvent mediated monomer effective potentials: How realistic are they?* (work in progress)

Part I

A QUANTUM STATISTICAL MODEL OF A THREE DIMENSIONAL LINEAR RIGID ROTATOR IN A BATH OF OSCILLATORS

Chapter 1

Generalities and the model

1.1 Generalities

The dielectric properties of polar fluids is a field of active research in Physics, Chemistry and technology. The study of the dynamics of the molecules of a dielectric medium furnishes useful informations on the reactivities of some molecules and the reaction constants of some reactions. This study over wide temperature and frequency ranges yields a good understanding of molecular structure and relaxation phenomena. Informations on the absorption and dispersion of electromagnetic waves through the atmosphere and other continuous media is readily obtained from the dielectric properties of atmospheric gases and the particles constituting the continuous media. A development of the qualitative and quantitative spectral analysis of atmospheric gas composition is also very essential for the mastery of the problem of atmospheric pollution and global warming.

An exhaustive interpretation of macroscopic observations of molecular systems requires a molecular study since observations are strongly related to molecular dynamics. A complete knowledge of the physical properties of molecular systems requires that the positions and velocities of its constituent particles be known at every instant. Such a knowledge is only obtainable for systems composed of very small number of particles. At the macroscopic level, we should be able to present the dynamics of a system of about 10^{23} interacting particles. This problem has been attempted using present day computers only for a few thousand particles. For macroscopic systems the statistical studies (involving collective or ensemble analysis) appear to be the unavoidable way to confront the problem.

The difficulty encountered in the description of large systems in terms of the dynamics of their individual particles has compelled physicists to restrict themselves to studies involving two types of well defined parameters; the first set of them being related to the geometry of the molecules (molecular forms and sizes) while the second is related to the internal structure of the molecules (average refractive indices, average dielectric constants, anisotropy, magnetic properties, etc). The birefringence permits us to come out with some valuable informations on the two sets of the parameters. For example, the birefringence of a molecular system permits the knowledge of the diffusion constant D for the rotational Brownian motion. D is known to be related to the form and dimensions of the molecule. **Perrin** [1, 2] showed that

$$D = \begin{cases} \frac{k_B T}{4\eta v}\frac{p^2}{1-p^2}\left(1 + \frac{1-2p^2}{2p\sqrt{1-p^2}}\arctan\frac{\sqrt{1-p^2}}{p}\right) & for \quad p < 1 \\ \frac{k_B T}{4\eta v}\frac{p^2}{p^4-1}\left(-1 + \frac{2p^2-1}{2p\sqrt{p^2-1}}\log\frac{p+\sqrt{p^2-1}}{p-\sqrt{p^2-1}}\right) & for \quad p > 1, \end{cases} \tag{1.1}$$

where k_B is the Boltzmann constant, T the absolute temperature, η the viscosity of the medium and p the ratio of the length of the longitudinal axis to that of the transverse axis of the molecule. Thus, if D is known, p or v can be deduced.

The most relevant dielectric properties of interest are the electric susceptibility $\chi(t)$ and the Kerr function $\Phi(t)$ [3, 4, 5, 50, 6]. It has been shown in linear response theory [7] that in the presence of an electric field, $\mathrm{E}(t)$, the polarisation is given by,

$$\mathbf{P(t)} = \int_{-\infty}^{\mathbf{t}} \chi(\mathbf{t} - \mathbf{t}')\mathbf{E}(\mathbf{t}')\mathbf{dt}, \tag{1.2}$$

where χ is the response function or the susceptibility. It depends only on the time interval $t - t'$ (that is, the time interval measured from the instant the stimulus is applied) and not on absolute time. χ is thus non zero only posterior to the application of the disturbance. In other words, $\chi(t - t') = 0$ for $t < 0$. This is the causality property. The argument $t - t'$ in Eq.(1.2) shows that the response at time t is an accumulated effect of the stimulus from the instant of its application (far past) to the time t. For this reason χ is also referred to as the memory function.

The frequency dependent complex susceptibility (necessary for spectral analysis) is obtained by taking the one sided Fourier transform of the polarisation [6] as,

$$\tilde{P}(\omega) = \tilde{\chi}(\omega)\tilde{E}(\omega) = \Big(P(0) - i\omega\int_0^\infty e^{-i\omega t}P_\alpha(t)dt\Big), \tag{1.3}$$

where $P_\alpha(t) = \langle \mu \cos\beta(t)\rangle$ is the mean polarisation parallel to the polarising field with $\beta(t)$ being the angle at time t between the direction of the applied field and the dipole moment vector. χ is a complex quantity with the real part χ' and imaginary part $-\chi''$. $\chi'(\omega)$ is responsible for the dispersive properties of most media while $\chi''(\omega)$, an always positive quantity, is the absorption or the loss factor.

Piekara and co-workers [8] proved that the permitivity variation tensor $\Delta\underline{\underline{\epsilon}}(E) = \underline{\underline{\epsilon}}(E) - \underline{\underline{\epsilon_0}}$ (where $\underline{\underline{\epsilon_0}} = \epsilon_0\underline{\underline{I}}$, with ϵ_0 being the permitivity of free space and $\underline{\underline{I}}$ the unit tensor) of a dielectric medium when the latter is subjected to a polarising field is a quadratic function of the polarising field. Indeed, when an optically isotropic dielectric is placed in a strong electric field, its refractive index undergoes a variation which depends on the relative orientation of the observing field with respect to the polarising field. Observations are performed using an analysing light source having a weak oscillating electric field. The direction of observation is that of the polarisation of the light source. The observed dielectric permitivity will, therefore, depend on the polarising field strength and the frequency of the analysing source, i.e., $\epsilon = \epsilon^\omega(E_p)$.

If the analysing field is parallel to the polarising field (longitudinal analysis), the measured change in permitivity tensor will be

$$\underline{\underline{\Delta\epsilon^\omega_{\parallel}}}(E_p) = \underline{\underline{\epsilon^\omega_{\parallel}}}(E_p) - \underline{\underline{\epsilon_0}}. \tag{1.4}$$

For perpendicular observation (transverse analysis)

$$\underline{\underline{\Delta\epsilon}}^{\omega}_{\perp}(E_p) = \underline{\underline{\epsilon}}^{\omega}_{\perp}(E_p) - \underline{\underline{\epsilon}}_0. \tag{1.5}$$

$\underline{\underline{\epsilon}}_0 = \epsilon_0 \underline{\underline{I}}$, with $\underline{\underline{I}}$ being the unit tensor. To each permitivity tensor corresponds a refractive index tensor $\underline{\underline{n}}$ defined by $\underline{\underline{n}} \cdot \underline{\underline{n}} = \underline{\underline{\epsilon}}^{\omega}(E_p)$. The optical birefringence is a measure of the quantity [9]

$$\Delta n = \Delta n_{\parallel} - \Delta n_{\perp} = K E_p^2, \tag{1.6}$$

where K is the **Kerr** constant which is characteristic of the dielectric medium under consideration. Under strong fields K becomes field dependent.

The classical fundamental theory of the Kerr effect proposed by **Voight** considers the electron theory of an atom as anharmonic oscillators while **Langevin** describes it as a statistical re-orientation of optically active molecules by a static electric field. Langevin assumes that the molecules of various substances are optically and electrically anisotropic in nature, their interactions with an external electric field tending to give them lower potential energy configurations or orientations but this is constantly counteracted by thermal motions. A competition process then sets in leading to a statistical re-orientation of the molecules.

If the z axis of the laboratory frame is assimilated to the direction of the external pertubation, Molecular dynamic studies reveal that Δn is a measure of $\langle u_z u_z - u_x u_x \rangle$ (where u_α is the α component of the molecular orientation unit vector) which can easily be shown to be the ensemble average of the second order associated Legendre polynomials of the dipole moment orientation unit vector component parallel to the external perturbation (u_z). We, therefore, define the Kerr electric birefringence as [3, 4, 5]

$$\Phi(t) = \langle u_z u_z - u_x u_x \rangle = \frac{1}{2} \left\langle (3 u_z u_z - \underline{\underline{1}}) \right\rangle, \tag{1.7}$$

where the angle brackets $\langle \ldots \rangle$ denote ensemble averaging, u_z is the z (direction of the polarising field) component of $\mathbf{u}$ and u_x any component of $\mathbf{u}$ perpendicular to the field.

In this part of the thesis, we are interested in the molecular origin of the electric polarisation or susceptibility and the electric birefringence or the Kerr effect. The polarisation is a measure of the mean dipole moment vector of the molecular system when the latter is subjected to an external electric field. To tackle this problem, we consider the rotational motion of a system of rotators embedded in a sea of non interacting bath oscillators. This problem has been undertaken in recent years by many authors [3, 4, 5], with all approaches based on classical methods using either the Smoluchowski equation or the generalised Liouville equation also called the Fokker-Planck-Kramer (FPK) equation. In the latter, the molecular orientation distribution function is expanded as a linear combination of the associated Legendre polynomials in $\cos\beta$ [3, 4, 5] (where β is the angle between the rotator's principal axis and the direction of the applied electric field). The coefficients of the respective polynomials are related to the most relevant dielectric properties such as the electrical susceptibility and birefringence or the Kerr effect. We shall consider the simple case of a quasi-free rotator undergoing intermittent instantaneous collisions with a bath of bosonic oscillators. These collisions lead to heat transfer from the host bath to the rotators.

Though much work has been done to give the theoretical description of the spectra of fluids, few have successfully formulated an analytical description of absorption spectra over

wide temperature and frequency ranges. Most of the theories are based on phenomenological models that yield parameter dependent results. Special emphasis has been given to the classical analysis of the problem. Most of the results published, thus far, have not gone beyond explaining the observations on classical systems, though it is well known that for systems composed of small molecules at low temperatures quantum aspects may influence their physical properties [11, 12]. For example, Birnbaum [11] and Frenkel [12] observed fine structures on the far infrared absorption spectra of HCl in argon, NH_3 in Sulphur hexafloride and DCl in non polar solvents. Gross [13] and Morita et al. [14] attributed this fine structures to quantum effects.

Progress in the theory of dielectrics has been greatly motivated by the development of two statistical mechanics methods: (i) the kinetic equation method [15] and (ii) the autocorrelation function (ACF) method [16]. The former is based on developing and solving kinetic equations for the one particle probability function $f(\mathbf{r}, \mathbf{p}; t)$ (or density operator $\hat{\rho}(\hat{\mathbf{r}}, \hat{\mathbf{p}}; t)$) of molecules in phase space (or in the Hilbert space of the molecular dynamical variables), while the ACF method, for the electric susceptibility is based on the Kubo linear response theory [17]. Most of the works based on the kinetic equation method exploit the impact approximation approach characterised by two criteria (i) that only binary collisions are considered and that (ii) the duration of collision is very small compared to the system characteristic times $(I/k_BT)^{0.5}$, $I/\hbar$ and system relaxation time τ_R. This latter condition restricts the validity of the resulting theory to the centre of the far infrared lines. Baranger [18] developed a general quantum theory for the impact approximation including line coupling. Rosenkranz [19] and Smith [20] established a formulation of line coupling. By truncating the well-known BBGKY (Bogoliubov-Born-Green-Kirkwood-Yvon) hierarchy of equations for the n particle density matrix at the two particle level and solving for the two particles $\rho^{(2)}(1, 2; t)$ in terms of the one particle $\rho^{(1)}(1; t)$, Roney [21] developed a kinetic equation for the one particle distribution function in which the collision term was independent of radiation frequency. Very recently Roney [22] exploited the previously derived kinetic equation to obtained absorption line shapes whose basic features are same as the VVW (van Vleck-Weisskopf) line form. Fano [23] laid the foundation for a theory in which collision is radiation frequency dependent. A wide range of models [24, 25, 26, 27] make use of the ACF method with each differing from the other in the interpretation of the changes of the physical characteristics of motion (momentum, orientation and energy) of the molecules as a result of collision. For the **J** diffusion model [16, 28], for example, the molecular orientation is unaltered after impact, while the magnitude and direction of the angular momentum are changed. Huber and van Vleck [29] emphasised on the importance of the application of the Kubo fluctuation dissipation theorem [30, 31] to the shape theory.

Since 1994, our group has been developing a new quantum approach for the description of dielectric and electro-optical properties of materials [32, 33, 34]. In our descriptions, we have shown that widely published classical results [4, 5, 27, 35, 36, 37, 38, 39, 40, 41, 42, 43, 44, 45, 46, 47] are well recovered as limiting cases of our more general quantum theory. Our quantum results faithfully reproduce the main features of absorption and dispersion spectra, demonstrating how line widths and shifts depend on the rotator and bath characteristics.

In this chapter we derive a master equation describing the evolution of the orientation probability density operator of a system of linear rigid rotators in a bath of non interacting harmonic oscillators [32, 33, 34]. The rest of the chapter is organised as follows: In section 2, we present the derivation of the Master Equation and section 3 is devoted to the study of the stability of the solutions of the master equation.

1.2 The model

Let us consider a symmetric rigid linear rotator, fixed at its centre but free to rotate about the latter [6]. The rotator is in a bath of nonpolar, mutually non interacting harmonic oscillators that interact harmonically with one or the other end of the rotator. Only the rotational degrees of freedom of the rotator are considered. In addition to an anisotropic polarisability tensor, the rotator possesses a permanent dipole moment susceptible of interacting with an applied electric field. In the quantum treatment, the Hilbert space associated with this model is the tensorial product of the Hilbert space associated with the rotator system $\mathcal{H}_S$ and of the bath system $\mathcal{H}_B$:

$$\mathcal{H} = \mathcal{H}_S \otimes \mathcal{H}_B. \tag{1.8}$$

In our model the following assumptions are made:

- The bath oscillator-rotator system is homogeneous;
- The rotator has a needle shape [10], so that the moment of inertia about its longitudinal axis is zero while that measured about a transverse axis passing through its centre is nonzero. The bath effect on the rotator is conceived as a quantum noise described by a collision operator in the considered dynamical equation.
- The rotator-rotator interaction is neglected, as we consider an infinitely dilute solution of rotators in the bath, that is, the ratio of the concentration of rotators to that of the bath is very small. Thus one rotator can be studied independently of the others.

1.2.1 The system Hamiltonian

The bath-rotator system Hamiltonian is the one used in [6]:

$$\hat{H}_T = \hat{H} + \hat{H}_E, \tag{1.9}$$

where $\hat{H} = \hat{H}_S + \hat{H}_B + \hat{H}_{SB}$. $\hat{H}_S$ is the Hamiltonian of the isolated rotator, $\hat{H}_B$ that of the bath and $\hat{H}_{SB}$ is the bath-rotator interaction Hamiltonian. We assume that there is no interaction between the rotators, so that its Hamiltonian is simply the kinetic energy term:

$$\hat{H}_S = \frac{\hat{\mathbf{P}}^2}{2m} = -\frac{\hbar}{2I}\left(\frac{1}{\sin\hat{\beta}}\frac{\partial}{\partial\hat{\beta}}\sin\hat{\beta}\frac{\partial}{\partial\hat{\beta}} + \frac{1}{\sin^2\hat{\beta}}\frac{\partial^2}{\partial\hat{\alpha}^2}\right). \tag{1.10}$$

The eigenfunctions of $\hat{H}_S$ are the spherical harmonics $Y_l^m(\hat{\alpha},\hat{\beta})$, where l and m are, respectively, the orbital and magnetic quantum numbers meanwhile $\hat{\alpha}$ and $\hat{\beta}$ are, respectively, the polar and the azimuthal angles. The eigenvalues of $\hat{H}_S$ are $E_l = \frac{\hbar}{2I}l\,(l+1)$. I is the rotator moment of inertia.

We define, respectively, the creation and annihilation operators

$$\hat{\mathbf{a}}_\nu^\dagger = \sqrt{\frac{\omega_\nu}{2\hbar}}\hat{\mathbf{q}}_\nu - i\sqrt{\frac{1}{2\hbar\omega_\nu}}\hat{\mathbf{p}}_\nu \quad \text{and} \quad \hat{\mathbf{a}}_\nu = \sqrt{\frac{\omega_\nu}{2\hbar}}\hat{\mathbf{q}}_\nu + i\sqrt{\frac{1}{2\hbar\omega_\nu}}\hat{\mathbf{p}}_\nu, \tag{1.11}$$

of the νth bath oscillator and the occupation number $\hat{\mathrm{N}}_\nu = \hat{\mathbf{a}}_\nu \cdot \hat{\mathbf{a}}_\nu^\dagger$, where $\hat{\mathbf{q}}_\nu$, $\hat{\mathbf{p}}_\nu$ and ω_ν are the corresponding generalised coordinates, momenta and the characteristic angular frequency, respectively. $\hat{\mathbf{a}}_\nu^\dagger$ and $\hat{\mathbf{a}}_\nu$ verify the commutation relation

$$\left[\hat{\mathbf{a}}_\nu, \hat{\mathbf{a}}_{\nu'}^\dagger\right] = \hat{I}\delta_{\nu\nu'}, \tag{1.12}$$

where $\hat{I}$ is a unit tensor and $\dagger$ denotes the hermitian conjugate. The bath Hamiltonian, corresponding to that of a harmonic oscillator, can then be written as

$$\hat{H}_B = \sum_\nu \hbar\omega_\nu \left(\hat{N}_\nu + \frac{\hat{I}}{2}\right). \tag{1.13}$$

The rotator-bath interaction is assumed to be of the form

$$\hat{H}_{SB} = \sum_\nu c_\nu \hat{\mathbf{q}}_\nu \cdot \hat{\mathbf{u}} = \sum_\nu c_\nu \sqrt{\frac{\hbar}{2\omega_\nu}} \left(\hat{\mathbf{a}}_\nu^\dagger + \hat{\mathbf{a}}_\nu\right) \cdot \hat{\mathbf{u}}, \tag{1.14}$$

with $\hat{\mathbf{u}}$ being a unit vector defining the orientation of the rotator. c_ν is the coupling constant.

The electric field term resulting from the interaction between the permanent dipole (μ) and the induced dipole moments with the applied electric field, is found to be [4]

$$\hat{H}_E = -\mu E \cos\hat{\beta} - \frac{\alpha_{\|} - \alpha_\perp}{2} E^2 \cos^2\hat{\beta} - \frac{\alpha_\perp}{2} E^2 \hat{I} \tag{1.15}$$

where $\alpha_{\|}$ and $\alpha_\perp$ are the rotator polarisability tensor components parallel and perpendicular to the molecular principal axise, respectively. We have assumed that the electric field is applied along the z-axis of the laboratory frame.

1.2.2 The Master Equation

We denote the rotator-bath probability density operator by $\hat{\rho}(t) \equiv \hat{\rho}(\mathbf{S}, \mathbf{B}; t)$, where $\mathbf{S}$ and $\mathbf{B}$ represent, respectively, the sets of rotator and bath variables. $\hat{\rho}(t)$ must verify the normalisation relation

$$Tr\hat{\rho}(t) = 1, \tag{1.16}$$

where Tr denotes trace norm over the rotator-bath space. It is expressed mathematically as $Tr\hat{\rho}(t) = Tr_B \otimes Tr_S \hat{\rho}(t) = Tr_S \otimes Tr_B \hat{\rho}(t)$.

When an external stimulus (electric, magnetic, mechanical, etc.) is applied to the rotator-bath system for a long time and is suddenly withdrawn, the system density operator relaxes to the canonical equilibrium expression,

$$\hat{\rho}^{eq} = \frac{\exp\left[-\beta\left(\hat{H}_s + \hat{H}_B + \hat{H}_{SB}\right)\right]}{Tr\left[\exp\left[-\beta\left(\hat{H}_s + \hat{H}_B + \hat{H}_{SB}\right)\right]\right]}, \quad \text{with } \beta = \frac{1}{k_B T}. \tag{1.17}$$

We want to derive the equation for the calculation of the dielectric properties of the rotator system. The first step in this derivation should be aimed at decoupling the rotator system from the bath variables, conserving in the final equations only collective characteristics of the bath such as its temperature, friction coefficients and characteristic frequencies. This task is feasible

through the use of projection operator techniques [48, 49, 50]. We define a projection operator $\hat{P}$ which acts on any rotator-bath observable, for example $\hat{\rho}(t)$, as

$$\hat{P}\hat{\rho}(t) = \hat{\rho}_B^{eq} \otimes \hat{\rho}_S(t). \tag{1.18}$$

Remark that $\hat{P}$ verifies the properties of projection operators. $\hat{\rho}(t)$ obeys the conservation law which is expressed here by the **Liouville** equation,

$$\frac{\partial}{\partial t}\hat{\rho}(t) + i\hat{L}\hat{\rho}(t) = 0, \tag{1.19}$$

where $\hat{L}$ is the Liouville operator defined over any dynamical variable $\hat{X}$ as follows:

$$\hat{L}\hat{X} = \begin{cases} \frac{i}{\hbar}\left[\hat{H}, \hat{X}\right] & \text{for quantum systems} \\ -\left\{\hat{H}, \hat{X}\right\} & \text{for classical systems.} \end{cases}$$

$[,]$ denotes the commutator symbol and $\{,\}$ the Poisson brackets.

Two coupled equations can be written (by writing $\hat{\rho} = (\hat{P} + \hat{P}')\hat{\rho}$ in the second term of Eq.(1.19) and multiplying the resulting equation from the left by $\hat{P}$ and $\hat{P}'$, respectively, noting that $\hat{P}$ is time independent) describing the time evolution of the relevant part $\hat{P}\hat{\rho}(t)$ and the non-relevant part $\hat{P}'\hat{\rho}(t) \equiv \left(\hat{I} - \hat{P}\right)\hat{\rho}(t)$ of the density operator. These read:

$$\frac{\partial}{\partial t}\hat{P}\hat{\rho}(t) = -\hat{P}i\hat{L}\hat{P}\hat{\rho}(t) - \hat{P}i\hat{L}\hat{P}'\hat{\rho}(t), \tag{1.20}$$

$$\frac{\partial}{\partial t}\hat{P}'\hat{\rho}(t) = -\hat{P}'i\hat{L}\hat{P}\hat{\rho}(t) - \hat{P}'i\hat{L}\hat{P}'\hat{\rho}(t). \tag{1.21}$$

On solving Eq.(1.21) for $\hat{P}'\hat{\rho}(t)$ using the initial condition $\hat{P}'\hat{\rho}(t=0) = 0$ (which means that initially the rotator is not coupled to the bath) and substituting into Eq.(1.20) while using the property

$$e^{\hat{P}'\hat{X}} = \hat{P} + \hat{P}'e^{\hat{X}} \tag{1.22}$$

for commuting $\hat{P}$ and $\hat{X}$; and taking trace over bath variables, it can be shown that the relevant part (related to the rotator probability density operator $\hat{\rho}_S$, through $\hat{\rho}_S(t) = Tr_B\left[\hat{P}\hat{\rho}(t)\right]$) verifies the integro-differential equation [50],

$$\frac{\partial\hat{\rho}_S(t)}{\partial t} = -iTr_B\left(\hat{P}\hat{L}\hat{P}\hat{\rho}(t)\right) - \int_0^t Tr_B\left[\hat{P}\hat{L}\left(\hat{P} + \hat{P}'e^{-i\hat{L}(t-\tau)}\right)\hat{P}'\hat{L}\hat{P}\hat{\rho}(\tau)\right]d\tau. \tag{1.23}$$

In the absence of an external field, the Liouville operator is made of three terms ($\hat{L} = \hat{L}_S + \hat{L}_B + \hat{L}_{SB}$). It was shown in [50], after a rather lengthy algebra, that the above equation can be written as

$$\frac{\partial\hat{\rho}_S}{\partial t} + i\hat{L}_S\hat{\rho}_S(t) = -\int_0^t Tr_B\left[\hat{L}_{SB}e^{i\hat{L}_0\tau}\hat{L}_{SB}e^{-i\hat{L}_0\tau}\hat{\rho}_B^{eq} \otimes \hat{\rho}_S(t)\right]d\tau, \tag{1.24}$$

where $\hat{L}_0 = \hat{L}_S + \hat{L}_B$. If the rotator longest relaxation time is very short compared with the observation time, we can assume that the collision term on the right hand side of Eq.(1.24) is short lived and extend the integration to infinity.

In order to be able to handle the last term in Eq.(1.24) the following points should be mentioned:

- We shall make use of the relation

$$e^{-i\hat{L}_0\tau}\hat{A} = e^{-i\frac{\hat{H}_0}{\hbar}\tau}\hat{A}e^{i\frac{\hat{H}_0}{\hbar}\tau}, \tag{1.25}$$

where $\hat{L}_0$ is the Liouvillian corresponding to the Hamiltonian $\hat{H}_0 = \hat{H}_S + \hat{H}_B$.

- We shall use the following expansion of the rotator unit vector (in the spherical harmonic basis) [6, 50]

$$\hat{\mathbf{u}} = \sum_{l=1}^{\infty}\left(\hat{\mathbf{u}}_l^+ + \hat{\mathbf{u}}_l^-\right), \tag{1.26}$$

where $\hat{\mathbf{u}}_l^- = \left(\hat{\mathbf{u}}_l^+\right)^\dagger$ and

$$\begin{aligned}
\hat{u}_{lx}^+(t) &= \frac{1}{2}\sum_{m=-l}^{l} \mid l,m > \Big[< l-1, m+1 \mid A(l,m) - < l-1, m-1 \mid B(l,m)\Big], \\
\hat{u}_{ly}^+(t) &= \frac{1}{2i}\sum_{m=-l}^{l} \mid l,m > \Big[< l-1, m+1 \mid A(l,m) + < l-1, m-1 \mid B(l,m)\Big], \\
\hat{u}_{lz}^+(t) &= \sum_{m=-l}^{l} \mid l,m >< l-1, m \mid C(l,m),
\end{aligned} \tag{1.27}$$

with

$$\begin{aligned}
A(l,m) &= \sqrt{\frac{(l-m)(l-m-1)}{(2l-1)(2l+1)}}, \quad B(l,m) = \sqrt{\frac{(l+m)(l+m-1)}{(2l-1)(2l+1)}}, \\
C(l,m) &= \sqrt{\frac{(l-m)(l+m)}{(2l-1)(2l+1)}}.
\end{aligned} \tag{1.28}$$

- We introduce the time displacement operator $\hat{U}(t) = e^{i\hat{L}_S t}$ so that for any dynamical variable in the rotator space, if $\hat{X}_S$ is the variable at time $t = 0$, then at $t \neq 0$.

$$\hat{X}_S(t) = \hat{U}(t)\hat{X}_S = e^{i\hat{L}_S t}\hat{X}_S. \tag{1.29}$$

It follows from this and the eigenvalue equation that

$$\hat{\mathbf{u}}(t) = e^{i\hat{L}_S t}\sum_{l=1}^{\infty}\left(\hat{\mathbf{u}}_l^- + \hat{\mathbf{u}}_l^+\right) = \sum_{l=1}^{\infty}\left(e^{i\omega_l t}\hat{\mathbf{u}}_l^+ + e^{-i\omega_l t}\hat{\mathbf{u}}_l^-\right), \tag{1.30}$$

where ω_l is the rotator angular frequency when it is in the quantum energy level l. In a similar manner, the generalised co-ordinate and momentum vectors of the bath molecules at any instant can be given in terms of their characteristic frequencies and the initial co-ordinates and momenta.

- We shall use the property of the occupation number operator $\hat{N}_\nu$,

$$Tr_B\left(\hat{\mathbf{a}}_\nu^\dagger \cdot \hat{\mathbf{a}}_{\nu'}\hat{\rho}_B^{eq}\right) = N(\omega_\nu)\delta_{\nu\nu'}, \tag{1.31}$$

where $\delta_{\nu\nu'}$ is the Kronecker delta symbol; and the other properties

$$Tr_B\left(\hat{\mathbf{q}}_\nu \cdot \hat{\mathbf{q}}'_\nu \hat{\rho}_B^{eq}\right) = \frac{\hbar}{\omega_\nu}\left(N(\omega_\nu) + \frac{1}{2}\right)\delta_{\nu\nu'}$$

and

$$Tr_B\left(\hat{\mathbf{q}}_\nu \cdot \hat{\mathbf{p}}_{\nu'} \hat{\rho}_B^{eq}\right) = i\hbar\delta_{\nu\nu'}.$$

When Eq.(1.24) is revisited, bearing in mind the above points where necessary, we obtain the Master Equation:

$$\frac{\partial}{\partial t}\hat{\rho}_S(t) + i\hat{L}_S\hat{\rho}_S(t) = -\hat{K}\hat{\rho}_S(t), \tag{1.32}$$

where the collision term characterising the bath effect ($\hat{K}\hat{\rho}_S(t)$) is written explicitly as,

$$\begin{aligned}\hat{K}\hat{\rho}_S(t) \;=\; & \sum_\nu \frac{c_\nu^2}{2\hbar\omega_\nu}\sum_{l=1}^{\infty}\Bigg\{\pi\delta(\omega_l-\omega_\nu)\Big[\hat{\mathbf{u}};\Big(N(\omega_\nu)+\frac{1}{2}\Big)\left[\hat{\mathbf{u}}_l^+ + \hat{\mathbf{u}}_l^-, \hat{\rho}_S(t)\right] \\ & -\frac{\omega_l}{2\omega_\nu}\left[\hat{\mathbf{u}}_l^+ - \hat{\mathbf{u}}_l^-, \hat{\rho}_S(t)\right]_+\Big] - i\Big(\frac{1}{(\omega_l-\omega_\nu)_p}+\frac{1}{(\omega_l+\omega_\nu)_p}\Big)\Big[\hat{\mathbf{u}}; \\ & \Big(N(\omega_\nu)+\frac{1}{2}\Big)\left[\left(\hat{\mathbf{u}}_l^+ - \hat{\mathbf{u}}_l^-\right), \hat{\rho}_S(t)\right] - \frac{\omega_l}{2\omega_\nu}\left[\left(\hat{\mathbf{u}}_l^+ + \hat{\mathbf{u}}_l^-\right), \hat{\rho}_S(t)\right]\Big]\Bigg\}.\end{aligned} \tag{1.33}$$

The index p denotes the principal value. We assimilate the bath system to a gas of phonons whose spectral density $g(\omega_\nu)$ is given by

$$\frac{\pi}{2}\frac{g(\omega_\nu)c(\omega_\nu)^2}{\omega_\nu^2} = \zeta\frac{\omega_D^2}{(\omega_D^2+\omega_\nu^2)}, \tag{1.34}$$

where ζ is the friction coefficient, $c_\nu = c(\omega_\nu)$ the coupling constant and ω_D, the Debye frequency, is the upper limit of the bath frequencies. If we approximate the discrete sum over ν in Eq.(1.33) by a continuous one over ω_ν as

$$\sum_\nu (\ldots) \approx \int d\omega_\nu g(\omega_\nu)(\ldots), \tag{1.35}$$

it can be shown that the collision term $\hat{K}\hat{\rho}_S(t)$ is,

$$\begin{aligned}\hat{K}\hat{\rho}_S(t) \;=\; & \frac{\zeta}{I}\sum_{l=1}^{\infty} l\Big\{A_l^*\hat{\mathbf{u}}.\hat{\mathbf{u}}_l^-\hat{\rho}_S(t) - A_l\hat{\mathbf{u}}.\hat{\rho}_S(t)\hat{\mathbf{u}}_l^+ + B_l\hat{\mathbf{u}}.\hat{\mathbf{u}}_l^+\hat{\rho}_S(t) \\ & -B_l^*\hat{\mathbf{u}}.\hat{\rho}_S(t)\hat{\mathbf{u}}_l^- - A_l^*\hat{\mathbf{u}}_l^-.\hat{\rho}_S(t)\hat{\mathbf{u}} + A_l\hat{\rho}_S(t)\hat{\mathbf{u}}_l^+.\hat{\mathbf{u}} \\ & +B_l^*\hat{\rho}_S(t)\hat{\mathbf{u}}_l^-\hat{\mathbf{u}} - B_l\hat{\mathbf{u}}_l^+\hat{\rho}_S(t).\hat{\mathbf{u}}\Big\},\end{aligned} \tag{1.36}$$

where

$$A_l = \frac{\omega_D^2}{\omega_D^2+\omega_l^2}\Big(1 + N(\omega_l) + i\Big(\kappa(x_l, x_D) - \frac{\omega_l}{2\omega_D}\Big)\Big), \tag{1.37}$$

$$B_l = \frac{\omega_D^2}{\omega_D^2 + \omega_l^2}\Big(N(\omega_l) + i\Big(\kappa(x_l, x_D) + \frac{\omega_l}{2\omega_D}\Big)\Big), \tag{1.38}$$

with

$$\kappa(x_l, x_D) = -\Big(\frac{1}{x_D} + 2\sum_{n=1}^{\infty} \frac{x_l^2 - 2\pi x_D n}{(x_D + 2\pi n)(x_l^2 + 4\pi^2 n^2)}\Big) \tag{1.39}$$

and

$$x_j = \beta\hbar\omega_j, \;\; \beta = \frac{1}{k_B T}, \;\; n \in Z^+. \tag{1.40}$$

A_l^* and B_l^* are the complex conjugates of A_l and B_l, respectively. k_B is the Boltzmann constant, T the absolute temperature, ζ the friction coefficient and $N(\omega_l)$ the occupation number of the rotator quantum level l.

Eq.(1.32) is the required master equation governing the evolution of the rotator probability density operator. The collision term imposes that the weak coupling limit must be characterised by the inequalities [45] (see also [6]):

$$\frac{\zeta}{I} << \frac{k_B T}{\hbar} \tag{1.41}$$

and

$$\frac{\zeta}{I} << \omega_D. \tag{1.42}$$

It has been shown in [6, 45] that in the case where the first inequality is verified, the coupling effect on the density matrix can be neglected. The classical Brownian and the rotating wave approximation limits are determined by the value of the mean thermal agitation frequency $\omega_{mean} = (k_B T/I)^{0.5}$. In the former, ω_{mean} is of the same order of magnitude as the characteristic frequency ζ/I. In this case, the rotator energy is of the same order as the thermal energy, that is, $\hbar^2 l(l+1)/2I \sim k_B T$. Here we assume that $\omega_D \to \infty$. The rotating wave approximation limit [49] concerns the weak coupling assumption, $\zeta/I << \omega_{mean}$. In this case we use a theorem by Davies [51, 52, 53] on weak coupling as described in [6], which states that

1. if the spectrum of $\hat{H}_S$ is discrete and
2. if there exists a $\delta > 0$, such that

$$\int_0^{\infty} dt' \Big|\sum_{\nu} Tr_B\left(\hat{\rho}_B^{eq}\hat{\mathbf{q}}_\nu \cdot \hat{\mathbf{q}}_\nu(-t')\right)\Big|(1+t')^{\delta} < +\infty, \tag{1.43}$$

then, replacing $\hat{H}_{SB}$ by $\lambda\hat{H}_{SB}$, where λ is a coupling parameter for all τ and all reduced matrix operator $\hat{\rho}_s$, one obtains

$$\lim_{\lambda\to 0} \sup_{0\le\lambda^2 t\le\tau} \|Tr_B\left(e^{-i\hat{L}t}\hat{\rho}_S \otimes \hat{\rho}_B^{eq}\right) - e^{(-i\hat{L}_s + \lambda^2\mathcal{K}^\sharp t)}\hat{\rho}_S\| = 0, \tag{1.44}$$

where $\|\ldots\|$ designates the trace norm and

$$\mathcal{K}^\sharp\hat{\rho}_S = \lim_{T\to+\infty} \frac{1}{2T}\int_{-T}^{T} dt e^{i\hat{L}_S t}\hat{K}e^{-i\hat{L}_S t}\hat{\rho}_S. \tag{1.45}$$

The two conditions (1) and (2) are essentially satisfied by our model. This theorem can be understood in the sense that as the coupling parameter ζ becomes vanishingly small the collision operator $\hat{K}$ can be replaced by its time average $\hat{K}^\sharp$. The advantage of using $\hat{K}^\sharp$ is two fold. Firstly, it commutes with the relevant density operator $\hat{\rho}_S$ and secondly, does not contain the off-diagonal terms that are responsible for mathematical difficulties.

1.3 The stability of the Master Equation

The stability of the master equation (1.32) can be analysed by assuming its solutions to exist and be of the form

$$\hat{\rho}_S(t) = \hat{\rho}_S^{eq}\hat{\psi}(t). \tag{1.46}$$

We then define a Liapounov function $tr_S\left(\hat{\rho}_S^{eq}\hat{\psi}(t)^2\right)$. On substituting this solution in the master equation and multiplying both sides of the resulting equation by $\hat{\psi}(t)$ while taking trace we obtain:

$$\begin{aligned}\frac{d}{dt}\sum_{l=0}^{\infty}\sum_{m=-l}^{l}(\rho_S^{eq})_{l,l}^{m}\frac{|\psi_{ll}^{m}(t)|^2}{2} &= -2B\Re\sum_{l=0}^{\infty}\sum_{m=-l}^{l}\left(A_l l^2 + B_{l+1}(l+1)^2\right)(\rho_S^{eq})_{l,l}^{m}\,|\psi_{l,l}^{m}(t)|^2 \\ &\times\frac{1}{2l+1} + 2B\Re\sum_{l=0}^{\infty}\sum_{m=-l}^{l}A_l\frac{l^2}{2l+1}(\rho_S^{eq})_{l,l}^{m}\,|\psi_{l-1,l-1}^{m}(t)|^2 \\ &+2B\Re\sum_{l=0}^{\infty}\sum_{m=-l}^{l}B_{l+1}\frac{(l+1)^2}{2l+1}(\rho_S^{eq})_{l,l}^{m}\,|\psi_{l+1,l+1}^{m}(t)|^2, \end{aligned}\tag{1.47}$$

where $B = \zeta/I$ and $\Re$ denotes real part. We have assumed that the system is near equilibrium so that all off-diagonal terms in the probability density matrix are neglected. If $\hat{\psi}(t)$ is independent of the rotator variables, $\psi_{l,l}^{m}(t)$ will be independent of l and m, then the right hand side (rhs) of Eq.(1.47) equals zero; the expression of the probability density operator is, thus, identically equal to that of the equilibrium distribution with matrix elements $(\rho_S^{eq})_{l,l}^{m}$. By translating l (i.e. by performing the transformations $l \to l+1$ and $l \to l-1$) in the second and third terms of the rhs of the above equation, we can show that the quantity to the right of the equality is always negative. This shows that the positive function whose time-derivative is at the left of Eq.(1.47) decreases exponentially to its equilibrium value when the field is switched off. This guarantees the stability of the solutions of Eq.(1.32).

Bibliography

[1] H. Benoît, *Ann. Phys.* **6**: 561, 1951

[2] F. Perrin, *J. Phys. Radium.* **5**: 497, 1934

[3] Y. P. Kalmykov. *J. Chem. Phys.* **95**: 9142, 1991

[4] M. N. Hounkonnou, A. Ronveaux and P. Navez, *J. Phys. A: Math. Gen.* **27**: 6635, 1994

[5] P. Navez, M. N. Hounkonnou, *J. Phys. A: Math. Gen.* **27**: 6657, 1994

[6] P. Navez and M. N Hounkonnou., *J. Phys. A: Math. Gen.* **28**: 6345, 1995

[7] Y. P. Kalmykov and S. V. Titov., *Adv. in Chem. Phys* **87** :31, 1994

[8] A. Piekara, *J. Chem. Phys.* **36**: 2145, 1962

[9] B. M. Ladanyi and T. Keyes, *Mol. Phys.* **34**(6): 1643, 1977

[10] W. T. Coffey, *J. Chem. Phys.* **95**: 2026, 1991

[11] G. Birnbaum *Mol. Phys.* **25**: 245, 1973

[12] D. Frenkel, *Rotational relaxation of linear molecules in dense noble gases*, Ph.D thesis, Amstradam, 1977

[13] E. P. Gross, *J. Chem. Phys.* **23**: 1415, 1955

[14] A. Morita, S. Walker and J. H. Calderwood,*J. Phys. D:App. Phys.* **9**: 2485, 1976

[15] V. I. Gaiduk and Yu P. I. Kalmykov, *J. Mol. Liq.* **34**: 1, 1987

[16] Y. P. Kalmykov and S. V. Titov, *A semi-classical theory of dielectric relaxation and absorption: memory function approach to extended diffusion models of molecular reorientation in fluids. Relaxation Phenomena in Condensed Matter*, Edited by W. Coffey, *Adv. Chem. Phys.*, LXXXVII: 31, 1994

[17] R. Kubo, *J. Phys. Soc. Jpn.* **12**: 570, 1957

[18] M. Baranger *Phys. Rev.* **111**: 481, 494, 1958

[19] P. W. Rosenkranz, *IEEE Trans. Antennas Propag.* **23**: 498, 1975

[20] E. W. Smith, *J. Chem. Phys.* **74**: 6658, 1981

[21] P. L. Roney, *J. Quant. Spectrosc. Radiat. Transfer* **15**: 361, 1975

[22] P. L. Roney, *J. Chem. Phys.* **101**(2): 1037, 1994

[23] U. Fano, *Phys. Rev.* **131**: 259, 1963

[24] R. Karplus and J. Schwinger, *Phys. Rev.* **74**: 1020, 1948

[25] E. P. Gross and J. L. Lebowitz, *Phys. Rev.* **104**: 1528, 1956

[26] J. J. O'Dwyer and E. Harting, *Prog. Diel.* **71**, 1967

[27] E. P. Gross, *J. Chem. Phys.* **23** (8): 1415, 1955

[28] R. E. D. mc Clung, *Adv. Mol. Relaxation Interact. Process* **10**: 83, 1977

[29] D. L. Huber and van Vleck, *Rev. Mod. Phys.* **38**: 187, 1966

[30] J. McConnell, *Rotational Brownian Motion and Dielectric Theory*, Academic Press, London, 1980

[31] R. Kubo, *Rep. Prog. Phys.* **29**: 255, 1966

[32] P. Navez and M. N. Hounkonnou, *J. Phys. A: Math. Gen.* **28**: 6345, 1995

[33] J. T. Titantah and M. N. Hounkonnou, *J. Phys. A* **30**: 6327, 1997

[34] J. T. Titantah and M. N. Hounkonnou, *J. Phys. A* **30**: 6347, 1997

[35] A. Morita, *J. Phys. D* **11** L9: 4708, 1978

[36] A. Morita and H. Watanabe, *J. Chem. Phys.* **70**: 4708, 1979

[37] M. Matsumoto, H. Watanabe and K. Yoshioka, *J. Phys. Chem.* **74**: 2182, 1970

[38] W. T. Coffey, *J. Chem. Phys.* **93**: 724, 1990

[39] W. T. Coffey, *J. Chem. Phys.* **95**: 2026, 1991

[40] A. Morita, *J. Chem. Phys.* **76**: 3198, 1982

[41] M. N. Hounkonnou, A. Ronveaux and R. P. Hazoumé, *Physica* **179**: 569, 1991

[42] M. N. Hounkonnou, *J. Chem. Soc. Faraday Trans.* **87**: 297, 1991

[43] M. N. Hounkonnou and A. Ronveaux, *Acta. Phys.* **82**: 425, 1992

[44] J. C. Filippini, *Ph.D Thesis*, Université de Grenoble-France, 1972

[45] P. Navez, *Thèse de Doctorat ès Sciences* Université Catholique de Louvain-Belgium, 1995

[46] W. T. Coffey and B. V. Paranjape, *Proc. R. Ir.* Acad. **78**: 17, 1978

[47] A. Morita and H. Watanabe, *Phys. Rev.* **35**: 2690, 1987

[48] H. Grabert, *Projection Operator Technique in Nonequilibrium Statistical Mechanics*, Springer-Verlag, Berlin, 1982

[49] C. W. Gardiner, *Quantum Noise*, Springer Verlag Berlin, 1991

[50] J. T. Titantah, *Mémoire de Diplôme d'Etudes Approfondies DEA*, IMSP, 1995

[51] P. Navez and M. N. Hounkonnou, *J. Phys. A: Math. Gen.* **27**: 6657, 1994

[52] E. B. Davies, *Math. ann.* **219**: 147, 1976

[53] H. Spohn, *Rev. Mod. Phys.* **53**: 569, 1980

[54] R. Kubo, M. Toda and N. Hashitsume, *Statistical Physics II, Nonequilibrium Statistical Mechanics* (Springer-Verlag, Berlin), 1985

Chapter 2

Electric birefringence induced by a constant field in relaxation regime

2.1 Introduction

The Kerr effect relaxation resulting from the sudden removal of a dc field previously applied to a system of dilute rigid linear polar rotators in a sea of non interacting bath harmonic oscillators is presented. In the Quantum Mechanics model proposed, we take account of permanent and induced dipole effects while the inertial effect is described by a collision operator. Hyperpolarisabilities are neglected. We use the generalised master equation derived in chapter 1 [1, 2] to calculate the Kerr relaxation function $\Phi(t)$. In the search for this function, we [3] define matrix elements $\varphi_{l,l}(t)$ and $\varphi_{l,l+2}(t)$ whose knowledge at all times t, completely gives $\Phi(t)$. We recover the classical limits of the quantum expressions. A quantum result valid for the rotating wave approximation (RWA) limit is given.

This chapter is organised as follows. In section 2, a brief description of the relaxational problem is given, in section 3 master equations are derived for well defined matrix elements; these are solved for different physical conditions leading to the classical Brownian limit and the rotating wave approximation limit, respectively, and finally section 4 is devoted to the derivation of the energy balance equation and entropy calculation.

2.2 The relaxation regime

Let us consider a polar, symmetric, rigid, linear rotator, fixed at its center but free to rotate about the latter [1]. The rotator is in a bath of non polar mutually non interacting harmonic oscillators that interact harmonically with one or the other end of the rotator.

We analyse the relaxational process (associated to the Kerr effect) following the sudden removal of a constant electric field that has been acting on the system for quite a long time. The field removal condition is characterised by the interaction between the rotator dipole moment (permanent ($\underline{\mu}$) and induced ($\underline{\underline{\alpha}} \cdot \underline{E}$)) and the applied electric field $\underline{E}$. For a linear molecule the polarisability tensor has three non-zero components in a frame whose axes coincide with the molecular principal axes - one component parallel to the longitudinal axis and two equal

transverse components. The interaction of the rotator with the field thus reads

$$\hat{H}_E(t) = \begin{cases} -\mu E \cos\hat{\beta} - \frac{\alpha_{\parallel}-\alpha_{\perp}}{2} E^2 \cos^2\hat{\beta} - \frac{\alpha_{\perp}}{2} E^2 \hat{I} & \text{if } t < 0 \\ 0 & \text{if } t \geq 0, \end{cases} \tag{2.1}$$

where $\alpha_{\parallel}$ and $\alpha_{\perp}$ are, respectively, the rotator polarisability tensor components parallel and perpendicular to the molecular principal axis. It is assumed that the electric field is applied along the z-axis of the laboratory frame. The evolution of the rotator probability density operator is governed by the master equation (see Eq.(1.32)) [1]:

$$\frac{\partial\hat{\rho}_S(t)}{\partial t} + \frac{i}{\hbar}\left[\hat{H}_S, \hat{\rho}_S(t)\right] = -\hat{K}\hat{\rho}_S(t), \tag{2.2}$$

where $\hat{K}$ is explicitly given in chapter 1.

We consider the field removal initial condition

$$\hat{\rho}_S(t=0) = \hat{\rho}_S^{eq}(E \neq 0) = \frac{tr_B\left[e^{-\beta(\hat{H}_S+\hat{H}_B+\hat{H}_{SB}+\hat{H}_E)}\right]}{tr\left[e^{-\beta(\hat{H}_S+\hat{H}_B+\hat{H}_{SB}+\hat{H}_E)}\right]}, \tag{2.3}$$

which corresponds to the canonical equilibrium density operator of the bath-rotator system in the presence of the electric field. On performing a perturbative expansion in $\beta\hat{H}_E$, knowing that $\hat{H}_E$ does not commute with $\hat{H} = \hat{H}_S + \hat{H}_B + \hat{H}_{SB}$, we obtain (see appendix A.1)

$$\hat{\rho}_S(t=0) = \frac{e^{-\beta\hat{H}_S}}{tr_S e^{-\beta\hat{H}_S}} - \frac{\beta}{tr_S e^{-\beta\hat{H}_S}}\int_0^1 d\alpha e^{-\alpha\beta\hat{H}_S}\hat{H}_E e^{-(1-\alpha)\beta\hat{H}_S} + \frac{\beta^2}{tr_S e^{-\beta\hat{H}_S}}\int_0^1 d\alpha\alpha \times \int_0^1 d\alpha' e^{-(1-\alpha')\alpha\beta\hat{H}_S}\hat{H}_E e^{-\alpha'\alpha\beta\hat{H}_S}\hat{H}_E e^{-(1-\alpha)\beta\hat{H}_S} + \ldots \tag{2.4}$$

The symbols tr_S, tr_B and tr denote, respectively, trace norms over the rotator and bath Hilbert spaces and the coupled rotator-bath Hilbert space.

2.3 The Kerr Effect Function

2.3.1 The master equations for the matrix elements

As it was pointed out earlier, the Kerr effect or the electric birefringence expresses the modification in the refractive index tensor of a medium as a result of the passage of an electric field through it. For rigid, linear molecules, the refractive index tensor $\underline{\underline{n}}$ is written as

$$\underline{\underline{n}} = n\underline{\underline{1}} + \frac{A}{2} < (3\hat{\mathbf{u}}\hat{\mathbf{u}} - \underline{\underline{1}}) >, \tag{2.5}$$

where $\hat{\mathbf{u}}$ is the molecule orientation unit vector, which here, is the dipole moment orientation unit vector and n is the isotropic refractive index (in the absence of any external stress). A is

a constant expressing the intrinsic birefringent properties of the medium. The Kerr function $\Phi(t)$ is related to the component $< (3\hat{u}_z\hat{u}_z - \hat{\underline{1}}) >$ as

$$\Phi(t) = \frac{1}{2} < (3\hat{u}_z\hat{u}_z - \hat{\underline{1}}) > . \tag{2.6}$$

We define the field removal reduced spectral function $\Delta n_r(\omega)$ as

$$\Delta n_r(\omega) = \frac{1}{\Phi(0)}\Big(\Phi(0) - i\omega \int_0^\infty \Phi(t)e^{-i\omega t}dt\Big). \tag{2.7}$$

On using the spherical harmonic representation of the unit vector $\hat{\mathbf{u}}$ (see Eq.(1.26)) and the probability density operator $\hat{\rho}_S(t)$ while defining matrix elements

$$\varphi_{l,l}(t) = \sum_{m=-l}^{l} (l(l+1) - 3m^2) < l, m|\hat{\rho}_S(t)|l, m > \tag{2.8}$$

and

$$\varphi_{l,l+2}(t) = \sum_{m=-l}^{l} \left[\frac{(l+1-m)(l+1+m)(l+2-m)(l+2+m)}{(2l+1)(2l+3)^2(2l+5)}\right]^{1/2} < l, m|\hat{\rho}_S(t)|l+2, m >, \tag{2.9}$$

we obtain

$$\Phi(t) = \sum_{l=1}^{\infty} \left\{ \frac{1}{(2l-1)(2l+3)}\varphi_{l,l}(t) + \frac{3}{2}\Big(\varphi_{l,l+2}(t) + \varphi^*_{l,l+2}(t)\Big)\right\}. \tag{2.10}$$

Let us derive the master equations verified by the matrix elements. To get the equation for $\varphi_{l,l}(t)$, we multiply through the master equation (1.32) from the left by $\sum_{m=-l}^{l}(l(l+1) - 3m^2)|l, m >< l, m|$ and take trace. On using some properties similar to (see appendix A.2)

$$\sum_{m=-l}^{l} (l(l+1) - 3m^2) < l, m \mid \hat{\mathbf{u}}_l^+ \hat{\rho}_S(t)\hat{\mathbf{u}}_{l+1}^+ \mid l, m >= -3\varphi_{l-1,l+1}(t)(1 - \delta_{l,0}), \tag{2.11}$$

we get:

$$\begin{aligned}
\frac{\partial}{\partial t}\varphi_{l,l}(t) \;=\; & -2B\Re\Big[(A_l l^2 + B_{l+1}(l+1)^2)\frac{\varphi_{l,l}(t)}{2l+1} - A_{l+1}(l+1)\frac{(2l-1)l}{(2l+1)(2l+3)} \\
& \times\varphi_{l+1,l+1}(t) - B_l l\frac{(l+1)(2l+3)}{(2l+1)(2l-1)}\varphi_{l-1,l-1}(t)(1-\delta_{l0}) \\
& -3(B_l l + A_{l+1}(l+1))\varphi_{l-1,l+1}(t)(1-\delta_{l0})\Big].
\end{aligned} \tag{2.12}$$

The initial condition (2.4) together with some algebra [4] lead to (see appendix A.3)

$$\begin{aligned}
\varphi_{l,l}(t=0) \;=\; & \frac{e^{-\beta E_l}}{\sum_{l'=0}^{\infty}(2l'+1)e^{-\beta E_{l'}}}\left\{\frac{l(l+1)(2l+3)}{15}\left[\frac{1}{2}\beta\Delta\alpha E^2 + \frac{\beta^2\mu^2E^2}{\beta(E_l - E_{l-1})}\right.\right. \\
& \left.\times\Big\{\frac{1}{\beta(E_l - E_{l-1})}(e^{\beta(E_l - E_{l-1})} - 1) - 1)\Big\}\right] + \frac{1}{15}l(l+1)(2l-1)\left[\frac{1}{2}\beta\Delta\alpha E^2\right. \\
& \left.\left. + \frac{\beta^2\mu^2E^2}{\beta(E_{l+1} - E_l)}\Big\{1 - \frac{1}{\beta(E_{l+1} - E_l)}(1 - e^{-\beta(E_{l+1} - E_l)})\Big\}\right]\right\}.
\end{aligned} \tag{2.13}$$

To get the equation verified by $\varphi_{l,l+2}(t)$, we multiply through Eq.(1.32) from the right by $\hat{u}^+_{l+2z}\hat{u}^+_{l+1z}$ and take trace. The use of similar properties as those used in Eq.(2.12) yields

$$\begin{aligned}\frac{\partial}{\partial t}\varphi_{l,l+2}(t) &- \frac{i\hbar}{I}(2l+3)\varphi_{l,l+2}(t) = -B\Bigg[\Bigg\{(A^*_l l^2 + B_{l+1}(l+1)^2)\frac{1}{2l+1} \\ &+(A_{l+2}(l+2)^2 + B^*_{l+3}(l+3)^2)\frac{1}{2l+5}\Bigg\}\varphi_{l,l+2}(t) - \frac{l+2}{2l+3}(B^*_l l \\ &+B_{l+2}(l+2))\varphi_{l-1,l+1}(t)(1-\delta_{lo}) - \frac{l+1}{2l+3}\Big(A^*_{l+1}(l+1) + A_{l+3}(l+3)\Big) \\ &\times\varphi_{l+1,l+3}(t) - 2\frac{\Big(A_{l+1}(l+1) + B^*_{l+2}(l+2)\Big)}{(2l+1)(2l+3)^2(2l+5)}\varphi_{l+1,l+1}(t)\Bigg]. \end{aligned} \tag{2.14}$$

The initial condition on $\varphi_{l,l+2}(t)$ is

$$\begin{aligned}\varphi_{l,l+2}(t=0) &= \frac{e^{-\beta E_l}}{\sum_{l'=0}^{\infty}(2l'+1)e^{-\beta E_{l'}}}\frac{2(l+1)(l+2)}{15(2l+3)}\Bigg[\frac{1}{2\beta(E_{l+2}-E_l)}(1-e^{\beta(E_{l+2}-E_l)}) \\ &\times\Delta\alpha\beta E^2 + \frac{\beta^2\mu^2E^2}{\beta(E_{l+1}-E_l)}\Bigg\{\frac{1}{\beta(E_{l+2}-E_l)}(1-e^{-\beta(E_{l+2}-E_l)}) \\ &-\frac{1}{\beta(E_{l+2}-E_{l+1})}\Big(e^{-\beta(E_{l+1}-E_l)} - e^{-\beta(E_{l+2}-E_l)}\Big)\Bigg\}\Bigg]. \end{aligned} \tag{2.15}$$

In Eqs.(2.12) and (2.14), $B = \zeta/I$. The exact expression for $\Phi(t)$ can be obtained if equations (2.12) and (2.14) are exactly solved using initial conditions (2.13) and (2.15). This quantum approach should generalise all results obtained using classical and semi-classical methods [5, 6, 7]. Let us now consider the case of the classical Brownian limit.

2.3.2 The classical Brownian limit

The classical Brownian limit is characterised by the inequalities [1]:

$$a \equiv \frac{\hbar^2}{Ik_BT} << 1 \text{ and } \frac{\omega_{mean}}{\omega_D} << 1, \tag{2.16}$$

which express the idea that the rotators perform slow random rotational motions compared to thermal motions and the fact that the thermal agitation frequencies will hardly ever attain the upper limit which corresponds to the Debye limit. Also, the rotator energy spectrum is regularly continuous. Though the quantum number l can assume large values, the quantity $al = \left(\hbar^2/Ik_BT\right)l$ is considered to be always very small compared to 1. We perform changes of functions

$$\varphi_{l,l}(t) = \frac{a}{2}l(l+1)(2l+1)exp\Big[-\frac{\hbar^2}{2Ik_BT}l(l+1)\Big]\psi_l(t), \tag{2.17}$$

$$\varphi_{l,l+2}(t) = \frac{a}{2}\frac{(l+1)(l+2)}{2l+3}exp\Big[-\frac{\hbar^2}{2Ik_BT}l(l+1)\Big]\Big(\varphi_l + i(2l+3)\chi_l(t)\Big) \tag{2.18}$$

while using the continuum hypothesis:

$$\frac{a}{2}l(l+1) \to x \tag{2.19}$$

and letting $\psi(x,t)$, $\varphi(x,t)$ and $\chi(x,t)$ be the continuum analogs of the discrete functions $\psi_l(t)$, $\varphi_l(t)$ and $\chi_l(t)$, Eqs.(2.12) and (2.14) reduce to second order coupled partial differential equations when we use:

$$\begin{aligned}\psi_{l-1}(t) &\approx \psi(x,t) - al\psi_x(x,t) + \frac{a^2l^2}{2}\psi_{xx}(x,t) + O_1(a^2)\\ \psi_{l+1}(t) &\approx \psi(x,t) + a(l+1)\psi_x(x,t) + \frac{a^2(l+1)^2}{2}\psi_{xx}(x,t) + O_2(a^2),\end{aligned} \tag{2.20}$$

where $O_i(a^2)$ $(i=1,2)$ is a vanishing function of a for small a.

On using the passage from discrete to continuous sum

$$\sum_{l=1}^{\infty} U_l(t) \to \frac{1}{\sqrt{2a}}\int_0^{\infty}\frac{dx}{\sqrt{x}}U(x,t), \tag{2.21}$$

we obtain the expression for the Kerr function

$$\Phi(t) = \frac{1}{4}\int_0^{\infty} dx e^{-x}(\psi(x,t) + 3\varphi(x,t)). \tag{2.22}$$

Let

$$F(x,t) = \psi(x,t) + 3\varphi(x,t), \tag{2.23}$$

then for dimensionless time $\tau = Bt$, the differential equations read:

$$\frac{\partial}{\partial\tau}F(x,\tau) + 3\alpha x\chi(x,\tau) = 2\Big[xF_{xx}(x,\tau) + (1-x)F_x(x,\tau)\Big], \tag{2.24}$$

$$\frac{\partial}{\partial\tau}\chi(x,\tau) - \frac{\lambda}{3}(F(x,\tau) - \psi(x,\tau)) = 2\Big[x\chi_{xx}(x,\tau) + (2-x)\chi_x(x,\tau) - \frac{1}{2}\chi(x,\tau)\Big], \tag{2.25}$$

$$\frac{\partial}{\partial\tau}\psi(x,\tau) = 2\Big[x\psi_{xx}(x,\tau) + (1-x)\psi_x(x,\tau) - \frac{1}{x}\psi(x,\tau) + \frac{1}{4x}F(x,t)\Big], \tag{2.26}$$

where

$$\alpha = \frac{8\hbar}{IaB} \text{ and } \lambda = \frac{\hbar}{IB}. \tag{2.27}$$

The initial condition on $F(x,\tau)$ is

$$F(x,0) = \frac{4E^2}{15}\left(\frac{\Delta\alpha}{k_BT} + \frac{\mu^2}{(k_BT)^2}\right) = 4\Phi_{static}. \tag{2.28}$$

In matrix form

$$\underline{\underline{D}}_{\tau,x}\underline{M}(\tau,x) = \underline{0}, \tag{2.29}$$

with

$$\underline{M}(\tau,x) = \begin{pmatrix} F(\tau,x)\\ \chi(\tau,x)\\ \psi(\tau,x)\end{pmatrix}, \tag{2.30}$$

$$\underline{\underline{D}}_{\tau,x} = \begin{pmatrix} \frac{\partial}{\partial\tau} - 2\Big[x\frac{\partial^2}{\partial x^2} + (1-x)\frac{\partial}{\partial x}\Big] & 3\alpha x & 0 \\ -\frac{\lambda}{3} & \frac{\partial}{\partial\tau} - 2\Big[x\frac{\partial^2}{\partial x^2} + (2-x)\frac{\partial}{\partial x} - \frac{1}{2}\Big] & \frac{\lambda}{3} \\ -\frac{1}{2x} & 0 & \frac{\partial}{\partial\tau} - 2\Big[x\frac{\partial^2}{\partial x^2} \\ & & +(1-x)\frac{\partial}{\partial x}\Big] + \frac{2}{x} \end{pmatrix}. \tag{2.31}$$

The initial condition on $\underline{M}(x,\tau)$ is

$$\underline{M}(x,0) = \Phi_{static}\begin{pmatrix} 4 \\ 0 \\ 1 \end{pmatrix}. \tag{2.32}$$

The spatial parts of the diagonal terms in the differential operator $\underline{\underline{D}}_{\tau,x}$ are related to the differential operator whose eigen functions are nothing but the generalised Laguerre polynomials $L_j^m(x)$ that verify the following properties [6, 8]:

$$(x\frac{d^2}{dx^2} + (m+1-x)\frac{d}{dx} + j)L_j^m(x) = 0, \tag{2.33}$$

$$xL_j^{m+1}(x) = (m+j+1)L_j^m(x) - (j+1)L_{j+1}^m(x), \tag{2.34}$$

$$L_j^m(x) = L_j^{m+1}(x) - L_{j-1}^{m+1}(x), \tag{2.35}$$

$$(x\frac{d}{dx} - x + m)L_j^m(x) = (j+1)L_{j+1}^{m-1}(x), \tag{2.36}$$

$$(\frac{d}{dx} - 1)L_j^m(x) = -L_j^{m+1}(x). \tag{2.37}$$

The orthogonality property of the $L_j^m(x)$ is written as

$$\int_0^\infty dx e^{-x}x^m L_j^m(x)L_{j'}^m(x) = \delta_{jj'}. \tag{2.38}$$

We, thus, look for solutions to the system (2.29) in the form

$$\underline{M}(x,\tau) = \sum_{j=0}^{\infty}\begin{pmatrix} f_j(\tau)L_j^0(x) \\ c_j(\tau)L_j^1(x) \\ d_j(\tau)L_j^0(x) \end{pmatrix}. \tag{2.39}$$

On using this in the system (2.24)-(2.26) while making use of the properties (2.33)-(2.37), we obtain the differential difference equations:

$$(\frac{d}{d\tau} + 2j)f_j(\tau) + 3\alpha((j+1)c_j(\tau) - jc_{j-1}(\tau)) = 0, \tag{2.40}$$

$$(\frac{d}{d\tau} + 2j + 1)c_j(\tau) - \frac{\lambda}{3}(f_j(\tau) - f_{j+1}(\tau)) + \frac{\lambda}{3}(d_j(\tau) - d_{j+1}(\tau)) = 0, \tag{2.41}$$

$$2(2j+1)(\frac{d}{d\tau}+2j)d_j(\tau)+4d_j(\tau)-2j(\frac{d}{d\tau}+2j-2)d_{j-1}(\tau)$$
$$-2(j+1)(\frac{d}{d\tau}+2j+2)d_{j+1}(\tau)-f_j(\tau)=0. \tag{2.42}$$

The Kerr function becomes,

$$\Phi(\tau)=\frac{1}{4}f_0(\tau). \tag{2.43}$$

On taking the Laplace transforms of (2.40)-(2.42) and searching for $f_0(s')$ (where $s=s'B$ is the Laplace variable) as a continued fraction [9], we obtain the Kerr function

$$\tilde{\Phi}(s')=\cfrac{\frac{E^2}{15B}\left(\frac{\Delta\alpha}{k_BT}+\frac{\mu^2}{(k_BT)^2}\right)}{s'+\cfrac{6\gamma}{s'+1+\cfrac{10\gamma}{s'+2+\cfrac{16\gamma}{s'+3-\cfrac{4\gamma}{(s'+2)(s'+4)}+\cfrac{16\gamma}{s'+4+\cfrac{24\gamma}{s'+5-\frac{4\gamma}{(s'+4)(s'+6)}+\frac{24\gamma}{s'+6+\ldots}}}}}}}, \tag{2.44}$$

where $\gamma=\alpha\lambda/8=Ik_BT/\zeta^2$.

The continued fraction (2.44). as the exact expression of the Kerr relaxation function in the classical limit obtained from the generalised quantum equations (2.12) and (2.14), is analogous to the result previously obtained by Hounkonnou et al., and generalises all approximate solutions published in the literature. All the higher-order solutions of the Kerr effect relaxation obtained, for example, by Kalmykov et al. [5] are simply some approximations of the successive convergents, up to the third order, of (2.44). These are well characterised in [6].

Let us define

$$\Delta n_r(s')=\frac{B\tilde{\Phi}(s')}{\frac{E^2}{15}\left(\frac{\Delta\alpha}{k_BT}+\frac{\mu^2}{(k_BT)^2}\right)}. \tag{2.45}$$

The characteristic times $\tau^{(i)}$, corresponding to the ith convergent of (2.44), can be calculated using:

$$\tau^{(i)}=\frac{1}{B}\Delta n_r^{(i)}(0). \tag{2.46}$$

Note that on replacing s' by $i\omega'$ ($\omega'=\frac{\omega}{B}$) in the *zero*th convergent to get the frequency picture, we obtain

$$\Delta n_r^{(0)}(\omega)=\frac{B\tau_{D2}}{1+i\omega\tau_{D2}}. \tag{2.47}$$

This is the rotational diffusion limit [5, 6, 10], with relaxation time

$$\tau^{(o)}=\tau_{D2}\equiv\frac{\zeta}{6k_BT}. \tag{2.48}$$

The first convergent,

$$\Delta n_r^{(1)}(\omega)=\frac{(i\omega+B)\tau_{D2}}{1+i\omega\tau_{D2}-(\frac{I\omega^2}{6k_BT})} \tag{2.49}$$

gives the same characteristic time as that obtained for $\Delta n_r^{(0)}(\omega)$. The second convergent gives

$$\tau^{(2)} = (1 + 5\gamma)\tau_{D2}. \tag{2.50}$$

This result coincides precisely with those obtained by Kalmykov et al. [5], Hounkonnou et al. [6], Burshtein and Temkin [11]. The third convergent gives

$$\tau^{(3)} = (1 + 5\gamma - \frac{40}{3}\gamma^2)\tau_{D2}. \tag{2.51}$$

For small γ, that is equivalent to small inertia and/or large friction, $\tau^{(3)} \to \tau^{(2)}$.

A more relevant form for the quantity $\Delta n_r(\omega)$ is its representation in the complex plane $\Delta n_r(\omega) = \Delta n_r'(\omega) - i\Delta n_r''(\omega)$. The real part is related to the dispersion factor while the imaginary part accounts for absorption.

Figure 2.1 shows the frequency dependence of the real parts of the first three convergents of $\Delta n_r(\omega)$. Note that all curves tend asymptotically to zero. Figure 2.2 shows the evolution of the loss factor $\Delta n_r''(\omega)$.

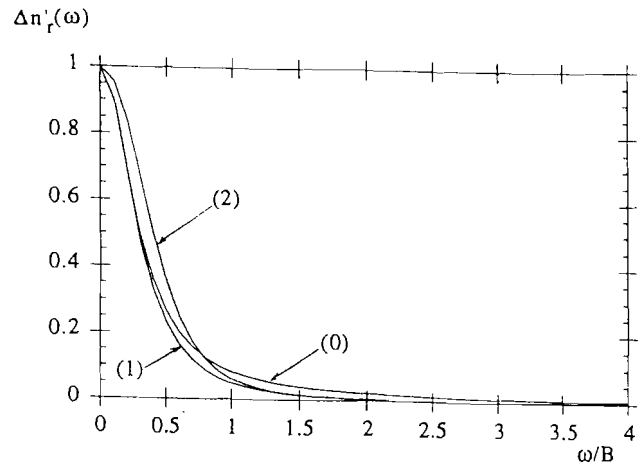

Figure 2.1: Normalised dispersion coefficient $\Delta n_r'(\omega)$ plots against the reduced frequency ω/B for Debye diffusion limit (0), the first (1) and the second (2) convergents in the classical Brownian limit for $\gamma = 0.05$.

2.3.3 The rotating wave approximation (RWA) limit

With the replacement of $\hat{K}$ by $\hat{K}^\natural$ for weak coupling [1] as was pointed out in chapter 1, we can ignore all off diagonal terms in Eqs.(2.12) and (2.14). We assume that ω_D is very large compared to both ω_l and ω_{mean} though the latter may attain relatively high values. All terms like $\varphi_{l\pm1,l\pm1}$, $\varphi_{l\pm1,l+2\pm1}$ and all coupling terms are ignored in the master equations ((2.12) and (2.14)) which now read:

$$(\frac{\partial}{\partial t} + \Gamma_l)\varphi_{l,l}(t) = 0 \tag{2.52}$$

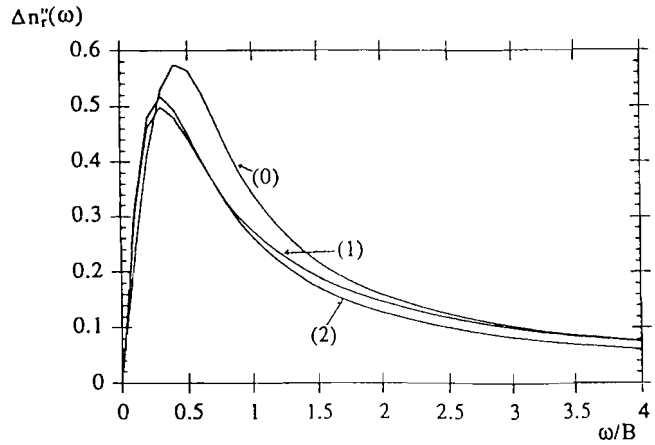

Figure 2.2: Normalised loss factor $\Delta n_r''(\omega)$ plots against the reduced frequency ω/B for Debye diffusion limit (0), the first (1) and the second (2) convergents in the classical Brownian limit for $\gamma = 0.05$.

and

$$\Big[\frac{\partial}{\partial t} - i\Big(\frac{\hbar}{I}(2l+3) + \Delta\omega_{l+2}\Big) + \Gamma_{l+2}\Big]\varphi_{l,l+2}(t) = 0, \tag{2.53}$$

where the positive half widths Γ and the frequency shifts $\Delta\omega$ for $\omega_l/\omega_D \to 0$ are:

$$\Gamma_l = 2B\Big[l^2(1+N(\omega_l)) + (l+1)^2 N(\omega_{l+1})\Big]\frac{1}{2l+1}, \tag{2.54}$$

$$\begin{aligned}\Gamma_{l+2} = B\Big[&l^2(1+N(\omega_l))\frac{1}{2l+1} + (l+1)^2 N(\omega_{l+1})\frac{1}{2l+1} \\ &+(l+2)^2(1+N(\omega_{l+2}))\frac{1}{2l+5} + (l+3)^2 N(\omega_{l+3})\frac{1}{2l+5}\Big]\end{aligned} \tag{2.55}$$

and

$$\begin{aligned}\Delta\omega_{l+2} = -2Ba^2(2l+3)\sum_{n=1}^{\infty}\frac{(2\pi n)^5}{[(2\pi n)^2 + a^2l^2][(2\pi n)^2 + a^2(l+1)^2]} \\ \times\frac{1}{[(2\pi n)^2 + a^2(l+2)^2][(2\pi n)^2 + a^2(l+3)^2]}\Big\{1 + \frac{a^2}{(2\pi n)^2}(l^2+3l+3)\Big\}.\end{aligned} \tag{2.56}$$

It is important to remark here that Eq.(2.52) describes the time relaxation of the diagonal elements of the quantum canonical probability density matrix element. This equation shows that under weak coupling the system remains close to the electric field imposed equilibrium for a relatively long time since each of its quantum states has a relaxation time which is inversely proportional to the friction coefficient ($\tau_{rel} \propto 1/\Gamma_l$). From the expression of Γ_l it is obvious

that high energy states relax faster than low energy ones. Observed relaxation will therefore be accounted for by low energy states. The non diagonal matrix elements relax in a similar manner but are accompanied by oscillations with frequencies that correspond to the $l \to l+2$ rotational transitions.

Eqs.(2.52) and (2.53) have solutions

$$\varphi_{l,l}(t) = \frac{E^2}{15}\Big(\frac{\Delta\alpha}{k_BT} + \frac{\mu^2}{(k_BT)^2}\Big) l(l+1)(2l+1)\exp\Big[-\frac{\hbar^2}{2Ik_BT}l(l+1)\Big] \times \frac{1}{\sum_{l'=0}^{\infty}(2l'+1)\exp\Big[\frac{-\hbar^2}{2Ik_BT}l'(l'+1)\Big]}\exp(-\Gamma_l t), \tag{2.57}$$

$$\varphi_{l,l+2}(t) = \frac{E^2}{15}\Big(\frac{\Delta\alpha}{k_BT} + \frac{\mu^2}{(k_BT)^2}\Big) \frac{(l+1)(l+2)}{(2l+3)\sum_{l'=0}^{\infty}(2l'+1)\exp\Big[-\frac{\hbar^2}{2Ik_BT}l'(l'+1)\Big]} \times \exp\Big[-\frac{\hbar^2}{2Ik_BT}l(l+1)\Big]\exp\Big[-\Gamma_{l+2}t + i(\frac{\hbar}{I}(2l+3) + \Delta\omega_{l+2})t\Big]. \tag{2.58}$$

On substituting these into Eq.(2.10) and taking the one-sided Fourier transform,

$$\tilde{\Phi}(\omega) = \int_0^{\infty} dt e^{-i\omega t}\Phi(t), \tag{2.59}$$

we get the frequency picture of the Kerr function

$$\tilde{\Phi}(\omega) = \tilde{\Phi}'(\omega) - i\tilde{\Phi}''(\omega), \tag{2.60}$$

where

$$\begin{aligned}\tilde{\Phi}'(\omega') &= \frac{\frac{E^2}{15B}(\frac{\Delta\alpha}{k_BT} + \frac{\mu^2}{(k_BT)^2})}{\sum_{l'=0}^{\infty}(2l'+1)\exp\Big[-\frac{\hbar^2}{Ik_BT}l'(l'+1)\Big]}\sum_{l=0}^{\infty}\frac{(l+1)exp\Big[-\frac{\hbar^2}{Ik_BT}l(l+1)\Big]}{2l+3} \\ &\times\Bigg\{\frac{l(2l+1)}{2l-1}\frac{G_l}{\omega'^2+G_l^2} + \frac{3}{2}(l+2)M_l\Bigg(\frac{1}{M_l^2+(\omega'-\frac{\hbar}{IB}(2l+3)-W_l)^2} \\ &+\frac{1}{M_l^2+(\omega'+\frac{\hbar}{IB}(2l+3)+W_l)^2}\Bigg)\Bigg\}\end{aligned} \tag{2.61}$$

and

$$\begin{aligned}\tilde{\Phi}''(\omega') &= \frac{\frac{E^2}{15B}(\frac{\Delta\alpha}{k_BT} + \frac{\mu^2}{(k_BT)^2})}{\sum_{l'=0}^{\infty}(2l'+1)exp\Big[-\frac{\hbar^2}{Ik_BT}l'(l'+1)\Big]}\sum_{l=0}^{\infty}\frac{(l+1)exp\Big[-\frac{\hbar^2}{Ik_BT}l(l+1)\Big]}{2l+3} \\ &\times\Bigg\{\frac{l(2l+1)}{2l-1}\frac{\omega'}{\omega'^2+G_l^2} + \frac{3}{2}(l+2)\Bigg(\frac{\omega'-\frac{\hbar}{IB}(2l+3)-W_l}{M_l^2+(\omega'-\frac{\hbar}{IB}(2l+3)-W_l)^2} \\ &+\frac{\omega'+\frac{\hbar}{IB}(2l+3)+W_l}{M_l^2+(\omega'+\frac{\hbar}{IB}(2l+3)+W_l)^2}\Bigg)\Bigg\},\end{aligned} \tag{2.62}$$

with $\omega' = \omega/B$, $G_l = \Gamma_l/B$, $M_l = \Gamma_{l+2}/B$ and $W_l = \Delta\omega_{l+2}/B$.

The spectral function $\Delta n_r(\omega)$ is deduced from Eq.(2.7) as:

$$\Delta n_r(\omega) = \Delta n_r'(\omega') - i\Delta n_r''(\omega'), \tag{2.63}$$

where

$$\begin{aligned}\Delta n_r'(\omega') &= \frac{\hbar^2}{2Ik_BT}\sum_{l=0}^{\infty}\frac{(l+1)\exp\left[-\frac{\hbar^2}{Ik_BT}l(l+1)\right]}{2l+3}\left\{\frac{l(2l+1)}{2l-1}\frac{\omega'^2}{\omega'^2+G_l^2}\right.\\ &+\frac{3}{2}(l+2)\left(2+\frac{\omega'\left(\omega'-\frac{\hbar}{IB}(2l+3)-W_l\right)}{M_l^2+(\omega'-\frac{\hbar}{IB}(2l+3)-W_l)^2}\right.\\ &\left.\left.+\frac{\omega'\left(\omega'+\frac{\hbar}{IB}(2l+3)+W_l\right)}{M_l^2+(\omega'+\frac{\hbar}{IB}(2l+3)+W_l)^2}\right)\right\}\end{aligned} \tag{2.64}$$

and

$$\begin{aligned}\Delta n_r''(\omega') &= \frac{\hbar^2}{2Ik_BT}\sum_{l=0}^{\infty}\frac{(l+1)exp[-\frac{\hbar^2}{Ik_BT}l(l+1)]}{2l+3}\left\{\frac{l(2l+1)}{2l-1}\frac{G_l\omega'}{\omega'^2+G_l^2}\right.\\ &+\frac{3}{2}(l+2)\left(\frac{M_l\omega'}{M_l^2+(\omega'-\frac{\hbar}{IB}(2l+3)-W_l)^2}\right.\\ &\left.\left.+\frac{M_l\omega'}{M_l^2+(\omega'+\frac{\hbar}{IB}(2l+3)+W_l)^2}\right)\right\}.\end{aligned} \tag{2.65}$$

We have described a model Hamiltonian of a system of polar, linear, rigid rotators in a bath of non polar harmonic oscillators. Quantal equations are given for well defined matrix elements that have been used to calculate the Kerr function. We have recovered the classical Brownian limit developed by many workers [5, 6, 7]. A quantal expression for the Kerr function (Eq.(2.60)) which is valid for weak coupling (van Hove limit) [12, 13], has been given. It is the Van Vleck Weisskopf line form for the Kerr function obtained via a mathematical theorem by E. B. Davies for the master equation in the interaction picture. In this limit, we ignore all "off diagonal" terms in the equations governing the evolution of the matrix elements. Neilsen and Gordon [14] concluded from their impact calculations on rotational line broadening of HCl by argon, that off diagonal elements of the $\sigma - matrix$ have little influence on the spectral shape for low densities (densities lower than 1500 amagats).

The exact Kerr effect corresponding to the Classical Brownian limit is given by the continued fraction in Eq.(2.44). The convergence of this fraction is governed by the parameter $\gamma = (Ik_BT/\zeta^2)$. This convergence is assured for small γ, that is, for small inertia and/or large friction. The different convergents of Eq.(2.44) can, therefore, only be applicable to light rotators in dense bath media. This means that collisions between the rotators and the bath oscillators are frequent and we observe continuous absorption/dispersion spectra as seen in Figures 2.1 and 2.2. The relaxation time, being the time over which an initial polarisation decays in zero field, must increase with increasing collision frequencies since collisions hinder the drift motion of dipoles which is the agency causing changes in polarisation. The characteristic frequency $B = \zeta/I$, is an increasing function of density and pressure [15] of the host bath. It depends also on the rotator. For rotators with characteristics comparable with those of the

bath, collisions are likely to involve large exchanges of energies, for example, of the order of k_BT.

For large inertia and /or small friction, Eq.(2.44) becomes unsuitable for the analysis of the Kerr effect relaxation. For weak coupling (small ς), we expect that collisions be less frequent and that the system becomes strongly uncorrelated. This should lead to absorption/dispersion spectra characterised by well defined line shapes.

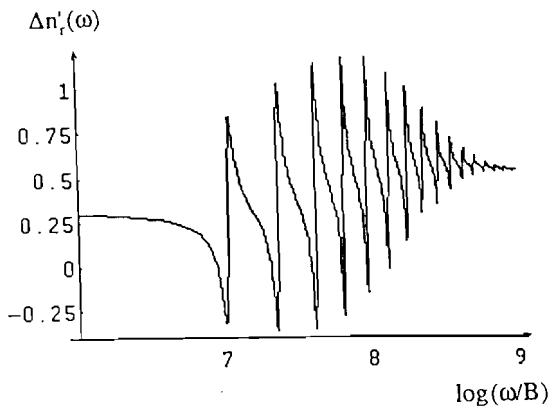

Figure 2.3: Normalised dispersion line-form $\Delta n'_r(\omega)$ against the Neperian logarithm of the reduced frequency $\ln(\omega/B)$ in the van Hove limit for $B/\omega_{mean} = 0.001$, and $\hbar^2/(Ik_BT) = 0.05$.

Figures 2.3 and 2.4 show the frequency dependence of the real and the imaginary parts of the quantity $\Delta n_r(\omega)$, respectively. These curves are obtained for the particular values of the parameters $a = (\hbar^2/Ik_BT) = 0.05$ and $B/\left(k_BT/I\right)^{0.5} = 0.001$. All these curves qualitatively well reproduce the absorption and dispersion behaviours of fluids exhibiting quantum effects as depicted by experiments [16]. The latter portray absorption/dispersion resonance lines at well defined frequencies. For large frequencies ($\nu > 10^{14}Hz$), as seen on the graphs, all resonance phenomena disappear giving rise to zero absorption, whereas dispersion tends asymptotically to a constant nonzero value. For low frequencies ($\nu < 10^{11}Hz$), resonances are absent but start appearing for frequencies above $10^{11}Hz$ and become populous in the range $10^{11}Hz < \nu < 10^{14}Hz$. We can note that the classical limit gives only one of these absorption lines and that the resonances observed are largely due to low energy rotators ($l < 10$). It is also important to note that the particular values affixed to the parameters of the model are those of HCl at temperatures between 150K and 300K. Frenkel [16] experimented that for HCl (0.06 amagat) at about 180K in Xe (1.05 amagat), absorption lines appear in the range $10cm^{-1} \leq 1/\lambda \leq 300cm^{-1}$. Our approach gives practically the same range with identical line positions.

These results confirm all deductions made using a similar approach on the electric susceptibility in [1]. Our results and those of the latter paper are, thus, in good agreement with experimental results [14, 16]. The coherency between theory and the experiments acts as a stimulant to further investigations of quantum effects on dielectric properties of polar fluids in

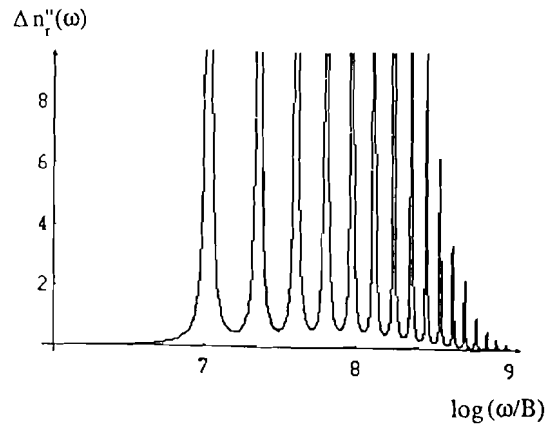

Figure 2.4: Normalised absorption (loss factor) line-form $\Delta n_r''(\omega)$ against the Neperian logarithm of the reduced frequency $\ln(\omega/B)$ in the van Hove limit for $B/\omega_{mean} = 0.001$, and $\hbar^2/(Ik_BT) = 0.05$.

non-polar thermalised media.

2.4 Energy balance equation and Entropy Calculation

In the absence of the field, there is no external work on the system and the internal energy change of the rotator is equal to the heat change. The energy balance equation is thus

$$\frac{d}{dt}U = \frac{d}{dt}Q, \tag{2.66}$$

where

$$U(t) = \sum_{l=0}^{\infty}\sum_{m=-l}^{l} < l,m|H_S\hat{\rho}_S(t)|l,m > . \tag{2.67}$$

The master equation then gives

$$\frac{d}{dt}Q = 2B[k_BT - U(t)]. \tag{2.68}$$

$2B$ is the rate at which heat is transferred from the bath to the rotator.

In the presence of the field

$$\frac{d}{dt}U = \frac{d}{dt}Q + \frac{d}{dt}W, \tag{2.69}$$

where

$$\frac{d}{dt}W = \frac{d}{dt}\sum_{l=0}^{\infty}\sum_{m=-l}^{l} < l,m|\hat{H}_E\hat{\rho}_S(t)|l,m > . \tag{2.70}$$

Note that

$$\sum_{l=0}^{\infty}\sum_{m=-l}^{l} < l,m|\hat{H}_E\hat{\rho}_S(t)|l,m >= -E\chi(t) - \frac{\Delta\alpha}{3}E^2\Phi(t) - \frac{\alpha_{\|}+2\alpha_{\perp}}{6}E^2, \tag{2.71}$$

where $\chi(t) = \langle\mu_E\rangle$ and $\Phi(t)$ is the Kerr effect function. In the case of a dc field, the energy balance equation becomes

$$\frac{d}{dt}Q = 2B[k_BT - U(t)] - E\frac{d}{dt}\chi(t) - \frac{\Delta\alpha}{3}E^2\frac{d}{dt}\Phi(t). \tag{2.72}$$

These results are identical to those previously obtained [45] via the Fokker-Planck equation. Q is the heat transfered to the rotator from the host bath and the work done by the electric field. In the case where the electric field is applied in the far past and removed at $t = 0$, $\chi(t)$ and $\Phi(t)$ are exponential decreasing functions of time, decreasing initially rapidly and tending to zero values for large times. Hence, the rate of heat transfer is initially high but reduces to the bath term at the equilibrium state.

We now proceed to analyse the evolution of the entropy from when the system is in equilibrium in the presence of an electric field till when the thermal equilibrium in the absence of the field is attained. In this analysis, we consider that the external electric field is so weak that the system is not far from the thermal equilibrium state. We, therefore, suppose $\hat{\rho}_S(t)$ to be of the form [17]:

$$\hat{\rho}_S(t) = \hat{\rho}^{eq}_{S\infty}(\hat{I} + \hat{g}(t)). \tag{2.73}$$

where $\hat{\rho}^{eq}_{S\infty}$ is the thermal equilibrium probability density operator in zero field condition. The normalisation condition on $\hat{\rho}_S(t)$ requires that $Tr_S\,(\hat{\rho}^{eq}_{S\infty}\hat{g}(t)) = 0$. The initial condition on $\hat{\rho}_S(t)$ is given in Eq.(2.4).

The Boltzmann entropy formula.

$$S(t) = -k_B < \hat{\rho}_S(t)\ln\hat{\rho}_S(t) > \tag{2.74}$$

yields, to first order in $\hat{g}(t)$,

$$S(t) = S_\infty + k_B\sum_l(\beta E_l - 1 + \ln Z_\infty)G_{l,l}(t), \tag{2.75}$$

where

$$Z_\infty = \sum_l\sum_{m=-l}^{l} < l,m \mid \exp -\beta\hat{H}_S \mid l,m >= \frac{2Ik_BT}{\hbar^2}, \tag{2.76}$$

$$S_\infty = -k_B\sum_l\sum_{m=-l}^{l} < l,m \mid \hat{\rho}^{eq}_{S\infty}\ln\hat{\rho}^{eq}_{S\infty} \mid l,m >= k_B\Big(1 + \ln(\frac{2Ik_BT}{\hbar^2})\Big), \tag{2.77}$$

$$G_{l,l}(t) = \sum_{m=-l}^{l} < l,m \mid \hat{\rho}^{eq}_{S\infty}\hat{g}(t) \mid l,m >= \sum_{m=-l}^{l}\rho^{eq}_{l,l}g^m_{l,l}(t). \tag{2.78}$$

The density operator $\hat{\rho}_S(t)$ must obey the Master Equation (1.32), in particular $\hat{\rho}^{eq}_{S\infty}$ verifies it since it is an asymptotic solution. $\hat{\rho}^{eq}_{S\infty}\hat{g}(t)$ is governed by the equation

$$\hat{\rho}^{eq}_{S\infty}\frac{\partial}{\partial t}\hat{g}(t) = -\hat{K}\Big(\hat{\rho}^{eq}_{S\infty}\hat{g}(t)\Big). \tag{2.79}$$

On multiplying through this by $\sum_{m=-l}^{l} \mid l,m >< l,m \mid$ and taking trace, we obtain

$$\frac{\partial}{\partial t}G_{l,l}(t) = -2BRe\Big[(A_l l^2 + B_{l+1}(l+1)^2)\frac{G_{l,l}(t)}{2l+1} - A_{l+1}\frac{(l+1)^2}{2l+3} \times G_{l+1,l+1}(t) - B_l\frac{l^2}{2l-1}G_{l-1,l-1}(t)(1-\delta_{l0})\Big]. \quad (2.80)$$

It is easily seen from Eq.(2.4) that the initial condition on $G_{l,l}(t)$ is

$$G_{l,l}(t=0) = \frac{\hbar^2}{36Ik_BT}\Big(\frac{\mu E}{k_BT}\Big)^2\frac{e^{-\beta E_l}}{Z_\infty}(2l+1)(\beta E_l - 1). \quad (2.81)$$

The entropy therefore relaxes from the initial equilibrium value

$$S(0) = k_B\Big[1 + \ln(\frac{2Ik_BT}{\hbar^2}) + \frac{\hbar^2}{36Ik_BT}\Big(\frac{\mu E}{k_BT}\Big)^2\Big]. \quad (2.82)$$

We perform the change of function

$$G_{l,l}(t) = \frac{\hbar^2}{36Ik_BT}\Big(\frac{\mu E}{k_BT}\Big)^2\frac{e^{-\beta E_l}}{Z_\infty}(2l+1)Y_l(t), \quad (2.83)$$

where $Y_l(t)$ has initial condition $Y_l(0) = \beta E_l - 1$. Then, the continuum approximations lead to

$$\frac{\partial}{\partial \tau}Y(x,\tau) = 2\Big[xY_{xx}(x,\tau) + (1-x)Y_x(x,\tau) + \frac{1}{2}Y(x,\tau)\Big], \quad (2.84)$$

where $Y(x,\tau)$ is the continuum analog of $Y_l(\tau)$). Solutions are sought, as a linear combination of the Laguerre polynomials

$$Y(x,\tau) = \sum_{j=0}^{\infty} y_j(\tau)L_j(x). \quad (2.85)$$

The initial condition on $G_l(t)$ leads to

$$Y(x,\tau) = y_1(\tau)L_1(x). \quad (2.86)$$

with $y_1(t) = -e^{-Bt}$. We recover the expression for the entropy

$$S(t) = k_B\Big[1 + \ln(\frac{2Ik_BT}{\hbar^2}) + \frac{\hbar^2}{36Ik_BT}\Big(\frac{\mu E}{k_BT}\Big)^2 e^{-Bt}\Big]. \quad (2.87)$$

Remark that the equilibrium state in the presence of the external field is more stable than that in its absence. This could be predicted, since an external electric field will favour statistical reorientation of dipole moments in its direction, thus increasing the order in the whole system.

Bibliography

[1] P. Navez and M. N. Hounkonnou, *J. Phys. A: Math. Gen.* **28**: 6345, 1995

[2] J. T. Titantah, *Mémoire de Diplôme d'Etudes Approfondies (DEA)*, IMSP, 1995

[3] J. T. Titantah and M. N. Hounkonnou, *J. Phys. A: Math. Gen.* **30**: 6327, 1997

[4] I. S. Gradshteyn and I. M. Rizhik, *Table of Integrals, Series, and Products*, Academic Press New York and London, 1965

[5] Y. P. Kalmykov, *J. Chem. Phys.* **95**: 9142, 1991

[6] M. N. Hounkonnou, A. Ronveaux and P. Navez, *J. Phys. A: Math. Gen.* **27**: 6635, 1994

[7] P. Navez and M. N. Hounkonnou, *J. Phys. A: Math. Gen.* **27**: 6657, 1994

[8] M. Abramowitz and I. A. Stegun, *Handbook of Mathematical functions* (New York: Dover), 1972

[9] R. A. Sack, *Proc. Phys. Soc.* **B70**: 402, **B70**: 414, 1957

[10] P. Debye, *Polar Molecules Chemical Catalog*, New York, 1929

[11] A. I. Burshstein and S. I. Temkin, *Spectroscopy of Molecular Rotation in Gases and Liquids* (Novosibirsk: Nauka): 53, 1982

[12] L. Van Hove, *Physica* **21**: 517, 1955

[13] L. Van Hove, *Physica* **23**: 441, 1957

[14] T. J. Balle, E. J. Campbell, M. R. Keenan and W. H. Flygare, *J. Chem. Phys.* **72**: 922, 1980

[15] E. P. Gross, *J. Chem. Phys.* **23** (8): 1415, 1955

[16] D. Frenkel, *Rotational relaxation of linear molecules in dense noble gases* Ph.D thesis, Amstradam, 1977

[17] R. Kubo, M. Toda and N. Hashitsume, *Statistical Physics II, Nonequilibrium Statistical Mechanics* (Springer-Verlag, Berlin), 1985

Chapter 3

Dielectric property dynamics induced by a dc field

Summary

With the aid of the master equation derived in chapter 1, which for commodity purposes will henceforth be referred to as the Hounkonnou-Navez (HN) master equation, the dielectric properties of a polar fluid in a constant electric field regime is analysed. Master equations are given for well-defined matrix elements $\sigma_{l,l+1}(t)$, $\varphi_{l,l}(t)$ and $\eta_{l,l+2}(t)$. While the electric susceptibility describes low energy rotational transitions, the Kerr effect, involves both low and high energy transitions. For the quantum electric susceptibility, the linear response limit is considered while the Kerr effect accounts for higher order electric field effects. The classical Brownian limit of the quantum equations recover most results published so far. The convergence of the classical results (which are in the form of continued fractions) are guaranteed for large friction and/or small inertia; and low frequencies. Quantum expressions, valid for weak coupling (small friction and/or large inertia) are obtained via a rigorous mathematical theorem on weak coupling. They are the an-Vleck-Weisskopf line forms for the electric susceptibility and the Kerr function. More importantly, explicit expressions are given for the frequency shifts and line widths. We demonstrate the transition from quantum to classical effects as the the friction/inertia parameter (ζ/I) increases. A temperature dependent cross-over is found.

3.1 Introduction

In chapter 2, we presented the analysis of the Kerr effect relaxation of a system of polar linear rigid rotators in interaction with a bath of harmonic oscillators [1]. This, we did using the master equation derived by us [2] for quantum systems. In this chapter [3], we make use of this equation to calculate the electric susceptibility and the Kerr function for the case where a constant unidirectional electric field is suddenly applied to the system. This problem has been tackled classically by Morita and Watanabe [4], using the rotational Smoluchowski equation. Kalmykov and Titov [5] presented a semi-classical approach based on the **J** diffusion model. Their analysis was limited to the electric susceptibility calculation. In the same paper, they used the ACF method on the Van Vleck-Weisskopf model. This model supposes that, after every

collision, the molecule can be found in any possible state with the probability proportional to the Boltzmann distribution corresponding to the instantaneous Hamiltonian of the system. Their results could be recovered from those obtained by us in this chapter for the weak coupling or the rotating wave approximation limit (RWA). These classical theories together with our recent works [6, 7] effectively describe the high density spectra of polar fluids.

This chapter is arranged as follows. In section 2, the Master equation governing the time evolution of the rotator probability density operator is given. In section 3, master equations are given for some well defined matrix elements. In section 4, the electric susceptibility and the Kerr function are calculated for the classical Brownian limit. In section 5, the RWA limit is considered. In section 6, we end with discussions.

3.2 The field dependent Master equation

The evolution of the rotator reduced probability density operator in the presence of an external electric field $\hat{\rho}_S(t)$ is governed by the HN master equation [1, 2]

$$\frac{\partial \hat{\rho}_S(t)}{\partial t} + \frac{i}{\hbar}\Big[\hat{H}_S, \hat{\rho}_S(t)\Big] + \hat{K}\hat{\rho}_S(t) = -\frac{i}{\hbar}\Big[\hat{H}_E, \hat{\rho}_S(t)\Big], \tag{3.1}$$

with the collision term $\hat{K}\hat{\rho}_S(t)$ explicitly given in chapter 1. This equation is the same as those used in [1, 2] but for the fact that there is an explicit presence of the electric field. This, because, we are interested in the investigation of how a thermally equilibrated system in the the absence of any stress will relax to the new equilibrium in the presence of a stress. In other words, is the relaxation following the sudden application of a dc field explained by the same mechanism as the relaxation following its sudden removal?

An appropriate initial condition for the above master equation is the canonical probability density operator of the free rotator in the absence of the electric field.

If $Q(t)$ is the heat gained by the rotator from the bath and as a result of the work done by the electric field on the dipole through the interaction with the dipole moment μ, we write the energy balance equation

$$\frac{d}{dt}Q(t) = \frac{d}{dt}U(t) + \frac{d}{dt}W(t), \tag{3.2}$$

where $U(t)$, the internal energy of the rotator and $W(t)$, the work done by the field are defined as:

$$U(t) =< \hat{H}_S\hat{\rho}_S(t) > \text{ and } W(t) =< \hat{H}_E\hat{\rho}_S(t) >, \tag{3.3}$$

with the angle brackets $< ... >$ denoting ensemble averaging. On using the HN master equation (3.1), we get, for a constant field,

$$\frac{d}{dt}Q(t) = 2B(k_BT - U(t)) + \frac{4\mu E_c}{3}\sum_{l=0}^{\infty}\frac{\hbar}{I}(l+1)^2\frac{e^{\beta E_l}}{Z}\mathcal{I}m\sigma_{l,l+1}(t) \tag{3.4}$$

to second order in electric field strength. $\mathcal{I}m$ denotes the imaginary part, $B = (\zeta/I)$ is the rotator-bath characteristic frequency. To get this equation, we made use of the change of function,

$$\sum_{m=-l}^{l} C(l+1,m)\rho^m_{l,l+1}(t) = \sum_{m=-l}^{l} C(l+1,m)^2\sigma_{l,l+1}(t)\frac{e^{-\beta E_l}}{Z}, \tag{3.5}$$

where Z is the free rotator partition function; $E_l = (\hbar^2/2I)l(l+1)$ is the rotator rotational kinetic energy and $C(l,m) = \sqrt{\frac{(l-m)(l+m)}{(2l-1)(2l+1)}}$. $\sigma_{l,l+1}(t)$ is independent of m. The matrix elements $\rho^m_{l,l'}(t)$ are defined as

$$\rho^m_{l,l'}(t) =< l,m \mid \hat{\rho}_S(t) \mid l',m > . \tag{3.6}$$

Remark that in the absence of the field $Q = U$ and the internal energy of the rotator tends asymptotically to that of the thermal bath. The energy balance equation is very important as it describes well the process of energy transfer from the bath to the rotator or vice versa. The matrix elements $\sigma_{l,l+1}(t)$ determine explicitly the electric susceptibility; the latter, thus, plays a vital role in the energy transfer processes.

3.3 The Master equations for matrix elements

We want to calculate the electric polarisation $P(t)$ defined as the ensemble average of the component of the rotator dipole moment parallel to the applied electric field which we assume directed along the z-axis of the laboratory frame [6, 7, 8, 9]

$$P(t) = \sum_{l=0}^{\infty} \sum_{m=-l}^{l} < l,m \mid \hat{\mu}_z \hat{\rho}_S(t) \mid l,m >, \tag{3.7}$$

where $\hat{\mu}_z = \mu \hat{u}_z$, with $\hat{u}_z$ the z component of the rotator orientation operator. On using the spherical harmonic representation of $\hat{u}_z$ in Eq.(1.26), we get

$$P(t) = \frac{2\mu}{3} \sum_{l=0}^{\infty} (l+1) \frac{e^{-\beta E_l}}{Z} \Re \sigma_{l,l+1}(t), \tag{3.8}$$

where $\Re$ denotes the real part.

The Kerr function is the ensemble average of the second order Legendre polynomial $P_2(\cos\beta)$ [6, 7, 8, 9]

$$\Phi(t) = \frac{1}{2} \sum_{l=0}^{\infty} \sum_{m=-l}^{l} < l,m \mid (3\hat{u}_z^2 - 1)\hat{\rho}_S(t) \mid l,m > . \tag{3.9}$$

On defining matrix elements (differently from those in chapter 2) $\varphi_{l,l}$ and $\eta_{l,l+2}$ through

$$\sum_{m=-l}^{l} \frac{l(l+1) - 3m^2}{(2l-1)(2l+3)} < l,m \mid \hat{\rho}_S(t) \mid l,m > = \frac{2}{15} \frac{e^{-\beta E_l}}{Z} \frac{l(l+1)(2l+1)}{(2l-1)2l+3)} \varphi_{l,l}(t) \tag{3.10}$$

and

$$\sum_{m=-l}^{l} \left[\frac{\left((l+1)^2 - m^2\right)\left((l+2)^2 - m^2\right)}{(2l+1)(2l+3)^2(2l+5)} \right] < l,m \mid \hat{\rho}_S(t) \mid l+2,m >= \sum_{m=-l}^{l} \frac{\left((l+1)^2 - m^2\right)\left((l+2)^2 - m^2\right)}{(2l+1)(2l+3)^2(2l+5)} \frac{e^{-\beta E_l}}{Z} \eta_{l,l+2}(t), \tag{3.11}$$

after using the spherical harmonic representation of u_z (Eq.(1.26)) we get,

$$\Phi(t) = \frac{2}{15}\sum_{l=0}^{\infty}\frac{e^{-\beta E_l}}{Z}\frac{(l+1)}{(2l+3)}\left\{\frac{l(2l+1)}{(2l-1)}\varphi_{l,l}(t) + 3(l+2)\Re\eta_{l,l+2}(t)\right\}. \tag{3.12}$$

We now give the master equations verified by the different matrix elements $\sigma_{l,l+1}$, $\varphi_{l,l}(t)$ and $\eta_{l,l+2}(t)$.

To get the equation verified by $\sigma_{l,l+1}$, we multiply through the HN master equation (3.1) from the left by $\sum_{m=-l}^{l} C(l+1,m)|l+1,m><l,m|$ and take trace. The use of properties similar, in some way, to that proved in appendix A.2 leads to

$$\begin{aligned}
&\sum_{m=-l}^{l}\frac{1}{Z}\Big[C(l+1,m)^2 e^{-\beta E_l}\Big(\frac{\partial}{\partial t} - \frac{i\hbar}{I}(l+1)\Big)\sigma_{l,l+1}(t)\\
&+B\Big\{C(l+1,m)^2 e^{-\beta E_l}\Big[(A_l^* l^2 + B_{l+1}(l+1)^2)\frac{1}{2l+1}\\
&+(A_{l+1}(l+1)^2 + B_{l+2}^*(l+2)^2)\frac{1}{2l+3}\Big]\sigma_{l,l+1}(t)\\
&-C(l,m)^2 e^{-\beta E_{l-1}}\frac{l+1}{2l+1}\Big[(B_l l + (l+1)B_{l+1}^*\Big]\sigma_{l-1,l}(t)(1-\delta_{lo})\\
&-C(l+2,m)^2 e^{-\beta E_{l+1}}\frac{l+1}{2l+3}\Big[A_{l+1}^*(l+1) + A_{l+2}(l+2)\Big]\sigma_{l+1,l+2}(t)\\
&-C(l+1,m)^2\frac{l+1}{(2l+1)(2l+3)}\Big[A_{l+1}^*(l+1) + B_{l+1}^*(l+1)\Big]\sigma_{l,l+1}^*(t)\Big\}\Big]\\
&= i\sum_{m=-l}^{l}\Big[\frac{\mu E(t)}{\hbar}\Big\{C(l+1,m)^2(\rho_{l+1,l+1}^m(t) - \rho_{l,l}^m(t))\\
&+C(l,m)^2 C(l+1,m)^2\frac{e^{-\beta E_{l-1}}}{Z}\eta_{l-1,l+1}(t)(1-\delta_{l,0})\\
&-C(l+1,m)^2 C(l+2,m)^2\frac{e^{-\beta E_l}}{Z}\eta_{l,l+2}(t)\Big\}\\
&+\frac{\Delta\alpha E(t)^2}{2\hbar}\Big\{\Big[C(l,m)^2 - C(l+2,m)^2\Big]C(l+1,m)^2\frac{e^{-\beta E_l}}{Z}\sigma_{l,l+1}(t)\\
&-C(l,m)^2 C(l+1,m)^2\frac{e^{-\beta E_{l-1}}}{Z}\sigma_{l-1,l}(t)(1-\delta_{l,0})\\
&+C(l-1,m)^2 C(l,m)^2 C(l+1,m)^2\frac{e^{-\beta E_{l-2}}}{Z}\lambda_{l-2,l+1}(t)(1-\delta_{l,0})(1-\delta_{l,1})\\
&-C(l+1,m)^2 C(l+2,m)^2 C(l+3,m)^2\frac{e^{-\beta E_l}}{Z}\lambda_{l,l+3}(t)\\
&+C(l+1,m)^2 C(l+2,m)^2\frac{e^{-\beta E_{l+1}}}{Z}\sigma_{l+1,l+2}(t)\Big\}\Big].
\end{aligned} \tag{3.13}$$

The equation for $\varphi_{l,l}$ is obtained by multiplying through the master equation by $\Big\{(l(l+1)-$

$3m^2)/\left[(2l-1)(2l+3)\right\}|l,m><l,m|\Big]$ and taking trace to get

$$\sum_{m=-l}^{l}\Bigg[\frac{\partial}{\partial t}\frac{l(l+1)-3m^2}{(2l-1)(2l+3)}\rho^m_{l,l}(t)$$
$$+2BRe\Bigg\{\frac{\left[A_l l^2+B_{l+1}(l+1)^2\right]}{2l+1}\frac{l(l+1)-3m^2}{(2l-)(2l+3)}\rho^m_{l,l}(t)$$
$$-A_{l+1}l\frac{(l+1)(l+2)-3m^2}{(2l+1)(2l+3)^2}\rho^m_{l+1,l+1}(t)$$
$$-B_l l\frac{l(l-1)-3m^2}{(2l-1)^2(2l+3)}\rho^m_{l-1,l-1}(t)(1-\delta_{l0})$$
$$-3\frac{\left[B_l l+A_{l+1}(l+1)\right]}{(2l+1)(2l+3)}C(l,m)^2C(l+1,m)^2\frac{e^{-\beta E_{l-1}}}{Z}\eta_{l-1,l+1}(t)(1-\delta_{l0})\Bigg\}\Bigg]$$
$$=\frac{2}{Z}\sum_{m=-l}^{l}\frac{l(l+1)-3m^2}{(2l-1)(2l+3)}\Bigg\{\frac{\mu E(t)}{\hbar}\Big[C(l+1,m)^2e^{-\beta E_l}\mathcal{I}m\sigma_{l,l+1}(t)$$
$$-C(l,m)^2\frac{e^{-\beta E_{l-1}}}{Z}\mathcal{I}m\sigma_{l-1,l}(t)(1-\delta_{l,0})\Big]+\frac{\Delta\alpha E(t)^2}{2\hbar}$$
$$\times\Big[C(l+1,m)^2(C(l+1,m)^2e^{-\beta E_l}\mathcal{I}m\eta_{l,l+2}(t)$$
$$-C(l-1,m)^2(C(l,m)^2e^{-\beta E_{l-2}}\mathcal{I}m\eta_{l-2,l}(t)(1-\delta_{l,0})(1-\delta_{l,1})\Big]\Bigg\}. \tag{3.14}$$

$\mathcal{I}m$ denotes the imaginary part.

Finally, the equation for $\eta_{l,l+2}$ is got by multiplying through the master equation (3.1) from the left by $\sum_{m=-l}^{l}C(l+1,m)C(l+2,m)\mid l+2,m><l,m\mid$ and taking trace:

$$\sum_{m=-l}^{l}\Bigg[C(l+1,m)^2C(l+2,m)^2\frac{e^{-\beta E_l}}{Z}[\frac{\partial}{\partial t}-\frac{i\hbar}{I}(2l+3)]\eta_{l,l+2}(t)$$
$$+B\Bigg\{C(l+1,m)^2C(l+2,m)^2\frac{e^{-\beta E_l}}{Z}\Big\{\left[A^*_l l^2+B_{l+1}(l+1)^2\right]\frac{1}{2l+1}$$
$$+\left[A_{l+2}(l+2)^2+B^*_{l+3}(l+3)^2\right]\frac{1}{2l+5}\Big\}\eta_{l,l+2}(t)$$
$$-\frac{l+2}{2l+3}C(l,m)^2C(l+1,m)^2\frac{e^{-\beta E_{l-1}}}{Z}\left[B_l l+B_{l+2}(l+2)\right]\eta_{l-1,l+1}(t)(1-\delta_{lo})$$
$$-C(l+2,m)^2C(l+3,m)^2\frac{e^{-\beta E_{l+1}}}{Z}\frac{l+1}{2l+3}\Big[A^*_{l+1}(l+1)$$
$$+A_{l+3}(l+3)\Big]\eta_{l+1,l+3}(t)-2\frac{\left[A^*_{l+1}(l+1)+B_{l+2}(+2)\right]}{(2l+3)^2}$$
$$\times\frac{(l+1)(l+2)-3m^2}{(2l+1)(2l+5)}\varphi_{l+1,l+1}(t)\Bigg\}\Bigg]=i\sum_{m=-l}^{l}\Bigg[\frac{\mu E(t)}{\hbar}$$
$$\times\Bigg\{C(l+1,m)^2C(l+2,m)^2\frac{e^{-\beta E_{l+1}}}{Z}\sigma_{l+1,l+2}(t)$$

$$
\begin{aligned}
&-C(l+1,m)^2C(l+2,m)^2\frac{e^{-\beta E_l}}{Z}\sigma_{l,l+1}(t)+C(l,m)^2C(l+1,m)^2C(l+2,m)^2\\
&\times\frac{e^{-\beta E_{l-1}}}{Z}\lambda_{l-1,l+2}(t)(1-\delta_{l,0})-C(l+1,m)^2C(l+2,m)^2(l+3,m)^2\frac{e^{-\beta E_l}}{Z}\lambda_{l,l+3}(t)\Big\}\\
&-\frac{\Delta\alpha E(t)^2}{2\hbar}\Big\{C(l+1,m)^2C(l+2,m)^2\Big(\rho^m_{l,l}(t)-\rho^m_{l+1,l+1}(t)\Big)\\
&-\Big[C(l,m)^2+C(l+1,m)^2-C(l+2,m)^2C(l+3,m)^2\Big]\\
&\times C(l+1,m)^2C(l+2,m)^2\frac{e^{-\beta E_l}}{Z}\eta_{l,l+2}(t)-C(l+1,m)^2C(l+2,m)^2\\
&\times\Big(C(l-1,m)^2C(l,m)^2\frac{e^{-\beta E_{l-2}}}{Z}\zeta_{l-2,l+2}(t)(1-\delta_{l,0})(1-\delta_{l,1})\\
&-C(l+3,m)^2C(l+4,m)^2\frac{e^{-\beta E_l}}{Z}\zeta_{l,l+4}(t)\Big)\Big\}\Big].
\end{aligned}
\tag{3.15}
$$

The new matrix elements $\lambda_{l,l+3}(t)$ and $\zeta_{l,l+4}(t)$ are defined through

$$
\begin{aligned}
&C(l+1,m)C(l+2,m)C(l+3,m)\,\langle l,m\mid\hat{\rho}_S(t)\mid l+3,m\rangle\\
&\qquad=\Big[C(l+1,m)C(l+2,m)C(l+3,m)\Big]^2\lambda_{l,l+3}(t),\\
&C(l+1,m)C(l+2,m)C(l+3,m)C(l+4,m)\,\langle l,m\mid\hat{\rho}_S(t)\mid l+4,m\rangle\\
&\qquad=\Big[C(l+1,m)C(l+2,m)C(l+3,m)C(l+4,m)\Big]^2\zeta_{l,l+4}(t).
\end{aligned}
\tag{3.16}
$$

The initial conditions on $\sigma_{l,l+1}(t)$, $\varphi_{l,l}(t)$ and $\eta_{l,l+2}(t)$ are

$$
\sigma_{l,l+1}(t=0)=\varphi_{l,l}(t=0)=\eta_{l,l+2}(t=0)=0. \tag{3.17}
$$

For commodity, Eqs.(3.13), (3.14) and (3.15) shall henceforth be referred to as Hounkonnou-Titantah (HT) equations for the electric susceptibility and the Kerr effect, as they will frequently be used in subsequent works. Eq.(3.13) will be referred as HT1, (3.14) as HT2 and (3.15) as HT3.

Remark that any matrix element $K_{l,l+n}$ (with $n\neq 0$) is at least an n-order electric field term. In particular, $\varphi_{l,l}(t)$ is a second order term. This follows from HT1 that the polarisation is an odd function of electric field strength $E(t)$. Thus, polarisation reverses as field reverses. On the contrary, the electric birefringence is an even function of $E(t)$. The modification in the refractive index tensor is thus, independent of the field orientation except with respect to that of the polarising field. In the analysis of the electric susceptibility, we limit ourselves to the linear response regime while the Kerr effect will be given to the second order in the electric field strength. In the $\sigma_{l,l+1}(t)$ equation (HT1), we, therefore, ignore third order terms like $E(t)\eta_{l,l+2}(t)$ and $E(t)^2\sigma_{l,l+1}(t)$; and fifth order terms like $E(t)^2\lambda_{l,l+3}(t)$ while retaining first order terms like $E(t)\rho^m_{l,l}(t)$ in which case we consider the canonical thermal equilibrium density matrix element in zero field ($\rho^m_{l,l}(t)=(\rho^m_{l,l})^{eq}=e^{-\beta E_l}/Z$). In the $\eta_{l,l+2}(t)$ (HT3) and $\varphi_{l,l}(t)$ (HT2)

equations, fourth order field terms like $E(t)^2\eta_{l,l+2}(t)$, $E(t)\lambda_{l,l+3}(t)$ and sixth order $E(t)^2\zeta_{l,l+4}(t)$ are ignored. The appropriate reduced HT equations are, thus:

i) the reduced HT1:

$$\Big(\frac{\partial}{\partial t}-\frac{i\hbar}{I}(l+1)\Big)\sigma_{l,l+1}(t)+B\Big[\Big\{\Big(A_l^*l^2+B_{l+1}(l+1)^2\Big)\frac{1}{2l+1}+(A_{l+1}(l+1)^2$$
$$+B_{l+2}^*(l+2)^2)\frac{1}{2l+3}\Big\}\sigma_{l,l+1}(t)-e^{\beta\left(E_l-E_{l-1}\right)}\frac{l}{2l+1}\Big[B_ll$$
$$+(l+1)B_{l+1}^*\Big]\sigma_{l-1,l}(t)(1-\delta_{l0})-e^{-\beta(E_{l+1}-E_l)}\frac{l+2}{2l+3}\Big[A_{l+1}^*(l+1)$$
$$+A_{l+2}(l+2)\Big]\sigma_{l+1,l+2}(t)-\frac{l+1}{(2l+1)(2l+3)}\Big[A_{l+1}^*(l+1)$$
$$+B_{l+1}^*(+1)\Big]\sigma_{l,l+1}^*(t)\Big]=-i\frac{\mu E(t)}{\hbar}\Big(1-e^{-\beta\left(E_{l+1}-E_l\right)}\Big); \tag{3.18}$$

ii) the reduced HT2:

$$\frac{\partial}{\partial t}\varphi_{l,l}(t)+2BRe\Big\{\frac{(A_ll^2+B_{l+1}(l+1)^2)}{2l+1}\varphi_{l,l}(t)-A_{l+1}(l+1)\frac{(l+2)(2l-1)}{(2l+1)^2}$$
$$\times e^{-\beta\left(E_{l+1}-E_l\right)}\varphi_{l+1,l+1}(t)-B_ll\frac{(l-1)(2l+3)}{(2l+1)^2}e^{\beta\left(E_l-E_{l-1}\right)}\varphi_{l-1,l-1}(t)(1-\delta_{l0})-$$
$$-3\frac{(B_ll+A_{l+1}(l+1))}{(2l+1)^2}e^{\beta\left(E_l-E_{l-1}\right)}\eta_{l-1,l+1}(t)(1-\delta_{l0})\Big\}=\frac{\mu E(t)}{\hbar}$$
$$\times\Big(\frac{2l-1}{2l+1}Im\sigma_{l,l+1}(t)-e^{\beta\left(E_l-E_{l-1}\right)}\frac{2l+3}{2l+1}Im\sigma_{l-1,l}(t)(1-\delta_{l,0})\Big) \tag{3.19}$$

and

iii) the reduced HT3:

$$\Big[\frac{\partial}{\partial t}-\frac{i\hbar}{I}(2l+3)\Big]\eta_{l,l+2}(t)+B\Big[\Big\{\Big[A_l^*l^2+B_{l+1}(l+1)^2\Big]\frac{1}{2l+1}+\Big[A_{l+2}(l+2)^2$$
$$+B_{l+3}^*(l+3)^2\Big]\frac{1}{2l+5}\Big\}\eta_{l,l+2}(t)-\frac{l}{2l+1}e^{\beta(E_l-E_{l-1})}$$
$$\times\Big[B_l^*l+B_{l+2}(l+2)\Big]\eta_{l-1,l+1}(t)(1-\delta_{l0})-e^{-\beta\left(E_{l+1}-E_l\right)}\frac{l+3}{2l+5}$$
$$\times\Big[A_{l+1}^*(l+1)+A_{l+3}(l+3)\Big]\eta_{l+1,l+3}(t)-\frac{2}{(2l+1)(2l+5)}$$
$$\times\Big[A_{l+1}^*(l+1)+B_{l+2}(+2)\Big]\varphi_{l+1,l+1}(t)\Big]=i\frac{\mu E(t)}{\hbar}$$
$$\times\Big(e^{-\beta\left(E_{l+1}-E_l\right)}\sigma_{l+1,l+2}(t)-\sigma_{l,l+1}(t)\Big)-i\frac{\Delta\alpha E(t)^2}{2\hbar}\Big(1-e^{-\beta\left(E_{l+2}-E_l\right)}\Big). \tag{3.20}$$

$\Delta\alpha=(\alpha_{\|}-\alpha_{\perp})$. If the reduced HT1, HT2 and HT3 equations are solved exactly, for all l and all model parameters such as temperature T, inertial effects $B=\zeta/I$ and moderate fields,

then the exact analysis of the dielectric properties of polar or polarisable fluids is accessible for a wide range of temperatures and frequencies. In the paragraph that follows, we present a low frequency analysis of this problem. This is the classical Brownian limit which is a highly explored aspect of the problem [6, 7, 8, 9].

It is important to point out here that the HT1 equation can be used as a starting point in the investigation of nonlinear effects on polarisation.

3.4 The classical Brownian limit

In the classical Brownian limit [7, 10], the bath is much faster than the rotator, in other words, the rotator frequencies $\omega_l = \hbar l/I$ are much smaller than its mean thermal agitation frequency $\omega_{mean} = \left(k_B T/I\right)^{0.5}$ which in turn is much smaller than the typical oscillator frequency ω_D. The spectrum of $\hat{H}_S$ is assumed to be continuous. These hypotheses justify the limits:

$$a = \frac{(\hbar/I)^2}{(k_B T/I)} \to 0 \text{ and } \frac{k_B T}{I\omega_D^2} \to 0 \tag{3.21}$$

and approximation

$$\frac{a}{2} l(l+1) \to x. \tag{3.22}$$

The transformation (3.22) is similar to the one used in [6, 7] on the Fokker-Planck-Kramers equation where $x = \frac{I\Omega^2}{2k_B T}$, with Ω being the angular velocity of the rotator.

On letting

$$\sigma_{l,l+1}(t) = \sigma_{1l}(t) + i(l+1)\sigma_{2l}(t), \tag{3.23}$$

$$\eta_{l,l+2}(t) = \eta_{1l}(t) + i(2l+3)\eta_{2l}(t) \tag{3.24}$$

while taking $\varphi(x,t)$, $\sigma_1(x,t)$, $\sigma_2(x,t)$, $\eta_1(x,t)$ and $\eta_2(x,t)$ as the continuum analogs of $\varphi_{l,l}(t)$, σ_{1l}, σ_{2l}, $\eta_{1l}(t)$ and $\eta_{2l}(t)$, respectively, we obtain the system of coupled partial second order differential equations:

$$\Big[\frac{\partial}{\partial\tau} - 2\Big(x\frac{\partial^2}{\partial x^2} + (1-x)\frac{\partial}{\partial x}\Big)\Big]\sigma_1(x,\tau) + 2b_2 x\sigma_2(x,\tau) = 0, \tag{3.25}$$

$$\Big[\frac{\partial}{\partial\tau} - 2\Big(x\frac{\partial^2}{\partial x^2} + (2-x)\frac{\partial}{\partial x} - \frac{1}{2}\Big)\Big]\sigma_2(x,\tau) - b_1\sigma_1(x,\tau) = -b_1\frac{\mu E(\tau)}{k_B T}, \tag{3.26}$$

$$\begin{aligned}&\Big[\frac{\partial}{\partial\tau} - 2\Big(x\frac{\partial^2}{\partial x^2} + (1-x)\frac{\partial}{\partial x}\Big)\Big]\varphi(x,\tau) + \frac{3}{2x}(\varphi(x,\tau) - \eta_1(x,\tau))\\ &= 2b_2\frac{\mu E(\tau)}{k_B T}\Big[x\frac{\partial}{\partial x} - x + 1\Big]\sigma_2(x,\tau) - 3b_2\frac{\mu E(\tau)}{k_B T}\sigma_2(x,\tau),\end{aligned} \tag{3.27}$$

$$\begin{aligned}&\Big[\frac{\partial}{\partial\tau} - 2\Big(x\frac{\partial^2}{\partial x^2} + (1-x)\frac{\partial}{\partial x}\Big)\Big]\eta_1(x,\tau) + 8b_2 x\eta_2(x,\tau) - \frac{1}{2x}(\varphi(x,\tau)\\ &-\eta_1(x,\tau)) = -2b_2\frac{\mu E(\tau)}{k_B T}\Big[x\frac{\partial}{\partial x} - x + 1\Big]\sigma_2(x,\tau) + b_2\frac{\mu E(\tau)}{k_B T}\sigma_2(x,\tau),\end{aligned} \tag{3.28}$$

$$\Big[\frac{\partial}{\partial\tau} - 2\Big(x\frac{\partial^2}{\partial x^2} + (2-x)\frac{\partial}{\partial x} - \frac{1}{2}\Big)\Big]\eta_2(x,\tau) - b_1\eta_1(x,\tau)$$
$$= \frac{b_1}{2}\frac{\mu E(\tau)}{k_B T}\Big[\frac{\partial}{\partial x} - 1\Big]\sigma_1(x,\tau) - b_1\frac{\Delta\alpha E(\tau)^2}{2k_B T}, \tag{3.29}$$

where $b_1 = \hbar/(IB)$, $b_2 = \hbar/(aIB)$ and $\tau = Bt$ is a dimensionless time.

3.4.1 The dc field susceptibility

On using the continuum approximation on equation (3.8) we get

$$P(\tau) = \frac{\mu}{3}\int_0^\infty dx e^{-x}\sigma_1(x,\tau). \tag{3.30}$$

Remark that the spatial parts of the differential operators defining the various functions are related to those of the generalised Laguerre polynomials $L_j^m(x)$ (for $x \in [0,\infty)$) whose properties are given in chapter 2 (see Eqns. (2.33)-(2.38)). We look for solutions to the system (3.25)-(3.26) in the form:

$$\begin{pmatrix} \sigma_1(x,\tau) \\ \sigma_2(x,\tau) \end{pmatrix} = \sum_{j=0}^{\infty}\begin{pmatrix} S_j^0(\tau)L_j(x) \\ S_j^1(\tau)L_j^1(x) \end{pmatrix}. \tag{3.31}$$

Using this together with the orthogonality property of the Laguerres in Eq.(3.30), we get

$$P(\tau) = \frac{\mu}{3}S_0^0(\tau). \tag{3.32}$$

The properties of $L_j^m(x)$ applied to Eqs.(3.25) and (3.26) give the differential difference equations for the coefficients $S_j^0(\tau)$ and $S_j^1(\tau)$ as:

$$\Big(\frac{d}{d\tau} + 2j\Big)S_j^0(\tau) + 2b_2\Big[(j+1)S_j^1(\tau) - jS_{j-1}^1(\tau)\Big] = 0 \tag{3.33}$$

and

$$\Big(\frac{d}{d\tau} + 2j + 1\Big)S_j^1(\tau) - b_1\Big[S_j^0(\tau) - S_{j+1}^0(\tau)\Big] = -b_1\frac{\mu E(\tau)}{k_B T}\delta_{j,0}, \tag{3.34}$$

with $S_j^0(0) = S_j^1(0) = 0$. For commodity reasons, Eqs.(3.32), (3.33) and (3.34) will be referred to, in subsequent works, as the classical HT equations for the electric polarisation.

On taking the Fourier transforms of Eqs.(3.32), (3.33) and (3.34), for $E(t) = E_c$, while searching for $S_0^0(\omega' = \omega/B)$ as a continued fraction, we obtain the spectral function or the reduced susceptibility

$$\begin{aligned}\chi_r^*(\omega') &= i\omega'\tilde{P}(i\omega')/P(0) \\ &= \cfrac{2\gamma}{2\gamma + i\omega'(i\omega'+1) + \cfrac{2\gamma i\omega'}{i\omega' + 2 + \cfrac{4\gamma}{i\omega' + 3 + \cfrac{4\gamma}{i\omega' + 4 + \cfrac{6\gamma}{i\omega' + 5 + \ldots}}}}},\end{aligned} \tag{3.35}$$

where $\gamma = Ik_BT/\zeta^2$. The convergence of this fraction is governed by the parameter $\gamma = (Ik_BT/\zeta^2)$. For low frequencies ($\omega' = \omega/B << 1$), it converges strongly. This expression, thus, explicitly describes the low frequency spectrum of classical fluids.

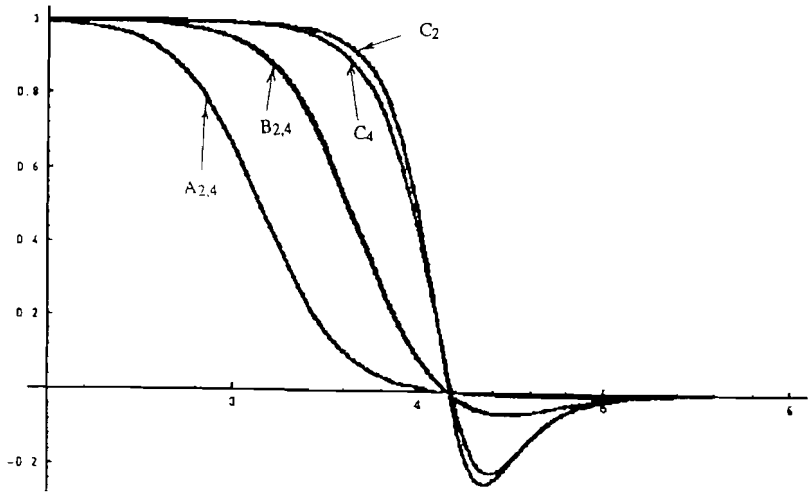

Figure 3.1: The plot of the real part of the normalised susceptibility versus $\log_{10}(\omega/10^9)$ for $\left(\frac{k_BT}{I}\right)^{0.5} = 10^{13} rad/s$: (A) $\gamma = 0.005$, (B) $\gamma = 0.05$ and (C) $\gamma = 0.5$. The subscripts 2 and 4 in $A_{2,4}$ stand for the order of convergence of the continued fraction (3.35).

Figure 3.1 shows the variation of the real part of the normalised complex susceptibility as a function of $\log_{10}(\omega/10^9)$ for different values of $\gamma = k_BT/(IB^2)$. For each value of this parameter, the second and fourth convergents of Eqs.(3.35) are plotted. Curves $A_{2,4}$ are the plots for $\gamma = 0.005$. A_2 and A_4 coincide exactly for the whole frequency spectrum. Similarly $B_{2,4}$ are the plots for $\gamma = 0.05$. Once more, the convergents coincide. Finally, C_2 and C_4 are those for $\gamma = 0.5$. They are distinct for a wide range of frequencies. Remark that all six curves present kink shapes with the kink frequency ranges and steepness increasing with increasing γ. The curves are drawn for a constant value of the mean thermal agitation frequency $\omega_{mean} = \left(k_BT/I\right)^{0.5} = 10^{13} rad/s$. From $\omega \geq 1.6 \times 10^{13} rad/s$, dispersion (the real part) becomes negative reaching a minimum value at a frequency of about $2.5 \times 10^{13} rad/s$ and increasing uniformly to zero for very high frequencies.

Figure 3.2 shows the imaginary part of the normalised susceptibility as a function of $\log_{10}(\omega/10^9)$. The curves $A'_{2,4}$, $B'_{2,4}$, C'_2 and C'_4 are defined in a similar manner as in figure 3.1. This figure illustrates exactly absorption resonance. From the curves, we remark that resonance frequencies and resonance band widths depend strongly on friction ζ, through $\gamma = Ik_BT/\zeta^2$. For large friction ($\gamma = 0.005$), resonance occurs at a frequency of $10^{12} rad/s$ with band width $\Delta\omega = 2.8 \times 10^{12} rad/s$. For moderate friction, ($\gamma = 0.05$), it occurs at $4.5 \times 10^{12} rad/s$ with a width $\Delta\omega = 1.4 \times 10^{13} rad/s$ and finally, at $1.1 \times 10^{13} rad/s$ for $\gamma = 0.5$. It is important to remark that the relative positions of resonances are independent of the order of convergence of the continued fraction (3.35) for given value of γ, but the order influences the magnitude of the

loss factor (imaginary part) and the real part of the electric susceptibility. The convergence of the continued fraction (3.35) is thus, guaranteed for large frictions and/or small inertial effects.

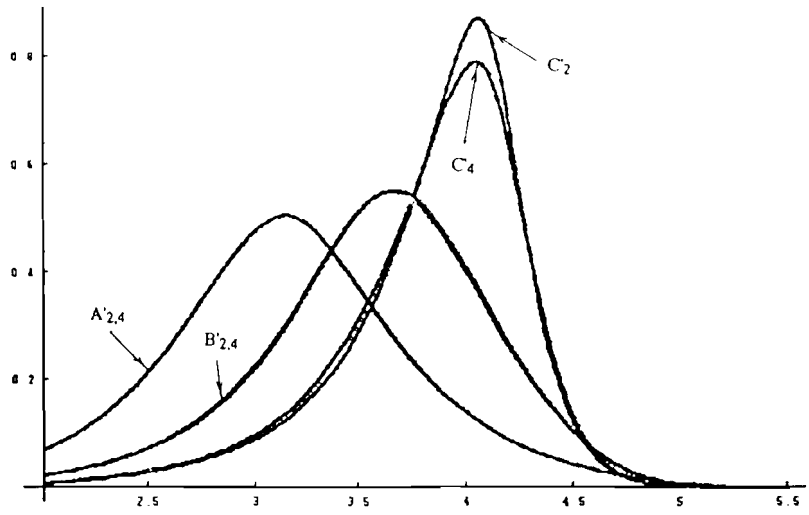

Figure 3.2: The plot of the imaginary part of the normalised susceptibility versus $\log_{10}(\omega/10^9)$ for $\left(\frac{k_BT}{I}\right)^{0.5} = 10^{13} rad/s$: (A') $\gamma = 0.005$, (B') $\gamma = 0.05$ and (C') $\gamma = 0.5$. The subscripts 2 and 4 in $A'_{2,4}$ stand for the order of convergence of the continued fraction (3.35).

3.4.2 The Kerr function

We apply the continuum approximation on Eq.(3.12) to get

$$\Phi(t) = \frac{1}{30}\int_0^\infty dx e^{-x}\Big(\varphi(x,t) + 3\eta_1(x,t)\Big). \tag{3.36}$$

On performing the change of function

$$\phi(x,t) = \varphi(x,t) + 3\eta_1(x,t), \tag{3.37}$$

in the system (3.27)-(3.29) and looking for solutions in the form

$$\begin{pmatrix} \varphi(x,\tau) \\ \phi(x,\tau) \\ \eta_2(x,\tau) \end{pmatrix} = \sum_{j=0}^{\infty} \begin{pmatrix} X_j(\tau)L_j(x) \\ Y_j^0(\tau)L_j(x) \\ Y_j^1(\tau)L_j^1(x) \end{pmatrix}, \tag{3.38}$$

the Kerr function reads,

$$\Phi(\tau) = \frac{1}{30}Y_0^0(\tau) \tag{3.39}$$

and the coefficients $X_j(\tau)$, $Y_j^0(\tau)$ and $Y_j^1(\tau)$ verify the coupled differential difference equations:

$$\Big[(2j+1)\Big(\frac{d}{d\tau}+2j\Big)+2\Big]X_j(\tau)-j\Big(\frac{d}{d\tau}+2j-2\Big)X_{j-1}(\tau)$$
$$-(j+1)\Big(\frac{d}{d\tau}+2j+2\Big)X_{j+1}(\tau)-\frac{1}{2}Y_j^0(\tau)=b_2\frac{\mu E(\tau)}{k_BT}$$
$$\times\Big[-2j(j-1)S_{j-2}^1(\tau)+j(4j+5)S_{j-1}^1(\tau)-(j+1)(2j+3)S_j^1(\tau)\Big], \tag{3.40}$$

$$\Big(\frac{d}{d\tau}+2j\Big)Y_j^0(\tau)+24b_2\Big((j+1)Y_j^1(\tau)-jY_{j-1}^1(\tau)\Big)=-4b_2\frac{\mu E(\tau)}{k_BT}jS_{j-1}^1, \tag{3.41}$$

$$\Big(\frac{d}{d\tau}+2j+1\Big)Y_j^1(\tau)-\frac{b_1}{3}\Big(Y_j^0(\tau)-Y_{j+1}^0(\tau)\Big)$$
$$+\frac{b_1}{3}\Big(X_j(\tau)-X_{j+1}(\tau)\Big)=-b_1\frac{\mu E(\tau)}{k_BT}S_j^0-b_1\frac{\Delta\alpha E(\tau)^2}{k_BT}\delta_{j,0}. \tag{3.42}$$

For same reasons as above, Eqs.(3.39), (3.40), (3.41) and (3.42) will be termed the classical HT equations for the optical Kerr effect.

On solving the system (3.40)-(3.42) for Y_0^0 in the Laplace variable we obtain the Kerr function:

$$\tilde{\Phi}(s')=\frac{1}{15B}\frac{(\alpha_{\|}-\alpha_{\perp})E_c^2}{k_BT}$$
$$\times\frac{1}{s'}\left(1+R\frac{\frac{4\gamma}{s'+2}}{2\gamma+s'(s'+1)+\cfrac{2\gamma s'}{s'+2+\cfrac{4\gamma}{s'+3+\cfrac{4\gamma}{s'+4+\cfrac{6\gamma}{s'+5+\ldots}}}}}\right)$$
$$\times\frac{6\gamma}{s'(s'+1)+4\gamma\frac{2s'+3}{s'+2}+\cfrac{8\gamma s'}{s'+2+\cfrac{16\gamma}{s'+3-\cfrac{4\gamma}{(s'+2)(s'+4)}+\cfrac{16\gamma}{s'+4+\cfrac{24\gamma}{s'+5-\cfrac{4\gamma}{(s'+4)(s'+6)}+\cfrac{24\gamma}{s'+6+\ldots}}}}}}, \tag{3.43}$$

with $R=\mu^2/\Big[(\alpha_{\|}-\alpha_{\perp})k_BT\Big]$. The corresponding spectral function is

$$\Delta n^{\star}(\omega')=\left(1+R\frac{\frac{4\gamma}{i\omega'+2}}{2\gamma+i\omega'(i\omega'+1)+\cfrac{2\gamma i\omega'}{i\omega'+2+\cfrac{4\gamma}{i\omega'+3+\cfrac{4\gamma}{i\omega'+4+\cfrac{6\gamma}{i\omega'+5+\ldots}}}}}\right)\times$$
$$\times\frac{6\gamma}{i\omega'(i\omega'+1)+4\gamma\frac{2i\omega'+3}{i\omega'+2}+\cfrac{8\gamma i\omega'}{i\omega'+2+\cfrac{16\gamma}{i\omega'+3-\cfrac{4\gamma}{(i\omega'+2)(i\omega'+4)}+\cfrac{16\gamma}{i\omega'+4+\cfrac{24\gamma}{i\omega'+5-\cfrac{4\gamma}{(i\omega'+4)(i\omega'+6)}+\cfrac{24\gamma}{i\omega'+6+\ldots}}}}}}. \tag{3.44}$$

Remark that the steady state Kerr function [11] is recovered from Eq.(3.43) as

$$\Phi_{stat} = \lim_{s'\to 0}\left[s'B\tilde{\Phi}(s')\right] = \frac{E_c^2}{15}\left(\frac{\alpha_{\|}-\alpha_{\perp}}{k_BT} + (\frac{\mu}{k_BT})^2\right). \tag{3.45}$$

Let us point out here, the specific character of the Kerr response function which stands as a product of continued fractions as opposed to that of the relaxation regime [1] where it is a simple continued fraction.

Figures 3.3 and 3.4 are the plots of the real and the imaginary parts of the Kerr spectral function (3.44) as functions of $\log_{10}(\omega/10^9)$ for differing values of the parameter R for $\left(\frac{k_BT}{I}\right)^{0.5} = 10^{13} rad/s$ and $\gamma = 0.05$. Curve (1) illustrates the case of highly polarisable non polar systems ($R = 0$), (2) the case of polarisable polar systems ($R = 1$) and (3) that of highly polar ones, ($R = 100$). In each case, the third convergent is considered.

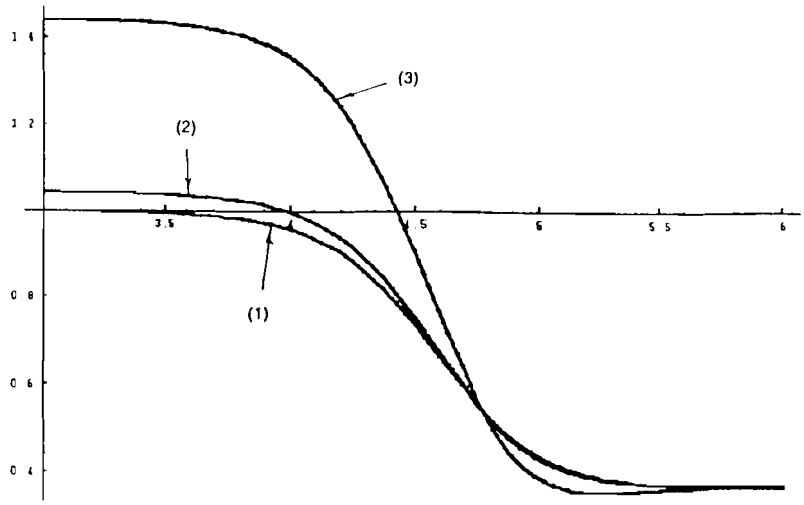

Figure 3.3: The real part of the normalised classical Kerr spectral function versus $\log_{10}(\omega/10^9)$ for $\left(\frac{k_BT}{I}\right)^{0.5} = 10^{13} rad/s$ and $\gamma = 0.05$: (1) $R = 0$, (2) $R = 1$ and (3) $R = 100$.

3.5 The rotating wave approximation (RWA) limit

In this limit, we assume that the solution of the rotators in the bath is highly diluted so that the pressure and consequently friction are very now. The coupling parameter B or the characteristic rotator-bath frequency is very small compared to the rotator lines $\omega_l = (\hbar l/I)$. The dynamics of the rotator is virtually governed by the free rotation in the orienting field. Coupling affects only the frequency shifts and line widths.

Using the mathematical theorem on weak coupling [2, 12] quoted in chapter 1, all "off-diagonal terms" and couplings between matrix elements can be ignored in Eqs.(3.18), (3.19) and (3.20) so that they become:

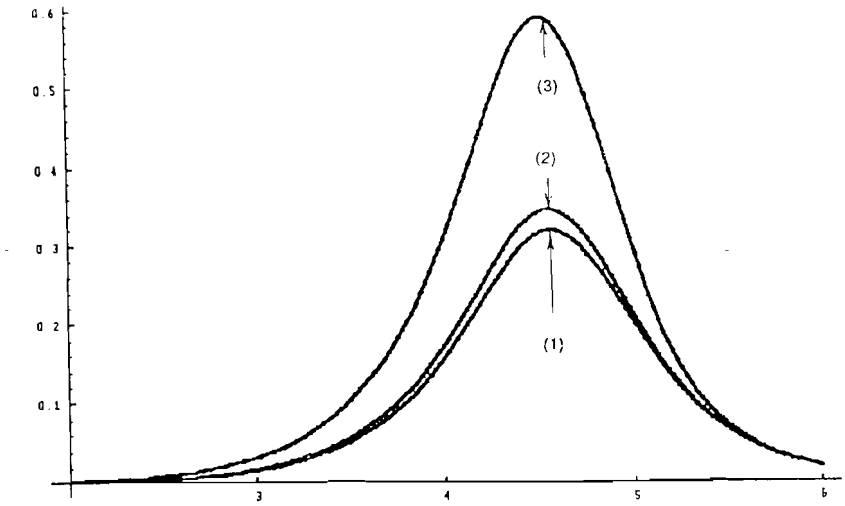

Figure 3.4: The imaginary part of the normalised classical Kerr spectral function versus $\log_{10}(\omega/10^9)$ for $\left(\frac{k_BT}{I}\right)^{0.5} = 10^{13} rad/s$ and $\gamma = 0.05$: (1) $R = 0$, (2) $R = 1$ and (3) $R = 100$.

$$\Big(\frac{\partial}{\partial t} - i(\omega_{l+1} + \Delta\omega_{l+1}) + \Gamma_{l+1}\Big)\sigma_{l,l+1}(t) = -i\frac{\mu E(t)}{\hbar}\Big(1 - e^{-\beta\left(E_{l+1}-E_l\right)}\Big), \tag{3.46}$$

$$\Big(\frac{\partial}{\partial t} + \gamma_l\Big)\varphi_{l,l}(t) = \frac{\mu E(t)}{\hbar}\left(\frac{2l-1}{2l+1}\mathcal{I}m\sigma_{l,l+1}(t) - e^{\beta\left(E_l-E_{l-1}\right)}\frac{2l+3}{2l+1}\mathcal{I}m\sigma_{l-1,l}(t)(1-\delta_{l,0})\right), \tag{3.47}$$

$$\Big(\frac{\partial}{\partial t} - i(\omega_{2l+3} + \Delta\omega_{2l+3}) + \Gamma_{2l+3}\Big)\eta_{l,l+2}(t) = i\frac{\mu E(t)}{\hbar}\Big(e^{-\beta\left(E_{l+1}-E_l\right)}\sigma_{l+1,l+2}(t)$$
$$-\sigma_{l,l+1}(t)\Big) - i\frac{\Delta\alpha E(t)^2}{2\hbar}\Big(1 - e^{-\beta\left(E_{l+2}-E_l\right)}\Big), \tag{3.48}$$

with initial conditions $\sigma_{l,l+1}(0) = \varphi_{l,l}(0) = \eta_{l,l+2}(0) = 0$. We define the dimensionless line widths and frequency shifts:

$$\gamma'_l = \frac{I}{\hbar}\gamma_l = \frac{2BI}{\hbar}\frac{1}{2l+1}\left[l^2 + \frac{l^2}{e^{\beta\hbar\omega_l} - 1} + \frac{(l+1)^2}{e^{\beta\hbar\omega_{l+1}} - 1}\right] \tag{3.49}$$

$$\Gamma'_{l+1} = \frac{1}{2}\Big(\gamma'_l + \gamma'_{l+1}\Big), \tag{3.50}$$

$$\Gamma'_{2l+3} = \frac{1}{2}\Big(\gamma'_l + \gamma'_{l+2}\Big), \tag{3.51}$$

$$\Delta\omega'_{l+1} = -\frac{4\hbar^3 B}{Ik_B^2T^2}(2l+3)\sum_{n=0}^{\infty}\frac{(2n\pi)^3}{\Big[(2n\pi)^2+(al)^2\Big]} \times\frac{1}{\Big[(2n\pi)^2+(a(l+1))^2\Big]\Big[(2n\pi)^2+(a(l+2))^2\Big]}, \tag{3.52}$$

$$\Delta\omega'_{2l+3} = -\frac{4\hbar^3 B}{Ik_B^2T^2}(2l+3)\sum_{n=0}^{\infty}\frac{(2n\pi)^5\Big(1+\frac{a}{(2n\pi)^2}(l^2+3l+3)\Big)}{\Big[(2n\pi)^2+(al)^2\Big]\Big[(2n\pi)^2+(a(l+1))^2\Big]} \times\frac{1}{\Big[(2n\pi)^2+(a(l+2))^2\Big]\Big[(2n\pi)^2+(a(l+3))^2\Big]}, \tag{3.53}$$

where $a=\frac{\hbar^2}{Ik_BT}$. These functions well indicate how line widths and frequency shifts respond to changing physical parameters like inertia, friction and temperature, thus their utility in exploring the influence of the parameter variations on spectral lines. Note that in our dimensionless frequency unit we define the quantum state frequency $\omega'_l = l$. Eqs.(3.8) and (3.46) will be called the quantum HT equations for the electric susceptibility while (3.12), (3.47) and (3.48) are those of the Kerr effect. The classical and quantum HT equations for the electric susceptibility and the Kerr optical effect so termed are very general in field type. The description of dielectric relaxation phenomena could also be done using these equations, putting in them $E(t)=0$ and setting appropriate initial conditions.

3.5.1 The dc field susceptibility

In constant field, Eq.(3.46) is solved to get

$$\begin{aligned}\sigma_{l,l+1}(t) = {} & \frac{(\mu E_c/\hbar)\Big[1-\exp[-\frac{\hbar^2}{Ik_BT}(l+1)]\Big]}{\Gamma_{l+1}^2+(\omega_{l+1}+\Delta\omega_{l+1})^2}\Bigg\{\Big(\omega_{l+1}+\Delta\omega_{l+1}\Big)\Big[1-e^{-\Gamma_{l+1}t} \\ & \times\cos(\omega_{l+1}+\Delta\omega_{l+1})t\Big]-\Gamma_{l+1}\sin\Big[(\omega_{l+1}+\Delta\omega_{l+1})t\Big]e^{-\Gamma_{l+1}t} \\ & -i\Bigg(\Gamma_{l+1}\Big[1-e^{-\Gamma_{l+1}t}\cos(\omega_{l+1}+\Delta\omega_{l+1})t\Big]+(\omega_{l+1}+\Delta\omega_{l+1}) \\ & \times\sin\Big[(\omega_{l+1}+\Delta\omega_{l+1})t\Big]e^{-\Gamma_{l+1}t}\Bigg)\Bigg\}.\end{aligned} \tag{3.54}$$

We deduce the steady state matrix elements

$$\sigma_{l,l+1}^{st} = \frac{(\mu E_c/\hbar)\Big(1-\exp[-\frac{\hbar^2}{Ik_BT}(l+1)]\Big)}{\Gamma_{l+1}^2+(\omega_{l+1}+\Delta\omega_{l+1})^2}\Big((\omega_{l+1}+\Delta\omega_{l+1})-i\Gamma_{l+1}\Big). \tag{3.55}$$

The steady state polarisation can then be calculated. It is found to be the usual $P=\mu^2E/3k_BT$ with a friction dependent correction which decreases proportionately as ζ^2/Ik_BT but since this result has been obtained in the limit of small friction and/or high inertia, the additional term becomes insignificant.

On defining the deviation at time t from the above steady state value, $\Delta\sigma_{l,l+1}(t) = \sigma^{st}_{l,l+1} - \sigma_{l,l+1}(t)$, and spectral function

$$\Delta\tilde{\sigma}_{l,l+1}(\omega) = \sigma^{st}_{l,l+1} - i\omega\int_0^\infty \Delta\sigma_{l,l+1}(t)e^{-i\omega t}dt, \tag{3.56}$$

we obtain from equation (3.8), the reduced susceptibility

$$\Delta\chi^*_r(\omega') = \Delta\chi'_r(\omega') - i\Delta\chi''_r(\omega'), \tag{3.57}$$

where

$$\begin{aligned}\Delta\chi'_r(\omega') &= \sum_{l=0}^{\infty}(l+1)(l+1+\Delta\omega'_{l+1})\left(e^{-\beta E_l} - e^{-\beta E_{l+1}}\right)\\ &\times\frac{(l+1+\Delta\omega'_{l+1})^2 - \omega'^2 + \Gamma'^2_{l+1}}{\left[\left(l+1+\Delta\omega'_{l+1}\right)^2 - \omega'^2 + \Gamma'^2_{l+1}\right]^2 + 4\omega'^2\Gamma'^2_{l+1}}\end{aligned} \tag{3.58}$$

and

$$\begin{aligned}\Delta\chi''_r(\omega') &= \sum_{l=0}^{\infty}2(l+1)(l+1+\Delta\omega'_{l+1})\left(e^{-\beta E_l} - e^{-\beta E_{l+1}}\right)\times\\ &\times\frac{\omega'\Gamma'_{l+1}}{\left[\left(l+1+\Delta\omega'_{l+1}\right)^2 - \omega'^2 + \Gamma'^2_{l+1}\right]^2 + 4\omega'^2\Gamma'^2_{l+1}},\end{aligned} \tag{3.59}$$

with $\omega' = \omega I/\hbar$.

Figure 3.5 shows the plots of the normalised dispersion coefficient (1) and loss factor (2) as functions of the dimensionless frequency $\omega' = \omega I/\hbar$ for weak coupling ($B = 10^{-3}\omega_{mean}$) with $\hbar^2/(Ik_BT) = 0.05$. The loss factor, an entirely positive quantity, presents an oscillatory character for $1 \leq \omega' \leq 10$ and vanishes for very high frequencies. Dispersion also shows this oscillatory behaviour but for high frequencies, it reverses sign and tends asymptotically to zero.

3.5.2 The Kerr function

Eqs.(3.47) and (3.48) give the integral form for $\varphi_{l,l}(t)$ and $\eta_{l,l+2}(t)$:

$$\begin{aligned}\varphi_{l,l}(t) &= \frac{\mu E}{\hbar}\frac{2l-1}{2l+1}\exp(-\gamma_l t)\int_0^t dt'\exp(\gamma_l t')\mathcal{I}m\sigma_{l,l+1}(t')\\ &-\frac{\mu E}{\hbar}e^{-al}\frac{2l+3}{2l+1}\exp(-\gamma_l t)\int_0^t dt'\exp(\gamma_l t')\mathcal{I}m\sigma_{l-1,l}(t')\end{aligned} \tag{3.60}$$

and

$$\eta_{l,l+2}(t) = i\frac{\mu E}{\hbar}e^{-a(l+1)}\exp\left[-\left\{\Gamma_{2l+3} - i\left(\omega_{2l+3} + \Delta\omega_{2l+3}\right)\right\}t\right]$$

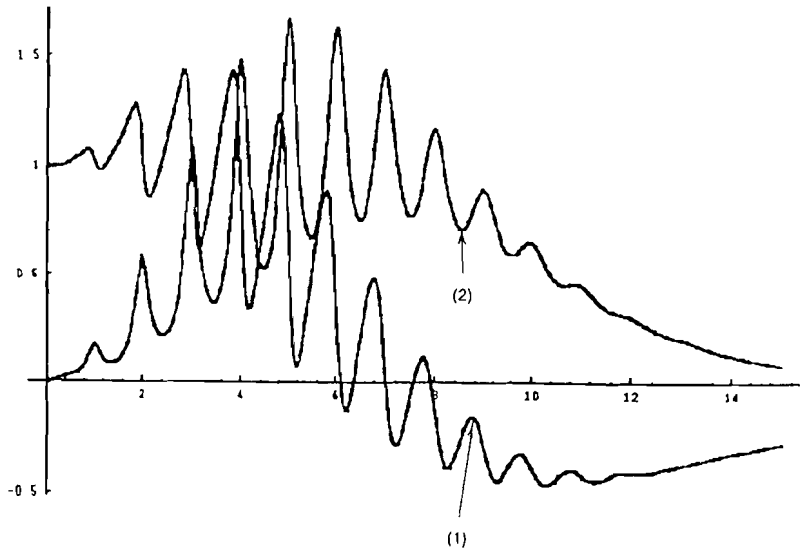

Figure 3.5: The plot of the real (1) and the imaginary (2) parts of normalised susceptibility versus the dimensionless frequency $\omega' = \omega/\left(\hbar/I\right)$ for $a = \hbar^2/(Ik_BT) = 0.05$, $B = 0.001\omega_{mean}$ (RWA).

$$
\begin{aligned}
&\times\int_0^t dt' \exp\Big[\Big\{\Gamma_{2l+3} - i\Big(\omega_{2l+3} + \Delta\omega_{2l+3}\Big)\Big\}t'\Big]\sigma_{l+1,l+2}(t') \\
&-i\frac{\mu E}{\hbar}\exp\Big[-\Big\{\Gamma_{2l+3} - i\Big(\omega_{2l+3} + \Delta\omega_{2l+3}\Big)\Big\}t\Big] \\
&\times\int_0^t dt' \exp\Big[\Big\{\Gamma_{2l+3} - i\Big(\omega_{2l+3} + \Delta\omega_{2l+3}\Big)\Big\}t'\Big]\sigma_{l,l+1}(t') \\
&-i\frac{\Delta\alpha E_c^2}{2\hbar}(1 - e^{-a(2l+3)})\exp\Big[-\Big\{\Gamma_{2l+3} - i\Big(\omega_{2l+3} + \Delta\omega_{2l+3}\Big)\Big\}t\Big] \\
&\times\int_0^t dt' \exp\Big[\Big\{\Gamma_{2l+3} - i\Big(\omega_{2l+3} + \Delta\omega_{2l+3}\Big)\Big\}t'\Big],
\end{aligned}
\tag{3.61}
$$

where $a = \hbar^2/(Ik_BT)$. On substituting for $\sigma_{l,l+1}$ as obtained previously, we easily show that

$$
\varphi_{l,l}(t) = \varphi_{l,l}^{st} - \Delta\varphi_{l,l}(t), \tag{3.62}
$$

with

$$
\varphi_{l,l}^{st} = \frac{\mu^2E^2}{\hbar^2}\Re\left[\frac{\frac{2l+3}{2l+1}(e^{al} - 1)}{\gamma_l\Big[\Gamma_l + i(\omega_l + \Delta\omega_l)\Big]} - \frac{\frac{2l-1}{2l+1}(1 - e^{-a(l+1)})}{\gamma_l\Big[\Gamma_{l+1} + i(\omega_{l+1} + \Delta\omega_{l+1})\Big]}\right] \tag{3.63}
$$

and

$$
\begin{aligned}
\Delta\varphi_{l,l}(t) = \frac{\mu^2E^2}{\hbar^2}\Re\Bigg[&\Bigg\{\frac{2l+3}{2l+1}(e^{al} - 1)\frac{1}{\gamma_l\Big[\Gamma_l + i(\omega_l + \Delta\omega_l)\Big]} - \frac{2l-1}{2l+1} \\
&\times(1 - e^{-a(l+1)})\frac{1}{\gamma_l\Big[\Gamma_{l+1} + i(\omega_{l+1} + \Delta\omega_{l+1})\Big]}\Bigg\}\exp(-\gamma_l t) + \frac{2l+3}{2l+1}(e^{al} - 1)
\end{aligned}
$$

$$\times\frac{\exp\Big[-\big(\Gamma_l+i(\omega_l+\Delta\omega_l)\big)t\Big]}{\Big[\gamma_l-\Gamma_l-i(\omega_l+\Delta\omega_l)\Big]\Big[\Gamma_l+i(\omega_l+\Delta\omega_l)\Big]}-\frac{2l-1}{2l+1}(1-e^{-a(l+1)})$$
$$\times\frac{\exp\Big[-\big\{\Gamma_{l+1}+i(\omega_{l+1}+\Delta\omega_{l+1})\big\}t\Big]}{\Big[\gamma_l-\Gamma_{l+1}-i(\omega_{l+1}-\Delta\omega_{l+1})\Big]\Big[\Gamma_{l+1}+i(\omega_{l+1}+\Delta\omega_{l+1})\Big]}\Bigg]. \tag{3.64}$$

Similarly,

$$\Delta\eta_{l,l+2}(t)=\eta^{st}_{l,l+2}-\eta_{l,l+2}(t)=\frac{\mu^2E^2}{\hbar^2}\Bigg[\Bigg(\frac{1-e^{-a(l+1)}}{\Gamma_{2l+3}-\Gamma_{l+1}-i(\omega_{l+2}+\Delta\omega_{l+2})}$$
$$-\frac{e^{-a(l+1)}(1-e^{-a(l+2)})}{\Gamma_{2l+3}-\Gamma_{l+2}-i(\omega_{l+1}+\Delta\omega_{l+1})}-\frac{i}{R}\Big(1-e^{-a(2l+3)}\Big)\Bigg)$$
$$\times\frac{\exp\Big[-\big\{\Gamma_{2l+3}-i(\omega_{2l+3}+\Delta\omega_{2l+3})\big\}t\Big]}{\Big[\Gamma_{2l+3}-i(\omega_{2l+3}+\Delta\omega_{2l+3})\Big]}-\Big(1-e^{-a(l+1)}\Big)$$
$$\times\frac{\exp\Big[-\big\{\Gamma_{l+1}-i(\omega_{l+1}+\Delta\omega_{l+1})\big\}t\Big]}{\Big[\Gamma_{l+1}-i(\omega_{l+1}+\Delta\omega_{l+1})\Big]\Big[\Gamma_{2l+3}-\Gamma_{l+1}-i(\omega_{l+2}+\Delta\omega_{l+2})\Big]}$$
$$+\frac{e^{-a(l+1)}\Big(1-e^{-a(l+2)}\Big)\exp\Big[-\big\{\Gamma_{l+2}-i(\omega_{l+2}+\Delta\omega_{l+2})\big\}t\Big\}}{\Big[\Gamma_{l+2}-i(\omega_{l+2}+\Delta\omega_{l+2})\Big]\Big[\Gamma_{2l+3}-\Gamma_{l+2}-i(\omega_{l+1}+\Delta\omega_{l+1})\Big]}\Bigg] \tag{3.65}$$

with

$$\eta^{st}_{l,l+2}=\frac{\mu^2E^2}{\hbar^2}\Bigg(\frac{(1-e^{-a(l+2)})e^{-a(l+1)}}{\Gamma_{l+2}-i(\omega_{l+2}+\Delta\omega_{l+2})}-\frac{(1-e^{-a(l+)})}{\Gamma_{l+1}-i(\omega_{l+1}+\Delta\omega_{l+1})}$$
$$-\frac{i}{R}(1-e^{-a(l+2)})\Bigg)\frac{1}{\Gamma_{2l+3}-i(\omega_{2l+3}+\Delta\omega_{2l+3})}, \tag{3.66}$$

On defining a spectral function similar to that of the polarisation, for all frequency $\omega=(\hbar/I)\omega'$, we get, after using Eq.(3.12), that

$$\Delta\tilde{\Phi}^*(\omega')=\Delta\tilde{\Phi}'(\omega')-i\Delta\tilde{\Phi}''(\omega'). \tag{3.67}$$

It is important to give a physical meaning to $\Delta\tilde{\Phi}(\omega')$. Its time picture depicts the deviation at time t from its steady state value $\frac{E^2}{15}\Big((\mu/k_BT)^2+(\Delta\alpha/k_BT)\Big)$. $\Delta\Phi(t)$ therefore describes the transient state following the sudden application of the constant electric field. It can also be called a relaxation function. Using the spectral function $\Delta\tilde{\Phi}(\omega)$ observed spectra may be accounted for. This method of characterising dielectrics should be capable of recovering results furnished by the field removal relaxation method [1, 2]. On the other hand, some new important features will appear. The field removal relaxation reveals only one type of rotational transition ($l\rightarrow l+2$) but due to the fact that the new approach couples both susceptibility and the Kerr function (cf. Eqs.(3.18), (3.19),(3.20)), $l\rightarrow l+1$ also intervenes in the relaxation mechanism. This method is therefore important as spectral lines not accounted for by the the usual method appears naturally.

Regardless of the complicated mathematical form of the real and the imaginary parts of this function, their significance for the interpretation of relevant physical properties of dielectric media earns them being written out explicitly as:

$$
\begin{aligned}
\Delta\tilde{\Phi}'(\omega') \;=\; & \frac{1}{15}\Big(\frac{\mu E_c}{k_B T}\Big)^2 \sum_{l=0}^{\infty} \frac{l+1}{a(2l+3)} e^{-\beta E_l} \Big\{ -l(1-e^{-a(l+1)})\gamma'_l \Gamma'_{l+1} \Big/ \Big[\Big(\Gamma'^2_{l+1} \\
& + (l+1+\Delta\omega'_{l+1})^2 \Big) \Big(\gamma'^2_l + \omega'^2 \Big) \Big] + \frac{l(2l+3)}{2l-1} (e^{al}-1)\gamma'_l \Gamma'_l \Big/ \\
& \Big[\Big(\Gamma'^2_l + (l+\Delta\omega'_l)^2 \Big) \Big(\gamma'^2_l + \omega'^2 \Big) \Big] - l(1-e^{-a(l+1)}) \Big\{ \Big[\Gamma'_{l+1}(\gamma'_l - \Gamma'_{l+1}) \\
& + (l+1+\Delta\omega'_{l+1})^2 \Big] \Big[\Gamma'^2_{l+1} + (l+1+\Delta\omega'_{l+1})^2 - \omega'^2 \Big] \\
& + 2\omega'^2 \Gamma'_{l+1}(\gamma'_l - \Gamma'_{l+1}) \Big\} \Big/ \Big[\Big\{ (\gamma'_l - \Gamma'_{l+1})^2 + (l+1+\Delta\omega'_{l+1})^2 \Big\} \\
& \times \Big\{ \Big(\Gamma'^2_{l+1} + (l+1+\Delta\omega'_{l+1})^2 - \omega'^2 \Big)^2 + 4\omega'^2 \Gamma'^2_{l+1} \Big\} \Big] \\
& + \frac{l(2l+3)}{(2l-1)} (e^{al}-1) \Big\{ \Big[\Gamma'_l(\gamma'_l - \Gamma'_l) + (l+\Delta\omega'_l)^2 \Big] \Big[\Gamma'^2_l + (l+\Delta\omega'_l)^2 - \omega'^2 \Big] \\
& + 2\omega'^2 \Gamma'_l(\gamma'_l - \Gamma'_l) \Big\} \Big/ \Big[\Big\{ \Big(\gamma'_l - \Gamma'_l \Big)^2 + (l+\Delta\omega'_l)^2 \Big\} \Big\{ \Big(\Gamma'^2_l \\
& + (l+\Delta\omega'_l)^2 - \omega'^2 \Big)^2 + 4\omega'^2 \Gamma'^2_l \Big\} \Big] - 3(l+2)(1-e^{-a(l+2)}) e^{-a(l+1)} \\
& \times \Big\{ \Big[\Gamma'_{2l+3} - \Gamma'_{l+2} \Big) \Gamma_{2l+3} - (2l+3+\Delta\omega'_{2l+3})(l+1+\Delta\omega'_{l+1}) \Big] \\
& \times \Big[\Gamma'^2_{2l+3} + (2l+3+\Delta\omega'_{2l+3})^2 - \omega'^2 \Big] + 2\omega'^2 \Gamma'_{2l+3}(\Gamma'_{2l+3} - \Gamma'_{l+2}) \Big\} \Big/ \\
& \Big[\Big\{ (\Gamma'_{2l+3} - \Gamma'_{l+2})^2 + (l+1+\Delta\omega'_{l+1})^2 \Big\} \Big\{ \Big(\Gamma'^2_{2l+3} + (2l+3+\Delta\omega'_{2l+3})^2 \\
& - \omega'^2 \Big)^2 + 4\omega'^2 \Gamma'^2_{2l+3} \Big\} \Big] + 3(l+2)(1-e^{-a(l+1)}) \Big\{ \Big[(\Gamma'_{2l+3} - \Gamma_{l+1}) \Gamma_{2l+3} \\
& - (2l+3+\Delta\omega'_{2l+3})(l+2+\Delta\omega'_{l+2}) \Big] \Big[\Gamma'^2_{2l+3} + (2l+3+\Delta\omega'_{2l+3})^2 \\
& - \omega'^2 \Big] + 2\omega'^2 \Gamma'_{2l+3}(\Gamma'_{2l+3} - \Gamma'_{l+1}) \Big\} \Big/ \Big[\Big\{ (\Gamma'_{2l+3} - \Gamma'_{l+1})^2 \\
& + (l+2+\Delta\omega'_{l+2})^2 \Big\} \Big\{ \Big(\Gamma'^2_{2l+3} + (2l+3+\Delta\omega'_{2l+3})^2 - \omega'^2 \Big)^2 \\
& + 4\omega'^2 \Gamma'^2_{2l+3} \Big\} \Big] - 3(l+2)(1-e^{-a(l+1)}) \Big\{ \Big[(\Gamma'_{2l+3} - \Gamma_{l+1}) \Gamma_{l+1} \\
& - (l+2+\Delta\omega'_{l+2})(l+1+\Delta\omega'_{l+1}) \Big] \Big[\Gamma'^2_{l+1} + (l+1+\Delta\omega'_{l+1})^2 - \omega'^2 \Big] \\
& + 2\omega'^2 \Gamma'_{l+1}(\Gamma'_{2l+3} - \Gamma'_{l+1}) \Big\} \Big/ \Big[\Big\{ \Gamma'_{2l+3} - \Gamma'_{l+1} \Big)^2 + (l+2+\Delta\omega'_{l+2})^2 \Big\} \\
& \times \Big\{ \Big(\Gamma'^2_{l+1} + (l+1+\Delta\omega'_{l+1})^2 - \omega'^2 \Big)^2 + 4\omega'^2 \Gamma'^2_{l+1} \Big\} \Big] + 3(l+2)(1-e^{-a\,l+2)}) \\
& \times e^{-a(l+1)} \Big\{ \Big[(\Gamma'_{2l+3} - \Gamma_{l+2}) \Gamma_{l+2} - (l+1+\Delta\omega'_{l+1})(l+2+\Delta\omega'_{l+2}) \Big] \\
& \times \Big[\Gamma'^2_{l+2} + (l+2+\Delta\omega'_{l+2})^2 - \omega'^2 \Big] + 2\omega'^2 \Gamma'_{l+2}(\Gamma'_{2l+3} - \Gamma'_{l+2}) \Big\} \Big/ \\
& \Big[\Big\{ \Big(\Gamma'_{2l+3} - \Gamma'_{l+2} \Big)^2 + (l+1+\Delta\omega'_{l+1})^2 \Big\} \times
\end{aligned}
$$

$$\times\Big\{\Big(\Gamma'^2_{l+2}+(l+2+\Delta\omega'_{l+2})^2-\omega'^2\Big)^2+4\omega'^2\Gamma'^2_{l+2}\Big\}\Big]$$
$$+\frac{3}{R}(l+2)(1-e^{-a(2l+3)})\Big[\Big(\Gamma'^2_{2l+3}+(2l+3+\Delta\omega'_{2l+3}\Big)^2$$
$$-\omega'^2\Big]\Big/\Big[\Big(\Gamma'^2_{2l+3}+(2l+3+\Delta\omega'_{2l+3})^2-\omega'^2\Big)^2+4\omega'^2\Gamma'^2_{2l+3}\Big]\Big\} \tag{3.68}$$

and

$$\Delta\tilde{\Phi}''(\omega') = \frac{1}{15}\Big(\frac{\mu E_c}{k_BT}\Big)^2\sum_{l=0}^{\infty}\frac{(l+1)\omega'}{a(2l+3)}e^{-\beta E_l}\Big\{-l\Big(1-e^{-a(l+1)}\Big)\Gamma'_{l+1}\Big/\Big[\Big\{\Gamma'^2_{l+1}$$
$$+(l+1+\Delta\omega'_{l+1})^2\Big\}(\gamma'^2_l+\omega'^2)\Big]+\frac{l(2l+3)}{2l-1}(e^{al}-1)\Gamma'_l\Big/\Big[\Big\{\Gamma'^2_l$$
$$+(l+\Delta\omega'_l)^2\Big\}(\gamma'^2_l+\omega'^2)\Big]-l(1-e^{-a(l+1)})\Big\{2\Gamma'_{l+1}\Big[\Big(\gamma'_l-\Gamma'_{l+1}\Big)\Gamma'_{l+1}$$
$$+(l+1+\Delta\omega'_{l+1})^2\Big]-(\gamma'_l-\Gamma'_{l+1})\Big[\Gamma'^2_{l+1}+(l+1+\Delta\omega'_{l+1})^2-\omega'^2\Big]\Big\}\Big/$$
$$\Big[\Big\{(\gamma'_l-\Gamma'_{l+1})^2+(l+1+\Delta\omega'_{l+1})^2\Big\}\Big\{\Big(\Gamma'^2_{l+1}+(l+1+\Delta\omega'_{l+1})^2-\omega'^2\Big)^2$$
$$+4\omega'^2\Gamma'^2_{l+1}\Big\}\Big]+\frac{l(2l+3)}{(2l-1)}(e^{al}-1)\Big\{2\Gamma'_l\Big[(\gamma'_l-\Gamma'_l)\Gamma'_l+(l+\Delta\omega'_l)^2\Big]-(\gamma'_l-\Gamma'_l)$$
$$\times\Big[\Gamma'^2_l+(l+\Delta\omega'_l)^2-\omega'^2\Big]\Big\}\Big/\Big[\Big\{(\gamma'_l-\Gamma'_l)^2+(l+\Delta\omega'_l)^2\Big\}\Big\{\Big(\Gamma'^2_l+(l+\Delta\omega'_l)^2$$
$$-\omega'^2\Big)^2+4\omega'^2\Gamma'^2_l\Big\}\Big]-3(l+2)(1-e^{-a(l+2)})e^{-a(l+1)}\Big\{2\Gamma_{2l+3}$$
$$\times\Big[(\Gamma'_{2l+3}-\Gamma'_{l+2})\Gamma_{2l+3}-(2l+3+\Delta\omega'_{2l+3})(l+1+\Delta\omega'_{l+1})\Big]-(\Gamma'_{2l+3}-\Gamma'_{l+2})$$
$$\times\Big[(2l+3+\Delta\omega'_{2l+3})^2-\omega'^2+\Gamma'^2_{2l+3}\Big]\Big\}\Big/\Big[\Big\{(\Gamma'_{2l+3}-\Gamma'_{l+2})^+(l+1+\Delta\omega'_{l+1})^2\Big\}$$
$$\times\Big\{\Big(\Gamma'^2_{2l+3}+(2l+3+\Delta\omega'_{2l+3})^2-\omega'^2\Big)^2+4\omega'^2\Gamma'^2_{2l+3}\Big\}\Big]+3(l+2)(1-e^{-a(l+1)})$$
$$\times\Big\{2\Gamma_{2l+3}\Big[(\Gamma'_{2l+3}-\Gamma'_{l+1})\Gamma'_{2l+3}-(2l+3+\Delta\omega'_{2l+3})(l+2+\Delta\omega'_{l+2})\Big]$$
$$(\Gamma'_{2l+3}-\Gamma'_{l+1})\Big[\Gamma'^2_{2l+3}-\omega'^2+\Gamma'^2_{2l+3}\Big]\Big\}\Big/\Big[\Big\{(\Gamma'_{2l+3}-\Gamma'_{l+1})^2$$
$$+(l+2+\Delta\omega'_{l+2})^2\Big\}\Big\{\Big(\Gamma'^2_{2l+3}+(2l+3+\Delta\omega'_{2l+3})^2-\omega'^2\Big)^2$$
$$+4\omega'^2\Gamma'^2_{2l+3}\Big\}\Big]-3((l+2)(1-e^{-a(l+1)})\Big\{2\Gamma_{l+1}\Big[(\Gamma'_{2l+3}-\Gamma'_{l+1})\Gamma_{l+1}$$
$$+(l+2+\Delta\omega'_{l+2})(l+1+\Delta\omega'_{l+1})\Big]-(\Gamma'_{2l+3}-\Gamma'_{l+1})\Big[\Gamma'^2_{l+1}-\omega'^2$$
$$+(l+1+\Delta\omega'_{l+1})^2\Big]\Big\}\Big/\Big[\Big\{(\Gamma'_{2l+3}-\Gamma'_{l+1})^2+(l+2+\Delta\omega'_{l+2})^2\Big\}$$
$$\times\Big\{\Big(\Gamma'^2_{l+1}+(l+1+\Delta\omega'_{l+1})^2-\omega'^2\Big)^2+4\omega'^2\Gamma'^2_{l+1}\Big\}\Big]$$
$$+3(l+2)(1-e^{-a(l+2)})e^{-a(l+1)}\Big\{2\Gamma_{l+2}\Big[(\Gamma'_{2l+3}-\Gamma'_{l+2})\Gamma'_{l+2}$$
$$-(l+1+\Delta\omega'_{l+1})(l+2+\Delta\omega'_{l+2})\Big]-(\Gamma'_{2l+3}-\Gamma'_{l+2})\Big[\Gamma'^2_{l+2}$$
$$-\omega'^2+(l+2+\Delta\omega'_{l+2})^2\Big]\Big\}\Big/\Big[\Big\{(\Gamma'_{2l+3}-\Gamma'_{l+2})^2+(l+2+\Delta\omega'_{l+2})^2\Big\}\times$$

$$\times\Big\{\Big(\Gamma'^2_{l+2}+(l+1+\Delta\omega'_{l+1})^2-\omega'^2\Big)^2+4\omega'^2\Gamma'^2_{l+2}\Big\}\Big]$$
$$+\frac{6}{R}(l+2)(1-e^{-a(2l+3)})\Gamma'_{2l+3}\Big/\Big[\Big(\Gamma'^2_{2l+3}+(2l+3+\Delta\omega'_{2l+3})^2$$
$$-\omega'^2\Big)^2+4\omega'^2\Gamma'^2_{2l+3}\Big]\Big\}, \tag{3.69}$$

where $R=\mu^2/(\Delta\alpha k_BT)$. In spite of a number of publications giving theoretical description of polar fluids, the problem of formulating analytical description of relevant spectra over wide frequency range has not yet been solved. The above expressions, explicitly reveal a detailed dependence on temperature and inertial effects through the shifts and widths and could directly be exploited to analyse observed spectra and give valuable informations about molecular structure and characteristic times of molecular rotational motions.

3.6 Discussions

i) Figure 3.1 is the normalised plot of the classical dispersion factor (the real part of the complex susceptibility) versus $\log_{10}(\omega/10^9)$ for $(k_BT/I)^{0.5}=10^{13}rad/s$: (A)$\gamma=Ik_BT/\zeta^2=0.005$, (B) $\gamma=0.05$ and (C) $\gamma=0.5$. The subscripts 2 and 4 in $A_{2,4}$ stand for the order of convergence of the continued fraction (3.35). From this figure, we observe that the dispersion factor vanishes at same frequency ($\omega_c=1.6\times10^{13}rad/s$) for all γ values. The more γ increases. the more the dispersion factor kink gets strong but tends asymptotically to a limit form that presents a square wall at the upper part (y-positive) and a sharp concavity at the bottom (y-negative). The well depth appearing at the bottom is the more important, the more γ increases. This phenomenon could be interpreted from the molecular structure of the medium. Indeed, large γ values ($\gamma\geq0.5$) correspond to small friction (ζ) for which the bath of oscillators is less concentrated. Collisions between the rotator and bath oscillators are less frequent. thus the bath-rotator system is less dispersive. Dispersion, then, changes very little over a wide frequency range ($0-4\times10^{12}rad/s$) but falls abruptly to zero at a cut-off frequency equal to ω_c. Contrarily to the case of large γ, small γ ($\gamma\leq0.005$) corresponds to large friction ζ, that means a highly concentrated bath, giving the medium a more dispersive character. Dispersion, thus, varies conspicuously with increasing frequency up till ω_c. ω_c is, thus, the frequency beyond which every medium becomes less dispersive than the vacuum. On limiting the analysis to the electric susceptibility, therefore, all media are transparent to electromagnetic waves of frequency far above the cut-off frequency. The less concentrated the bath is, the highly reduced its dispersivity is (the deeper the well).

ii) Absorption resonance frequencies as well as its maxima increase with increasing γ. Free particles absorb radiations more than bound ones. This explains the observation that less dense media will absorb more than denser ones (see figure 3.2). Quantum effects start appearing when the medium characteristic frequency is of the order of $\hbar/I\sim10^{13}rad/s$. This effect manifests for weak couplings (the rotating wave approximation) which here correspond to small friction (or large γ). This explains why as γ increases, resonance frequencies grow, approaching the quantum range.

iii) For same bath concentration ($\gamma=0.05$):

a) for same R values (polar or non polar molecules), there exists an initial frequency range over

which the refraction coefficient remains constant (see figure 3.3). This widens as the dipole moment of the molecules increases. For example, for non polar molecules ($R = 0$), this range length is of the order $3 \times 10^{12} rad/s$ while for molecules with equal permanent and induced moment energy contribution ($R = 1$), it is $6.3 \times 10^{12} rad/s$ and for purely polar ones ($R \to \infty$), it stands at about $10^{13} rad/s$,
b) a steady state value of the refraction coefficient is practically attained at a frequency of $5.0 \times 10^{14} rad/s$ independent of the degree of polarisation of the molecules.
c) there exists a specific frequency characterising the bath structure at which, what ever the molecular electronic structure, the Kerr refraction coefficient is always the same. It occurs at $6.3 \times 10^{13} rad/s$ for $\gamma = 0.05$. At this frequency, appear the Kerr absorption maxima which are more pronounced, the more polar the molecules are.

A general view of the Kerr classical dispersion spectrum is a sluggish variation for low frequencies $0 < \omega < 10^{13} rad/s$, followed by abrupt falls for frequencies between 10^{13} and $10^{14} rad/s$. Above this value, it attains a steady positive value of 0.4 in the normalised units (see figure 3.3). The quantum one starts with a small constant negative value (for molecules with $\hbar/I \sim 4 \times 10^{12} rad/s$ e.g. HCl) for frequencies lower than $10^{13} rad/s$ (for less polar systems) and beyond this frequency value spectral lines start appearing (see figures 3.6 and 3.7 (1)).

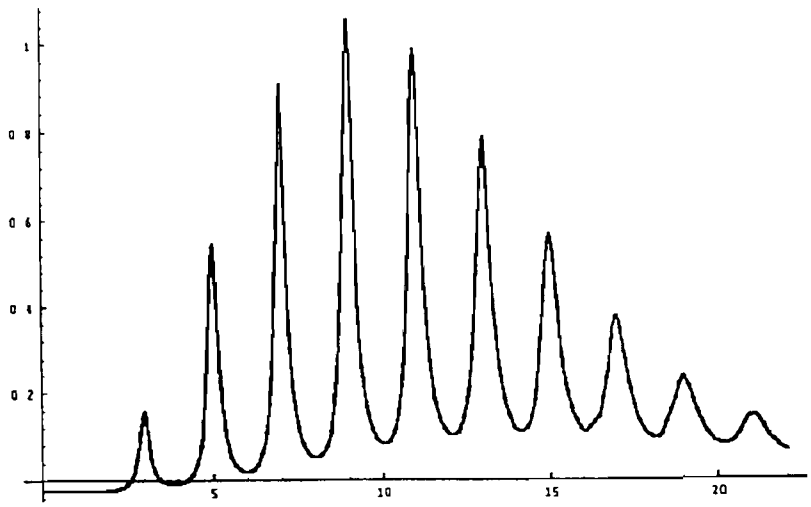

Figure 3.6: The plot of the real part of normalised Kerr spectral function versus the dimensionless frequency $\omega' = \omega/\left(\hbar/I\right)$ for $a = \hbar^2/(Ik_BT) = 0.05$, $R = 0$ and $B = 0.001\omega_{mean}$ (RWA).

iv) For fixed inertia/temperature parameter ($a = \hbar^2/(Ik_BT) = 0.05$), we observe, as the coupling parameter $s = B/\omega_{mean}$ (with $\omega^2_{mean} = k_BT/I$) decreases from 5.0×10^{-3} through 2.5×10^{-3} to 1.0×10^{-3}, a transition from a continuous spectrum (1) through broadened lines (2) to separate line-forms (3) (see figure 3.8). This phenomenon was observed experimentally by Frenkel [16] for HCl in argon while varying argon density. Indeed, the line width at half height varies proportionately with the friction parameter B as portrayed by equation (3.49). As B increases, thus, lines broaden out and fuse up forming a continuous spectrum. This explains

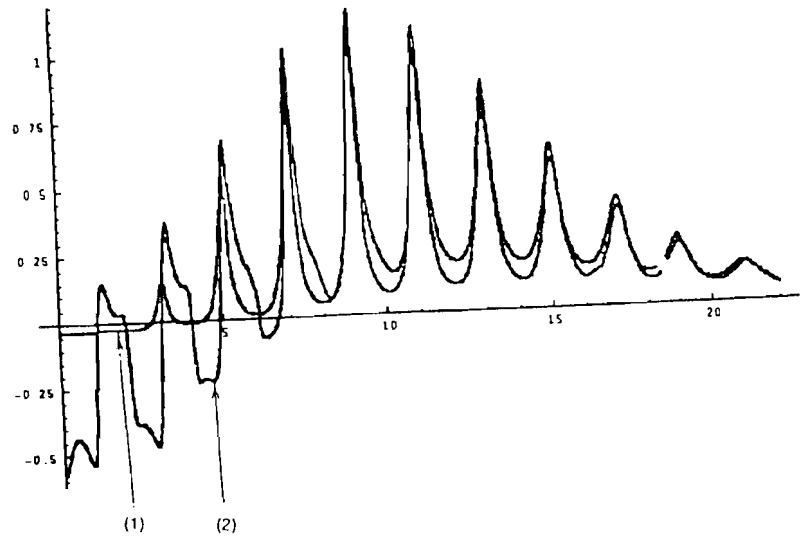

Figure 3.7: The plot of the real part of normalised Kerr spectral function versus the dimensionless frequency $\omega' = \omega/\left(\hbar/I\right)$ for $a = \hbar^2/(Ik_BT) = 0.05$, $B = 0.001\omega_{mean}$: (1) $R = 1$ and (2) $R = 100$ (RWA). y-units are same as in figure 3.6

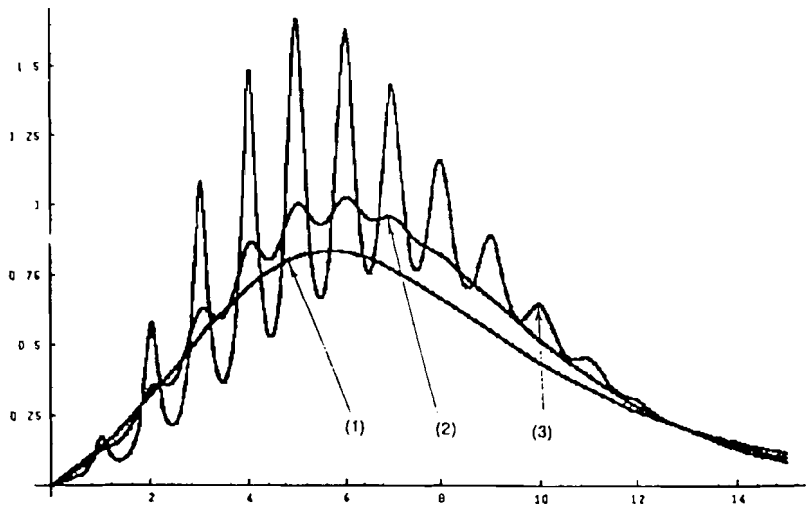

Figure 3.8: The plot of the imaginary part of normalised susceptibility versus the dimensionless frequency $\omega' = \omega/\left(\hbar/I\right)$ for $a = \hbar^2/(Ik_BT) = 0.05$: (1) $B = 0.0050\omega_{mean}$, (2) $B = 0.0025\omega_{mean}$ and (3) $B = 0.0010\omega_{mean}$ (RWA).

the fact that when B for a medium approaches ω_{mean}, the medium acquires typical classical behaviours. On the contrary, when B is very small compared to ω_{mean}, particles are far apart, colliding less frequently leading to highly uncorrelated collisions. This results to pure discrete spectra. Let us make notice of the fact that the calculated line shifts (Eq.(3.52)) have negligible influence on the spectral line positions ($\Delta\omega'_{l+1} \approx -as(2l+3) \sim -10^{-4}(2l+3)$ as opposed to $\omega'_{l+1} = l+1$). This was also observed by Frenkel using impact cross section calculations.

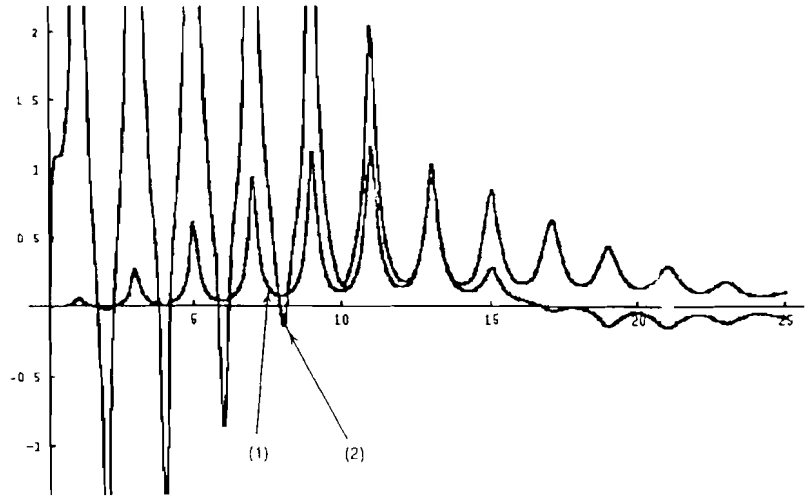

Figure 3.9: The imaginary part of normalised Kerr spectral function versus the dimensionless frequency $\omega' = \omega/\left(\hbar/I\right)$ for $a = \hbar^2/(Ik_BT) = 0.05$, $B = 0.001\omega_{mean}$: (1) $R = 1$ and (2) $R = 100$ (RWA).

v) For the same friction parameter $B = \zeta/I = 0.001\left(k_BT/I\right)^{0.5}$, for $a = 0.05$ and for $R \neq 0$, the Kerr spectra present distortions with amplitudes increasing with increasing R (see figures 3.7(2) and 3.9(2)). For non polar systems, the imaginary part of the Kerr spectral function shows a usual line shape (see figure 3.10), meanwhile for polar ones lines start with very pronounced peaks, then falling into weak negative value peaks which vanish for large frequencies (see figure 3.9).

The distorsions observed in the Kerr low frequency dispersion spectrum of polar fluids result from the mixing of lines corresponding to transitions between small quantum number l levels. Remark that, while the electric susceptibility allows for only lines corresponding to the selection rule $\Delta l = l_f - l_i = \pm 1$, to be computed, the Kerr effect accounts for transitions of the form $\Delta l = l_f - l_i = \pm 2$

We have investigated theoretically, the effect of bath concentration or friction on observed spectra of polar fluids. Bath concentration affects considerably the shape (line-width) of spectra. The classical continuous ones, observable for low frequency ranges, have been highlighted while far infra-red lines have been analysed for less concentrated host bath. Our theory permits the exploration of the spectra of polar fluids over wide temperature and frequency ranges.

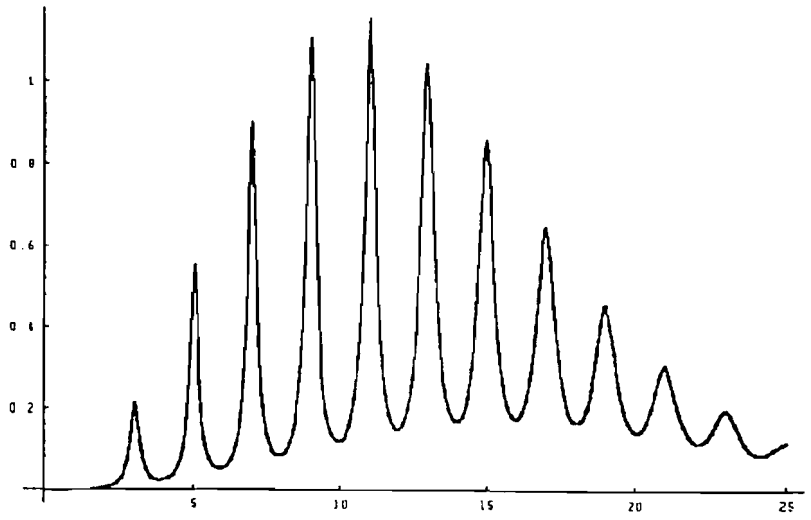

Figure 3.10: The imaginary part of normalised Kerr spectral function versus the dimensionless frequency $\omega' = \omega/\left(\hbar/I\right)$ for $a = \hbar^2/(Ik_BT) = 0.05$, $R = 0$ and $B = 0.001\omega_{mean}$ (RWA).

Bibliography

[1] J. T. Titantah and M. N. Hounkonnou, *Phys. A: Math. Gen.* **30**: 6327, 1997

[2] P. Navez and M. N. Hounkonnou, *J. Phys. A: Math. Gen.* **28**: 6345, 1995

[3] J. T. Titantah and M. N. Hounkonnou, *J. Phys. A: Math. Gen.* **30**: 6347, 1997

[4] A. Morita and H. Watanabe, *J. Chem. Phys.* **70** (10): 4708, 1979

[5] Y. P. Kalmykov and S. V. Titov, *A semi- classical theory of dielectric relaxation and absorption: memory function approach to extended diffusion models of molecular reorientation in fluids* Relaxation Phenomena in Condensed Matter, edited by W. Coffey, *Adv. Chem. Phys.*, LXXXVII: 31, 1994

[6] M. N. Hounkonnou, A. Ronveaux and P. Navez, *J. Phys. A: Math. Gen.* **27**: 6635, 1994

[7] P. Navez and M. N. Hounkonnou, *J. Phys. A: Math. Gen.* **27**: 6657, 1994

[8] V. I. Gaiduk and Yu P. Kalmykov, *J. Mol. Liq.* **34**: 1, 1987

[9] Y. P. Kalmykov and K. P. Quinn, *J. Chem. Phys.* **95** (12): 9142, 1991

[10] H. Spohn, *Rev. Mod. Phys.* **53**: 569, 1980

[11] M. Doi and S. F. Edwards, *The Theory of Polymer Dynamics*, Clarendon Press Oxford, 1986

[12] E. B. Davies, *Math. Ann.* **219**: 147, 1976

Chapter 4

steady state dielectric properties induced by ac and dc field coupling

Summary

The long time effect of a radio frequency (rf) ac field superimposed on a dc field on the electric susceptibility and the Kerr optical functions of polarisable fluids in inert solvent is analysed. The results obtained for the classical Brownian limit, valid for dense solvent media, well reproduce classical results published in the literature with excellent precisions in inertia, density and temperature dependences. The low density limit yields absorption-dispersion lines whose widths and shifts are density, inertia and temperature dependent. While the low density and/or large inertia susceptibility is explicitly written out as a continued fraction got by solving an infinite hierarchy of differential coupled equations, that of the Kerr effect is given in the form of successive convergents of the solutions of an infinite hierarchy of differential difference triplets. The polarisation/ac field phase difference is analysed. The effects of the constant field strength and the ac field frequency on the Kerr function are explored.

4.1 Introduction

In the last chapter [1], we used the master equation derived in chapter 1 [2] (which we named "the HN master equation" in the last chapter) to verify the dielectric properties of a system of polar rotators in interaction with a constant electric field of strength E_c. The effects of inertia and bath concentration were intensively explored. Using the rotational Smoluchowski equation [3], Morita et al. [4] and Matsumoto et al. [5] presented studies of this problem but the former laid much interest on the effect of the applied field on the Kerr effect relaxation that results from the sudden application of the dc field. By averaging the Langevin equation, Coffey [6, 7] tackled the problem emphasising on the effects of inertia.

In the present chapter, we consider the effect of coupling a constant dc field with a radio frequency ac field [8]. In the course of this work, we adopt the notations of chapter 3 [1] so that we can directly exploit existing results therein. The polarisation and the Kerr functions can be calculated using the Hounkonnou-Titantah (HT) quantum relations[1] (see Eqs.(3.8) and 3.12)

$$P(t) = \frac{2\mu}{3}\sum_{l=0}^{\infty}(l+1)\frac{e^{-\beta E_l}}{Z}\Re\sigma_{l,l+1}(t), \tag{4.1}$$

$$\Phi(t) = \frac{2}{15}\sum_{l=0}^{\infty}\frac{e^{-\beta E_l}}{Z}\frac{(l+1)}{(2l+3)}\left\{\frac{l(2l+1)}{(2l-1)}\varphi_{l,l}(t) + 3(l+2)\Re\eta_{l,l+2}(t)\right\}, \tag{4.2}$$

where Z is the one particle free rotator canonical partition function and $\Re$ denotes the real part. The reduced HT equations for the matrix elements $\sigma_{l,l+1}(t)$, $\varphi_{l,l}(t)$, and $\eta_{l,l+2}(t)$ [1] are given in chapter 3 (see Eqs.(3.19)-(3.20) with initial conditions (3.17)).

4.2 The electric susceptibility and the Kerr functions

In this section, the calculations of the electric susceptibility and the Kerr functions are done in the usual two physical limits: the classical Brownian limit and the rotating wave approximation (RWA) limit. In each case, we analyse the long time effect; that is, we consider times very long compared to the period of collision $\tau = 1/B$, the Debye relaxation time $\tau_D = \zeta/(2Ik_BT)$ and the mean thermal angular time $\left(I/k_BT\right)^{0.5}$.

4.2.1 The classical Brownian limit

This limit is characterised by slow moving rotators entering into instantaneous collisions with the bath of fast moving oscillators. Inertial effects are very important for understanding line shapes. With the aid of the Fokker-Planck- Kramer (FPK) equation [9, 10, 11, 12, 13], Hounkonnou et al. [12, 14, 15, 16] presented the steady state analysis of the electric polarisation and the Kerr optical function in a radio frequency ac field; while their electric susceptibility function was given as a continued fraction, the Kerr function was in the form of exponential integrals. Filippini [17] measured experimentally the Kerr dispersion constant when an ac field superimposed on a unidirectional field is applied to a liquid. Coffey and Paranjape [18], Morita [3], Morita and Watanabe [19], gave theoretical descriptions of these phenomena using pure classical diffusion equations.

The electric susceptibility

In the classical limit, quantum equations reduce to the classical HT equations for the electric susceptibility [1] as given in chapter 3 (see Eqs.(3.32)-(3.34)).

$$P(\tau) = \frac{\mu}{3}S_0^0(\tau), \tag{4.3}$$

$$\left(\frac{d}{d\tau} + 2j\right)S_j^0(\tau) + 2b_2\left[(j+1)S_j^1(\tau) - jS_{j-1}^1(\tau)\right] = 0 \tag{4.4}$$

and

$$\left(\frac{d}{d\tau} + 2j + 1\right)S_j^1(\tau) - b_1\left[S_j^0(\tau) - S_{j+1}^0(\tau)\right] = -b_1\frac{\mu E_a}{k_BT}\left(\tau + \cos\omega\tau\right)\delta_{j,0}, \tag{4.5}$$

where $\tau = Bt$, $\omega' = \omega/B$ are dimensionless time and frequency, respectively; $r = E_c/E_a$ measures the ratio of the constant field strength to the amplitude of the ac field. $b_1 b_2 = \gamma = Ik_BT/\zeta^2$, where ζ is the coupling coefficient. In the steady state regime, we search for $S_j^m(\tau)$ in the forms:

$$\begin{aligned} S_0^0(\omega',\tau) &= \frac{\mu E_a}{k_BT}\Big[r + S_0^{0\prime}(\omega')e^{i\omega'\tau} + (S_0^{0\prime}(\omega'))^* e^{-i\omega'\tau}\Big], \\ S_j^0(\omega',\tau) &= \frac{\mu E_a}{k_BT} S_j^{0\prime}(\omega')e^{i\omega'\tau} + C.C. \text{ for } j \neq 0, \\ S_j^1(\omega',\tau) &= \frac{\mu E_a}{k_BT} S_j^{1\prime}(\omega')e^{i\omega'\tau} + C.C. \text{ for all } j. \end{aligned} \tag{4.6}$$

On substituting these into the hierarchy (4.4) -(4.5) and solving for $S_0^{0\prime}(\omega')$, we get

$$S_0^{0\prime}(\omega') = \cfrac{\gamma}{2\gamma + i\omega'\left[1 + i\omega' + \cfrac{2\gamma}{2 + i\omega' + \cfrac{4\gamma}{3 + i\omega' + \cfrac{4\gamma}{4 + i\omega' + \cfrac{6\gamma}{5 + i\omega' + \ldots}}}}\right]}, \tag{4.7}$$

then using (4.3), we deduce the polarisation

$$P(\omega',\tau) = \frac{\mu^2 E_a}{3k_BT}\left\{\frac{r}{2} + \cfrac{\gamma e^{i\omega'\tau}}{2\gamma + i\omega'\left[1 + i\omega' + \cfrac{2\gamma}{2 + i\omega' + \cfrac{4\gamma}{3 + i\omega' + \cfrac{4\gamma}{4 + i\omega' + \ldots}}}\right]} + C.C.\right\}. \tag{4.8}$$

In the absence of the dc field ($r = 0$), the result of Gross [20] on generalised Brownian motion is recovered. We define a reduced susceptibility $\chi_r(\omega',\tau)$ as

$$\chi_r(\omega',\tau) = r + 2 \mid S_0^{0\prime}(\omega') \mid \cos\Big(\omega'\tau - \alpha(\omega')\Big), \tag{4.9}$$

where $\alpha(\omega',)$, the phase difference between the exciting ac field and the dielectric response function (the polarisation), furnishes valuable informations on the absorption properties of the medium under investigation. It is given by

$$\tan\alpha(\omega') = -\frac{\mathcal{I}mS_0^{0\prime}(\omega')}{\Re S_0^{0\prime}(\omega')}. \tag{4.10}$$

On neglecting inertial effects in (4.7), we obtain the Debye limit

$$S_0^{0\prime}(\omega') = \frac{1}{2(1 + i\omega\tau_D)} \tag{4.11}$$

in usual frequency units. In this case, the phase is given by $\tan\alpha(\omega) = \omega\tau_D$ with $\tau_D = \zeta/(2k_BT)$. The lowest inertial limit, corresponding to the Rocard formula,

$$S_0^{0\prime}(\omega') = \frac{1}{2(1 + i\omega\tau_D - (I\omega^2/2k_BT))}, \tag{4.12}$$

leads to the phase expression $\tan\alpha(\omega) = \omega\tau_D/\left(1-(I\omega^2/2k_BT)\right)$ which yields a maximum phase of $\pi/2$ for frequency of $\sqrt{2}$ times mean thermal agitation frequency ($\omega_{mean} = \left(k_BT/I\right)^{0.5}$). At this frequency value, the rate of energy absorption from the surrounding bath by the rotators is in phase with the forcing field (since the rate of heat exchange between the rotator and the surrounding is proportional to minus the rate of change of the induced polarisation [1, 21, 22] as seen in chapters 2 and 3). On defining a new dimensionless frequency $\nu = \omega/\omega_{mean}$ in (4.7), we rewrite $S_0^{0\prime}$ as

$$S_0^{0\prime}(\nu) = \cfrac{1}{2 + i\nu/\sqrt{\gamma} - \nu^2 + \cfrac{2i\sqrt{\gamma}\nu}{2 + i\sqrt{\gamma}\nu + \cfrac{4\gamma}{3 + i\sqrt{\gamma}\nu + \cfrac{4\gamma}{4 + i\sqrt{\gamma}\nu + \ldots}}}}. \tag{4.13}$$

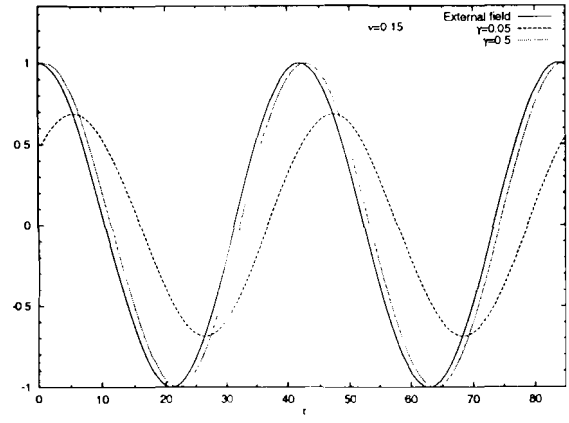

Figure 4.1:
Function $\cos\nu\tau$ (—), the reduced susceptibility $\chi_r(\nu,\tau)$ for the parameter $\gamma = Ik_BT/\zeta^2 = 0.05$ (---) and $\gamma = 0.5$ (····) against the dimensionless time $\tau = \omega_{mean}t$, provided the fixed reduced frequency $\nu = \omega/\omega_{mean} = 0.15$ and dc field parameter $r = 0$ ($\omega_{mean} = (k_BT/I)^{0.5}$ and $r = E_c^2/(E_c^2 + E_a^2)$).

Figures 4.1 and 4.2 show the plots of the external exciting field $\cos\nu\tau$ and those of the reduced susceptibility $\chi_r(\nu,\tau)$ as functions of the dimensionless time τ (with $\tau = t\omega_{mean}$) for $\nu = 0.15$, 4.00, respectively, and for different values of γ. For fixed ω_{mean}, we analyse the effect of friction ζ on the phase, through $\gamma = Ik_BT/\zeta^2$. Figure 4.3 shows a 3-D plot of $\chi_r(\nu,\tau)$ for $\gamma = 0.05$.

Figure 4.4 shows a 3-D plot of the tangent of the phase angle as a function of the reduced frequency ν and γ. The peaks are found to shift towards larger frequency values as γ increases. It is important to note that while the Debye theory predicts such phenomena only for infinite frequencies ($\tan\alpha(\omega) = \omega\tau_D$) and the Rocard lowest inertial limit predicts a phase difference of $\pi/2$ between the applied field and the material response at $\nu = \sqrt{2}$, our results extensively portrays the effect of inertia on this phase difference. The pioneering investigations of inertial effects in Debye relaxation date back to the work by Sack in 1957 [9] in which he expressed the dielectric property as a continued fraction.

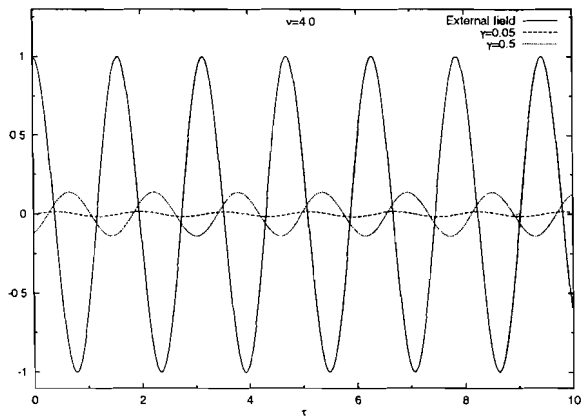

Figure 4.2:
Function $\cos \nu\tau$ (—), the reduced susceptibility $\chi_r(\nu, \tau)$ for the parameter $\gamma = 0.05$ (---) and $\gamma = 0.5$ (····) against the dimensionless time $\tau = \omega_{mean}t$, provided the fixed reduced frequency $\nu = 4.00$ and $r = 0$.

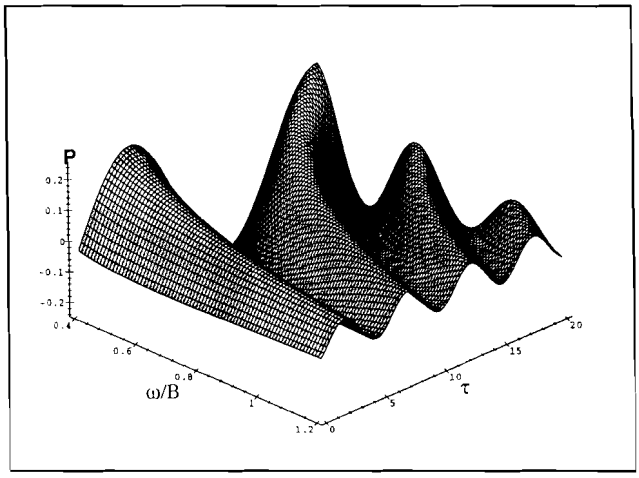

Figure 4.3:
3D plot of the reduced polarisation $\chi_r(\omega', \tau)$ for the inertial parameter $\gamma = 0.05$ and $r = 0$ against the dimensionless time and frequency $\tau = Bt$ $(B = \zeta/I)$ and $\omega' = \omega/B$, respectively.

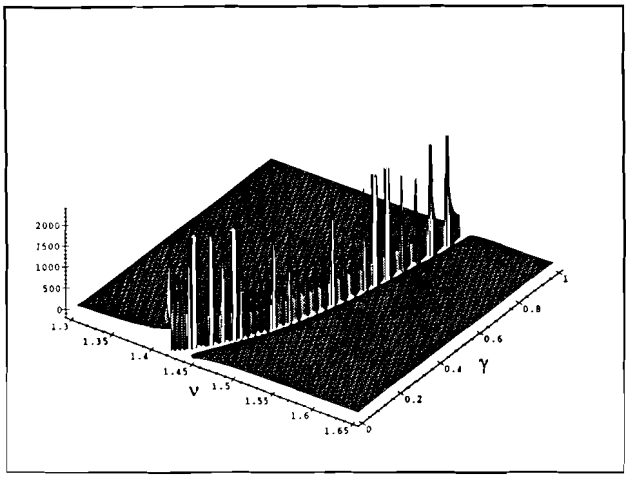

Figure 4.4:
3D plot of function $\tan\alpha(\nu,\gamma)$ against the dimensionless frequency $\nu = \omega/\omega_{mean}$ and the inertia parameter γ (classical result).

The Kerr function

The classical HT equations [1] for the optical Kerr function are (see Eqs.(3.39)-(3.42)):

$$\Phi(\tau) = \frac{1}{30}Y_0^0(\tau) \tag{4.14}$$

with

$$\begin{aligned}&\Big(\frac{d}{d\tau}+2j\Big)Y_j^0(\tau)+24b_2\Big((j+1)Y_j^1(\tau)-jY_{j-1}^1(\tau)\Big)\\&=-4b_2\frac{\mu E_a}{k_BT}(r+\cos\omega'\tau)S_{j-1}^1(\tau)(1-\delta_{j,0}),\end{aligned} \tag{4.15}$$

$$\begin{aligned}&\Big(\frac{d}{d\tau}+2j+1\Big)Y_j^1(\tau)-\frac{b_1}{3}\Big(Y_j^0(\tau)-Y_{j+1}^0(\tau)\Big)+\frac{b_1}{3}\Big(X_j(\tau)-X_{j+1}(\tau)\Big)\\&=-b_1\frac{\mu E_a}{k_BT}(r+\cos\omega'\tau)S_j^0(\tau)-b_1\frac{\Delta\alpha E_a^2}{k_BT}(r+\cos\omega'\tau)^2\delta_{j,0},\end{aligned} \tag{4.16}$$

$$\begin{aligned}&\Big[(2j+1)\Big(\frac{d}{d\tau}+2j\Big)+2\Big]X_j(\tau)-j\Big(\frac{d}{d\tau}+2j-2\Big)X_{j-1}(\tau)\\&-(j+1)\Big(\frac{d}{d\tau}+2j+2\Big)X_{j+1}(\tau)-\frac{1}{2}Y_j^0(\tau)=b_2\frac{\mu E_a}{k_BT}(r+\cos\omega'\tau)\\&\times\Big[-2j(j-1)S_{j-2}^1(\tau)+j(4j+5)S_dj-1^1(\tau)-(j+1)(2j+3)S_j^1(\tau)\Big],\end{aligned} \tag{4.17}$$

where $b_1 = \frac{\hbar}{IB}$ and $b_2 = \frac{\hbar}{aIB}$. Steady state solutions are sought in the forms:

$$X_j(\omega',\tau) = \Big(\frac{\mu E_a}{k_BT}\Big)^2\Big[X_{j,0}(\omega') + X_{j,1}(\omega')e^{i\omega'\tau} + X_{j,2}(\omega')e^{2i\omega'\tau} + C.C.\Big],$$
$$Y_j^0(\omega',\tau) = \Big(\frac{\mu E_a}{k_BT}\Big)^2\Big[Y_{j,0}^0(\omega') + Y_{j,1}^0(\omega')e^{i\omega'\tau} + Y_{j,2}^0(\omega')e^{2i\omega'\tau} + C.C.\Big],$$
$$Y_j^1(\omega',\tau) = \Big(\frac{\mu E_a}{k_BT}\Big)^2\Big[Y_{j,0}^1(\omega') + Y_{j,1}^1(\omega')e^{i\omega'\tau} + Y_{j,2}^1(\omega')e^{2i\omega'\tau} + C.C.\Big], \qquad (4.18)$$

where C.C. denotes complex conjugate. Knowing the forms of S_j^m (obtained by solving system (3.33)-(3.34)), we obtain the three systems of hierarchies (each system being a set of three coupled equations (triplets)) given in appendix B.1. The technique adopted in solving these triplets is based on convergents. Remark that the systems could be written in matrix forms of infinite dimensions. The notion of convergence can be seen as limiting the dimensions of the matrices. The zeroth convergent consists of considering only equations involving just $j = 0$. The first convergent is the modification of the zeroth by including $j = 1$ terms. The former is the solution of a 3×3 matrix equation, while the latter is that of a 6×6 matrix equation. Reliable spectral informations can only be got from at least a 6×6 matrix equation. The expressions for $Y_{0,0}^0(\omega')$, $Y_{0,1}^0(\omega')$ and $Y_{0,2}^0(\omega')$ obtained for $j = 1$ are given in appendix B.2, where $E^2 = E_a^2 + E_c^2$ and $K_0 = \Big(\frac{\mu}{K_BT}\Big)^2 + \frac{\Delta\alpha}{K_BT}$. We can now write the Kerr function as

$$\Phi(\omega',\tau) = \frac{1}{30}E^2K_0\Big[Y_{0,0}^0(\omega') + Y_{0,1}^0(\omega')\exp(i\omega'\tau) + Y_{0,2}^0(\omega')\exp(2i\omega'\tau) + C.C.\Big]. \qquad (4.19)$$

Remark that in the expressions for $Y_{0,0}^0(\omega')$, $Y_{0,1}^0(\omega')$ and $Y_{0,2}^0(\omega')$ we have replaced the field parameter $r = E_c/E_a$ with a more convenient one $r = E_c^2/E^2$ and the quantity R is replaced by $\alpha = \frac{\Delta\alpha/(k_BT)}{K_0}$. With these new parameters, the limiting cases are better understood; for example $r = 0$ corresponds to pure ac field effects and $\alpha = 0$ demonstrates the properties of a non polarisable but polar molecule. Note that both parameters are such that $0 \leq r \leq 1$ and $0 \leq \alpha \leq 1$. The Kerr function (Eq.(4.19)) presents very interesting properties. It expresses the time, radio frequency (rf), rotator-bath parameters and more importantly the E_c/E_a dependences of the Kerr electric birefringence (KEB). For infinitely high frequencies, the function reduces to the steady state expression

$$\Phi_\infty = \frac{E_c^2}{15}\Big((\frac{\mu^2}{k_BT})^2 + \frac{\Delta\alpha}{k_BT}\Big) + \frac{E_a^2}{30}\frac{\Delta\alpha}{k_BT}. \qquad (4.20)$$

The effect of the ac field is felt only when $\Delta\alpha = \alpha_{||} - \alpha_\perp \neq 0$. This result is consistent with that of Doi and Edwards [11]. At very high frequencies, ac field effects on dipole moments average out. Also, in the absence of the dc field ($r = 0$), the term $Y_{0,1}^0(\omega')$ vanishes and the result for pure ac field is recovered.

It is important to note that, while all these results are deduced as the classical limit of a quantum theory, they recover recent results such as those of Déjardin et al. [23] and Hounkonnou et al. [12] based on the Fokker-Planck equation. More recently Déjardin et al. [24] used the Smoluchowski equation to analyse the effect of a dc field on the relaxation time of the dynamic Kerr function. A similar procedure was adopted by Coffey et al. [25] to tackle the same problem.

4.2.2 The rotating wave approximation (RWA) limit

In this limit, the solution of the rotators in the bath is assumed highly diluted, the pressure and friction are very low. The coupling parameter B or the characteristic rotator-bath frequency is very small compared to the rotator lines $\omega_l = (\hbar l/I)$. The dynamics of the rotator is mainly governed by free rotations and interactions with the re-orienting fields. Bath coupling affects only the frequency shifts and line widths. The absorption lines are the neat spectral lines corresponding to the different l transitions owing to non negligible Planck constant $2\pi\hbar$ and finite inertia [20]. The transition frequencies are

$$\omega_{l->l\pm\Delta l} = \mid E_{l\pm\Delta l} - E_l \mid /\hbar = (2l + 1 + \Delta l)\hbar/2I$$

for transitions from l to $l\pm\Delta l$. At the level of linear response, $\Delta l = 1$ and $\omega_{l+1} = (l+1)\hbar/I$. For the lowest order nonlinear effect (the Kerr effect to the second order in electric field), $\Delta l = 2$ and $\omega_{2l+3} = (2l + 3)\hbar/I$.

The relevant dielectric matrix elements are governed by the quantum HT equations for the electric susceptibility and the Kerr optical functions [1] (see Eqs.(3.8), (3.12), 3.46)-(3.48)):

$$\Big(\frac{\partial}{\partial t} - i(\omega_{l+1} + \Delta\omega_{l+1}) + \Gamma_{l+1}\Big)\sigma_{l,l+1}(t) = -i\frac{\mu E_a}{\hbar}(r + \cos\omega t)\Big(1 - e^{-\beta(E_{l+1}-E_l)}\Big), \tag{4.21}$$

$$\Big(\frac{\partial}{\partial t} + \gamma_l\Big)\varphi_{l,l}(t) = \frac{\mu E_a}{\hbar}(r + \cos\omega t)\left(\frac{2l-1}{2l+1} Im\sigma_{l,l+1}(t) - e^{\beta(E_l-E_{l-1})}\frac{2l+3}{2l+1} Im\sigma_{l-1,l}(t)(1-\delta_{l,0})\right), \tag{4.22}$$

$$\Big(\frac{\partial}{\partial t} - i(\omega_{2l+3} + \Delta\omega_{2l+3}) + \Gamma_{2l+3}\Big)\eta_{l,l+2}(t) = i\frac{\mu E_a}{\hbar}(r + \cos\omega t)\Big(e^{-\beta(E_{l+1}-E_l)}\sigma_{l+1,l+2}(t) - \sigma_{l,l+1}(t)\Big) - i\frac{\Delta\alpha E_a^2}{2\hbar}(r + \cos\omega t)^2\Big(1 - e^{-\beta(E_{l+2}-E_l)}\Big) \tag{4.23}$$

with $\sigma_{l,l+1}(0) = \varphi_{l,l}(0) = \eta_{l,l+2} = 0$. Here, we use the dimensionless line widths and frequency shifts of Eqs.(3.49) and (3.53). These functions well indicate how line widths and frequency shifts respond to changing physical parameters like inertia, friction and temperature, thus their utility in exploring the influence of the parameter variations on spectral lines. Note that, in our dimensionless frequency units, we define the quantum state frequency $\omega'_l = l$.

The electric susceptibility

We are interested in the steady state regime. On solving Eq.(4.21) for this, we get

$$\sigma^{st}_{l,l+1}(\omega,t) = (\mu E_a/\hbar)\Big(1 - \exp[-\frac{\hbar^2}{Ik_BT}(l+1)]\Big)\left\{\frac{r}{\omega_{l+1} + \Delta\omega_{l+1} + i\Gamma_{l+1}} + \frac{e^{i\omega t}}{2(\omega_{l+1} + \Delta\omega_{l+1} - \omega + i\Gamma_{l+1})} + \frac{e^{-i\omega t}}{2(\omega_{l+1} + \Delta\omega_{l+1} + \omega + i\Gamma_{l+1})}\right\}. \tag{4.24}$$

The polarisation is deduced as

$$P(\omega,t) = \frac{\mu^2 E_a}{3k_BT}\sum_{l=0}^{\infty}\Big(e^{-\beta E_l}-e^{-\beta E_{l+1}}\Big)\frac{l+1}{a}\Big(l+1+\Delta\omega'_{l+1}\Big)$$
$$\times\Bigg\{r\Big/\Big[\Big(l+1+\Delta\omega'_{l+1}\Big)^2+\Gamma'^2_{l+1}\Big]+\Bigg(\Big[\Big(l+1+\Delta\omega'_{l+1}\Big)^2-\omega'^2+\Gamma'^2_{l+1}\Big]\cos\omega t$$
$$+2\Gamma'_{l+1}\omega'\sin\omega t\Bigg)\Big/\Bigg(\Big[\Big(l+1+\Delta\omega'_{l+1}\Big)^2-\omega'^2+\Gamma'^2_{l+1}\Big]^2+4\omega'^2\Gamma'^2_{l+1}\Bigg)\Bigg\}. \quad (4.25)$$

These are the Van Vleck-Weisskopf line forms for the electric susceptibility for which sharp separate lines result for small widths at half heights Γ_{l+1}. For line coupling and subsequent line overlaps to be absent, thus, Γ_{l+1} should be small compared to line spacings which for the electric susceptibility stands at $\hbar/I$. Remark that the Boltzmann weight $e^{-\beta E_l}$ appearing in the last expression renders small quantum number transitions more probable. An appropriate Taylor expansion of the Bose-Einstein factor appearing in the expression of the half width shows that a necessary condition for dominant separate lines is expressed by the inequality $(B/\omega_{mean})^2 << a^3/4 = (\hbar^2/Ik_BT)^3/4$.

For $r = 0$, we define the reduced susceptibility

$$\chi_r(\omega,t) = \cos\Big(\omega t-\alpha(\omega)\Big) \quad (4.26)$$

where $\alpha(\omega)$, the phase difference between the exciting field and the induced polarisation, is given by

$$\tan\alpha(\omega) = \Bigg[\sum_{l=0}^{\infty}\Big(e^{-\beta E_l}-e^{-\beta E_{l+1}}\Big)(l+1)\Big(l+1+\Delta\omega'_{l+1}\Big)\Gamma'_{l+1}\omega'\Big/$$
$$\Bigg(\Big[\Big(l+1+\Delta\omega'_{l+1}\Big)^2-\omega'^2+\Gamma'^2_{l+1}\Big]^2+4\omega'^2\Gamma'^2_{l+1}\Bigg)\Bigg]\Big/$$
$$\Bigg[\sum_{l=0}^{\infty}\Big(e^{-\beta E_l}-e^{-\beta E_{l+1}}\Big)(l+1)\Big(l+1+\Delta\omega'_{l+1}\Big)\Big(\Big(l+1+\Delta\omega'_{l+1}\Big)^2$$
$$-\omega'^2+\Gamma'^2_{l+1}\Big)\Big/\Bigg(\Big[\Big(l+1+\Delta\omega'_{l+1}\Big)^2-\omega'^2+\Gamma'^2_{l+1}\Big]^2+4\omega'^2\Gamma'^2_{l+1}\Bigg)\Bigg]. \quad (4.27)$$

Note that for usual temperatures and simple linear molecules like HCl and DCl [26, 27], the frequency shift has a negligible contribution as it varies as $\Delta\omega'_{l+1} \sim -10^{-4}(2l+3)$ compared to the corresponding line $l+1$.

The Kerr function

On using the expression for $\sigma^{st}_{l,l+1}(\omega,t)$ (Eq.(4.24)) into Eqs.(4.22) and (4.23) and solving the resulting equations for the steady state matrix elements $\varphi^{st}_{l,l}(\omega,t)$ and $\eta^{st}_{l,l+2}(\omega,t)$, we deduce that the Kerr function comprises three terms: a frequency dependent time constant term $\Phi_0(\omega)$, an $\omega-$frequency time dependent term $\Phi_1(\omega)e^{i\omega t}$ and a $2\omega-$ frequency time dependent one $\Phi_2(\omega)e^{2i\omega t}$ with their respective complex conjugates. In other words,

$$\Phi(\omega,t) = \Phi_0(\omega)+\Phi_1(\omega)e^{i\omega t}+\Phi_2(\omega)e^{2i\omega t}+C.C., \quad (4.28)$$

where $\Phi_0(\omega)$, $\Phi_1(\omega)$ and $\Phi_2(\omega)$ are explicitly written out in appendix B.3.

Relation (4.28) shows how frequency-time dependent Kerr optical function depends on field parameters like frequency and field strengths, on the molecular parameters like moment of inertia, dipole moment and polarisability, on the bath frictional parameter and on the temperature. Despite the fact that these results have been obtained in the limit of small coupling parameter B, they can still be used as first approximation to interpret experimental results on dense bath but at very low temperatures. We point out again that, unlike earlier works on electric susceptibility which have always considered that observed spectra are mainly accounted for by transitions involving $\Delta l = \pm 1$, these results on the Kerr optical effect predict, not only $\Delta l = \pm 1$ transitions, but also those with $\Delta l = \pm 2$.

4.3 Discussions

1) In constant temperature conditions, the response of a dielectric material to a low frequency external ac field is strong and is in phase with the latter for low frictional oscillator-bath and /or large inertia molecules ($\gamma = 0.5$ in Figure 4.1). From the energetic point of view, this in-phase aspect favours the external field effect on the rotator-bath system and thus increases the system's ability to capture energy from the surrounding. On the other hand, a totally different phenomenon is observed for high frequencies where a weak response sets in, tending to annihilate the field effect by appearing in anti-phase with it (Figure 4.2). The first convergent of the classical susceptibility function corresponding to the Rocard result (the first approximation of the inertia effect) gives a maximum phase for a frequency of $\omega = \sqrt{2}\omega_{mean}$ whatever the γ value. At this frequency value collisions result to large energy exchanges of the order of k_BT. For higher γ values, there is a departure from this frequency value (see Figure 4.4).
2) The manifestation of quantum effects depends, not only on the coupling parameter ($B = \zeta/I$) but also on the temperature-inertia parameter $a = \hbar^2/(Ik_BT)$. This allows us to define a necessary condition for the domination of quantum effects. The inequality

$$s = B/\omega_{mean} = 1/\sqrt{\gamma} << \frac{1}{2}\left(\hbar^2/Ik_BT\right)^{3/2} = a^{3/2}/2 \tag{4.29}$$

expresses this condition. For example, for $a = 0.05$, as the parameter s decreases from 0.025 through 0.010 to 0.001, we observe a passage from a continuous classical spectrum through broadened lines to well defined discrete lines (Figure 4.5) meanwhile for $a = .5$ quantum effects are already present even for $s = .08$ (see Figure 4.6). This observation is also important for the Kerr spectra (see Figure 4.14). In the previous chapter[1], we had already remarked that, as the coupling parameter $s = B/\omega_{mean}$ decreases under fixed a, a transition from the usual continuous classical spectrum through broadened lines to separate line-forms was observed. This phenomenon was also observed experimentally by Frenkel [16] on HCl in argon while varying argon density at very low temperatures. A recent experimental study of the linear and nonlinear dielectric spectra of 4, 4'-n-pentyl-cyanobiphenyl (5CB) was undertaken by De Smet et al. [28]. But the study concerned large molecules at room temperatures. This limited the interpretation of the results in the framework of classical theories well predicted by Coffey et al. [18] and Alexiewicz et al. [29].
3) The time variation of the classical Kerr electric birefringence (KEB) is characterised by oscillations about $\tau - \omega$ dependent time constant values which decrease with decreasing τ and

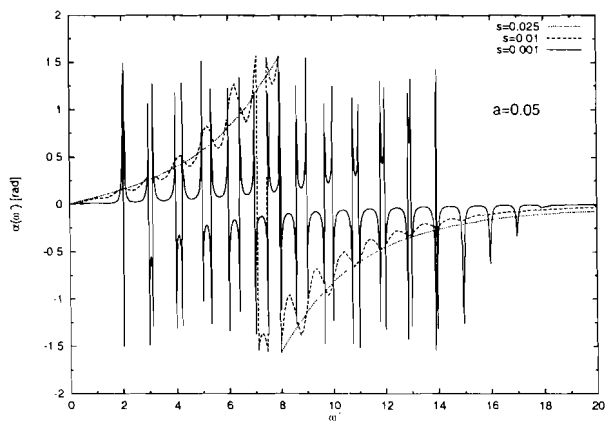

Figure 4.5:
Plots of the phase difference $\alpha(\omega')$ (in rad) between the ac field and response function against the dimensionless frequency $\omega' = \omega/(\omega_q)$ for the ratio $a = (\omega_q/\omega_{mean})^2 = 0.05$ ($\omega_q = \hbar/I$) for the friction parameter $s = 1/\sqrt{\gamma} = 0.025$ (···), $s = 0.01$ (---) and $s = 0.001$ (—) (RWA).

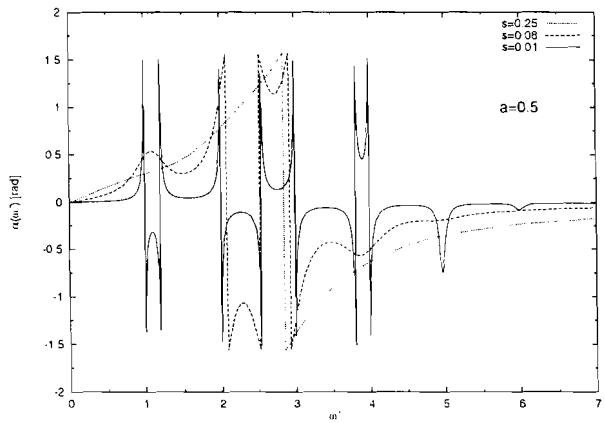

Figure 4.6:
Plots of the phase difference $\alpha(\omega')$ (in rad) between the ac field and response function against the dimensionless frequency $\omega' = \omega/\omega_q$ for the ratio $a = (\omega_q/\omega_{mean})^2 = 0.5$ ($\omega_q = \hbar/I$) for the friction parameter $s = 1/\sqrt{\gamma} = 0.25$ (···), $s = 0.08$ (---) and $s = 0.01$ (—) (RWA).

with increasing frequency. The 2ω-harmonic component is dominant for small r and large α values while the single ω one dominates for intermediate and higher r values (see Figures 4.7-4.9). Physically, the doubling of period takes place by a process of progressive crushing of intermediate peak values in the KEB curve shape with increasing r. This period change is noticed by a set of pronounced transitions of non sinusoidal periodic regimes which takes place between two sinusoidal regime limits corresponding to the extreme r values ($E_a << E_c$ and $E_a >> E_c$).

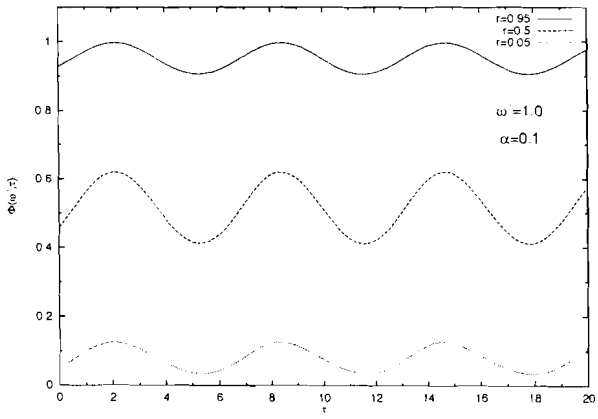

Figure 4.7:
Plots of the classical Kerr function against the reduced time $\tau = Bt$ for the field ratio $r = 0.95$ (—), $r = 0.5$ (---) and $r = 0.05$ (···), provided $\omega/B = 1.0$, $\gamma = 0.05$ and the polarisability/permanent dipole moment parameter $\alpha = 0.1$ ($\alpha = \Delta\alpha/k_BT/\left((\mu/k_BT)^2 + \Delta\alpha/k_BT\right)$).

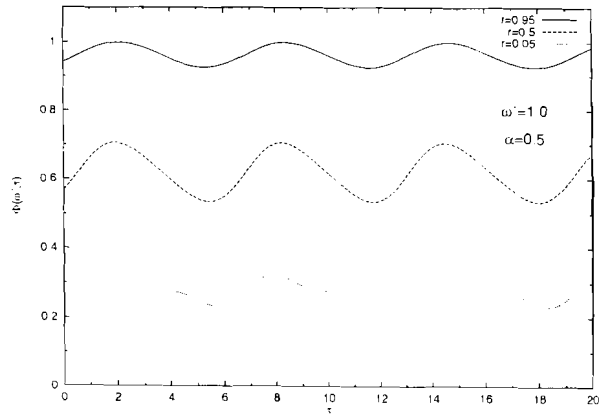

Figure 4.8:
Plots of the classical Kerr function against the reduced time $\tau = Bt$ for the field ratio $r = 0.95$ (—), $r = 0.5$ (---) and $r = 0.05$ (···). provided $\omega/B = 1.0$, $\gamma = 0.05$ and $\alpha = 0.5$.

4) For constant bath parameters and for small and intermediate E_c/E_a ratio, the Kerr effect

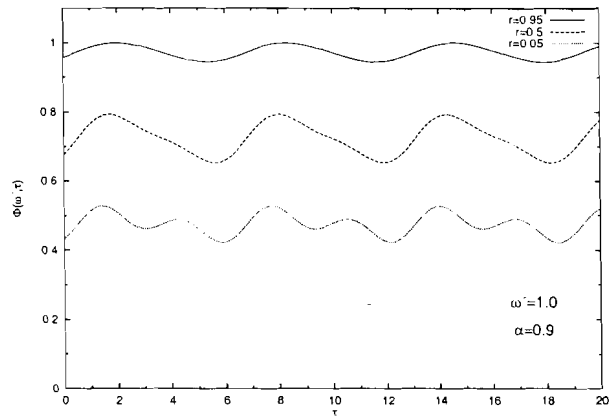

Figure 4.9:
Plots of the classical Kerr function against the reduced time $\tau = Bt$ for the field ratio $r = 0.95$ (—), $r = 0.5$ (---) and $r = 0.05$ (····), provided $\omega/B = 1.0$, $\gamma = 0.05$ and $\alpha = 0.9$.

increases with increasing α, presenting small amplitude distortions that disappear to form secondary peaks as α grows, portraying the progressive appearance of the 2ω-harmonic component (See Figures 4.10-4.12).

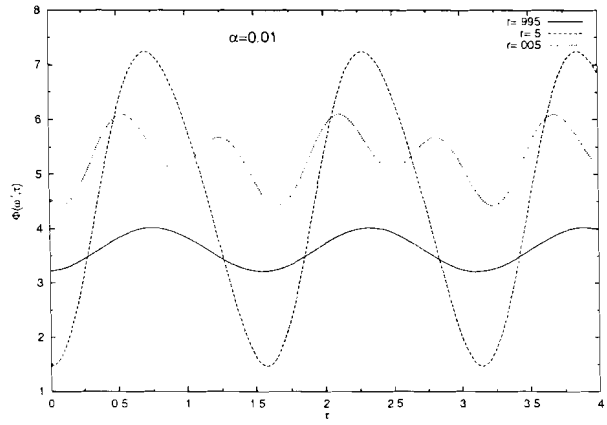

Figure 4.10:
Plots of the quantum Kerr function $\Phi(\omega, t)$ against the dimensionless time $\tau = t/(\hbar/I)$ for the field ratio $r = 0.995$ (—), $r = 0.5$ (- --) and $r = 0.005$ (····), provided $\omega = \hbar/I$, $\alpha = 0.1$, $a = 0.05$ and $s = 0.01$.

5) The Kerr spectral function for ac-dc coupling is

$$\begin{aligned}\tilde{\Phi}(\omega,\Omega) &= \Big[2Re\Phi_0(\omega)\delta(\Omega) + \Phi_1(\omega)\delta(\Omega-\omega) + \Phi_1^*(\omega)\delta(\Omega+\omega) \\ &\quad +\Phi_2(\omega)\delta(\Omega-2\omega) + \Phi_2^*(\omega)\delta(\Omega+2\omega)\Big]. \end{aligned} \tag{4.30}$$

This shows that for an ac field of given frequency, all three terms cannot be measured simultaneously. The ac-dc field coupling on dielectrics, therefore, proves to be very useful as,

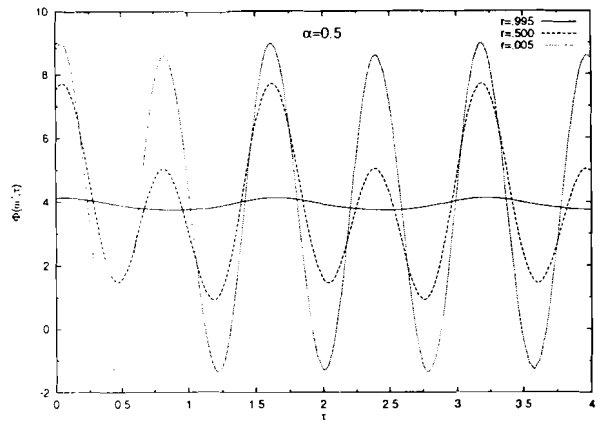

Figure 4.11:
Plots of the quantum Kerr function $\Phi(\omega, t)$ against the dimensionless time $\tau = t/(\hbar/I)$ for the field ratio $r = 0.995$ (—), $r = 0.5$ (---) and $r = 0.005$ (····), provided $\omega = \hbar/I$, $\alpha = 0.5$, $a = 0.05$ and $s = 0.01$.

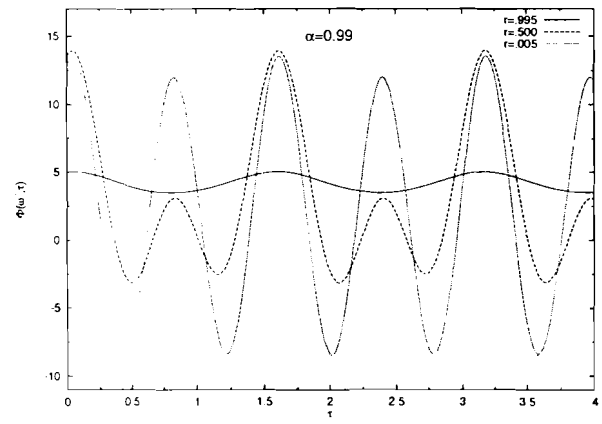

Figure 4.12:
Plots of the quantum Kerr function $\Phi(\omega, t)$ against the dimensionless time $t' = t/(\hbar/I)$ for the field ratio $r = 0.995$ (—), $r = 0.5$ (---) and $r = 0.005$ (····), provided $\omega = 4\hbar/I$, $\alpha = 0.99$, $a = 0.05$ and $s = 0.01$.

depending on the harmonic component observed, we are able to predict the relative strengths of permanent dipole to induced dipole effects. The 2ω-component dominates for polarisable fluids (large α) while the ω-one dominates for less polarisable (but polar) fluids (small α). More importantly, the observation of 2ω-harmonic component may also entail that the most probable rotational lines involve transitions like $l \rightarrow l \pm 2$ while the observation of ω harmonics concerns transitions $l \rightarrow l \pm 1$. This last point is very important when E_c and E_a are of the same order of magnitudes. The curves on figure 4.13 show the frequency dependence of the real parts of the ω and the $2\omega-$components of the quantum Kerr functions. While the $2\omega-$component is significant for relatively low frequencies, the $\omega-$component persists into high frequency regions.

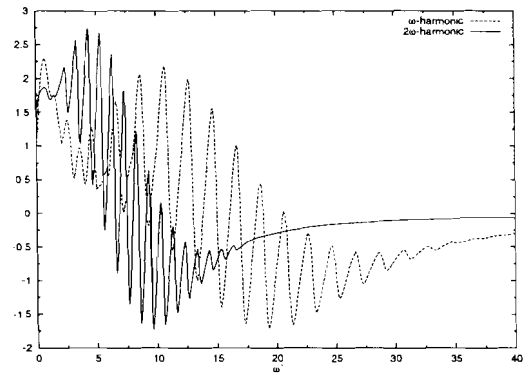

Figure 4.13:
Plot of the real part of the ω-harmonic component (---) and the 2ω-harmonic component (—) of the quantum Kerr function against the dimensionless frequency $\omega/(\hbar/I)$ for $a = 0.05$, $s = 0.01$, $\alpha = 0.4$ and $r = 0.5$).

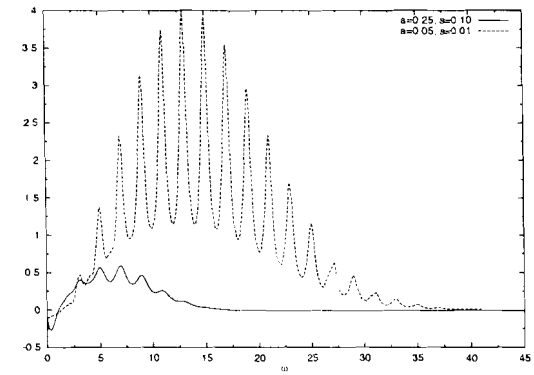

Figure 4.14:
Plot of the imaginary part of the ω-harmonic component of the quantum Kerr function against the dimensionless frequency $\omega/(\hbar/I)$ for: $a = 0.25$, $s = 1/\sqrt{\gamma} = 0.10$ (---) and $a = 0.05$, $s = 0.01$ (—), provided the friction parameter $s = 1/\sqrt{\gamma} = 0.01$ and the polarisability-dipole moment parameter $\alpha = 0.4$ and $r = 0.5$

Bibliography

[1] J. T. Titantah and M. N. Hounkonnou, *J. Phys. A* **30**: 6347, 1997

[2] P. Navez and M. N. Hounkonnou, *J. Phys. A: Math. Gen.* **28**: 6345, 1995

[3] A. Morita, *J. Phys. D* **11** L9: 4708, 1978

[4] A. Morita and H. Watanabe, *J. Chem. Phys.* **70**: 4708, 1979

[5] M. Matsumoto, H. Watanabe and K. Yoshioka, *J. Phys. Chem.* **74**: 2182, 1970

[6] W. T Coffey, *J. Chem. Phys.* **93**: 724, 1990

[7] W. T. Coffey, *J. Chem. Phys.* **95**: 2026, 1991

[8] J. T. Titantah and M. N. Hounkonnou, *J. Phys. A: Math. Gen.* **32**: 897, 1999

[9] J. Mc Connel, *Rotational Brownian motion and Dielectric Theory* (New York: Academic), 1980

[10] K. Lindenberg and B. J. West, *The Non Equilibrium Statistical Mechanics of Open and Closed systems* (New York:VCH), 1991

[11] A. Morita, *J. Chem. Phys.* **76**: 3198, 1982

[12] M. N. Hounkonnou, A. Ronveaux and P. Navez, *J. Phys. A* **27**: 6635, 1994

[13] P. Navez and M. N. Hounkonnou, *J. Phys. A: Math. Gen.* **27**: 6657, 1994

[14] M. N. Hounkonnou, A. Ronveaux and R. P. Hazoumé, *Physica* **179**: 569, 1991

[15] M. N. Hounkonnou, *J. Chem. Soc. Faraday Trans.* **87**: 297, 1991

[16] M. N. Hounkonnou and A. Ronveaux, *Acta. Phys.* **82**: 425, 1992

[17] J. C. Filippini, Ph.D Thesis, Université de Grenoble France, 1972

[18] W. T. Coffey and B. V. Paranjape, *Proc. R. Ir. Acad.* **78**: 17, 1978

[19] A. Morita andH. Watanabe, *Phys. Rev. E* **35**: 2690, 1987

[20] E. P. Gross, *J. Chem. Phys.* **23**: 1415, 1955

[21] J. T. Titantah and M. N. Hounkonnou, *J. Phys. A: Math. Gen.* **30**: 6327, 1997

[22] P. Navez, Thèse de Doctorat ès Sciences, Université Catholique de Louvain Belgium. 1997

[23] J. L. Déjardin, P. M. Déjardin and Yu. P. Kalmykov, *J. Chem Phys* **106** (4): 5824. 1996

[24] J. L. Déjardin, P. M. Déjardin and P. Yu. Kalmykov, *J. Chem. Phys.* **107** (2): 508, 1997

[25] W. T. Coffey, J. L. Déjardin and Yu. P. Kalmykov, *Phys. Rev. E* **54** (6): 6462, 1996

[26] A. Morita, S. Walker and J. H. Calderwood, *J. Phys. D: App.Phys.* **9**: 2485, 1976

[27] B. Stark, *Atomic and Molecular Constants from Microscopic Spectroscopy* (Berlin: Springer-Verlag), 1967

[28] K. De Smet, L. Hellemans, J. F. Rouleau and T. K. Bose, *Phys. Rev. E* **57** (2): 1384, 1998

[29] W. Alexiewicz and B. Kasprovicz-Kielich, *Modern Nonlinear Optics*, Part I, edited by M. Evans and S. Kielich (Wiley, New York), Vol 85, 1993

Conclusions and Perspectives of Part I

By exploiting the projection operator technique, we have derived a master equation for the probability density operator of a rotator embedded in a sea of bath harmonic oscillators. The effect of the bath on the rotator has been reduced to that of its concentration and temperature. The derivation of this equation is in line with the spirit of kinetic equation method. Depending on the strength of the rotator bath coupling with respect to thermal effects, two physical limits have been shown to follow naturally - the classical Brownian limit and the Rotating Wave Approximation limit.

Using the master equation, we have successfully studied the electric susceptibility and the Kerr function in both relaxation and "build-up" regimes. We have recovered widely published classical results on both dielectric properties. Our quantal results, though obtained as perturbative expansions around isolated spectral lines, adequately retrieve some of the published quantum results. The general features of our quantum results are very much like those of the Rosenkranz van Vleck-Weisskopf line forms. We have pointed out clearly how line widths and shifts depend on bath and rotator characteristics.

The effect of line coupling on the electric susceptibility and the Kerr effect appears through line mixing. This line mixing accentuates for the Kerr "build-up" with respect to susceptibility and Kerr relaxation as a result of the coupling of dipole moment transition matrix elements in the Kerr transition matrix, thus demonstrating that Kerr "build-up" mechanism differs greatly from Kerr relaxation mechanism.

A condition for dominant quantum effects on the dispersion and absorption spectra has been expressed by the inequality $\zeta << \frac{\hbar^3}{Ik_BT}$, which is usually verified for small molecules at low temperatures and/or low bath concentration or pressure. This condition is rarely verified by macromolecules (characterised by very large I), thus explaining why most experimental spectral results on systems composed of such molecules in usual polar solvents are adequately explained by even non inertial classical theories like the Debye theory.

By considering the steady state dielectric properties of a polar/polarisable fluid in ac/dc field coupling, we have stressed on the relative importance of permanent dipole to induced dipole moment effects on the Kerr electric birefringence. We have shown that, while the ω-harmonics are inherent of polar molecules, the observation of 2ω ones are a consequence of dominating induced polarisation. We have also discussed that line coupling becomes important when there is a competing tendency between permanent and induced dipole moments. Therefore, in strong fields it is most likely that line coupling becomes very severe.

One aspect that has not been addressed so far is that of collision/radiation coupling. Remark that on deriving the master equation (Eq.(1.32)) we quenched the field $E(t)$. In reality, $E(t)$

should be included in the dynamic equation so that we arrive at an equation of the form:

$$\frac{\partial \hat{\rho}_S(t)}{\partial t} + i\hat{L}_S\hat{\rho}_S(t) + i\hat{L}_E\hat{\rho}_S(t) = tr_B\left[\int_0^t d\tau i\hat{L}\hat{P}e^{-i\hat{L}(t-\tau)}\hat{P}'i\hat{L}e^{-i\hat{L}(t-\tau)}\hat{\rho}_S(t)\right] \qquad \text{(CI.1)},$$

where $\hat{L} = \hat{L}_S + \hat{L}_B + \hat{L}_{SB} + \hat{L}_E$. In this way, we are inevitably faced with collision/radiation coupling. Such a coupling should lead to radiation frequency dependent line widths and shifts. A possible extension of this work could be to incorporate this latter physically relevant situation into the dynamical equations.

Through out this part of the thesis, the calculation of the electric susceptibility has not exceeded the linear response limit valid for weak fields though the HT master equation (Eq.(3.13)) is capable of yielding higher order results. By defining new matrix elements $\pi_{l,l}(t)$ as

$$\sum_{m=-l}^{l}\left((\rho_S^{eq})_{l,l}^{m}\right)^{-1}\langle l,m|\rho(t)|l,m\rangle \equiv (2l+1)\left(1+\frac{1}{15}\pi_{l,l}(t)\right), \qquad \text{(CI.2)}$$

we can show that relevant polarisation related functions $\sigma_1(x,\tau)$ and $\sigma_2(x,\tau)$ (up to 3rd order in field strength), and $\pi(x,\tau)$ verify the equations:

$$\left[\frac{\partial}{\partial\tau} - 2\left(x\frac{\partial^2}{\partial x^2} + (1-x)\frac{\partial}{\partial x}\right)\right]\sigma_1(x,\tau) + \tau_D^{-1}x\frac{\partial}{\partial x}\sigma_2(x,\tau) = \frac{2}{5}\tau_D^{-1}\frac{\mu E(\tau)}{k_BT}$$
$$\times\left(x\frac{\partial}{\partial x} - x + 1\right)\eta_2(x,\tau) - \frac{1}{5}\tau_D^{-1}\frac{\Delta\alpha E(\tau)^2}{k_BT}\left(x\frac{\partial}{\partial x} - x + 1\right)\sigma_2(x,\tau), \qquad \text{(CI.3)}$$

$$\left[\frac{\partial}{\partial\tau} - 2\left(x\frac{\partial^2}{\partial x^2} + (2-x)\frac{\partial}{\partial x} - \frac{1}{2}\right)\right]\sigma_2(x,\tau) - B^{-1}\sigma_1(x,\tau) + B^{-1}\frac{\mu E(\tau)}{k_BT} = \frac{8}{15}\frac{\mu E(\tau)}{k_BT}$$
$$\times\left(\frac{\partial}{\partial x} - 1\right)\left[\pi(x,\tau) + \varphi(x,\tau)\right], \qquad \text{(CI.4)}$$

$$\left[\frac{\partial}{\partial\tau} - 2\left(x\frac{\partial^2}{\partial x^2} + (1-x)\frac{\partial}{\partial x}\right)\right]\pi(x,\tau) = 5\tau_D^{-1}\frac{\mu E(\tau)}{k_BT}\left(x\frac{\partial}{\partial x} - x + 1\right)\sigma_2(x,\tau), \qquad \text{(CI.5)}$$

where $\tau_D = \frac{\zeta}{2k_BT}$ is the Debye relaxation time and $B = \zeta/I$. The change of functions $\sigma_2 = \sigma_2$(of this thesis)$\times I/\hbar$, $\eta_2 = \eta_2$(of this thesis)$\times I/\hbar$, have been made to obtain the above system and the equations for η_1, η_2 and φ result from those used so far in this thesis.

The effect of strong field on quantum electric susceptibility can be investigated by truncating Eq.(3.13) to third order in field strength and applying the Rotating Wave Approximation criterion.

If the rotator is magnetically active (having a permanent magnetic dipole moment or easily polarisable), radiation is likely to result to electromagnetic interactions. There is therefore a possibility to include electromagnetic interactions in the analysis of electro-optical properties of such materials.

Appendix A

A.1 The initial condition on $\hat{\rho}_S(t)$

$$\hat{\rho}_S(t=0) = \frac{1}{tr_S tr_B e^{-\beta(\hat{H}+\hat{H}_E)}} tr_B e^{-\beta(\hat{H}+\hat{H}_E)}. \tag{A.1}$$

Let

$$\hat{Y}(\beta) = e^{-\beta(\hat{H}+\hat{H}_E)}, \tag{A.2}$$

then

$$\frac{d}{d\beta}\hat{Y}(\beta) = -\hat{Y}(\beta)\hat{H} - \hat{Y}(\beta)\hat{H}_E \tag{A.3}$$

with solution

$$\hat{Y}(\beta) = \hat{A}(\beta)e^{-\beta\hat{H}} \tag{A.4}$$

and

$$\hat{A}(\beta) = 1 - \int_0^1 d\alpha \hat{Y}(\alpha\beta)\beta\hat{H}_E e^{\alpha\beta\hat{H}}. \tag{A.5}$$

After performing similar expansion for $e^{-\beta\hat{H}} = e^{-\beta(\hat{H}_0+\hat{H}_{SB})}$, for small $\beta\hat{H}_{SB}$ and taking trace over bath variables ($\hat{H}_0 = \hat{H}_S + \hat{H}_B$), we obtain, to second order in $\beta\hat{H}_E$ that:

$$\hat{\rho}_S(t=0) = \frac{e^{-\beta\hat{H}_S}}{tr_S e^{-\beta\hat{H}_S}} - \frac{\beta}{tr_S e^{-\beta\hat{H}_S}} \int_0^1 d\alpha e^{-\alpha\beta\hat{H}_S}\hat{H}_E e^{-(1-\alpha)\beta\hat{H}_S} + \frac{\beta^2}{tr_S e^{-\beta\hat{H}_S}} \int_0^1 d\alpha\alpha \times \int_0^1 d\alpha' e^{-(1-\alpha')\alpha\beta\hat{H}_S}\hat{H}_E e^{-\alpha'\alpha\beta\hat{H}_S}\hat{H}_E e^{-(1-\alpha)\beta\hat{H}_S} + ... \tag{A.6}$$

A.2 Sample property proof

We want to prove that

$$\sum_{m=-l}^{l} (l(l+1) - 3m^2) < l,m \mid \hat{\mathbf{u}}_l^+ \hat{\rho}_S(t)\hat{\mathbf{u}}_{l+1}^+ \mid l,m > = -3\varphi_{l-1,l+1}(t)(1-\delta_{l0}). \tag{A.7}$$

On using the spherical harmonic expansion for $\hat{\mathbf{u}}$ (Eq.(1.26)) and the fact that $\langle lm \mid l'm' \rangle =$

$\delta_{ll'}\delta_{mm'}$, we get

$$\sum_{m=-l}^{l}(l(l+1)-3m^2)<l,m\mid\hat{\mathbf{u}}_l^+\hat{\rho}_S(t)\hat{\mathbf{u}}_{l+1}^+\mid l,m>$$
$$=\frac{1}{2}\sum_{m=-l}^{l}\sum_{m'=-l}^{l}\sum_{m''=-(l+1)}^{l+1}(l(l+1)-3m^2)\Big(-A(l,m')$$
$$\times B(l+1,m'')\hat{\rho}^{m'+1}_{l-1,l+1}(t)\delta_{m,m'}\delta_{m''+1,m}-B(l,m')A(l+1,m'')$$
$$\times\hat{\rho}^{m'-1}_{l-1,l+1}(t)\delta_{m,m'}\delta_{m''-1,m}+2C(l,m)C(l+1,m)\hat{\rho}^{m}_{l-1,l+1}(t)\delta_{m,m'}\delta_{m'',m}\Big)$$
$$\times(1-\delta_{l,0})=-3\sum_{m=-(l-1)}^{l-1}\left[\frac{(l-1-m)(l-1+m)(l+1-m)(l+1+m)}{(2l-1)(2l+1)^2(2l+3)}\right]^{\frac{1}{2}}$$
$$\times\hat{\rho}^{m}_{l-1,l+1}(t)(1-\delta_{l0})=-3\varphi_{l-1,l+1}(t)(1-\delta_{l0}),\qquad\text{(A.8)}$$

where $A(l,m)=\left[\frac{(l-m)(l-m-1)}{(2l-1)(2l+1)}\right]^{1/2}$, $B(l,m)=\left[\frac{(l+m)(l+m-1)}{(2l-1)(2l+1)}\right]^{1/2}$ and $C(l,m)=\left[\frac{(l-m)(l+m)}{(2l-1)(2l+1)}\right]^{1/2}$.

A.3 The initial condition on $\varphi_{l,l}(t)$

$$\varphi_{l,l}(t=0)=\sum_{l=-m}^{l}\Big(l(l+1)-3m^2\Big)<l,m\mid\hat{\rho}_S(t=0)\mid l,m>.\qquad\text{(A.9)}$$

On substituting $\hat{\rho}_S(t=0)$ (Eq.(A.6)) and using the properties

$$a)<l,m\mid e^{-\alpha\beta\hat{H}_S}\hat{H}_Ee^{-(1-\alpha)\beta\hat{H}_S}\mid l,m>=e^{-\beta E_l}<l,m\mid\beta\hat{H}_E\mid l,m>\qquad\text{(A.10)}$$

and

$$b)\quad<l,m\mid e^{-(1-\alpha')\alpha\beta\hat{H}_S}\beta\hat{H}_Ee^{-\alpha\alpha'\beta\hat{H}_S}\beta\hat{H}_Ee^{-(1-\alpha)\beta\hat{H}_S}\mid l,m>$$
$$=e^{-\beta E_l}\sum_{l'=0}^{\infty}\sum_{m'=-l'}^{l'}e^{-\alpha\alpha'\beta(E_{l'}-E_l)}\mid<l,m\mid\beta\hat{H}_E\mid l',m'>\mid^2\qquad\text{(A.11)}$$

we obtain after using the expression for $\hat{H}_E$ (Eq.(2.1)), that

$$\varphi_{l,l}(t=0)=\frac{1}{\sum_{l'=0}^{\infty}(2l'+1)e^{-\beta E_{l'}}}\sum_{m=-l}^{l}\Big(l(l+1)-3m^2\Big)e^{-\beta E_l}$$
$$\times\Big[1+\frac{\beta\alpha_\perp}{2}E^2+<l,m\mid\cos^2\beta\mid l,m>\frac{\beta\Delta\alpha}{2}E^2$$
$$+\beta^2\mu^2E^2\sum_{l''=0}^{\infty}\sum_{m''=-l''}^{l''}\mid<l,m\mid\cos\beta\mid l'',m''>\mid^2$$
$$\times\int_0^1d\alpha\alpha\int_0^1d\alpha'e^{-\alpha\alpha'\beta(E_{l''}-E_l)}\Big].\qquad\text{(A.12)}$$

This leads to the required expression when the expansion of $\cos\beta$ in the spherical harmonic basis is used.

Appendix B

B.1 Systems of hierarchies for $Y^m_{j,l}$ and $X_{j,l}$

Triplet 1.

$$
\begin{aligned}
&2jY^0_{j,0}(\omega') + 24b_2\Big((j+1)Y^1_{j,0}(\omega') - jY^1_{j-1,0}(\omega')\Big) = -2b_2S^1_{j-1}(\omega')(1-\delta_{j,0}),\\
&(2j+1)Y^1_{j,0}(\omega') - \frac{b_1}{3}\Big(Y^0_{j,0}(\omega') - Y^0_{j+1,0}(\omega')\Big) + \frac{b_1}{3}\Big(X_{j,0}(\omega') - X_{j+1,0}(\omega')\Big)\\
&= -\frac{b_1}{4}\Big[(2r^2 + 2r^2/R + 1/R)\delta_{j,0} + 2S^0_j(\omega')\Big],\\
&\Big[2j(2j+1)+2\Big]X_{j,0}(\omega') - j(2j-2)X_{j-1,0}(\omega) - (j+1)(2j+2)\Big)X_{j+1,0}(\omega')\\
&-1/2Y^0_{j,0}(\omega') = \frac{b_2}{2}\Big[-2j(j-1)S^1_{j-2}(\omega') + j(4j+5)S^1_{j-1}(\omega')\\
&-(j+1)(2j+3)S^1_j(\omega')\Big];
\end{aligned}
\tag{B.1}
$$

Triplet 2.

$$
\begin{aligned}
&\Big(i\omega' + 2j\Big)Y^0_{j,1}(\omega') + 24b_2\Big((j+1)Y^1_{j,1}(\omega') - jY^1_{j-1,1}(\omega')\Big)\\
&= -4rb_2S^1_{j-1}(\omega')(1-\delta_{j,0}),\\
&\Big(i\omega' + 2j + 1\Big)Y^1_{j,1}(\omega') - \frac{b_1}{3}\Big(Y^0_{j,1}(\omega') - Y^0_{j+1,1}(\omega')\Big)\\
&+\frac{b_1}{3}\Big(X_{j,1}(\omega') - X_{j+1,1}(\omega')\Big) = -r\frac{b_1}{4}\Big[(2+4/R)\delta_{j,0} + 4S^0_j\Big],\\
&\Big[(2j+1)\Big(i\omega' + 2j\Big) + 2\Big]X_{j,1}(\omega') - j\Big(i\omega' + 2j - 2\Big)X_{j-1,1}(\omega')\\
&-(j+1)\Big(i\omega' + 2j + 2\Big)X_{j+1,1}(\omega') - (1/2)Y^0_{j,1}(\omega') = b_2r\Big[-2j(j-1)S^1_{j-2}(\omega')\\
&+j(4j+5)S^1_{j-1}(\omega') - (j+1)(2j+3)S^1_j(\omega')\Big]
\end{aligned}
\tag{B.2}
$$

and

Triplet 3.

$$
\begin{aligned}
&\Big(2i\omega' + 2j\Big)Y^0_{j,2}(\omega') + 24b_2\Big((j+1)Y^1_{j,2}(\omega') - jY^1_{j-1,2}(\omega')\Big)\\
&= -2b_2S^1_{j-1}(\omega')(1-\delta_{j,0}),\\
&\Big(2i\omega' + 2j + 1\Big)Y^1_{j,2}(\omega') - \frac{b_1}{3}\Big(Y^0_{j,2}(\omega') - Y^0_{j+1,2}(\omega')\Big) +
\end{aligned}
$$

$$
\begin{aligned}
&+\frac{b_1}{3}\big(X_{j,2}(\omega') - X_{j+1,2}(\omega')\big) = -\frac{b_1}{4}\Big[\frac{1}{R}\delta_{j,0} + 2S_j^0\Big],\\
&\Big[(2j+1)\big(2i\omega' + 2j\big) + 2\Big]X_{j,2}(\omega') - j\big(2i\omega' + 2j - 2\big)X_{j-1,2}(\omega')\\
&-(j+1)\big(2i\omega' + 2j + 2\big)X_{j+1,2}(\omega') - \frac{1}{2}Y_{j,2}^0(\omega') = \frac{b_2}{2}\Big[-2j(j-1)S_{j-2}^1(\omega')\\
&+j(4j+5)S_{j-1}^1(\omega') - (j+1)(2j+3)S_j^1(\omega')\Big],
\end{aligned}
\tag{B.3}
$$

where $R = \mu^2/(\Delta\alpha k_B T)$. For simplicity, we have left out the primes on each S_j^m. i denotes the complex number $\sqrt{-1}$.

B.2 Expressions for $Y_{0,0}^0$, $Y_{0,1}^0$ and $Y_{0,2}^0$

$$
\begin{aligned}
Y_{0,0}^0(\omega') = \quad & \frac{1}{2}(\alpha + 2r - \alpha r) + (1-\alpha)(1-r)\Bigg\{(1 - \frac{i\omega'}{2})\\
&+\frac{2i\omega'}{3(2+5\gamma)}\Bigg[2 - \gamma - \cfrac{8\gamma}{2 + i\omega' + \cfrac{4\gamma}{3 + i\omega' + \cfrac{4\gamma}{4 + i\omega' + \ldots}}}\\
&+\cfrac{4\gamma^2/3}{4\gamma + (2+i\omega')\Big(3 + i\omega' + \cfrac{4\gamma}{4 + i\omega' + \cfrac{6\gamma}{5 + i\omega' + \cfrac{6\gamma}{6 + i\omega' + \ldots}}}\Big)}\Bigg]\Bigg\}\\
&\times\cfrac{\gamma}{2\gamma + i\omega'\Big(1 + i\omega' + \cfrac{2\gamma}{2 + i\omega' + \cfrac{4\gamma}{3 + i\omega' + \cfrac{4\gamma}{4 + i\omega' + \ldots}}}\Big)} +\\
&+\frac{64}{9}\frac{\gamma}{2+5\gamma}Y_{2,0}^0(\omega'),
\end{aligned}
\tag{B.4}
$$

$$
\begin{aligned}
Y_{0,1}^0(\omega') = \quad & \sqrt{r(1-r)}\Bigg\{(1 + 2/R)\frac{6\gamma(1+\alpha)}{1+i\omega'}\Big(2 + i\omega' + 4\gamma\frac{15 + 4i\omega'}{(3+i\omega')(4+i\omega')}\Big)\\
+\ & (1-\alpha)\Bigg[\frac{24\gamma}{(1+i\omega')(2+i\omega')}\Big(2 + i\omega' + 4\gamma\frac{15 + 4i\omega'}{(3+i\omega')(4+i\omega')}\Big)\\
+\ & \frac{8i\omega'\gamma}{1+i\omega'} - \frac{32i\omega'\gamma^2}{(1+i\omega')(3+i\omega')(4+i\omega')}\Bigg(\frac{6(1+i\omega')}{(2+i\omega')} -\\
-\ & \cfrac{4\gamma}{4\gamma + (2+i\omega')\Big(3 + i\omega' + \cfrac{4\gamma}{4 + i\omega' + \cfrac{6\gamma}{5 + i\omega' + \cfrac{6\gamma}{6 + i\omega' + \ldots}}}\Big)}\Bigg)
\end{aligned}
$$

$$
\begin{aligned}
&- \frac{192\gamma^2 i\omega'}{(1+i\omega')(3+i\omega')\Big(2+i\omega'+\dfrac{4\gamma}{3+i\omega'+\dfrac{4\gamma}{4+i\omega'+\dfrac{6\gamma}{5+i\omega'+\ldots}}}\Big)}\Bigg] \\
&\times \frac{\gamma}{2\gamma+i\omega'\Big(1+i\omega'+\dfrac{2\gamma}{2+i\omega'+\dfrac{4\gamma}{3+i\omega'+\dfrac{4\gamma}{4+i\omega'+\ldots}}}\Big)} + \\
&+ \frac{128\gamma^2/r}{3+i\omega'} Y^0_{2,1}(\omega')\Bigg\} \Big/ \Bigg\{ \Big(i\omega' + 4\gamma \frac{3+i\omega'}{(1+i\omega')(2+i\omega')}\Big)\Big(2+i\omega' \\
&+ 4\gamma \frac{15+4i\omega'}{(3+i\omega')(4+i\omega')}\Big) + \frac{8i\omega'\gamma}{1+i\omega'} \\
&- \frac{32i\omega'\gamma^2}{(1+i\omega')(2+i\omega')(3+i\omega')(4+i\omega')}\Bigg\},
\end{aligned}
\tag{B.5}
$$

$$
\begin{aligned}
Y^0_{0,2}(\omega') = \quad & (1-r)\Bigg\{ \frac{3\gamma\alpha}{1+2i\omega'}\Big(2+2i\omega'+4\gamma\frac{15+8i\omega'}{(3+2i\omega')(4+2i\omega')}\Big) \\
&+ (1-\alpha)\Bigg[6\gamma \frac{2+i\omega'}{(1+2i\omega')(2+2i\omega')}\Big(2+2i\omega'+4\gamma\frac{15+8i\omega'}{(3+2i\omega')(4+2i\omega')}\Big) \\
&+ \frac{8i\omega'\gamma}{1+2i\omega'} - \frac{96i\omega'\gamma^2}{(1+2i\omega')(3+2i\omega')\Big(2+i\omega'+\dfrac{4\gamma}{3+i\omega'+\dfrac{4\gamma}{4+i\omega'+\ldots}}\Big)} \\
&- 16i\omega'\gamma^2 \frac{\Big(3-\dfrac{4\gamma}{4\gamma+(2+i\omega')\Big(3+i\omega'+\dfrac{4\gamma}{4+i\omega'+\ldots}\Big)}+6i\omega'\Big)}{(1+2i\omega')(2+2i\omega')(3+2i\omega')(4+2i\omega')}\Bigg] \\
&\times \frac{\gamma}{2\gamma+i\omega'\Big(1+i\omega'+\dfrac{2\gamma}{2+i\omega'+\dfrac{4\gamma}{3+i\omega'+\dfrac{4\gamma}{4+i\omega'+\ldots}}}\Big)} \\
&+ \frac{128\gamma^2}{(1+2i\omega')(3+2i\omega')} Y^0_{2,2}(\omega')\Bigg\} \Big/ \Bigg\{ \Big[2i\omega' + 4\gamma \frac{3+4i\omega'}{(1+2i\omega')(2+2i\omega')}\Big] \\
&\times \Big[2+2i\omega'+4\gamma\frac{15+8i\omega'}{(3+2i\omega')(4+2i\omega')}\Big] + \\
&+ \frac{16i\omega'\gamma\Big((2+i\omega')(3+i\omega')(4+i\omega')-4\gamma\Big)}{(1+2i\omega')(2+2i\omega')(3+2i\omega')(4+2i\omega')}\Bigg\},
\end{aligned}
\tag{B.6}
$$

where $r = \frac{E_c^2}{E^2}$ with $E^2 = E_c^2 + E_a^2$ and $\alpha = \frac{\Delta\alpha/k_BT}{K_0}$ with $K_0 = \Delta\alpha/k_BT + (\mu/k_BT)^2$.

B.3 The dc, the ω and the 2ω components of the quantum Kerr function

$$
\begin{aligned}
\Phi_0(\omega') \;=\; & \frac{1}{60}E^2K_0\sum_{l=0}^{\infty}\frac{l+1}{a}\Bigg[(1-\alpha)\frac{l}{2l-1}\frac{1}{\gamma'_l}\Big(e^{-\beta E_{l-1}}-e^{-\beta E_l}\Big)\\
&\times\Bigg(2r\frac{\Gamma'_l+i(l+\Delta\omega'_l)}{(l+\Delta\omega'_l)^2+\Gamma'^2_l}+\frac{1}{2}(1-r)\frac{\Gamma'_l+i(l+\Delta\omega'_l-\omega')}{(l+\Delta\omega'_l-\omega')^2+\Gamma'^2_l}\Bigg)\\
&-\frac{l}{2l+3}(1-\alpha)\frac{1}{\gamma'_l}\Big(e^{-\beta E_l}-e^{-\beta E_{l+1}}\Big)\Bigg(2r\frac{\Gamma'_{l+1}+i(l+1+\Delta\omega'_{l+1})}{(l+1+\Delta\omega'_{l+1})^2+\Gamma'^2_{l+1}}\\
&+\frac{1}{2}(1-r)\frac{\Gamma'_{l+1}+i(l+1+\Delta\omega'_{l+1}-\omega')}{(l+1+\Delta\omega'_{l+1}-\omega')^2+\Gamma'^2_{l+1}}\Bigg)+\frac{3(l+2)}{2l+3}\frac{1}{(2l+3+\Delta\omega'_{2l+3})^2+\Gamma'^2_{2l+3}}\\
&\times\Bigg\{\Big(2l+3+\Delta\omega'_{2l+3}\Big)-i\Gamma'_{2l+3}\Big)\Bigg[\Big(e^{-\beta E_l}-e^{-\beta E_{l+1}}\Big)\\
&\times\Bigg(2r\frac{(l+1+\Delta\omega'_{l+1}-i\Gamma'_{l+1})}{(l+1+\Delta\omega'_{l+1})^2+\Gamma'^2_{l+1}}+\frac{1}{2}(1-r)\frac{(l+1+\Delta\omega'_{l+1}-\omega'-i\Gamma'_{l+1})}{(l+1+\Delta\omega'_{l+1}-\omega')^2+\Gamma'^2_{l+1}}\\
&+\frac{1}{2}(1-r)\frac{(l+1+\Delta\omega'_{l+1}+\omega'-i\Gamma'_{l+1})}{(l+1+\Delta\omega'_{l+1}+\omega')^2+\Gamma'^2_{l+1}}\Bigg)-\Big(e^{-\beta E_{l+1}}-e^{-\beta E_{l+2}}\Big)\\
&\times\Bigg(2r\frac{(l+2+\Delta\omega'_{l+2}-i\Gamma'_{l+2})}{(l+2+\Delta\omega'_{l+2})^2+\Gamma'^2_{l+2}}+\frac{1}{2}(1-r)\frac{(l+2+\Delta\omega'_{l+2}-\omega'-i\Gamma'_{l+2})}{(l+2+\Delta\omega'_{l+2}-\omega')^2+\Gamma'^2_{l+2}}\\
&+\frac{1}{2}(1-r)\frac{(l+2+\Delta\omega'_{l+2}+\omega'-i\Gamma'_{l+2})}{(l+2l+\Delta\omega'_{l+2}+\omega')^2+\Gamma'^2_{l+2}}\Bigg)\Bigg](1-\alpha)\\
&+\frac{\alpha}{2}\Big(e^{-\beta E_l}-e^{-\beta E_{l+2}}\Big)\Big(2l+3+\Delta\omega'_{2l+3}\Big)\Bigg\}\Bigg],
\end{aligned}
\tag{B.7}
$$

$$
\begin{aligned}
\Phi_1(\omega') \;=\; & \frac{\sqrt{r(1-r)}}{60}E^2K_0\sum_{l=0}^{\infty}\frac{l+1}{a}\Bigg[\frac{2(1-\alpha)(\gamma'_l-i\omega')}{\gamma'^2_l+\omega'^2}\Bigg\{\frac{l}{2l+3}\Big(e^{-\beta E_l}-e^{-\beta E_{l+1}}\Big)\\
&\times\Bigg(\frac{\Gamma'_{l+1}}{(l+1+\Delta\omega'_{l+1})^2+\Gamma'^2_{l+1}}+\frac{\Gamma'_{l+1}+i(l+1+\Delta\omega'_{l+1}+\omega')}{(l+1+\Delta\omega'_{l+1}+\omega')^2+\Gamma'^2_{l+1}}\\
&-\frac{\Gamma'_{l+1}+i(l+1+\Delta\omega'_{l+1}-\omega')}{(l+1+\Delta\omega'_{l+1}-\omega')^2+\Gamma'^2_{l+1}}\Bigg)-\frac{l}{2l-1}\Big(e^{-\beta E_{l-1}}-e^{-\beta E_l}\Big)\\
&\times\Bigg(\frac{\Gamma'_l}{(l+\Delta\omega'_l)^2+\Gamma'^2_l}+\frac{\Gamma'_l+i(l+\Delta\omega'_l+\omega')}{(l+\Delta\omega'_l+\omega')^2+\Gamma'^2_l}\\
&-\frac{\Gamma'_l+i(l+\Delta\omega'_l-\omega')}{(l+\Delta\omega'_l-\omega')^2+\Gamma'^2_l}\Bigg)\Bigg\}+\frac{3(l+2)}{2l+3}\times\\
&\times\frac{\Big(2l+3+\Delta\omega'_{2l+3}\Big)^2-\omega'^2-2i\omega'\Gamma'_{2l+3}}{\Big[(2l+3+\Delta\omega'_{2l+3})^2-\omega'^2+\Gamma'^2_{2l+3}\Big]^2+4\omega'^2\Gamma'^2_{2l+3}}\Bigg\{(1-\alpha)\Big(2l+3+\Delta\omega'_{2l+3}\\
&+\omega'-i\Gamma'_{2l+3}\Big)\Bigg[\Big(e^{-\beta E_l}-e^{-\beta E_{l+1}}\Big)\Bigg(\frac{l+1+\Delta\omega'_{l+1}-\omega'-i\Gamma'_{l+1}}{(l+1+\Delta\omega'_{l+1}-\omega')^2+\Gamma'^2_{l+1}}+
\end{aligned}
$$

$$
\begin{aligned}
&+\frac{l+1+\Delta\omega'_{l+1}-i\Gamma'_{l+1}-}{(l+1+\Delta\omega'_{l+1})^2+\Gamma'^2_{l+1}}\Big)-\Big(e^{-\beta E_{l+1}}-e^{-\beta E_{l+2}}\Big)\\
&\times\left(\frac{(l+2+\Delta\omega'_{l+2}-\omega'-i\Gamma'_{l+2})}{(l+2+\Delta\omega'_{l+2}-\omega')^2+\Gamma'^2_{l+2}}+\frac{l+2+\Delta\omega'_{l+2}-i\Gamma'_{l+2}}{(l+2+\Delta\omega'_{l+2})^2+\Gamma'^2_{l+2}}\right)\Bigg]\\
&+\Big(2l+3+\Delta\omega'_{2l+3}-\omega'+i\Gamma'_{2l+3}\Big)\Bigg[\Big(e^{-\beta E_l}-e^{-\beta E_{l+1}}\Big)\\
&\times\left(\frac{l+1+\Delta\omega'_{l+1}+\omega'+i\Gamma'_{l+1}}{(l+1+\Delta\omega'_{l+1}-\omega')^2+\Gamma'^2_{l+1}}+\frac{l+1+\Delta\omega'_{l+1}+i\Gamma'_{l+1}}{(l+1+\Delta\omega'_{l+1})^2+\Gamma'^2_{l+1}}\right)\\
&-\Big(e^{-\beta E_{l+1}}-e^{-\beta E_{l+2}}\Big)\left(\frac{l+2+\Delta\omega'_{l+2}+\omega'+i\Gamma'_{l+2}}{(l+2+\Delta\omega'_{l+2}-\omega')^2+\Gamma'^2_{l+2}}\right.\\
&\left.+\frac{l+2+\Delta\omega'_{l+2}+i\Gamma'_{l+2}}{(l+2+\Delta\omega'_{l+2})^2+\Gamma'^2_{l+2}}\right)\Bigg](1-\alpha)\\
&+\alpha(2l+3+\Delta\omega'_{2l+3})\Big(e^{-\beta E_l}-e^{-\beta E_{l+2}}\Big)\Bigg\}\Bigg],
\end{aligned}
\tag{B.8}
$$

$$
\begin{aligned}
\Phi_2(\omega') \;=\;& \frac{(1-r)}{60}E^2K_0\sum_{l=0}^{\infty}\frac{l+1}{a}\Bigg[\frac{2(1-\alpha)(\gamma'_l-2i\omega')}{\gamma'^2_l+4\omega'^2}\Bigg\{\frac{l}{2l+3}\Big(e^{-\beta E_l}-e^{-\beta E_{l+1}}\Big)\\
&\times\left(\frac{\Gamma'_{l+1}+i(l+1+\Delta\omega'_{l+1}+\omega')}{(l+1+\Delta\omega'_{l+1}+\omega')^2+\Gamma'^2_{l+1}}-\frac{\Gamma'_{l+1}+i(l+1+\Delta\omega'_{l+1}-\omega')}{(l+1+\Delta\omega'_{l+1}-\omega')^2+\Gamma'^2_{l+1}}\right)\\
&-\frac{l}{2l-1}\Big(e^{-\beta E_{l-1}}-e^{-\beta E_l}\Big)\Bigg[\frac{(\Gamma'_l+i(l+\Delta\omega'_l+\omega')}{(l+\Delta\omega'_l+\omega')^2+\Gamma'^2_l}\\
&-\frac{\Gamma'_l+i(l+\Delta\omega'_l-\omega')}{(l+\Delta\omega'_l-\omega')^2+\Gamma'^2_l}\Bigg]\Bigg\}+\frac{3(l+2)}{2l+3}\\
&\times\Bigg(\frac{2l+3+\Delta\omega'_{2l+3})^2-4\omega'^2-4i\omega'\Gamma'_{2l+3}}{\Big[(2l+3+\Delta\omega'_{2l+3})^2-4\omega'^2+\Gamma'^2_{2l+3}\Big]^2+16\omega'^2\Gamma'^2_{2l+3}}\Bigg\{\Big(2l+3+\Delta\omega'_{2l+3}\\
&+2\omega'-i\Gamma'_{2l+3}\Big)\Bigg(\Big(e^{-\beta E_l}-e^{-\beta E_{l+1}}\Big)\frac{l+1+\Delta\omega'_{l+1}-\omega'-i\Gamma'_{l+1}}{(l+1+\Delta\omega'_{l+1}-\omega')^2+\Gamma'^2_{l+1}}\\
&-\Big(e^{-\beta E_{l+1}}-e^{-\beta E_{l+2}}\Big)\frac{(l+2+\Delta\omega'_{l+2}+\omega'-i\Gamma'_{l+2})}{(l+2+\Delta\omega'_{l+2}+\omega')^2+\Gamma'^2_{l+2}}\Bigg)(1-\alpha)\\
&+\Big(2l+3+\Delta\omega'_{2l+3}-2\omega'+i\Gamma'_{2l+3}\Big)\Bigg(\Big(e^{-\beta E_l}-e^{-\beta E_{l+1}}\Big)\\
&\times\frac{l+1+\Delta\omega'_{l+1}+\omega'+i\Gamma'_{l+1})}{(l+1+\Delta\omega'_{l+1}+\omega')^2+\Gamma'^2_{l+1}}-\Big(e^{-\beta E_{l+1}}-e^{-\beta E_{l+2}}\Big)\\
&\times\frac{l+2+\Delta\omega'_{l+2}+\omega'+i\Gamma'_{l+2}}{(l+2+\Delta\omega'_{l+2}-\omega')^2+\Gamma'^2_{l+2}}\Bigg)(1-\alpha)\\
&+\alpha(2l+3+\Delta\omega'_{2l+3})\Big(e^{-\beta E_l}-e^{-\beta E_{l+2}}\Big)\Bigg\}\Bigg].
\end{aligned}
\tag{B.9}
$$

Part II

COMPUTER SIMULATION OF POLYMER SOLUTIONS

Chapter 5

Simulation techniques

5.1 Introduction

After the second world war, the computing skills and techniques developed during the war had to be shifted to more human problems. It was not till the early 1950s when computers became partly available for non military use. Metropolis [1], in 1953, got interested in seeing computing being used in wide range of human problems.

The basic laws of nature, in their raw forms, some times appear very difficult or even not possible to be treated analytically. The example of the interacting many body (more than 2 particles) problem is a shouting example. However, using a computer, this problem can be solved to a reasonable accuracy. Most of material science deals with problems of many interacting bodies. Analytical methods used in solving these problems have usually been based on simplifying assumptions that have often led to the theoretical prediction suffering from a loss of generality or completely unable to explain experimental observations. Also, at times, experimental analogs of theoretical predictions of some natural problems are not easy to come by. Computer experiments can then come in as substitute "experimental tests" of theories.

Problems in material science range from static to dynamic properties. While dynamic properties are dependent upon the type of dynamic the system undergoes, static properties are related to time equilibrium states of the system. The latter properties are functions of the possible conformations the system can acquire. While some static properties can be obtained from natural dynamics, others do not have natural dynamic analogs. Two methods of computer simulations, therefore arise naturally: the molecular dynamics (MD) and Monte Carlo (MC) simulation methods.

Molecular dynamics method [2, 3] is based on the real dynamics of the system. A sample of the system consisting of N particles is prepared in a well defined microscopic initial state (initial positions and velocities). Newton equations of motion are solved for all the (interacting) particles of the system and the time evolution yields the possibility to calculate the time averages of the properties of interest, MD thus exploits Boltzmann statistics to estimate experimentally relevant observables. Note that both static and dynamic properties are accessible in this technique. Remark that this brief description is similar to that of a real experiment. This means that MD simulations are very similar to real experiments. A detailed description of MD techniques and the application to polymers in solution will be given later. For now we will emphasise on the MC methods.

The second simulation method exploits the Gibbs approach of Statistical Mechanics. Equilibrium properties are evaluated for ensemble averages using Monte Carlo techniques to perform phase space integrals.

5.2 Monte Carlo techniques

Because MC methods are limited to static equilibrium properties, one can wonder what their advantages are with respect to the apparently more powerful MD method. The advantages are twofold. (a) In MD the realistic dynamic path is followed by the system while in MC, unphysical moves are allowed. This facilitates, in many cases, the effective sampling of the phase space. Examples are mixtures where A - B particle exchanges are allowed, CBMC method where a part of a polymer chain can be regrown, etc. (b) there exist physical phenomena that do not have natural dynamics. Examples include the lattice models and systems with discrete degrees of freedom like the Ising spins.

To see how MC comes in, we start from the classical expression of the partition function.

$$Q = c \int d\underline{p}^N d\underline{r}^N \exp\left[-\beta H\left(\underline{r}^N, \underline{p}^N\right)\right], \tag{5.1}$$

where $\underline{r}^N$ and $\underline{p}^N$, respectively, stand for the coordinates and momenta of the N-particles system, $\beta = \frac{1}{k_B T}$ (with k_B being the Boltzmann constant and T the absolute temperature). H is the Hamiltonian of the system and c is a constant. We know from quantum statistical mechanics that the expectation value of an observable $\mathcal{A}$ can be calculated from the knowledge of the probability $P_i(E_i)$ that the system is found in an energy state $\mid i >$. This expectation value $\langle \mathcal{A} \rangle$ is written as,

$$\langle \mathcal{A} \rangle = \sum_i P_i(E_i) \langle i \mid \mathcal{A} \mid i \rangle, \tag{5.2}$$

where $\langle i \mid \mathcal{A} \mid i \rangle$ is the expectation value of $\mathcal{A}$ in the quantum state $\mid i >$. For a system in equilibrium, P_i is given by the Boltzmann distribution,

$$P_i(E_i) = \frac{\exp\left(-\frac{E_i}{k_B T}\right)}{\sum_i \exp\left(-\frac{E_i}{k_B T}\right)}. \tag{5.3}$$

The classical limit of Eq.(5.2) is

$$\langle \mathcal{A} \rangle = \frac{\int d\underline{p}^N d\underline{r}^N \mathcal{A} \exp\left[-\frac{1}{k_B T}\left(\sum_i \frac{\underline{p}_i^{\,2}}{2m_i} + U(\underline{r}^N)\right)\right]}{\int d\underline{p}^N d\underline{r}^N \exp\left[-\frac{1}{k_B T}\left(\sum_i \frac{\underline{p}_i^{\,2}}{2m_i} + U(\underline{r}^N)\right)\right]}. \tag{5.4}$$

If $\mathcal{A}$ is uniquely a function of momenta, then $\langle \mathcal{A} \rangle$ can be treated analytically. But if it depends on coordinates, analytical procedures become limited to stringently simple cases. Computer analysis becomes inevitable for a wide range of real problems of this nature. Let us suppose that $\mathcal{A}$ does not depend on $\underline{p}^N$, then

$$\langle \mathcal{A} \rangle = \frac{\int \underline{r}^N \mathcal{A} \exp\left(-\frac{U(\underline{r}^N)}{k_B T}\right)}{\int d\underline{r}^N \exp\left(-\frac{U(\underline{r}^N)}{k_B T}\right)}. \tag{5.5}$$

There are many system configurations for which the Boltzmann factor

$$\exp\left(-\frac{U(\underline{r}^N)}{k_BT}\right) \Big/ \int d\underline{r}^N \exp\left(-\frac{U(\underline{r}^N)}{k_BT}\right) \equiv \exp\left(-\frac{U(\underline{r}^N)}{k_BT}\right) \Big/ Z$$

is infinitely small. In a **simple sampling** scheme (where all conformations are selected using a uniform distribution), most of the calculations will therefore be performed on points where this factor is negligible. In the **importance sampling**, we can oblige more computations in regions with large Boltzmann factors and few elsewhere. This is the main idea behind the Metropolis scheme.

5.2.1 The Metropolis method

In a Metropolis scheme we do not need to know the absolute probability of finding the system in a given configuration, but the simple knowledge of relative probabilities is sufficient. This relative probability is given by the Boltzmann factor.

The general approach in a Metropolis scheme is to prepare the system in a configuration denoted o (old). This starting configuration should be representative of the real system (with non negligible Boltzmann factor $N(o) = \exp\left(-\frac{U(o)}{k_BT}\right)/Z$). A new trial configuration n is generated by giving o a random displacement in phase space. The corresponding Boltzmann factor of n is $N(n) = \exp\left(-\frac{U(n)}{k_BT}\right)/Z$. $U(o)$ and $U(n)$ are, respectively, the old and new energies of the system. The condition of equilibrium is governed by the fact that the transition matrix element $\pi(o \rightarrow n)$ depicting the transition from the old to the new conformation and that of the reverse process $\pi(n \rightarrow o)$ must insure that any established equilibrium does not break down. This means that the number of conformations transformations transiting from o to any other conformation must be equal to the number leaving any other conformation to o. A much stronger condition is that, to preserve equilibrium, the number of moves from o to n must be balanced by the number of reverse moves. In other words,

$$N(o)\pi(o \rightarrow n) = N(n)\pi(n \rightarrow o), \tag{5.6}$$

where π is the probability that the system jumps from one configuration to the other. π is then considered to be the product of a trial move matrix $\alpha(o \rightarrow n)$ and an acceptance matrix $acc(o \rightarrow n)$ so that

$$N(o)\alpha(o \rightarrow n)acc(o \rightarrow n) = N(n)\alpha(n \rightarrow o)acc(n \rightarrow o). \tag{5.7}$$

Metropolis choses α to be symmetric ($\alpha(o \rightarrow n) = \alpha(n \rightarrow o)$), so that

$$\frac{acc(n \rightarrow o)}{acc(o \rightarrow n)} = \frac{N(n)}{N(o)} \tag{5.8}$$

and the acceptance condition is given by

$$acc(n \rightarrow o) = min\left(1, \exp\left[-\frac{1}{k_BT}\left(U(n) - U(o)\right)\right]\right). \tag{5.9}$$

Note that the α matrix is nonzero for transitions between "close" states in configurational space: in this case the acceptance rate has a good chance to be reasonable. The Metropolis scheme can, thus, be summarised as follows:

- prepare the system in an initial configuration,
- select a particle at random (for a mono-atomic system) at $\underline{r}$ and calculate its contribution to the total energy $U(\underline{r}^N)$
- give the particle a random move to $\underline{r}' = \underline{r} + d\underline{r}$ and calculate its new contribution to the total energy $U(\underline{r}'^N)$,
- calculate $\Delta U = U(\underline{r}'^N) - U(\underline{r}^N)$ and accept the move from $\underline{r}^N$ to $\underline{r}'^N$ if $\Delta U \leq 0$, else use Eq.(5.9).

If the move is accepted, the new configuration is conserved together with the corresponding values of the observables of interest, if not, the old configuration is retained and its statistics reconsidered for subsequent averaging.

5.2.2 The periodic boundary conditions

Most often, the systems we simulate are quite reduced such that if appropriate boundary conditions are not considered it may lead to very unrepresentative informations on the systems of interest. It should be noted that in a system of N-particles occupying a volume V, the fraction of particles at the surface bounding the volume is proportional to $N^{-1/3}$. This means that in a small system most of the particles will be at the surface and since surface particles interact differently from bulk ones, small systems will be ill-adapted to simulate (without any boundary conditions) bulk properties. A better way to avoid problems of this nature is to use the periodic boundary condition (PBC). This consists of repeating in a periodic manner the simulation cell in the whole space in such a way that an infinite system is obtained as shown on Figure 5.1.

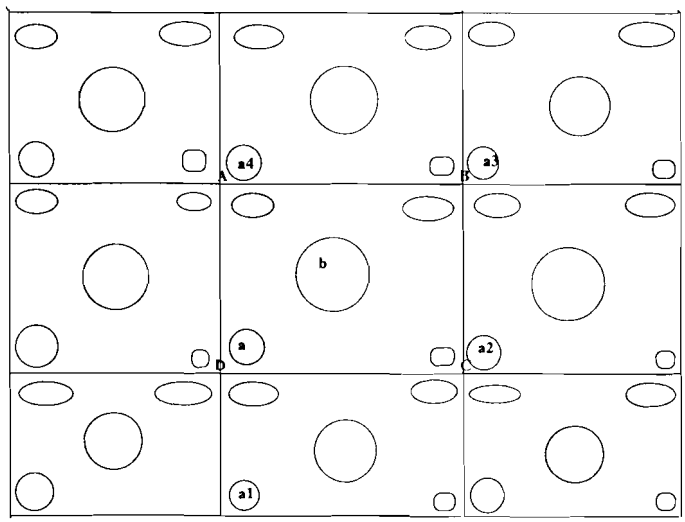

Figure 5.1: The periodic boundary condition

Most often the interactions between particles of the molecular system are of short range nature and are therefore usually truncated in space. Suppose r_c is the cutoff distance beyond

which the intermolecular potential is truncated. On calculating the intermolecular energies and forces of a particular molecule, (**b**, for example) only molecules of the simulation cell **ABCD** (e.g. **a** or its periodic images **a1**, **a2**, **a3**,...) which are found in a sphere of radius r_c, centred on the molecule, are considered. When PBC is used, r_c must be less than half the diameter of the simulation cell. PBC is used in MC and MD simulations and in both cases the choice of the size of the simulation cell should depend on the range of intermolecular potentials involved. The situation complicates for MD when hydrodynamic interactions (known to be of long range character) are present and when coulomb interactions of charged particles are involved. Recently, C. Pierleoni and J.-P. Ryckaert demonstrated how, in a MD calculation, the dynamic properties of a polymer solution undergoing a flow depend on the dimensions of the simulation cell [4].

5.2.3 The configurational biased Monte Carlo (CBMC)

The Metropolis scheme described earlier, based on one particle displacement, is best suited for mono-atomic systems, but when coupled with reptation moves, it can be used on macromolecules or polymers. This method is very inefficient for sampling the conformations of very large molecules since it will require very long time for the molecule to evolve from one independent configuration to the other. A long linear molecule is said to have moved from one independent configuration to the other when all its segments or monomers have undergone successful MC moves. Due to the inefficiency of the traditional Metropolis on macromolecules, a sampling method should be devised that will permit a quick sampling of the numerous conformations of large molecules without the latter getting locked up in a reduced portion of the configurational space. The method adopted for homopolymers is the configurational biased Monte Carlo coupled with reptation moves. By reptation move, we mean that a segment of fixed length of a long linear molecule is suppressed at one end of the molecule and reconstructed at the other end.

The original version of the CBMC [1, 5, 6] consists of generating a new trial conformation from an initial one by replacing a sequence of segments at one end of the chain with another sequence of same length at the other end. This reconstruction is done randomly. A uniform sampling of the chain would as usual be highly inefficient so that a bias should be introduced in this scheme such that overlaps with high energies are avoided. This bias must be removed by attributing to the new trial conformation a corrected statistical weight called the **Rosenbluth weight**. The highlights of the CBMC used in our simulations can be summarised as follows [3]:

- 1. Prepare the sample to be simulated in a particular conformation.
- 2. Randomly select one end of the polymer and suppress a portion of it of k (fixed) segments.

  Depending on the nature of the intra and inter molecular interactions (bending, torsional, excluded volume, external field, etc.) the reconstruction of the k segments is done segment by segment as follows:

- 3. Suppose $i-1$ segments or bonds (or i monomers: $2 \leq i \leq k$) have been successfully constructed. To place the segment i, *idir* trial orientations are chosen around the

ith monomer according to a distribution that may be uniform or depend on a certain orientational potential energy.

- 4. Calculate the Rosenbluth weight $W_i(n)$ (sum of the orientation related Boltzmann weights of the *idir* orientations) of the new trial orientation of the ith segment while selecting one of the orientations according to the Boltzmann weight associated to each trial orientation.
- 5. $idir - 1$ other orientations are chosen for the old conformation of segment i. These together with the original orientation of i constitute *idir* old orientations of i. The Rosenbluth factor $W_i(o)$ of the old configuration is evaluated.
- 6. Repeat points $3 - 5$ until all k segments are placed while calculating the overall Rosenbluth weights $W(n)$ (new) and $W(o)$ (old) as the products of those of the respective k segments.
- 7. Accept the new conformation with a probability

$$acc\,(o \rightarrow n) = min\left(1, \frac{W(n)}{W(o)}\right). \tag{5.10}$$

The acceptance rate and the time required to generate an independent configuration will depend on the choice of the couple $(k, idir)$. Large *idir* will result in large acceptance rate but slow sampling while large k will lead to fast sampling but little acceptance rate. The choice of an optimal couple that yields reasonable acceptance rate and samples a good portion of the molecule's possible configurations within a reasonably short time is very important. There is no conventional method of chosing this couple but by simple trials we can make a better choice. If the acceptance rate is r for reptation moves of k segment, the number of trial reptations needed to generate an independent conformation is $(N/(2k))^2/r$. For example, for a 1024 segments excluded volume chain in vacuum, when $k = 32$ an acceptance rate of $r = 0.35$ is obtained. The number of reptation moves thus needed for the chain molecule to change from one independent configuration to the other is about 730.

The CBMC method outlined above will be described in more detail when particular cases will be considered. In Chapter 6 and 7 we shall apply it to sample the configurations of a semi flexible necklace chain subjected to a traction force. In this model there is no explicit intra-molecular energy, excluded volume is enhanced by a hard sphere consideration. In chapter 7, we shall also consider the case of polyethylene, a polymer model characterised by several forms of intra-molecular energies.

5.3 Molecular Dynamics

We pointed out earlier that molecular dynamics simulation is very similar to real experiments [3]. It is a method of simulating classical equilibrium and transport properties of a material. This means that only systems of large particles or those free of high frequency vibrational motions are considered. This method consists of solving the following equations of motion of the system of N particles:

$$\dot{\underline{r}}_i(t) = \underline{v}_i(t), \tag{5.11}$$

$$\dot{\underline{v}}_i(t) = \frac{1}{m_i}\underline{F}_i(t), \tag{5.12}$$

where $\underline{r}_i$ and $\underline{v}_i$ are, respectively, the position and the velocity vectors of particle i ($1 \leq i \leq N$) with $\underline{F}_i$ being the total force due to its interactions with all other particles (plus possibly an external field). If the phase space trajectory resulting from these equations is known, a time average of the system properties over a long period of time should yield results to a good estimate of the equilibrium averages which can then be confronted with experiments.

Several methods exist for solving the equations of motion [2, 3]. Amongst them is the Verlet algorithm [3]. This algorithm is based on solving the conservative equations of motion (Eqs.(5.11) and (5.12)). This means that the algorithm is used for a micro-canonical system (constant N, volume V and energy E ensemble). Since we shall be interested in simulating a system in a canonical ensemble (constant N, V and temperature T), we must couple to the NVE algorithm a thermostating scheme. We shall, therefore, describe the velocity version of the Verlet algorithm coupled with a Nosé-Hoover [7] scheme. The velocity Verlet procedure is governed by the two equalities (consequences of Eqs. (5.11) and (5.12)):

$$\underline{r}_i(t + \Delta t) = \underline{r}_i(t) + \Delta t\underline{v}_i(t) + \frac{(\Delta t)^2}{2m_i}\underline{F}_i(t) \tag{5.13}$$

$$\underline{v}_i(t + \Delta t) = \underline{v}_i(t) + \frac{\Delta t}{2m_i}\left(\underline{F}_i(t) + \underline{F}_i(t + \Delta t)\right), \tag{5.14}$$

where Δt is the integration time step. Note that these equations describe a reversible phenomenon and that the knowledge of $\underline{v}_i(t + \Delta t)$ requires that of the force at that instant.

In order to render the simulation temperature conserving, Nosé [7, 8, 9] used an extended Langrangian approach in which he included two artificial conjugate coordinates (s and $\dot{s}$) characterising the heat bath. His Lagrangian was of the form:

$$\mathcal{L}_{Nose} = \sum_{i=1}^{N}\frac{1}{2}m_i s^2\underline{r}_i^2 - U(\underline{r}^N) + \frac{1}{2}Q\dot{s}^2 - \frac{g}{\beta}\ln s, \tag{5.15}$$

where Q is the coupling constant and $\beta = 1/(k_B T)$. Averaging in a micro-canonical ensemble corresponding to the constancy of the resulting Hamiltonian [3],

$$H_{Nose}(t) = \sum_{i=1}^{n}\frac{1}{2}\frac{\underline{p}_i(t)^2}{m_i} + U(\underline{r}^N) + \frac{1}{2}\epsilon^2(t)Q + \frac{g}{\beta}s(t), \tag{5.16}$$

leads to an NVT ensemble averaging on condition that $g = 3N$. In general, g represents the number of independent coordinates characterising the dynamics of the system. The new equations of motion are obtained via the Hamilton's equations:

$$\dot{\underline{r}}_i(t) = \frac{\underline{p}_i(t)}{m_i} = \underline{v}_i(t), \tag{5.17}$$

$$\dot{\underline{p}}_i(t) = \underline{F}_i(t) - \epsilon(t)\underline{p}_i(t), \tag{5.18}$$

$$\dot{\epsilon}(t) = \frac{gk_BT}{Q}\left[\sum_{i=1}^{N}\frac{1}{gk_BT}\frac{\underline{p}_i^2(t)}{m_i} - 1\right], \tag{5.19}$$

with $\epsilon(t) = \frac{d}{dt}\ln s(t)$. Coupling the velocity Verlet algorithm with the Nosé-Hoover equations of motion leads to the following system:

$$\underline{r}_i(t+\Delta t) = \underline{r}_i(t) + \Delta t \underline{v}_i(t) + \frac{(\Delta t)^2}{2}\left(\underline{F}_i(t)/m_i - \epsilon(t)\underline{v}_i(t)\right), \tag{5.20}$$

$$\underline{v}_i(t+\frac{\Delta t}{2}) = \underline{v}_i(t) + \frac{\Delta t}{2}\left(\underline{F}_i(t)/m_i - \epsilon(t)\underline{v}_i(t)\right), \tag{5.21}$$

$$\underline{v}_i(t+\Delta t) = \underline{v}_i(t+\frac{\Delta t}{2}) + \frac{\Delta t}{2}\left(\underline{F}_i(t+\Delta t)/m_i - \epsilon(t+\Delta t)\underline{v}_i(t+\Delta t)\right) \tag{5.22}$$

and

$$\epsilon(t+\Delta t) = \epsilon(t+\frac{\Delta t}{2}) + \left[\sum_{i=1}^{N} m_i \underline{v}_i^2(t) - g k_B T\right]\frac{\Delta t}{2Q}. \tag{5.23}$$

The Nosé-Hoover integration scheme is subdivided into two subroutines. In a first one

- $\underline{r}_i(t+\Delta t)$ is estimated using Eq.(5.20)
- $\underline{v}_i(t+\frac{\Delta t}{2})$ is estimated using Eq.(5.21)
- $\epsilon(t+\frac{\Delta t}{2})$ is estimated using

$$\epsilon(t+\frac{\Delta t}{2}) = \epsilon(t) + \left[\sum_{i=1}^{N} m_i \underline{v}_i^2(t) - g k_B T\right]\frac{\Delta t}{2Q}. \tag{5.24}$$

$\underline{v}_i(t+\frac{\Delta t}{2})$ and $\epsilon(t+\frac{\Delta t}{2})$ are then used in the second subroutine to solve for $\underline{v}_i(t+\Delta t)$ and $\epsilon(t+\Delta t)$ using Eqs.(5.22) and (5.23) via a Newton Raphson procedure. The Nosé-Hoover Hamiltonian (Eq. (5.16)) should be a constant of motion along the phase space trajectory of the system.

As an application of a constant temperature molecular dynamic simulation, we shall consider some static properties of a system of two pentamers in a bath of a mono-atomic solvent. We shall be interested in knowing how the effective potential between them depends on the distance between their respective centres of mass. This problem is best suited for a MD simulation approach because we are dealing here with a dense liquid system consisting of both flexible chain molecules and solvent molecules. For such systems no "clever" MC move is possible to enhance the convergence of averages. MD remains a very efficient method for dense systems, partly because calculations can easily be efficiently vectorised on parallelised or modern computers.

Bibliography

[1] N. Metropolis, A. W. Rosenbluth, M.N. Rosenbluth, A. N. Teller, and E. Teller, *J. Chem. Phys* **21**: 1087, 1953

[2] M. P. Allen and D. J. Tildesley, *Computer simulation of liquids*, Clarendon Press, Oxford, 1975

[3] D. Frenkel and B. Smit, *Understanding Molecular Simulation*, Academic Press, 1996.

[4] C. Pierleoni and J.-P. Ryckaert, *Mol. Phys.* **75**: 731, 1992

[5] M. N. Rosenbluth and A. W. Rosenbluth, *J. Chem. Phys.* **23**: 356, 1955

[6] M. Destrée, *Thèse de Doctorat*, Université Libre de Bruxelles, 1998

[7] S. Nosé, *J. Chem. Phys.* **81**: 511, 1984

[8] W. G. Hoover. *Phys. Rev.* **A81** 1695, 1985

[9] S. Nosé, *Mol. Phys.* **52**: 255, 1984

Chapter 6

On the stretched polymer statistical mechanics ensembles

Summary

Imposing to a single polymer chain of N monomers either a fixed pair of forces $\pm\mathbf{f}$ acting at the chain ends (stress ensemble) or a fixed end-to-end vector $\mathbf{R}$ (strain ensemble) does correspond to the use of different statistical mechanical ensembles and leads in general to distinct averages in conjugated ensembles. In particular, the elasticity laws $R_f = g(f)$, where R_f is the length of the average end-to-end vector $\langle \mathbf{R} \rangle_f$ in the stress ensemble, and $f_R = h(R)$, where h_R is the intensity of the average internal force $\langle \mathbf{f} \rangle_R$ in the strain ensemble, are not inverse functions. For these conjugated ensembles, the quantity $\Delta_f = f - h(g(f))$ and more generally $\Delta_O = \langle O \rangle_f - \langle O \rangle_R$ for an arbitrary single chain observable O, is studied systematically in this chapter for a large class of polymer models corresponding to chains at temperatures equal or above the theta point. The leading term $\Delta_f^{(2)}$ of an expansion of Δ_f in terms of successive moments of end-to-end vector fluctuations in the stress ensemble can be used to analyse the Δ_f scaling properties. For the gaussian and the freely jointed chain models, $\Delta_f \propto 1/N$ for $N >> 1$ with the particularity that, for the elasticity law, Δ_f strictly vanishes for the gaussian chain at finite N. For chains in good solvent, the usual result $\Delta_f \propto 1/N$ at fixed f is only valid in the highly stretched chain regime (Pincus regime). Large (N independent) ensemble effects of the order of 20% on Δ_f are noticed when the chain is stretched over a distance of the order of the unstretched chain root-mean-square end-to-end distance R_0. These effects decrease to 1% level for $R > 3R_0$. Monte-Carlo calculations for a chain model containing both excluded volume and finite extensibility features illustrate the distinction between the elasticity laws in the two ensembles over all stretching regimes. Our study suggests that the nature of the constraints used in the single chain experimental micro-manipulations could be relevant to the interpretation of elasticity law data.

6.1 Introduction

The study of the elastic behaviour of a single linear polymer is a standard application of statistical mechanical concepts [1, 2, 3, 4, 5]. In this field of renewed interest [6], it is sometimes

noticed (see [1, 4, 5, 7]) that ensembles corresponding to a fixed end-to-end vector $\underline{R}$ or to fixed stretching forces $\pm\underline{f}$ acting at the chain ends can lead to distinct elastic laws. Long ago, Flory pointed out [1] that these two conjugated single chain ensembles can be seen as polymer counterparts of, respectively, the constant volume and constant pressure ensembles of N-particle systems. In the latter case, away from phase transitions, there are correction terms of $O(N^{-\frac{1}{2}})$ for finite size effects on intensive properties like the energy per particle, the density or the pressure. To our knowledge, the nature of the equivalent correction terms for single stretched chain ensembles has never been discussed systematically (for arbitrary models). Elasticity laws relative to different single chain ensembles have been compared long ago for ideal chain models. For gaussian chains, the same linear elastic law follows independently of the ensemble chosen while for the freely jointed chain (FJC) made of N segments each of length b, the Langevin function relates the (imposed) force on chain ends to the average extension of the polymer while the inverse Langevin function gives the average internal force for a fixed end-to-end vector $\underline{R}$ up to correction terms which vanish in the limit of infinitely long chains (see page 321 in [1] and chapter 6 in [4]).

To which extent the elasticity behaviour of a single polymer chain with excluded volume (EV) interactions and finite extensibility (FE) is dependent upon the nature of the external constraint imposed at the chain ends is the central question on which we focus, although the general approach we take in the present chapter could be exploited in other applications. We prefer to leave for future works, the elasticity features of particular biological molecules [6] or universal properties of stretched polyelectrolytes [9]. The chain elasticity in the globular state (below the theta point) [8] will not be considered here as our analysis is restricted to single phase systems far from phase transition boundaries.

The correct statistical mechanical ensemble to associate with an experimental measurement probing single chain properties is an issue of great interest given the actual breakthrough of experimental set-ups probing directly single chain mechanical or thermodynamic properties like elasticity, finite extensibility or adsorption /desorption of a chain on/from a surface. In all these experiments, the ends of a single chain are controlled externally, either directly or indirectly.

In the original experiment of Bustamante's group [10], one end of a DNA chain is chemisorbed to a glass support while the other end is chemically bounded to a micron-sized bead to which well calibrated external forces can be imposed while the average position of the bead is being recorded by fluorescence microscopy. Along the same lines, the Brownian motion of a hairy polystyrene bead temporarily tethered to a glass surface by a single chain under bead-surface repulsive force conditions was analysed and the polymer "spring constant" determined [11].

J.L. Viovy and coworkers devised another set-up [12] where the chain is rigidly maintained by a mobile piezo-micromanipulator at one end and, at the other end, by a flexible tube through which light is deviated in a way which has been previously calibrated against known forces within the piconewton range. The light deflection angle is then a measure of the average internal contractile force for an imposed end-to-end vector. Atomic Force Microscopy (AFM) has been recently developed towards single chain force measurements probing the vertical stretching of a chain grafted on a surface [13] or detaching a single polyelectrolyte chain adsorbed on a charged surface [14, 15].

In order to focus on the single chain elasticity law of an N-segment linear polymer within an ensemble characterised either by a pair of fixed stretching forces applied at the chain ends or by a fixed end-to-end vector. we need to introduce some specific notations. Let us first consider

that the polymer ends are subjected to a pair of external forces $-\underline{f}$ and $+\underline{f}$ acting respectively on the beads indexed 0 and N. The resulting average end-to-end vector $\underline{R}_f \equiv \langle \underline{r}_N - \underline{r}_0 \rangle_f$, where $\underline{r}_i$ stands for the position vector of bead i and $\langle \ldots \rangle_f$ represents a fixed-f ensemble average, can be written as $\underline{R}_f = R_f \hat{\underline{f}} \equiv g(f)\hat{\underline{f}}$ where $\hat{\underline{f}} \equiv \frac{\underline{f}}{|\underline{f}|}$ is the unit vector pointing along the force $\underline{f}$. The relationship $R_f = g(f)$ gives the elasticity law in the f ensemble for f intensities defined, in principle, over the range $[0, \infty)$. When the same polymer is subjected to a fixed end-to-end vector $\underline{r}_N - \underline{r}_0 = \underline{R} \equiv R\hat{\underline{R}}$ of length R and direction $\hat{\underline{R}}$, an average internal force $\underline{f}_R = f_R \hat{\underline{R}} \equiv h(R)\hat{\underline{R}}$ develops within the polymer. These forces, namely $+\underline{f}_R$ and $-\underline{f}_R$, which act respectively on beads 0 and N, tend usually to contract the chain ($h(R) > 0$) but they sometimes act in the opposite direction, as when EV forces between end beads give rise to a repulsion at short distance ($h(R) < 0$). The relationship $f_R = h(R)$ is the elasticity law in the fixed-R ensemble which, in principle, covers values of R in the range $[0, \infty)$. We will consider the difference $\Delta_f = f - h(g(f))$ between force intensities as a measure of the non equivalence of the elasticity laws in both ensembles.

The fact that we focus on this particular manifestation of the distinction between both conjugated ensembles does not imply that it is the only one. Other single chain properties of a stretched polymer like its gyration tensor, the NMR residual dipolar interaction or the chain structure factor in scattering experiments should also depend upon the nature of the applied constraint. Even if these applications are not discussed in the present chapter, we give the theoretical basis to establish the connection between the averages of any observable calculated in the stress or in the strain ensembles.

The nature of the difference between the fixed-f and fixed-R single polymer conformational ensembles is formally similar for any particular R (or f) value but, as well qualitatively and quantitatively, the effect turns out to be radically different for the small and the large extension regimes defined, respectively, by $R/R_0 << 1$ and $R/R_0 >> 1$, where R_0 is the average (in the root-mean-square sense) of the unstretched chain end-to-end vector.

In the low f regime of the fixed-f ensemble, the EV chains are usual (weakly perturbed) 3D self-avoiding walks while in the low R limit of the fixed-R ensemble, all conformations are close to a cyclic structure and EV chain ends are mutually repelling due to forces which are largely of entropic origin: the members of both ensembles are thus forming two quite different families of conformations. It must be realised here that our attitude is quite formal as the relevance of the stress or strain ensembles considered in this work (and in standard textbooks [1. 5]) is of little experimental relevance in the $R/R_0 << 1$ regime. Real single chain elasticity experiments involving micro-manipulations on chain ends use needles, beads or microtubes on which chain ends are grafted: a more realistic study of the effects of the constraints on the single chain elasticity in the weak stretching regime should then include additional confinement effects.

Considering now the strong stretching regime of the fixed-f ensemble, it turns out that the end-to-end vector fluctuates only slightly around the mean so that both ensembles give almost the same averages for any single chain structural property. A systematic study of the ensemble influence on elasticity law will however allow us to investigate the interesting cross-over regime $R/R_0 \approx 1$ which should be experimentally relevant as confinement effects are probably negligible with respect to the ensemble effects discussed here. The difference Δ_f in the elasticity law will be discussed theoretically and then applied to different standard chain models in the continuous space. We will consider gaussian chains, freely jointed chains and EV

chains according to the end-to-end distribution obtained from Renormalisation Group Theory (RGT). A last model containing both EV and FE characteristics will also be discussed on the basis of extensive Monte-Carlo simulations. The adopted hard sphere necklace model is a semi-flexible chain with hard sphere repulsion terms between monomers. Both fixed-f and fixed-R elasticity laws can be extracted from such simulations which in addition, are useful to test the domain of validity of RGT and the nature of the cross-over behaviour between the scaling regime and the FE region, the latter region being actually the main focus of the new experiments on single molecule stretching. The technique we used in our simulations, namely the Configurational Biased Monte-Carlo method adapted to stretched chains, has also been implemented to study the elongation of a realistic chain model of polyethylene but this topic will be discussed in the next chapter [16].

It should be recalled at this point that Monte-Carlo calculations have been successfully applied within the context of a single stretched EV chain, starting with the pioneering work of Webman, Lebowitz and Kalos in 1981 [17] which demonstrated the existence of a Pincus blob regime in the intermediate regime of the elasticity law. The behaviour $R_f \propto f^{(1/\nu)-1}$, where $\nu \approx 0.6$ is the Flory scaling exponent for good solvent conditions, remains today a property which was originally predicted theoretically [18], subsequently checked by simulations [17], but not yet directly verified experimentally. Much later, Wittkop at al. [19] performed a more extensive Monte-Carlo study of the same single EV chain elasticity law, showing that RGT correctly predicts the cross-over between the linear stretching regime (at weak forces) and the Pincus blob regime. In 1995, Cifra and Bleha [20] studied the effect of varying the solvent quality on the elasticity law, in particular the separation between enthalpic and entropic contributions to the stretching force. Recently, Pierleoni et al. [21] reported Monte-Carlo results on the scattering structure factor of a stretched chain showing the signature of Pincus blobs on the structure factor. It is interesting to note that, with the exception of Cifra and Bleha's work which follows a fixed-R statistical mechanical formulation, all MC works mentioned above are formulated in the fixed-f ensemble. A different stretched chain ensemble where only one component of the end-to-end vector is constrained has been used in a recent series of MC studies [22, 23] aimed at studying the coil-globule phase transition under stretching. As transverse end-to-end vector fluctuations are sampled while they are frozen in the fixed R-ensemble, we consider that (where the vector $\underline{R}$ is fully constrained) the elasticity law in this unusual ensemble should be intermediate between the two cases discussed in the present chapter.

This chapter is organised as follows. In the next section, we start by defining quite generally the different single chain stretching domains to which we will refer throughout the chapter. In section 3, we recall the statistical mechanics formalism required to derive the elasticity law in both the fixed-f and the fixed-R ensembles which enables us to properly define the central quantity Δ_f mentioned earlier. In section 4 we establish a formal expansion of the average of an arbitrary observable $\langle O \rangle_f$ around $\langle O \rangle_R$ at $R = R_f$. For the particular case of Δ_f where O is simply chosen to be the internal force acting on chain ends, we find a leading term in the expansion, namely a second order expression $\Delta_f^{(2)}$, which turns out to be a good approximation of Δ_f in the $R/R_0 > 1$ stretching domain. In that case, scaling properties of Δ_f can be estimated from those of $\Delta_f^{(2)}$. The next section is concerned with the evaluation of Δ_f and $\Delta_f^{(2)}$ for specific models such as ideal chains (the gaussian and the FJC cases) and EV chains using the RGT end-to-end vector distribution of unstretched chains. In the second part of this

section, Monte-Carlo calculations relative to the hard-sphere necklace model are presented.

6.2 Single chain stretching domains

Consider a linear polymer of N Kuhn segments (we suppose $N >> 1$) each of size b undergoing Brownian motion in a solution at temperature T. The average end-to-end distance of the chain is $R_0 \approx bN^{\nu}$ where ν is the scaling exponent equal to $\nu = 0.5$ or $\nu \approx 0.6$ for Θ and good solvent conditions, respectively. When this polymer is subjected to stretching forces $\pm\underline{f}$ at its ends, the average end-to-end distance shows three distinct regimes which can be predicted by scaling arguments [17, 18, 24]

6.2.1 The linear regime

At small forces ($f < f^* \equiv \frac{k_B T}{R_0}$), the relative extension increases linearly with the global reduced force $\eta_g = \frac{fR_0}{k_B T}$

$$\frac{R_f}{R_0} = \frac{1}{3}\eta_g, \tag{6.1}$$

The effective spring constant k, which relates the extension R_f to the stretching force$f$, $f = kR_f$, is thus $k = \frac{3k_B T}{R_0^2}$.

6.2.2 The Pincus blob regime

For forces in the range $f^* < f < f^{**} \equiv \frac{k_B T}{b}$, i.e. when f lies in the domain where $\eta_g > 1$ and the local reduced force $\eta_l \equiv \frac{fb}{k_B T} < 1$, the universal scaling corresponds to the so-called Pincus blob behaviour [18, 24]

$$\frac{R_f}{R_0} = A\eta_g^{\left(\frac{1}{\nu}-1\right)}, \tag{6.2}$$

where A is a constant. When excluded volume forces are absent, one has $\nu = 0.5$ and $A = 1/3$ so that Eq.(6.2) extends the validity of the small force linear law of Eq.(6.1) up to f^{**}. For EV chains, $A \approx 0.46$ [17, 21].

6.2.3 The finite extensibility regime

Finally, when the force is such that $f \geq f^{**}$, the finite extensibility (FE) regime is entered and a model specific behaviour follows. This is the region which is most studied experimentally [6, 13].

6.2.4 The N dependence of R_f at fixed-f

For later purposes, it is useful to discuss at this stage the N dependence of the average end-to-end vector at fixed-f in the different domains. In the linear regime, the N dependence is related to the spring constant varying as $N^{-2\nu}$. For both the Pincus blob regime and the

finite extensibility regime (sometimes collectively denoted as the strong stretching regime in the following), the average extension scales like N at fixed-f, a behaviour expected when the extension of the stretched polymer overcomes the size of the unstretched chain [24].

6.2.5 Typical force cross-over values in experimental set-ups

Cross-over values f^* and f^{**} for some micro-manipulations on stretched macromolecules at 300K reported in the introduction are easily estimated on the basis of published values of the contour length L_c of individual chains and of the Kuhn segment length b which combine to give $R_0^2 = L_c b$. For a DNA chain of length $L_c \approx 30\mu m$ in physiological conditions for which $b = 0.1\mu m$ [10], one finds $f^* \approx 0.003pN$ and $f^{**} \approx 0.05pN$ and we note that, in reference [10], data points are reported for $f \geq f^{**}$. The AFM study of individual dextran filaments leads to $f^* = 0.2pN$ and $f^{**} = 7pN$ using $b = 0.6nm$ and $L_c \approx 1.\mu m$ [13]. Exploring the power law regime would be rather difficult as f should be of the order of a few pN while natural fluctuations seem to be of the order of $20pN$. Improved precision could however be obtained by averaging over many successive stress or strain cycles over the range of end-to-end vector lengths of interest [13].

6.3 Fixed f and fixed-R ensembles for a single polymer chain

6.3.1 A reminder of textbook statistical mechanics

We now establish the theoretical context more explicitly by starting from the equilibrium distribution function of the chain end-to-end vector $\underline{R} = \underline{r}_N - \underline{r}_0$ in the absence of external force defined as

$$W_0(\underline{R}, N) = \frac{\int d\underline{r}^N \delta\left(\underline{r}_N - \underline{r}_0 - \underline{R}\right) \exp\left[-\beta U\left(\underline{r}^N\right)\right]}{\int d\underline{r}^N \exp\left[-\beta U(\underline{r}^N)\right]} \equiv \frac{Z_R}{Z}, \tag{6.3}$$

where $\beta = \frac{1}{k_B T}$ is the reciprocal temperature, $\underline{r}_i$ is the ith bead position, $U(\underline{r}^N)$ is the effective potential energy with $\underline{r}^N$ representing the set of coordinates of the chain and δ is the Dirac delta function. The potential energy consists of a sum of bond length constraining potential terms (insuring the connectivity) and possibly EV pair interactions. The numerator Z_R and denominator Z in the above equation are single chain partition functions for a constrained and unconstrained end-to-end vector, respectively. For any cartesian component $\alpha = x, y, z$, the first moment of R_α with respect to W_0 vanishes due to space isotropy while the second moment gives $\frac{1}{3}R_0^2$.

In the fixed-R ensemble, the average of an observable $O(\underline{r}^N)$ is given by

$$\langle O \rangle_R = Z_R^{-1} \int d\underline{r}^N O(\underline{r}^N) \delta\left(\underline{r}_N - \underline{r}_0 - \underline{R}\right) \exp\left[-\beta U\left(\underline{r}^N\right)\right]. \tag{6.4}$$

Under the end-to-end vector constraint, the choice $O = -\frac{\partial U}{\partial \underline{r}_0}$ yields the average internal force $\underline{f}_R$ acting on the end-bead 0 which lies along $\underline{\hat{R}} = \frac{\underline{R}}{R}$ by symmetry. To see this explicitly, we start

from Eq.(6.4) where our choice of observable leads to an expression where the $\frac{\partial}{\partial \underline{r}_0}$ operation acts on U within the integral. First, the expression can be transformed by applying the derivative operation to the $\exp(-\beta U)$ factor itself. Integration by parts further shifts the application of the derivative operation to the δ function. Given the nature of the argument of the δ function appearing in Eq.(6.4), the gradient operation with respect to $\underline{r}_0$ can be substituted with a gradient with respect to $\underline{R}$ so that the expression turns out to be finally equivalent to the gradient of lnW_0 with respect to $\underline{R}$ (see Eq.(6.3)). Keeping consistency with notations used in the introduction, we thus have

$$\left\langle -\frac{\partial U}{\partial \underline{r}_0} \right\rangle_R = \left\langle +\frac{\partial U}{\partial \underline{r}_N} \right\rangle_R = -\frac{1}{\beta}\frac{\partial}{\partial \underline{R}} \left(\ln W_0(\underline{R}, N)\right) = f_R \hat{\underline{R}} \equiv h(R)\underline{R}. \tag{6.5}$$

The equation $f_R = h(R)$ defines the elasticity law in the R ensemble.

In the fixed-f ensemble, the end-to-end vector fluctuates around a non zero vector $\langle \underline{R} \rangle_f$ parallel to $\underline{f}$. The relevant partition function becomes [1]

$$Z_f(\underline{f}, N) = \int d\underline{R}\, Z_R \exp\left(\beta \underline{f} \cdot \underline{R}\right) = Z \int d\underline{R}\, W_0(\underline{R}, N) \exp\left(\beta \underline{f} \cdot \underline{R}\right). \tag{6.6}$$

The f ensemble average of a microscopic variable $O(\underline{r}^N)$ will be written as

$$\langle O \rangle_f = Z_f^{-1} \int d\underline{r}^N O(\underline{r}^N) \exp\left[-\beta \left(U(\underline{r}^N) - (\underline{r}_N - \underline{r}_0) \cdot \underline{f}\right)\right]. \tag{6.7}$$

It follows from above that the end-to-end vector averages are given as partial derivatives of Z_f according to

$$\langle \underline{R} \rangle_f = \frac{1}{\beta} \nabla_f \ln Z_f = R_f \hat{\underline{f}} \equiv g(f) \hat{\underline{f}}. \tag{6.8}$$

Let us calculate the fluctuation $\langle \delta R_\mu \delta R_\nu \rangle_f = \langle R_\mu R_\nu \rangle_f - \langle R_\mu \rangle_f \langle R_\nu \rangle_f$. By definition

$$\begin{aligned} \langle R_\mu R_\nu \rangle_f &= \frac{1}{Z_f} \int d\underline{R} R_\mu R_\nu Z_R \exp\left(\beta \underline{f} \cdot \underline{R}\right) \\ &= \frac{1}{Z_f} \frac{\partial}{\partial \beta f_\nu} \frac{\partial}{\partial \beta f_\mu} \int d\underline{R} Z_R \exp\left(\beta \underline{f} \cdot \underline{R}\right) \\ &= \frac{1}{Z_f} \frac{\partial}{\partial \beta f_\nu} \left[\frac{\partial}{\partial \beta f_\mu} Z_f\right] \end{aligned} \tag{6.9}$$

which according to Eq.(6.8) leads to

$$\langle \delta R_\mu \delta R_\nu \rangle_f = \frac{\partial}{\partial \beta f_\nu} \langle R_\mu \rangle_f . \tag{6.10}$$

Knowing that $\langle R_\mu \rangle_f = g(f)\frac{f_\mu}{f}$, $\langle \delta R_\mu \delta R_\nu \rangle_f$ becomes

$$\langle \delta R_\mu \delta R_\nu \rangle_f = \frac{1}{\beta} \left[\frac{f_\nu f_\mu}{f^2} \frac{\partial g(f)}{\partial f} + \frac{g(f)}{f} \left(\delta_{\mu\nu} - \frac{f_\mu}{f}\frac{f_\nu}{f}\right)\right], \tag{6.11}$$

which in tensor form is

$$\langle \delta \underline{R} \delta \underline{R} \rangle_f = \frac{1}{\beta^2} \nabla_{\underline{f}} \nabla_{\underline{f}} \ln Z_f = \frac{1}{\beta} \left(\frac{\partial g(f)}{\partial f} \hat{\underline{f}}\, \hat{\underline{f}} + \frac{g(f)}{f} (\underline{\underline{I}} - \hat{\underline{f}}\, \hat{\underline{f}})\right), \tag{6.12}$$

where $\underline{\underline{I}}$ is the unit tensor. Eq.(6.8) defines the elasticity law, $R_f = g(f)$, in the f-ensemble and states moreover that the average elongation in a direction transverse to $\underline{\hat{f}}$ vanishes by symmetry. Fluctuations are still given in terms of $g(f)$ and its first derivative. If we denote respectively as $\delta R_{\parallel}$ and $\delta R_{\perp}$ the longitudinal and transverse components of fluctuations in the fixed-f ensemble, we obtain from Eq.(6.8)

$$\left\langle \delta R_{\parallel}^2 \right\rangle_f = \frac{1}{\beta} \frac{\partial g(f)}{\partial f}, \tag{6.13}$$

$$\left\langle \delta R_{\perp}^2 \right\rangle_f = \frac{1}{\beta} \frac{g(f)}{f}. \tag{6.14}$$

The non-equivalence between fixed-f and fixed-R ensembles shows up in the fact that the relationships $f_R = h(R)$ (Eq.(6.5)) and $R_f = g(f)$ (Eq.(6.8)) are not inverse functions of one another. The function Δ_f introduced earlier to measure this ensemble difference can thus be expressed as $\Delta_f = f - h(g(f))$.

6.3.2 Elasticity laws in both stretched chain ensembles for specific models

In this subsection, our aim is simply to use the above theory to estimate the importance of the ensemble effects on the single polymer elasticity law for standard chain models. We will successively treat the universal models for ideal chains and for chains in good solvent and finally look to the freely jointed chain to appreciate the ensemble effects when finite extensibility is incorporated in the model.

Long chains at or above the theta point

If we restrict ourselves to theta and good solvent conditions, the single chain end-to-end distance equilibrium distribution $W_0(\underline{R}, N)$ evolves, as the number of monomers N gets larger, to an expression $W_0(\underline{R}, N) \propto \frac{C}{R_0^3} \hat{w}(x)$ where $\hat{w}(x)$ is a universal function of the reduced distance $x = \frac{R}{R_0}$ and where the explicit N dependence is left in the measure only. We have [26]

$$W_0(\underline{R}, N) = \frac{C}{R_0^3} x^{\gamma} exp\left(-Dx^{\delta}\right), \tag{6.15}$$

where C is a normalisation constant. The RGT parameters for good solvent chains are $D = 1.2063, \delta = (1-\nu)^{-1} = 2.4272$ and $\gamma = 0.275$ while, for gaussian chains, we simply have $D = \frac{3}{2}$, $\delta = 2.0$ and $\gamma = 0.0$.

Within the fixed-R ensemble, the force function $f_R = h(R)$ can be obtained by applying Eq.(6.5) to the particular expression (6.15). Using reduced quantities, one gets the general result

$$\beta R_0 f_R \equiv \eta_g = -\frac{\gamma}{x} + \frac{D}{(1-\nu)} x^{\frac{\nu}{(1-\nu)}}, \tag{6.16}$$

which reduces to the linear law $\beta R_0 f_R = 3x$ in the gaussian case. We apply Eqs.(6.6), (6.8) and (6.12) to the particular end-to-end distribution function (6.15) to get the elasticity law and the end-to-end vector fluctuations relative to the fixed-f ensemble. For gaussian chains,

the linear law $R_f = g(f) = R_0 \frac{\eta_g}{3}$ turns out to be strictly identical to the elasticity law already obtained in the fixed-R ensemble. The end-to-end vector fluctuations in the fixed-f ensemble, which can be obtained directly from $g(f)$ on the basis of Eqs.(6.13) and (6.14), are independent of f and thus identical to the unstretched case. For EV chains, the end-to-end vector moments in the f ensemble, namely R_f, $\left\langle \delta R_{\parallel}^2 \right\rangle_f$ and $\langle \delta R_{\perp}^2 \rangle_f$, can be estimated numerically along the lines developed for R_f only in ref. [19], on the basis of Eqs.(6.8), (6.13) and (6.14). For completeness, we give the expressions to be evaluated numerically in terms of the global reduced force η_g,

$$\frac{R_f}{R_0} \equiv x = \frac{1}{\eta_g}\left[\left(\frac{\eta_g c_2}{s_1}\right) - 1\right], \tag{6.17}$$

$$\frac{\left\langle \delta R_{\parallel}^2 \right\rangle_f}{R_0^2} = \frac{s_3}{s_1} - \left(\frac{c_2}{s_1}\right)^2 + \frac{1}{\eta_g^2}, \tag{6.18}$$

$$\frac{\langle \delta R_{\perp}^2 \rangle_f}{R_0^2} = \frac{1}{\eta_g^2}\left[\left(\frac{\eta_g c_2}{s_1}\right) - 1\right], \tag{6.19}$$

where we have defined

$$s_i(\eta_g) = \int_0^\infty dy exp\left[-Dy^{\frac{1}{1-\nu}}\right] y^{i+\gamma} sinh(\eta_g y), \tag{6.20}$$

$$c_j(\eta_g) = \int_0^\infty dy exp\left[-Dy^{\frac{1}{1-\nu}}\right] y^{j+\gamma} cosh(\eta_g y). \tag{6.21}$$

For chains in good solvent, satisfying the universal distribution function Eq.(6.15), the elasticity laws in fixed-f and fixed-R ensembles, i.e. Eqs.(6.17) and (6.16) respectively, are found to be largely different! This is shown in figure 6.1 where the universal behaviour of Δ_f/f is plotted against the reduced distance x. The difference is small (below 2%) for chains stretched over distances at least three times their typical unstretched chain value ($R > 3R_0$), it amounts to about 25% for $R \approx R_0$ and it rises to infinity as the distance gets closer and closer to zero. The elastic behaviour of chains in good solvent thus presents quantitative differences depending upon the nature of the stretching constraint. These effects, valid for arbitrary N (although we discard the very short chains because they somewhat differ from the universal behaviour), culminate at short end-to-end distances ($R < R_0$) where both distributions of conformations are intrinsically different as we mentioned in the introduction. For large extensions, finite extensibility effects which are disregarded in the chain universal models (Eq.(6.15)), should be taken into account. This will be considered in the next subsection with the FJC model. Let is finally remark that the ideal chain result $\Delta_f = 0$, which is valid for arbitrary N, is finally somewhat surprising when one considers that, at least at short end-to-end distances, the distribution of conformations is very different in both ensembles. We will see the origin of the absence of constraint effect on the elasticity properties of gaussian chains in the next section.

The FJC model: finite extensibility effects

The freely jointed chain model (FJC) is the prototype of ideal chain with limited extensibility. This model of N freely jointed rigid links each of length b evolves towards the gaussian model as N gets large, as long as the end-to-end distance R remains much smaller than the contour length of the chain $L_c = Nb$ [1, 4].

To analyse the elasticity law in the fixed-R ensemble for the FJC model, we exploit the known expression of $W_0(\underline{R}, N)$ which is an integral over reciprocal space [1]. The average force intensity $h(R)$ estimated using Eq.(6.5), requires an additional integral over reciprocal space to be calculated. We have

$$W_0(\underline{R}, N) = \frac{1}{2\pi^2 R} s_1' \tag{6.22}$$

$$h(R) = \frac{1}{R} - \frac{c_2'}{s_1'}, \tag{6.23}$$

where we have introduced more general compact notations (which will be useful for later purposes)

$$s_i' = \int_0^\infty dq q^i sin(qR) \left[\frac{sin(qb)}{qb}^N\right], \tag{6.24}$$

$$c_j' = \int_0^\infty dq q^j cos(qR) \left[\frac{sin(qb)}{qb}^N\right], \tag{6.25}$$

which will be used for odd i indices and even j indices only.

On the other hand, the partition function for the FJC at fixed-f can be evaluated analytically using Eq.(6.6). The average end-to-end vector [1] and its fluctuations at fixed-f (see Eqs.(6.13) and (6.14)) are easily obtained. One finds the classical result $\frac{R_f}{L_c} \equiv s = \mathcal{L}(\eta_l)$ where $\eta_l = \frac{bf}{k_B T}$ is the local reduced force, s is the relative extension and $\mathcal{L}(x) = coth(x) - 1/x$ is the well known Langevin function. Use of Eqs.(6.13) and (6.14) leads to fluctuation expressions $\left\langle \delta R_{\parallel}^2 \right\rangle_f = Nb^2 \left(1 - 2\mathcal{L}(\eta_l)/\eta_l - \mathcal{L}^2(\eta_l)\right)$ and $\langle \delta R_{\perp}^2 \rangle_f = Nb^2 \mathcal{L}(\eta_l)/\eta_l$.

In figure 6.2, we show the behaviour of $\frac{\Delta_f}{s}$ for various lengths of the FJC model ($N = 16$, $N = 32$, and $N = 64$) in terms of s corresponding to a range of forces $\eta_l \leq 4.0$. Such a figure is motivated by the fact; discussed in the following, that $\Delta_f \approx \frac{3s}{N}$ for small s and large N. About the distinction between both elasticity laws, one finds that $\frac{\Delta_f}{f}$ decreases below the 1% level for chains with $N > 100$ but amounts 10% for the $N = 16$ case at $s = 0.75$. The gaussian chain limit for the elasticity law ensemble difference (namely $\Delta_f/f = 0$) can indeed be recovered from the FJC result, for $s << 1$, when N goes to infinity.

6.4 The connection formulae between fixed-f and fixed-R ensembles

In the previous section, we have shown that single chain elasticity laws are in general different in different single stretched chain ensembles. While the effect is accidentally zero for gaussian chains, the relative difference Δ_f/f is below the percent level only when EV chains, independently of their length, are stretched over a distance which is larger than three times their unstretched end-to-end distance. Finally, for FJC chains, $\Delta_f/f \approx \frac{1}{N}$ over a large range of local reduced forces $\eta_l < 4$, provided N is larger than ≈ 15.

In the present section, we express the differences in the ensemble averages in terms of series expansions in order to interpret the properties of Δ_f which have summarised above. In order

to enlarge the potential applications of our theoretical developments, we will study the single stretched chain ensemble effects on the averages of an arbitrary structural property represented by an observable $O((\underline{r}_i)_{i=1,N})$. At the end of the section, we will return to the elasticity case on which we focus in this chapter.

6.4.1 General formalism

To be specific, we want to compare for an arbitrary observable O, its averages in the strain (fixed $\underline{R}$ vector) and in the stress (fixed $\underline{f}$ vector) conjugated ensembles. These ensembles imply vector constraints along the same direction (say along the z axis), namely $\underline{f} = (0, 0, f)$ and $\underline{R} = \underline{R}_f = (0, 0, R_f)$ where $R_f = g(f)$ (Eq.(6.8)).

On the basis of expressions (6.3), (6.4), (6.6) and (6.7), we can write the basic exact relationship linking ensemble averages, namely

$$\langle O \rangle_f = Z_f^{-1} \int d\underline{R} Z_R \langle O \rangle_R \exp\left(\beta \underline{R} \cdot \underline{f}\right) \equiv \int d\underline{R} M_f(\underline{R}) \langle O \rangle_R , \tag{6.26}$$

where the function $M_f(\underline{R})$ can be interpreted, using Eq.(6.6), as a probability distribution function associated to the fixed-R average which, by integration over the end-to-end vector space yields the fixed-f corresponding average.

In order to bridge the two ensemble averages in conjugated ensembles, the first idea would be to expand the r.h.s. of Eq.(6.26) around $(\langle O \rangle)_{\underline{R}=R_f\hat{\underline{f}}}$. This is formally possible by performing a simple Taylor expansion of the fixed-R observable average $\langle O \rangle_R$ around its value at $R = R_f$. Using expressions (6.7) and (6.3), integration of all expansion terms yields [25] an infinite series

$$\langle O \rangle_f = (\langle O \rangle_R)_{\underline{R}=R_f\hat{\underline{f}}} + \left(\frac{\partial}{\partial \underline{R}} \langle O \rangle_R\right)_{\underline{R}=R_f\hat{\underline{f}}} \cdot \langle \delta \underline{R} \rangle_f + \frac{1}{2} \left(\frac{\partial}{\partial \underline{R}} \frac{\partial}{\partial \underline{R}} \langle O \rangle_R\right)_{\underline{R}=R_f\hat{\underline{f}}} : \langle \delta \underline{R} \delta \underline{R} \rangle_f + \ldots , \tag{6.27}$$

where $\delta \underline{R} = \left(\underline{R} - R_f \hat{\underline{f}}\right)$ is the fluctuation measured in the fixed-f ensemble. The expansion in Eq.(6.27) (where we have conserved the first order term which is zero to indicate the series structure) is a basic relationship for the analysis of the ensemble difference for any single chain observable relative to a stretched chain.

The weakness of this approach is that the convergence of the series is difficult to apprehend without analysing more closely the position and the sharpness of the peak in the M_f function in the $\underline{R}$ space, in particular regarding the polymer size. To do so, we introduce the free energy $A(\underline{R}, N) = -\beta^{-1} ln Z_R(\underline{R}, N)$ (where the temperature dependence is not made explicit), so that M_f can be rewritten as

$$M_f(\underline{R}) = Z_f^{-1} \exp\left(-\beta\left(A - \underline{R} \cdot \underline{f}\right)\right) \tag{6.28}$$

$$Z_f = \int d\underline{R} \exp\left(-\beta\left(A - \underline{R} \cdot \underline{f}\right)\right) . \tag{6.29}$$

In order to clarify the important role of N in the connection formulae between ensembles, we rewrite the weight function (6.29) in terms of b, N and a new intensive variable $\underline{s} = \underline{R}/N$.

Using $R_0 = bN^\nu$, one gets

$$\langle O \rangle_f = \frac{1}{C} \int d\underline{s} \, \langle O \rangle_{Ns} \exp\left(-N\left[\beta a(s,N) - \beta \underline{s} \cdot \underline{f}\right]\right), \tag{6.30}$$

where $a(s,N)$ is the single chain free energy per bond when the chain end-to-end vector is constrained at $R = Ns$. The M_f peak position in $\underline{s}$ space is given by minimising the argument of the exponential. This leads to the implicit equation in $\underline{s}$,

$$f = \frac{\partial a(s,N)}{\partial \underline{s}}, \tag{6.31}$$

where, according to the above free energy definition and Eqs.(6.3) and (6.5), the r.h.s. is $h(Ns)$, the internal force in the fixed end-to-end vector ensemble. The peak position thus does not correspond exactly to $R_f \equiv g(f)$, but to $h^{-1}(f)$ so that the leading term in the expansion would be $\langle O \rangle_R$ around its value at $R = h^{-1}(f)$. Along the same lines, the dependence of $a(s,N)$ upon N makes it difficult to make general statements upon the evolution of the convergence with N. What can be shown on various polymer models is that as f is fixed and N increases, $a(s,N)$ becomes progressively N independent while the peak position evolves towards the conjugated ensemble value $R = R_f \equiv g(f)$.

This limiting behaviour as N becomes infinite has a clear mathematical meaning. However, we would like to comment here upon the point that fixed f stretching force, the infinite N limit for a stretched polymer has much less physical relevance than the well known thermodynamic limit which is used to establish the link between constant volume and constant pressure conjugated ensemble for an N particles system. The equivalence between ensembles in the thermodynamic limit is proved on the basis of an expression similar mathematically to Eq.(6.30) where the free energy per particle is function of the density only (thus independent of N). When the N infinity limit is taken at fixed density, the weight function becomes infinitely sharp and finite size corrections are found to be in N^{-1}. For the stretched polymer case, the number of monomers and the end-to-end vector are the extensive variables replacing respectively the number of particles and the volume, while the force and the average extension per bond $\underline{s}$ are the intensive variables playing respectively the role of the pressure and the (inverse) density. Polymers always have finite sizes and ensemble correction terms should be controlled systematically for the particular N value. To estimate a typical very large N value for real chains, let us consider a chain at theta point modeled as a bead-spring (gaussian) chain for which each spring is an elementary statistical segment representing a portion of the chain consisting typically of a few Kuhn segments. Taking a typical synthetic polymer like polystyrene, one has $N \approx 200$ for a very long polymer of about 10^6 Dalton.

6.4.2 Link between ensembles for specific chain models

We now consider for specific polymer models the difference between averages relative to the stretched chain conjugated ensembles through an analysis of the series developed in the previous subsection. Let us start by adopting for W_0 and its associated free energy expression the universal model function for theta point and good solvent polymers defined by the distribution (6.15). If we disregard irrelevant s independent terms, we find a free energy per link given by

$$\beta a(s,N) = -\frac{\gamma}{N} ln(\frac{s}{b}) + D(\frac{s}{b})^{1/(1-\nu)}. \tag{6.32}$$

We first restrict ourselves to the gaussian chain case because the absence of the term coupling N and s in Eq.(6.32) (because $\gamma = 0$) considerably simplifies the analysis. We will consider the EV chain in a second step.

Gaussian chain universal model

Substituting Eq.(6.32) in Eq.(6.30), we observe that the fixed R ensemble average is weighted by a gaussian function $M_f \propto \exp\left(-N\frac{3}{2b^2}(\underline{s} - \langle \underline{s} \rangle_f)^2\right)$. If we keep f fixed (or equivalently $\underline{s}$ fixed at $\langle \underline{s} \rangle_f$) but increase N, the width of the peak decreases without changing the position of the distribution maximum so that the contribution of $\langle O \rangle_{Ns}$ at $\underline{s} = \langle \underline{s} \rangle_f$ dominates more and more. One gets a series

$$\langle O \rangle_f = \langle O \rangle_{R_f} + \frac{1}{2}\left(\frac{\partial}{\partial \underline{s}}\frac{\partial}{\partial \underline{s}}\langle O \rangle_R\right)_{\underline{R}=N\langle \underline{s} \rangle_f} : \langle \delta \underline{s} \delta \underline{s} \rangle_f + \ldots \tag{6.33}$$

$$= \langle O \rangle_{R_f} + \frac{1}{N}\frac{b^2}{6} TRACE\left[\left(\frac{\partial}{\partial \underline{s}}\frac{\partial}{\partial \underline{s}}\langle O \rangle_R\right)_{\underline{R}=N\langle \underline{s} \rangle_f}\right] + \ldots, \tag{6.34}$$

where the next terms consist in ascending integer powers of N^{-1}. For non pathological $\langle O \rangle_R$ functions and for moderately large N, the above series should always converge to a finite value. Note that in the particular case where $\langle O \rangle_R$ is linear in $\underline{s}$ like it is precisely the case for the internal force $h(R)$ (see Eq.(6.16)), $\langle O \rangle_f$ is strictly equal to $\langle O \rangle_{R_f}$ for N finite and arbitrary because all terms of the series vanish! This explains the origin of the strict equivalence between elasticity laws relative to both ensembles which was noticed for gaussian chains with finite number of beads in the previous section.

To illustrate the general situation where $\langle O \rangle_R$ is a non linear local variable, we take the function $O = \exp\left(i\underline{q} \cdot \underline{u}_i\right)$ relevant in the scattering properties of a chain with N bonds represented by $\left[\left(\underline{u}_j\right)_{j=1,N}\right]$ while $\underline{q}$ is an arbitrary scattering vector. We thus consider a gaussian chain with N bonds of mean squared length b^2 which is subject to stretched chain conjugated ensembles. Either a force $\underline{f}$ is applied at both ends of the chain or a fixed end-to-end vector $\underline{R} = \frac{\beta}{3}Nb^2\underline{f}$ restricts the chain configurational space. The result is independent of the bond index and both averages are given by

$$\begin{aligned} \left\langle \exp\left(i\underline{q} \cdot \underline{u}_i\right)\right\rangle_R &= \exp\left[-\frac{b^2}{6}\left(1 - \frac{1}{N}\right)q^2 + i\left(\underline{q} \cdot \underline{s}\right)\right], \\ \left\langle \exp\left(i\underline{q} \cdot \underline{u}_i\right)\right\rangle_f &= \exp\left[-\frac{b^2}{6}q^2 + i\frac{1}{3}b^2\beta\left(\underline{q} \cdot \underline{f}\right)\right], \end{aligned} \tag{6.35}$$

where $\underline{s} = \frac{\underline{R}}{N}$. Both averages are found to be identical up to a factor $\exp\left(-\frac{b^2q^2}{6N}\right)$ affecting the fixed-R ensemble average. For a given force f, the ensemble equivalence is thus only recovered when N gets infinite. It can easily be shown that, as one expands the exponential correction term, the obtained infinite series in ascending powers in $\frac{1}{N}$ is equivalent to the series in Eq.(6.34).

EV chain universal model

For EV chains, the weight maximum is given by Eq.(6.31) using the free energy expression given by Eq.(6.32), which leads to the implicit equation

$$\beta s f - \frac{D}{(1-\nu)}(\frac{s}{b})^{\frac{1}{(1-\nu)}} = -\frac{\gamma}{N}, \tag{6.36}$$

whose solution s_{max} is N dependent. When the r.h.s. of Eq.(6.36) can be neglected, i.e. when $\beta f s >> \frac{0.275}{N}$, one finds $s_{max} = \left(\frac{(1-\nu)}{D}\right)^{\frac{(1-\nu)}{\nu}} (\beta f)^{\frac{(1-\nu)}{\nu}} b^{\frac{1}{\nu}}$ which gives an extension R_{max} following the Pincus scaling expression g(f) given by Eq.(6.2). Accordingly, the above condition can be interpreted as $R >> 0.275 r_{blob}$ which indicates that, for a fixed f value and thus for a fixed Pincus (tensile) blob size $r_{blob} = (\beta f)^{-1}$, the number of monomers should be such that the polymer extension is several times the blob size [24]. Physically, this means that the chain must be in the strong stretching regime ($\eta_g >> 1$). If this condition is met, one recovers the situation discussed earlier where the N factor preceding the brackets in Eq.(6.30) allows a steepest descent method approach to re-express the integral as a series of terms of ascending powers in N^{-1}.

Some comments about the FJC model

The link between stretched chain ensemble averages $\langle O \rangle_f$ and $\langle O \rangle_R$ for the FJC model furnishes additional insights about the FE effects. We first note that the stretched chain free energy $F(\underline{R}, N)$, its first derivative respect to R which is the force h(R), and, if required, its higher derivatives can be calculated numerically using expressions (6.23) and derivatives easily expressed in terms of higher order coefficients s'_i and c'_j defined earlier in Eq.(6.25). Using the above quantities calculated for N up to 64 over the range $0 \leq \eta_l \leq 4.00$ corresponding to $s \leq 0.75$, one expects that the s dependent part of the free energy per monomer presents a polymer size dependent term dominated by a $\frac{1}{N}$ and then a $\frac{1}{N^2}$ terms. Moreover, as $\Delta_f = f - h(g(f))$ for the FJC model should converge to zero in the N infinite limit at f arbitrary [1, 4], one should have

$$\beta a = \frac{1}{2}\left(3 + \frac{a'}{N} + \frac{a''}{N^2}\right)(\frac{s}{b})^2 + \frac{1}{4}\left(\frac{9}{5} + \frac{b'}{N} + \frac{b''}{N^2}\right)(\frac{s}{b})^4 + \ldots, \tag{6.37}$$

$$\beta h(R) b = (3 + \frac{a'}{N} + \frac{a''}{N^2})\frac{s}{b} + \left(\frac{9}{5} + \frac{b'}{N} + \frac{b''}{N^2}\right)\left(\frac{s}{b}\right)^3 + \ldots, \tag{6.38}$$

where a', a'', b' and b'' were determined empirically from fitting polynomials to the numerically determined free energy and derivatives. Using $a' = -3.00$, $b' = -4.50$, $a'' = 1.2684$, $b'' = 1.68$ one could explain the $\frac{\Delta_f}{s}$ dependence upon N and s.

The link between ensemble averages for an arbitrary observable $\langle O \rangle$ relative to the FJC model is given by Eqs.(6.28) and (6.29) where the free energy term is given by Eq.(6.37). The maximum of probability is given by the s implicit Eq.(6.38) which, at low N, gives an s_{max} value which is N dependent. As N increases, the r.h.s. of the Eq.(6.38) must evolve towards $\beta f b = \mathcal{L}^{-1}(s)$: this limit is obtained as soon as $N >> 1$. For $N >> 1$, the exponential argument in M_f probability is thus purely extensive in N, which leads to the equivalence between conjugated ensemble averages up to a correction dominated by a term in $\frac{1}{N}$.

6.4.3 A second order approximation applied to the elasticity case

The series expansion given by Eq.(6.27) defines a second order term which should dominate Δ_O for an arbitrary observable provided that we are close to the convergence regime of the particular chain model considered. We will again focus on the elasticity law and thus select the variable $O \equiv -\frac{\partial U}{\partial z_0}$ where z_0 is the z component of the end-bead 0 of position $\underline{r}_0$. In the fixed-f ensemble, mechanical equilibrium imposes $\left\langle -\frac{\partial U}{\partial z_0} \right\rangle_f = f$ while, in the fixed-R ensemble Eq.(6.5) gives $\left\langle -\frac{\partial U}{\partial z_0} \right\rangle_R = h(R)\frac{R_z}{R}$ where R_z is the z component of the end-to-end vector. The quantity Δ_f which was introduced earlier in this chapter as a measure of the distinction between the elasticity laws in both ensembles, can indeed be expressed as

$$\Delta_f \equiv \left\langle -\frac{\partial U}{\partial z_0} \right\rangle_f - \left\langle -\frac{\partial U}{\partial z_0} \right\rangle_R = f - \left(h(R)\frac{R_z}{R} \right)_{\underline{R}=\underline{R}_f} = f - h(R_f). \tag{6.39}$$

Adapting Eq.(6.27) to our case provides us with the following second order approximation for Δ_f,

$$\Delta_f^{(2)} = \frac{1}{2}\langle \delta\underline{R}\delta\underline{R} \rangle_f : \left(\frac{\partial}{\partial \underline{R}}\frac{\partial}{\partial \underline{R}} \left(h(R)\frac{R_z}{R} \right) \right)_{\underline{R}=\underline{R}_f} \equiv \frac{1}{2}\langle \delta\underline{R}\delta\underline{R} \rangle_f : \underline{T}, \tag{6.40}$$

where the tensor $\underline{T}$ is introduced for convenience. Using diagonal properties of the fluctuation tensor according to Eqs.(6.12), (6.13) and (6.14), Eq.(6.40) can be transformed, using Eq.(6.8), as

$$\Delta_f^{(2)} = \frac{1}{2}\left[\left\langle \delta R_{\parallel}^2 \right\rangle_f T_{zz} + \left\langle \delta R_{\perp}^2 \right\rangle_f (T_{xx} + T_{yy}) \right] \tag{6.41}$$

$$= \frac{1}{2\beta}\left[\frac{\partial g}{\partial f}\left(\frac{\partial^2 h}{\partial R^2} \right)_{R=g(f)} + \frac{g(f)}{f}\left[\frac{2}{R}\left(\frac{\partial h}{\partial R} - \frac{h}{R} \right) \right]_{R=g(f)} \right] \tag{6.42}$$

$$= \frac{1}{2\beta}\left[\frac{\partial g}{\partial f}\left(\frac{\partial^2 h}{\partial R^2} \right)_{R=g(f)} + \frac{2}{f}\left(\frac{\partial h}{\partial R} - \frac{h}{R} \right)_{R=g(f)} \right]. \tag{6.43}$$

Using Eqs.(6.5), (6.6) and (6.8), the expressions Δ_f and $\Delta_f^{(2)}$ can be evaluated for any model for which $W_0(\underline{R}, N)$ is known. In Figures 6.1 and 6.2, we show, respectively, $\Delta_f^{(2)}$ for the universal EV case and for the FJC model. For the RGT model, the approximation is quite good for the range $R \geq R_0$ but for $R < R_0$, the expansions we have discussed do not converge. For the FJC case, the second order estimate improves quickly as N gets larger.

Quite generally, at fixed f in the highly stretched chain regime, it can be expected that both $h(R)$ and R_f become linear in chain length N [24]. In that regime, Δ_f can be shown to vanish like $1/N$ for infinite chains, independently of the chain model. This can be proved using the approximation $\Delta_f^{(2)} \approx \Delta_f$ valid in that regime. One takes $R_f = Nz(f)$ and $f_R = h(R) = w(R/N)$ where $z(f)$ and $w(r)$ (with $r = R/N$) are almost inverse functions of each other. Substituting these formal expressions in $\Delta_f^{(2)}$ (Eq.(6.43)) gives

$$\Delta_f^{(2)} = \frac{1}{N}\left[\frac{\partial z}{\partial f}\left(\frac{\partial^2 w}{\partial r^2} \right)_{r=z(f)} + \frac{2}{f}\left(\frac{\partial w}{\partial r} - \frac{w}{r} \right)_{r=z(f)} \right], \tag{6.44}$$

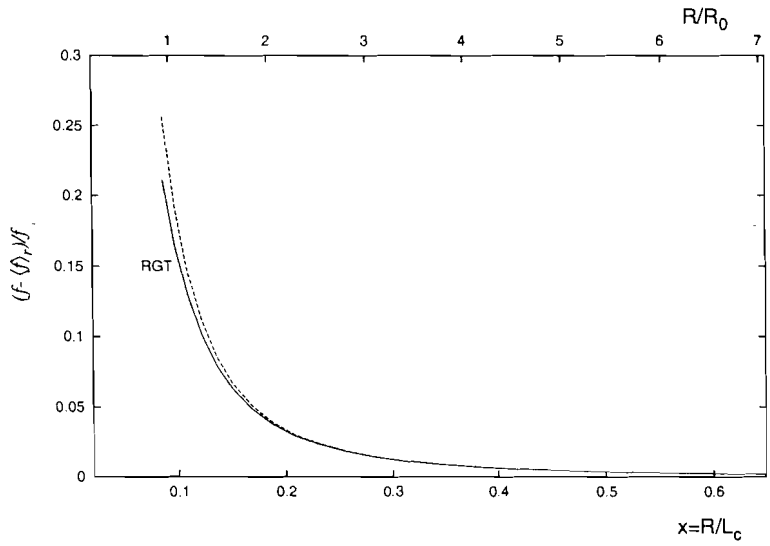

Figure 6.1: Δ_f/f is shown as a universal function of the reduced extension $x = R/R_0$ for the RGT model. The line (——) represents the direct differences while the dashed line (- - - -) shows the predictions of $\Delta_f^{(2)}$ according to Eq.(6.43).

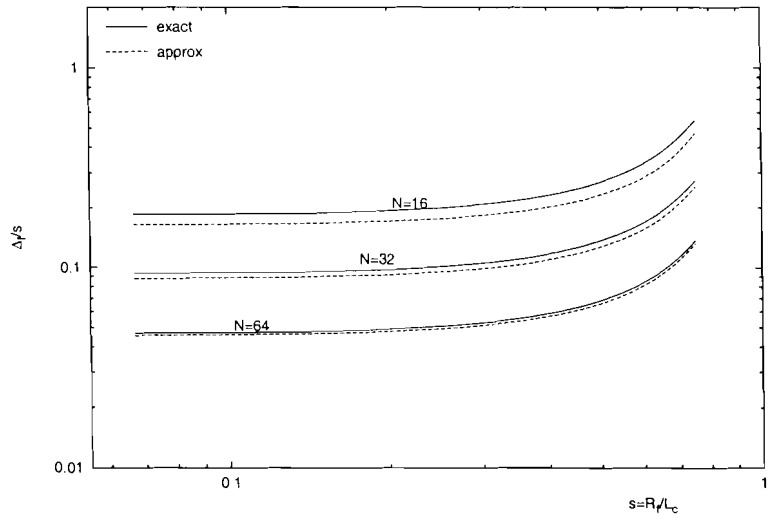

Figure 6.2: Δ_f/s is shown as a function of the reduced extension $s = R/L_c$ for the FJC model with N=16, 32, 64. The lines (——) represent the exact differences while the dashed lines (- - - -) show the predictions of $\Delta_f^{(2)}$ according to Eq.(6.43).

thus indicating a $1/N$ dependence at fixed-f (and thus at fixed $r = R/N$) in any strongly stretched regime such as the Pincus blob regime for EV chains or such as any type of FE regime.

6.4.4 Monte-Carlo calculations for the stretched hard-sphere necklace model

The semi-rigid necklace model we now consider consists in $N+1$ hard spheres linearly connected by N rigid bonds each of length b. This 3-D continuous space model is attractive as it combines most aspects of real polymers in good solvent conditions, namely EV and FE effects. We report in the following a Monte-Carlo study of a stretched polymer based on this model with a hard sphere diameter $\sigma = 0.65b$ which guarantees that EV interactions are operative at all length scales in the absence of external forces. The particular case $N = 400$ with unperturbed size $R_0 = 36.81b$ [21] was selected for our illustration as such a chain size is sufficiently long to display all stretching regimes of the elastic law.

The adopted MC method combines Configurational Bias sampling and reptation moves [27]. A stretched state of the polymer (i.e. under fixed external force $\pm\underline{f} = (0, 0, \pm f)$) is studied by adding to the potential energy term, a stretching work

$$T = -\underline{f} \cdot \underline{R}, \tag{6.45}$$

which is a function of the instantaneous value of the end-to-end vector $\underline{R}$. The MC procedure implemented follows the following points.

- 1. Suppose the molecule whose configurations are to be sampled has been succesfully generated.
- 2. One end of the polymer is randomly selected, a segment of fixed number of bonds k is then supressed at that end and reconstructed at the other end. The reconstruction is done segment by segment as follows.
- 3. Since the segments undergo unrestricted torsional rotations and bendings, to place the ith segment once $i-1$ segments ($2 \leq i \leq k$) have succesfully been placed, $idir$ bond vectors whose ends lie on a sphere of radius b (the bond length) and centred at the monomer $i-1$ are selected and accepted with a probabilty proportional to $\exp\left(\frac{fb}{k_BT}(\cos\phi - 1)\right)$, where ϕ is the angle the new bond vector makes with the external force of magnitude f.
- 4. Once these vectors are obtained. they are tested for overlap with already placed segments (with two segments said to overlap when their centres are separated by a distance less than σ). One of the nonoverlapping directions is randomly chosen then accepted and given a Rosenbluth weight $w_i(n)$ which is equal to the ratio of the number of nonoverlapping vectors to $idir$.
- 5. Simultaneously, $idir - 1$ other orientations are chosen around the old segment i in a similar manner. These together with the old position of segment i form a set of $idir$ old orientations. Overlapping is checked and the Rosenbluth of the old $w_i(o)$ is obtained.

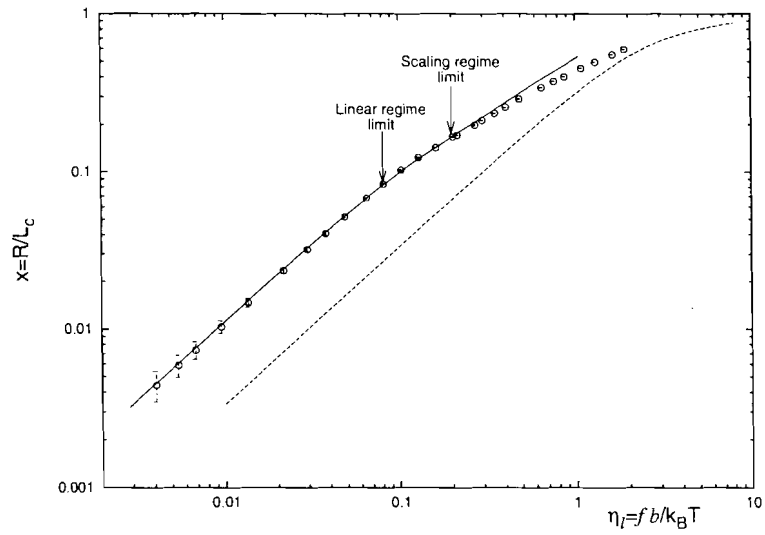

Figure 6.3: Elasticity law in the constant stress ensemble for the FJC model (- - - - -), the RGT prediction (——) and our fixed-f MC results (∘∘∘∘) adapted (for RGT) or calculated (by MC) for a 400 segments chain.

- 6. Procedures 3-5 are repeated until all k segments are reconstructed. The Rosenbluths of the new and old chains are, respectively,

$$w(n) = \prod_{i=1}^{k} w_i(n) \quad \text{and} \quad w(o) = \prod_{i=1}^{k} w_i(o). \tag{6.46}$$

- 7. Since no interaction energies are involved here, the acceptance condition is simply given by $acc\,(o \rightarrow n) = w(n)/w(o)$. The newly reconstructed segment is then accepted with a probability equal to $min\,[1, w(n)/w(o)]$.

It is important to state here that when we used $idir = 4$ and $k = 8$ for chains as long as 400 segments an acceptance rate of about 35% was obtained. This $idir$ and k values appeared to be the optimal values - ptimal in the sense that large $idir$ would enhance the acceptance rate but render longer, the time required to generate a new independent configuration, meanwhile large k would need shorter times but would diminish the acceptance rate.

Running the program for various f values gives the evolution of the average end-to-end vector $\underline{R}_f$, i.e. the $g(f)$ data shown in Figure 6.3, and its fluctuations shown in Figure 6.4. In Figure 6.3, the simulation points are compared with the RGT model prediction (Eq.(6.17)) for a polymer with unstretched size R_0 adjusted to the actual value of the 400 bonds polymer treated by MC, and also to the 400 bonds FJC prediction, a model to which our MC necklace model reduces when the hard-sphere interactions are suppressed. We observe that the MC results are quite well represented by the RGT curve at low forces [19]. Beyond $\eta_l \approx 0.3$, the data exhibit a smooth cross-over to a FJC behaviour.

Figure 6.4 shows the fluctuations of the end-to-end vector components of the same 400 segments EV chain treated by MC and the corresponding RGT predictions for longitudinal and transversal fluctuations. In terms of reduced quantities, the theoretical expressions given

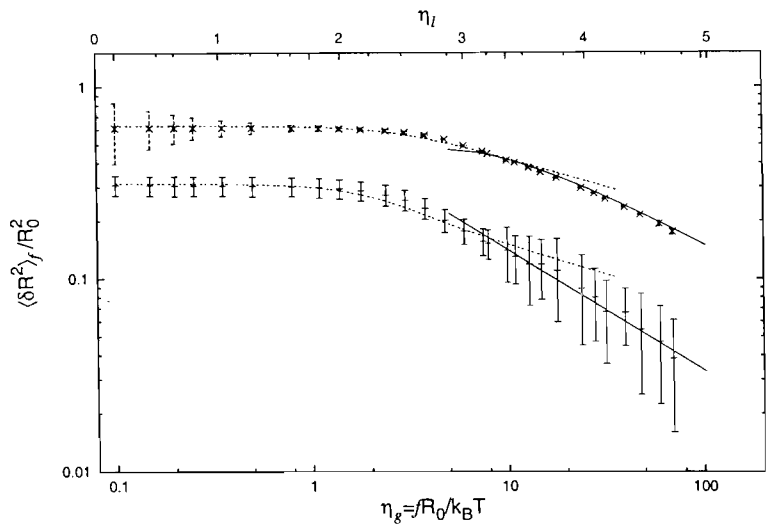

Figure 6.4: Fluctuations of the end-to-end vector components both parallel (lower) and perpendicular (upper) to the stretching force of a 400 segments EV chain. The dashed lines (----) give the RGT prediction. The continuous line (——) results from exploiting the link between the fixed-f end-to-end fluctuations and the $g(f)$ behaviour for the range $\eta_l > 0.2$, which is shown in figure 6.3 (see also text).

by Eqs.(6.18), (6.19), are seen to match the MC data up to $\eta_l \approx 0.3$. At higher forces, FE effects lead to a more rapid decrease of the fluctuations, a behaviour fully coherent with the corresponding $g(f)$ evolution given in Figure 6.3. This is actually shown by plotting in Figure 6.4 the (high stretching) expected behaviour of fluctuations as obtained by Eqs. (6.13), (6.14) applied to a smooth function fitting the $g(f)$ data in the $\eta_l > 0.3$ regime (see Figure 6.3). On the other hand, the unperturbed end-to-end vector distribution of the chain is needed to estimate the internal force at fixed end-to-end distance according to Eq.(6.5). It is useful to note that the distribution function of $\underline{R}$ in the presence of stretching forces, namely

$$W_f(\underline{R}, N) = \frac{\int d\underline{r}^N \delta\left(\underline{r}_N - \underline{r}_0 - \underline{R}\right) \exp\left[-\beta\left(U(\underline{r}^N) - (\underline{r}_N - \underline{r}_0)\cdot \underline{f}\right)\right]}{\int d\underline{r}^N \exp\left[-\beta\left(U(\underline{r}^N) - (\underline{r}_N - \underline{r}_0)\cdot \underline{f}\right)\right]} \tag{6.47}$$

can also be used to get the distribution in the absence of force, i.e. $W_0(\underline{R}, N)$ of Eq.(6.3), by exploiting the identity

$$W_0(\underline{R}, N) = \frac{Z_f}{Z} \exp\left(-\beta \underline{R}\cdot \underline{f}\right) W_f(\underline{R}, N), \tag{6.48}$$

where the Z and Z_f partition functions are defined by Eqs. (6.3) and (6.6) respectively. By superimposing the distributions W_0 obtained using Eq. (6.48) within our set of simulations at various fixed forces, the profile of W_0 was retrieved over a large range of R values as shown in Figure 6.5. This combination of biased samplings leads to a precise estimate of the distribution up to end-to-end distances of $R \approx 4.5R_0$, i.e. up to extensions of the order of 40% of the chain contour length where the probability density is reduced to 10^{-9} of its maximum value! As expected, the RGT curve shown in Figure 6.5 matches very well our data as long as FE

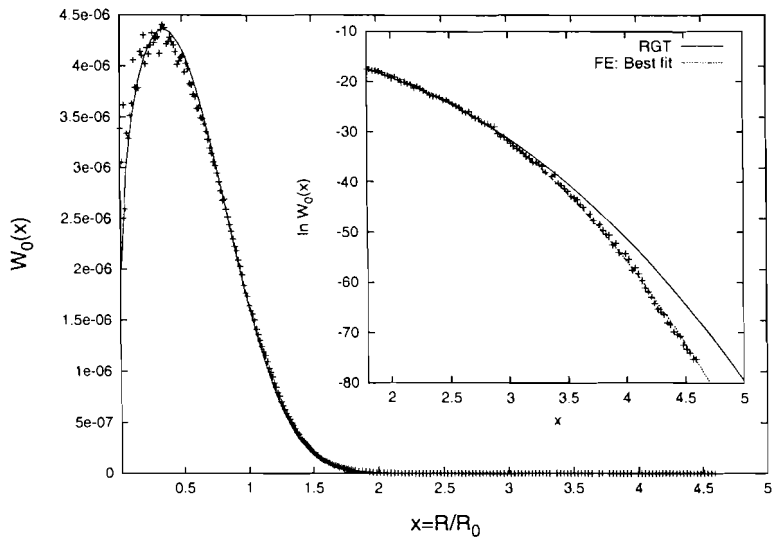

Figure 6.5: The equilibrium end-to-end vector distribution for a 400-segment excluded volume chain. The line shows the RGT model prediction for small and intermediate extensions. In the inset, we show the same function for extension values corresponding to rarely occurring highly stretched configurations so that FE deviations from the RGT prediction can be detected in our MC data

effects are not showing up. The cross-over to the FE regime seems to occur somewhere between $R = 2R_0$ and $R = 3R_0$ where we observe that $W_0(\underline{R}, N)$ starts decreasing more rapidly towards zero than expected from RGT. In order to reproduce this new behaviour by a smooth analytic function (to ease further derivation), we used for $R > 2R_0$ the same RGT expression (Eq.(6.15)) but with the exponent δ and the coefficient D considered as free fitting parameters. The inset of Figure 6.5 shows the resulting best fitting curve describing the data above $R = 2R_0$.

The fixed-R force $h(R)$ of the necklace chain can now be obtained according to Eq. (6.5) by combining two curves obtained by differentiation of lnW_0 functions, the first one on the basis the RGT function and the second one using the ad hoc fitting curve of lnW_0 in the FE regime, as discussed earlier in the Figure 6.5 data interpretation. The resulting function $h(R)$ is described by two portions valid in different R domains, as shown in Figure 6.6. The change of sign at $x \approx 0.35$ shows the specific distance where entropic forces equilibrate. In Figure 6.6, we further compare both elasticity laws and the validity of the bridge function $\Delta_f^{(2)}$. With respect to this latter point, the correction term does not perform so well at small stretching for reasons already explained above for the RGT case which is relevant in that regime.

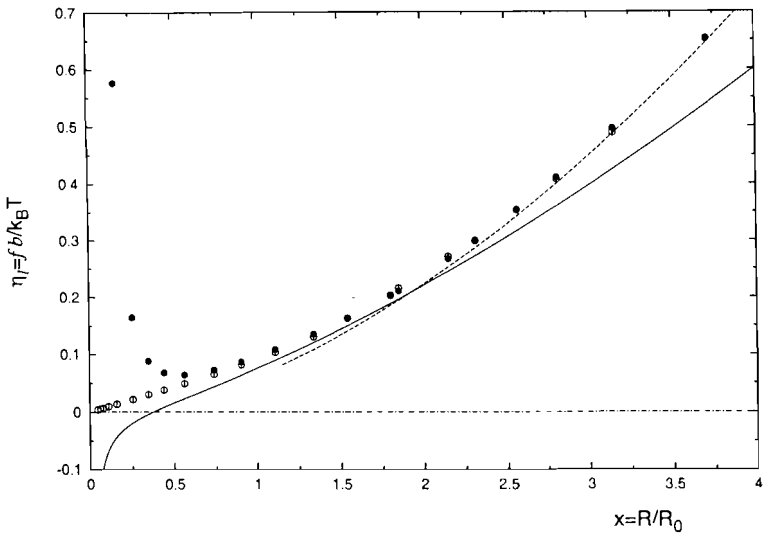

Figure 6.6: Force-extension relationships for the necklace EV model in the fixed $\underline{f}$ and the fixed $\underline{R}$ ensembles. The MC results for $g^{-1}(R)$ illustrate the elasticity law in the f ensemble ($\circ\circ\circ\circ$). For $h(R)$, the internal force in the fixed-R ensemble, the RGT prediction is represented (—) over the whole range of $x = R/R_0$ while the finite extensibility prediction using the fitting curve used in Figure 6.5 (see text) is shown in the domain of $x > 1$ (- - - -): the actual evolution of $h(R)$ in the simulation shifts from the first to the second curve in a smooth way. The filled circles show the fixed-f version deduced from fixed-R as $h(R) + \Delta_f^{(2)}$ using the the fluctuations of Figure 6.4.

Bibliography

[1] P. J. Flory, *Statistical Mechanics of Chain Molecules* Hanser Publ., Munich, 1989

[2] T. L. Hill, *An Introduction to Statistical Thermodynamics* Addison-Wesley Publ., Reading, 1960

[3] A. Y. Grosberg and A. R. Khokhlov, *Statistical Physics of Macromolecules* (AIP Press, New-York, 1994)

[4] L. R. G. Treloar, *The Physics of Rubber Elasticity* (3rd edition, Clarendon Press, Oxford, 1975)

[5] M. V. Volkenstein, *Configurational Statistics of Polymeric Chains (Interscience, New-York, 1963)*

[6] R. H. Austin, J. P. Brody, E. C. Cox, T. Duke, and W. Volkmuth, Phys. Today, **50***: 32, 1997*

[7] A. Kholodenko, M. Ballauff, and M. Aguero Granados, Physica **A260***: 261, 1998*

[8] A. Halperin, and E.B. Zhulina, Europhys. Lett. **15***: 417, 1991*

[9] P. Haronska, J. Wilder, and T. A. Vilgis, J. Phys. II **7***: 1273, 1997*

[10] S. B. Smith, L. Finzi, and C. Bustamante, Science **258**: *1122, 1992*

[11] H. Jensenius and G. Zocchi, Phys. Rev. Lett. **79**: *5030, 1997*

[12] P. Cluzel, A. Lebrun, C. Heller, R. Lavery, J.-L. Viovy, D. Chatenay, and F. Caron, Science **271**: *792, 1996*

[13] M. Rief, F. Oesterhelt, B. Heymann, and H. E. Gaub, Science **275**; *1295, 1997*

[14] X. Châtelier, T. J. Senden, J.-F. Joanny, and J.-M. Di Meglio, Europhys. Lett. **41**: *303, 1998*

[15] X. Châtelier and J.-F. Joanny, Phys. Rev. E **57**: *6923, 1998*

[16] J. T. Titantah, C. Pierleoni, and J.-P. Ryckaert, in preparation.

[17] I. Webman, J. L. Lebowitz, and M. H. Kalos, Phys. Rev. A **23**: *316, 1981*

[18] P. Pincus, Macromolecules **9**: *386, 1976*

[19] M. Wittkop, J.-U. Sommer, S. Kreitmeier, and D. Göritz, Phys. Rev. E **49**: *5472, 1994*

[20] P. Cifra and T. Bleha, J. Chem. Soc. Faraday Trans. **91**: *2465, 1995*

[21] C. Pierleoni, G. Arialdi, and J.-P. Ryckaert, Phys. Rev. Lett. **79**: *2990, 1997*

[22] M. Wittkop, S. Kreitmeier and D. Göritz, Phys. Rev. E **53**: *838, 1996*

[23] S. Kreitmeier, M. Wittkop, and D. Göritz, Phys. Rev. E **59**: *1982, 1999*

[24] P. G. de Gennes, Scaling Concepts in Polymer Physics *(*Cornell Univ. Press, Ithaca, 1979)

[25] J. L. Lebowitz, J. K. Percus, and L. Verlet, *Phys. Rev.* **153**: 153, 1967

[26] J. des Cloizeaux and G. Janninck, *Polymers in Solution: Their Modelling and Structure Clarendon Press, Oxford, 1990*

[27] D. Frenkel and B. Smit, *Understanding Molecular Simulation Academic Press, San Diego, 1996*

[28] M. Bishop, J. H. R. Clarke, A. Rey, and J. J. Freire, *J. Chem. Phys.* **95**: 4589, 1991

Chapter 7

Single polymer response to stretching forces

Summary

The elastic properties of two single polymer models in different solvent conditions are examined using Configurational Biased Monte-Carlo. For an excluded volume (EV) model and an atomistic polyethylene (PE) model, force-extension relations and other elastic properties reveal the usual three elastic regimes: the global regime, valid for weakly stretched chains; the scaling regime, where excluded volume forces start influencing the polymer properties and the local regime where finite extensibility sets in and the polymer experiences large internal rearrangements. In Θ-solvent conditions, PE is found to exhibit some molecular mass independent universalities, whereas in the presence of excluded volume forces the universalities become regime dependent. The decomposition of the elastic forces into enthalpic and entropic terms reveals a competition between the two terms over a wide range of extension. A magnetic field coupled to the stretching force induces a longitudinal residual dipole-dipole interaction whose magnitude grows, for weakly stretched chains, as the square of the stretching force but for a strongly stretched EV chain this interaction is found to follow a power law $\epsilon_{ij} \sim f^{3/2}$. An analogy between the thermodynamic function of a stretched strand composed of $|i-j|$ bonds and and the expectation value $\left\langle \exp\left(i\underline{q}\cdot(\underline{r}_i - \underline{r}_j)\right)\right\rangle_f$ of a portion of a polymer molecule between scattering centres i and j has led to important expressions for the static structure factor of stretched and unstretched chains. The celebrated Debye expression and the asymptotic $q^{-\frac{1}{\nu}}$ scaling predictions are easily recovered from the more general expressions.

7.1 Introduction

The study of the elasticity of single polymer molecules is essential for the understanding of the properties of a wide range of polymeric materials in solution and melts. The primary importance of this study lies in the subject of rubber (a material formed from cross-linking long flexible molecules) elasticity [1, 2, 3, 4]. It is well known [5] since Gough (1805), Lord Kelvin (1857) and Joule (1859) that rubber elasticity is predominantly of entropic origin. The pioneering theoretical works on this question date back to James and Guth (1942), Wall (1942,1943)

and Flory and Rehner (1943) who independently suggested that the elastic force was due to conformational entropy changes. In most of these theories, it is believed (through the affine deformation approximation) that the elastic properties of a polymer net-work depends intrinsically on those of the isolated strands comprising it. In this way the strand between two junctions of the net-work can be approximated to an isolated polymer molecule at whose ends (the junctions) equal and opposite forces act. These forces may also be experienced through nonascale devices like the atomic force microscope [6, 7] or through a strong velocity gradient on the polymer in solution [8, 9].

In biotechnology, the emergence of new techniques of manipulating single DNA molecules [10, 11], as pointed out in the previous chapter, offers a fertile ground for physicists to extend to this emerging science the knowledge acquired from the study of the elasticity of single polymer molecules. The coiled nature of DNA molecule renders its examination under a microscope very difficult but on stretching, a clearer picture of its structure can be obtained. The intensity of the stretching force needed to give the end bond distance of the molecule can help in the understanding of the mechanical properties of single molecules.

Various length scales can be used to describe the properties of a polymer molecule depending on the property of interest, its chemical nature or the environment in which the molecule finds itself. The scales range from the bond length through persistence length to the contour length; the hydrodynamic radius for a polymer in a solution undergoing a flow, the Bjerrum length $l_B = e^2/(4\pi\epsilon k_B T)$ and the Debye-Hückel electrostatic screening length $\kappa^{-1} \equiv (8\pi l_B n)^{-1/2}$ for a polyelectrolytes in salt solution of salt concentration n (ϵ being the dielectric constant of water) and many other length scales characterising an adsorbed polymer on a charged surface [6]. In a recent work aimed at investigating the effects of stretching on the single polymer scattering function of a single excluded volume (EV) polymer chain, the existence of tensile blobs [12] of sizes ξ_f (where $\xi_f^{-1} = f/k_B T$ with k_B the Boltzmann constant and f the strength of the tensile force) in long linear polymers were revealed through a cross-over in the scaling behaviour of the structure factor. Within the blobs, excluded volume interactions persist while for two monomers separated by a distance greater the the blob size, the former are screened out. The notion of blobs has gained a wide admiration and has been extended to include other terminologies like the hydrodynamic and electrostatic blobs.

The extension-force relationships of single polymers have been widely explored [13, 17, 18, 19]. Two methods largely explored in the previous chapter have often been used. On one hand uniform equal and opposite forces are applied at the ends of the polymer ("stress ensemble") and the mean elastic properties are evaluated [13, 17, 18]. Though this method is quite easy to handle in computer simulation (since no conformational constraints are involved) it is scarcely used in experimental works. On the other hand, most theoretical works on polymer elasticity are done in the "strain ensemble" in which the molecule is given a fixed length and the mean fluctuating force together with other elastic properties are calculated. In this ensemble, the important observable is the unperturbed end-to-end vector distribution function. This method introduces constraint complications which are hard to handle in computer simulation and require sophisticated codes like the concerted rotation [20] algorithm etc. This method also, has the shortcoming that most of the algorithms will not be able to explore configurations characterised by strong extension and those characterising cyclic conformations in excluded volume chains. des Cloizeaux [19], using renormalisation group theory (RGT), gave the probability distribution of the end-to-end vector (the basis of the latter method) for a chain in solvent but

this distribution function was short of demonstrating the finitely extensible character of most chain molecules.

The physical properties of polymer gels are intermediary between those of liquids and solids, respectively. While in the presence of a magnetic field, residual dipole-dipole interactions average out for unperturbed dilute polymer solutions comprising nuclei with non zero magnetic spins, for solids there is a net magnetisation. Concentrated polymer solutions and net-works should, therefore, portray peculiar magnetic relaxation properties over frequency scales of several decades. These properties would be enhanced by the presence of any permanent strain resulting from a solvent environment or a large velocity gradient or from an external stress on the polymer system, since such a stress reduces spatial fluctuations that are responsible for the averaging out of magnetic properties.

In this chapter, we investigate by computer simulation some interesting topics related to the elasticity of single polymers in solution like the force-extension relationships, the effect of stretching on: the various conformations of a macromolecule, the intensity of NMR dipolar interactions and on the neutron spectral intensity. The chapter is organised as follows: In section 2 a brief description of the models of interest and the Monte-Carlo procedures used are given. In section 3 the simulation results on the force-extension relationships and their comparisons with the predictions of some theoretical models are given, the effect of stretching on the gauche-trans populations of polyethylene is explored and finally the decoupling of the entropic elasticity from enthalpic one is attempted. In section 4 the elasticity related nuclear magnetic resonance observables are studied. In section 5 the effect of stretching on the scattering function of a single polymer is reviewed. The present chapter ends with discussions and a brief conclusion.

Basic features of single chain elasticity

As mentioned above, several important length scales can be used to characterise a polymer molecule: the bond length a denoting the length of a monomeric unit, the Kuhn length b, the unperturbed chain size $R_0 \equiv \left\langle (\underline{R}_N - \underline{R}_0)^2 \right\rangle^{1/2}$ and the contour length L_c. Depending on the magnitude of force used, the elasticity of single polymers can reveal insights into polymer structures at the monomeric ("local") level or the "global" level. Two reduced force scales can, therefore, be defined: the "global" reduced force $\eta_g \equiv \frac{R_0 f}{k_B T}$ (where f is the magnitude of the force) and the "local" reduced force $\eta_\ell \equiv \frac{fb}{k_B T}$. We can also define the bond reduced force η_a (to be useful in the analysis of the effect of stretching on the NMR residual dipolar interactions) as $\eta_a = fa/k_B T$, where a is the C-C bond length.

Most often the study of the elasticity of single polymers is limited to stress-strain relations. This property, known to be intimately related to the solvent quality characterising the polymer medium, is also very sensitive to the elastic regime considered. It has been pointed out in the last chapter that a single polymer subjected to a wide range of tensile forces is known to present the three basic elastic regimes:

- The weak stretching regime ($\eta_g < 2.5$): where the extension-force relationship is the linear (Hooke's) law,

$$\langle R \rangle_f / R_0 = \frac{1}{3} \eta_g, \tag{7.1}$$

irrespective of solvent quality.

- the strong stretching or the tensile blob regime ($2.5 < \eta_g$ and $\eta_\ell < 1$): Here, the elastic law depends on the solvent quality:
  - For Θ-conditions the elastic behaviour is governed by Hooke's law.
  - For good solvent conditions the Pincus-de Gennes [13] scaling law,

$$\frac{\langle R_f \rangle}{R_0} = A\eta_g^{\left(\frac{1}{\nu}-1\right)} \tag{7.2}$$

    reigns, where ν is the Flory excluded volume exponent. For an ideal chain ($A = 1/3$, $\nu = 0.5$) Eq.(7.2) reduces to Eq.(7.1). In the presence of excluded volume interactions, one has [12] $A = 0.46$, $\nu = 2/3$, which means that $\left\langle \underline{r}_{ij} \right\rangle_f = 0.46 R_0^{1/\nu} \times (f/k_BT)^{(1/\nu-1)}$, is linear in the number of monomers pertaining to the polymer at fixed f since $R_0 \sim N^\nu$. In Θ conditions the first two regimes merge up.

- The extra strong stretching or the FE regime ($\eta_\ell > 1$): In this region η_g looses its meaning. The polymer undergoes strong internal rearrangements. The reduced end-to-end vector $\langle \underline{R} \rangle_f / L_c$ becomes a universal function of the local reduced force, the universality being independent of solvent quality and chain size.

The elastic law in the first two regimes has been extensively investigated by mechanical means. The methods used range from the Pincus-de Gennes scaling considerations [13] to the renormalisation group theory (RGT) by des Cloizeaux et al. [19]. This latter theory demonstrates that the distribution of the end-to-end vector of a long linear polymer molecule can be written as in Eq.(6.15). The force-extension relationship (fixed R) is given by $\langle f \rangle_R / k_BT = -\partial/\partial R\,(lnW(R))$. By using the Legendre transformation, Wittkop et al. [18] used the RGT expression for $W(R)$ to study the force extension relationship in the fixed f ensemble.

The approach to the freely jointed chain-like elasticity has been studied thoroughly by Flory [2] and Treloar [1]. It will be useful however to re-interprete their findings to make a direct comparison with single chain elasticity properties of the broader class of polymer models considered in our thesis. We will also show that the FJC model validity in the high stretching regime is not entirely appropriate when we consider the elasticity of a realistic polymer like polyethylene at high stretching.

It will be interesting to enquire to know how other elasticity related polymer properties behave in each of these regions. It is in this perspective that we embark on the study of the effects of stretching on the residual dipolar interaction and the scattering of a polymer molecule. For the dipolar interaction, the quantity of interest is $\langle P_2(\cos\alpha_{kk'}) \rangle_f \equiv \left\langle \frac{3}{2}\cos^2\alpha_{kk'} - \frac{1}{2} \right\rangle_f$ which has often been approximated as [21]

$$\begin{aligned} \langle P_2(\cos\alpha_{kk'}) \rangle_f &= \frac{1}{15}\left(\frac{3}{2}\cos^2\theta - \frac{1}{2}\right)\Lambda\left(\frac{fa}{k_BT}\right)^2 \\ &\quad \times \left[\frac{3}{2}\cos^2\theta_{kk'} - \frac{1}{2}\right], \end{aligned} \tag{7.3}$$

where $\alpha_{kk'}$ is the angle between the vector joining the spin pair kk' and an external magnetic field, θ the angle between the external force acting on polymer ends and the external magnetic field, $\theta_{kk'}$ that between the spin pair vector and the skeletal bond vector to which the spin pair is attached and Λ a parameter of second order stiffness which will be defined later. For the first time, using a Monte-Carlo simulation, we present a quantitative study of $\langle P_2(\cos\alpha_{kk'})\rangle_f$, pointing out the limit of validity of the last equation and other related relations that will be given subsequently. In what concerns scattering, we are interested in the effect of a uni-axial force on the static structure function:

$$S_{\underline{f}}(\underline{q}) \equiv \frac{1}{N+1}\sum_{l=0}^{N}\sum_{j=0}^{N}\left\langle \exp\left[i\underline{q}\cdot\left(\underline{r}_l - \underline{r}_j\right)\right]\right\rangle_{\underline{f}}, \tag{7.4}$$

where $\underline{q}$ is the scattering vector and $\underline{r}_j$ denotes the cartesian coordinates of the scattering site j. It will be seen that this quantity (for small and intermediate q) is very insensitive to the detailed chemistry of the molecule.

7.2 Models and Monte-Carlo (MC) program

7.2.1 Models

Two models, one physical and the other taking into account some chemical details of the molecule are considered.

The bead rod EV chain

This is a physical model characterised by $N+1$ hard spheres each of diameter σ that are linearly connected by free rotating rigid bonds of length $a = b$. For $\sigma = 0$ the model reduces to the usual freely jointed chain (FJC) while for $\sigma > 0$ it is an excluded volume (EV) chain (good solvent conditions). To model the good solvent bead rod chain, we shall use $\sigma/a = 0.65$, a value which guarantees fully developed excluded volume statistics [22], a being taken as unit of length. For this EV model, one has $\eta_a \simeq \eta_\ell$, as the bond length and the Kuhn segment length are identical. In this model, the pair of spins which will be considered in the estimation of dipolar residual interactions is located along the skeleton bonds.

Atomistic model: Single polyethylene chain (- $(CH_2\text{-}CH_2)_n$-) in a solvent

In this model:

- the $N+1$ CH_2 (or CH_3) groups are modeled as united atoms (single force centres)
- C-C bond length (l_{cc}) and C-C-C bending angles (γ) are kept rigid
- restricted rotational motions of the polymer around the C-C bonds are described by a torsional potential energy equivalent to that of butane (function of the torsional angle ϕ - see Figure 7.1). Trans ($\phi \approx 0°$) gauche$^+$ ($\phi \approx 120°$) and the gauche$^-$ ($\phi \approx 240°$) are the three stable conformations. An energy difference of about 3 KJ/mol exists between the trans and the gauche states.

- Solvent effect is accounted for by an effective potential acting between any pair of C atoms separated by at least four successive bonds which is expressed as:

$$V(r) = 4\epsilon\left[\left(\frac{\sigma}{r}\right)^{12} - \lambda\left(\frac{\sigma}{r}\right)^{6}\right], \tag{7.5}$$

where λ is an ad hoc parameter modeling solvent quality:
$\rightarrow \lambda \approx 0$ is equivalent to good solvent conditions
$\rightarrow \lambda = 0.505$ at 400 K corresponds to Θ-condition (compensation of attractive/repulsive forces) [24]. The values of γ, ϵ and σ used are, respectively, $\gamma \approx 109.7°$, $\epsilon/k_B = 51.8$K and $\sigma = 3.74$Å.

For PE, it is important to remark that $\eta_\ell = (b/l_{cc})\eta_a$ where $b = 14.9$Å is the Kuhn segment length and $a = l_{cc} = 1.54$Å [24]. In this model, the pair of spins which will be considered in the estimation of dipolar residual interactions is the set of two H nuclei pertaining to a methylene group.

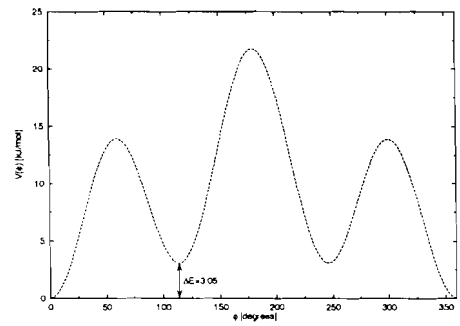

Figure 7.1: Polyethylene torsional potential

7.2.2 Monte-Carlo programs

Two Monte-Carlo programs, one for each model, were set up. They are capable of monitoring the static properties of the two model polymers both in the stretched and unstretched states.

The MC procedures we adopt for both models are based on configurational biased Monte-Carlo (CBMC) [25] coupled with reptation moves. That of the EV model has been described in the last chapter. In this section, we shall describe the CBMC adapted for use on stretched polyethylene.

The case of polyethylene is slightly more complicated since, the interactions are of differing origins: restricted torsional motion of the molecule, solvent mediated effective potential due to "far-off segments" (those separated by more than four bonds) modeled by interactions of the form (7.5), the usual pentane effect modeled by a Lennard-Jones type interaction ($\lambda = 1$) and finally the external work due to the traction force. In addition to this multiplicity in the sources of interactions, there is the bond angle constraint that must be taken into account during chain reconstruction.

Once the molecule to be simulated is entirely constructed, conformation sampling is executed as follows.

- 1. One end of the molecule is randomly chosen and a segment of k beads suppressed and reconstructed bead by bead at the other end as follows.

- 2. Once $i-1$ beads are successfully placed, the ith bead is placed by selecting *idir* bond vectors each of length b around bead $i-1$ and accepting with a probability proportional to $\exp\left(-\frac{1}{k_BT}U_{tors}(\phi_i)\right)$, where U_{tor} is the torsional potential energy, function of the dihedral angle (ϕ_i) of bead i. $\underline{\Omega}_i$, the orientation of i, is chosen on a cone whose axis is the $(i-1)$th bond orientation vector such that $\angle\,(\underline{\Omega}_{i-1}, \underline{\Omega}_i) = \gamma$ =constant where γ is the bond angle. The interaction energy U_{int}, corresponding to each of the *idir* positions is evaluated. This energy includes the excluded volume interactions of i with beads 1 through $i-3$ and the external field energy (T) on i.

- 3. The Rosenbluth weight [26] of i is calculated as

$$W_i(n) = \sum_{m=1}^{idir} \exp\left(-\frac{U_{int}^m(n)}{k_BT}\right), \tag{7.6}$$

  where the superscript m indicates that only the interaction energy of the mth orientation is considered.

- 4. One of the *idir* positions m is chosen and accepted with a probability

$$P_m(n) = \exp\left(-\frac{U_{int}^m(n)}{k_BT}\right)/W_i(n) \tag{7.7}$$

- 5. Procedures 2-4 are repeated for all the k beads and the Rosenbluth of the new segment $W(n)$ is obtained as the product of the Rosenbluths of each of the k beads.

$$W(n) = \prod_{i=1}^{k} w_i(n) \tag{7.8}$$

- 6. Similar procedures are done for the original segment of k bonds with one of the *idir* orientations of each of the k bonds being the original old orientation. The Rosenbluth of the old segment $W(o)$ is evaluated and the new segment configuration is accepted with a probability equal to $min\,[1, W(n)/W(o)]$. We next show that the condition of detailed balance renders this sampling that of a Boltzmann distribution.

Note that the three energy terms (torsional, excluded volume and external work) intervening in the sampling are separable. In the choices of the *idir* orientations, only lower torsional energy conformations are selected. Once this is done it will be legitimate to perform a sampling whereby the two remaining energy terms govern the acceptance criterion. The condition of detailed balance is expressed as

$$acc(o \to n)\alpha(o \to n)N(o) = acc(n \to o)\alpha(n \to o)N(n), \tag{7.9}$$

The transition probability $\alpha(a \to b)$ is equal to the product of those of the individual segments.

$$\begin{aligned} \alpha(o \to n) &= \prod_{l=1}^{k} P_l(n) = \frac{\exp\left(-\sum_{l=1}^{k} \frac{U^l_{int}(n)}{k_B T}\right)}{W(n)} \\ &= \frac{\exp\left(-\frac{U_{int}(n)}{k_B T}\right)}{W(n)} \\ \alpha(n \to o) &= \frac{\exp\left(-U_{int}(o)\right)}{W(o)}. \end{aligned} \tag{7.10}$$

It then follows from Eq.(7.9) and the acceptance criterion that

$$\frac{N(n)}{N(o)} = \exp\left[-\frac{U_{int}(n) - U_{int}(o)}{k_B T}\right], \tag{7.11}$$

which is the Boltzmann distribution.

7.3 Bead rod excluded volume chain versus atomistic polyethylene

7.3.1 Extension - force relationships

The elasticity of PE is studied for Θ and good solvent conditions. The extension-force relationship for the EV model is shown on Figure 7.2 for chain lengths varying from 64 to 6000 segments. The line shows the stress ensemble version of the renormalisation group theory [19],

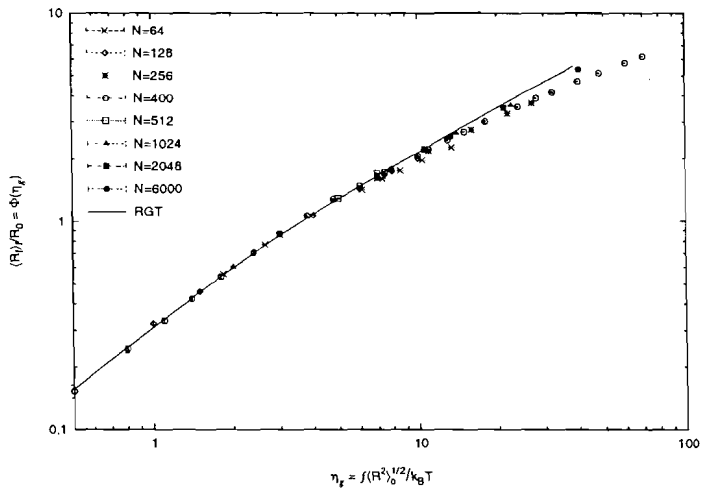

Figure 7.2: Reduced extension $x =< R_f > /R_0$ as a function of reduced force η_g for the EV model. The solid line gives the prediction of the RGT.

that is, the result obtained using eq.(6.17). We remark the good agreement between the simulation results and the RGT for both weak ($\eta_g < 3$) and strong ($fb/k_BT < 1 < fR_0/k_BT$)

stretchings (see Figure 7.2). It can also be noted that shorter chains depart from the RGT faster than longer ones. This is due to finite extensibility which shows up at a unique η_ℓ value ($\eta_\ell \approx 1$) which corresponds to η_g varying with chain size N as $\eta_g \sim N^\nu$. The extension-force relationships of an atomistic polyethylene are shown on Figures 7.3, 7.4 and 7.5. On Figure 7.3 good solvent results are presented. The three elastic regimes are clearly depicted. Shorter

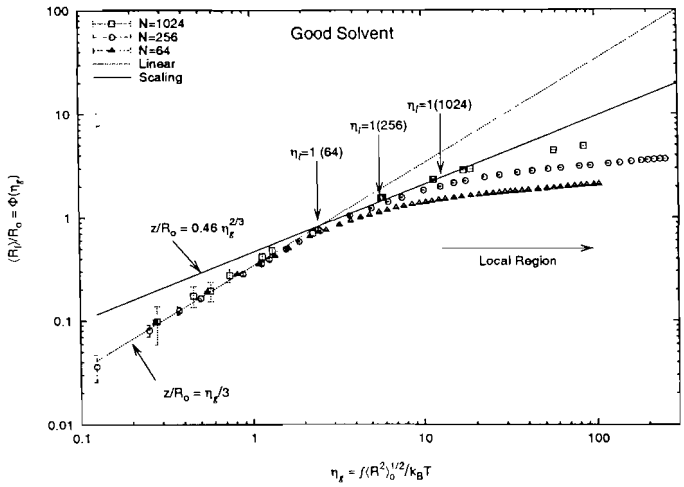

Figure 7.3: Reduced extension $x =< R_f > /R_0$ as a function of reduced force η_g for the PE model in good solvent.

chains again leave the scaling regime faster than longer ones. As the chains are stretched into the extra strong stretching regime, the reduced end-to-end extension $\langle R \rangle_f / L_c$ tends to a universal function of the force (see Figure 7.4), the universality being independent of chain size and solvent quality.

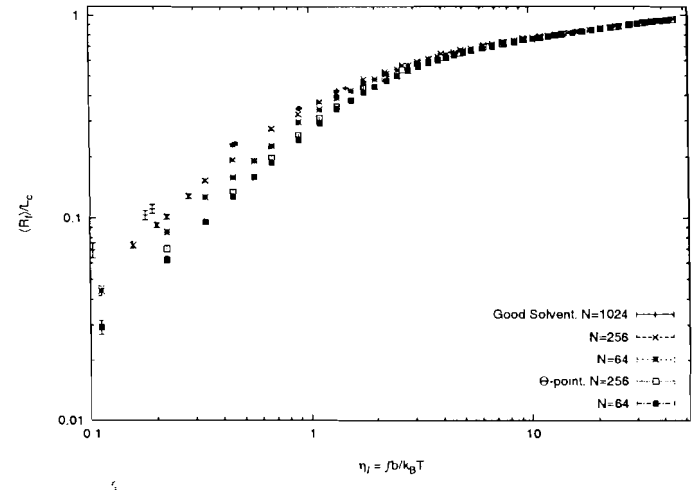

Figure 7.4: log − log plot of the reduced extensions $\langle R \rangle_f / L_c$ as functions of the local reduced force $\eta_\ell = fb/k_BT$ for PE in Θ and good solvent conditions. For weak and intermediate stretching good solvent results are chain dependent. For extra strong stretching all results, be it for good or Θ-solvents, converge to a unique curve.

One may be tempted to assert that under extra strong stretching, excluded volume effects are screened out completely so that the force-extension relationship is the FJC langevin formula. Figure 6.3 shows that though the elasticity of an EV chain approaches that of a FJC, it tends to the latter basically around maximum chain extension ($R \sim L_c$).

PE at Θ-point clearly shows a universality in $\langle R \rangle_f / L_c$ which is neither of the freely jointed Langevin type,

$$\frac{\langle R \rangle_f}{L_c} = L(fb/k_BT) \equiv \coth(fb/k_BT) - \frac{1}{(fb/k_BT)}, \tag{7.12}$$

nor of the Ha and Thirumalai semi-flexible chain model [27],

$$\frac{fR_0}{k_BT} = \frac{3(\langle R \rangle_f / R_0)}{\left[1 - (\langle R \rangle_f / L_c)^2\right]^2}, \tag{7.13}$$

but is sandwiched between the two (see Figure 7.5). Polyethylene, thus appears to be stiffer than the usual FJC but more flexible than a typical worm-like chain. It should be pointed out here that Eq.(7.13) is an approximate form for the real wormlike chain as it is derived via a mean field approach introduced by repacing the local constraint $\underline{u}^2(s) = 1$ with a global one $\langle \underline{u}^2(s) \rangle = 1$. Marko and Siggia [28] calculated the extension as a function of force for wormlike chains and found that their results fit well experimental data.

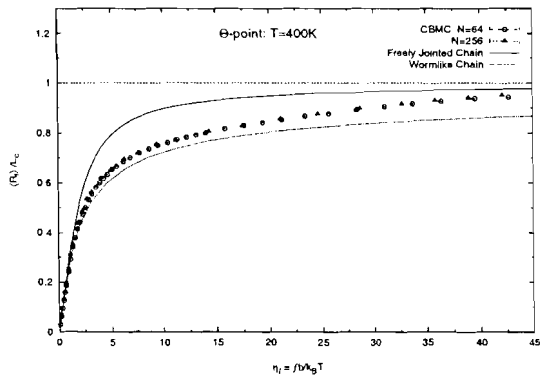

Figure 7.5: Linear plot of the reduced extension $\langle \underline{R} \rangle_f / L_c$ as a function of the local reduced force $\eta_\ell = fb/k_BT$ for PE at Θ-point. The results for the two chain sizes lie relatively well on a unique curve. The upper curve shows the prediction of the Langevin function while the lower one represents that of the corresponding worm-like model.

Let us give an outline of the proof of Eq.(7.13). To do this we shall follow the line of reasoning of Ha et al. [27] based on the semi-flexible chain Hamiltonian

$$\frac{\mathcal{H}}{k_BT} = \frac{l_p^{Ha}}{2} \int_0^{L_c} \left(\frac{\partial \underline{u}(s)}{\partial s} \right)^2 ds - \int_0^{L_c} \frac{\underline{f}(s)}{k_BT} \cdot \underline{u}(s)\, ds, \tag{7.14}$$

where l_p^{Ha} is the persistence length as defined by Ha et al. in [27], $\underline{u}(s) = \frac{\partial \underline{r}(s)}{\partial s}$ is the unit tangent vector along the molecular back-bone at a point characterised by the cartesian and curvilinear

coordinates $\underline{r}(s)$ and s, respectively, and $\underline{f}(s)$ is the external field at s. By introducing the local constraint $\underline{u}^2(s) = 1$ via an auxiliary field parameter $\lambda(s)$, Ha et al. defined a free energy F as

$$\exp\left(-\frac{F}{k_BT}\right) = \int_{-i\infty}^{i\infty} \mathcal{D}[\lambda(s)] \int \mathcal{D}[\underline{u}(s)] \exp\left[-\frac{1}{2}\int_0^{L_c} ds \int_0^{L_c} ds' \underline{u}(s) Q(s,s') \underline{u}(s') + \int_0^{L_c} \frac{\underline{f}(s)}{k_BT} \cdot \underline{u}(s)\, ds \right], \tag{7.15}$$

where

$$Q(s, s') = \left[-l_p^{Ha} \left(\frac{\partial}{\partial s}\right)^2 + 2\lambda(s) \right] \delta(s' - s) \tag{7.16}$$

and $\mathcal{D}[\lambda(s)]$ denotes the measure of $\lambda(s)$ over the continuous space on which s is defined. The variable $\lambda(s)$ that enforces the local constraint is evaluated by stationary phase approach which requires that at this λ the derivative of the integrand of Eq.(7.15) (with respect to $\lambda(s)$), denoted $\exp\left\{-\beta\mathcal{F}[\lambda(s), \underline{f}(s)]\right\}$ ($\beta = 1/k_BT$) be an extremum. This leads to the equation

$$\frac{3}{2}\left(\frac{2}{Q}\right)_{s,s} + \int_0^{L_c} ds' \int_0^{L_c} ds'' \frac{\underline{f}(s')}{k_BT} Q^{-1}(s,s') Q^{-1}(s,s'') \frac{\underline{f}(s'')}{k_BT} = 1. \tag{7.17}$$

It can be shown that $\mathcal{F}[\lambda(s), \underline{f}(s)]$ may be used as a generating function for calculating various orientation correlation functions. In other words

$$\langle (u_\alpha(s_1) - \bar{u}_\alpha(s_1))\,(u_\delta(s_2) - \bar{u}_\delta(s_2)) \ldots (u_\omega(s_n) - \bar{u}_\omega(s_n)) \rangle_f$$

can be calculated as follows

$$\begin{aligned} &\langle (u_\alpha(s_1) - \bar{u}_\alpha(s_1))\,(u_\delta(s_2) - \bar{u}_\delta(s_2)) \ldots (u_\omega(s_n) - \bar{u}_\omega(s_n)) \rangle_f \\ &= -\left[\frac{\partial}{\partial\beta f_\alpha(s_1)} \frac{\partial}{\partial\beta f_\delta(s_2)} \cdots \frac{\partial}{\partial\beta f_\omega(s_n)} \beta\mathcal{F}[\lambda(s), \underline{f}(s)] \right], \end{aligned} \tag{7.18}$$

where $\alpha, \delta, \ldots, \omega$ are the cartesian coordinates and $s_1, s_2, \ldots, s_n$ are the curvilinear coordinates along the chain backbone. For a uni-axial constant force $\underline{f}$, Ha et al. obtained, via an eigenfunction expansion, the following system:

$$\begin{aligned} &\frac{3}{4}\sqrt{\frac{2}{\lambda l_p^{Ha}}} \coth\left[\left(\frac{\lambda L_c^2}{2 l_p^{Ha}} \right)^{1/2} \right] + \frac{\beta^2 f^2}{4\lambda^2} = 1, \\ &\langle \underline{r} \rangle_f = (0, 0, z) \quad \text{with} \quad z = \frac{\underline{f}}{f} \cdot \frac{\partial\beta\mathcal{F}}{\partial\beta\underline{f}} = \frac{\beta f L_c}{2\lambda}, \end{aligned}$$

$$\begin{aligned} \langle \underline{u}(s) \cdot \underline{u}(s') \rangle_f &= \frac{3}{Q(s,s')} + \frac{\beta^2 f^2}{4\lambda^2} \\ &= \frac{3}{4}\sqrt{\frac{2}{\lambda l_p^{Ha}}} \frac{\cosh\left[\sqrt{\frac{\lambda}{2 l_p^{Ha}}} \left(L_c - 2 \mid s - s' \mid \right) \right]}{\sinh\left(\sqrt{\frac{\lambda L_c^2}{2 l_p^{Ha}}} \right)} + \frac{\beta^2 f^2}{4\lambda^2}. \end{aligned} \tag{7.19}$$

Eq.(7.13) is obtained by combining the first two equations of this system in the limit of very long chains (in this limit $\coth\left[\left(\lambda L_c^2/(2l_p^{Ha})\right)^{1/2}\right] = 1$) and requiring that the usual Hookian law at small forces be retrieved. This latter condition leads to a redefinition of the persistence length as $l_p = \frac{2}{3}l_p^{Ha}$, which is in conformity with the mapping of Eq.(7.20).

We map PE at Θ-point to the equivalent wormlike chain by defining the Kuhn segment length b ($b = 2l_p$) through:

$$R_0^2 = \left\langle R^2 \right\rangle_0 = L_c b \quad and \quad L_c = \mathcal{N} b, \tag{7.20}$$

where L_c and $\mathcal{N}$ are, respectively, the contour length and the number of Kuhn segments in the polymer. This mapping should be consistent with the other condition that the persistence length of the chain should read $l_p = b/2$, where the persistence length, l_p, is the correlation length of the polymer - l_p is the distance over which the correlation function of the unit tangent vector along the chain backbone ($\underline{u}(s)$),

$$C(s) = \langle \underline{u}(0) \cdot \underline{u}(s) \rangle_0 , \tag{7.21}$$

decorrelates. Despite the fact that the mapping (7.20) and the determination of l_p from $C(s)$ using the method described above are strictly correct only in the limit of very long chains as system (7.19) demonstrates, satisfactory results have been obtained even for very short chains. For a 64-segments polyethylene the mapping led to $b \sim 14.3$Å while the correlation function of Figure 7.6 gave $l_p \sim 7$Å, which are consistent with the experimental values of $l_p \sim 6.9 - 7.1$Å. This means that polyethylene chains as short as 64 C-C bonds are representative of the real molecule, at least as far as chain rigidity is concerned.

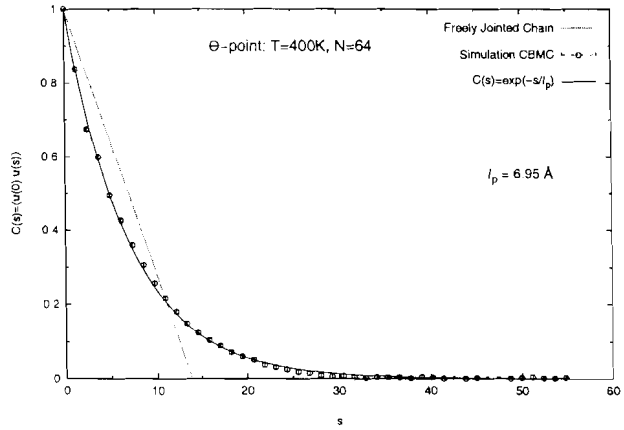

Figure 7.6: Tangent vector correlation function $C(s)$ of a 64 segments polyethylene at Θ-point. The straight line represents $C(s)$ for a freely jointed chain of *kuhn* length 14.3Å

At this juncture it will be nice to examine how the detailed chemical properties of a polymer molecule influences the stress-strain relation. There is no doubt that solvent quality plays a magnificent rule in polymer properties. A critical look at Figures 7.2 and 7.3 reveals that there is a clear influence of chain size on the elasticity of PE

7.3.2 The dependence of the gauche-trans populations on stretching

The populations of the two main stable conformations of polyethylene (gauche and trans) corroborate the fact that for weak stretching the internal degrees of freedom of the chains are very little affected, but under strong stretching, there is a massive switch-over from the mixed gauche-trans conformations to all trans zig-zag conformations.

For weakly stretched chains, there are more trans conformations in excluded volume chains than in Θ ones as Figure 7.7 shows.

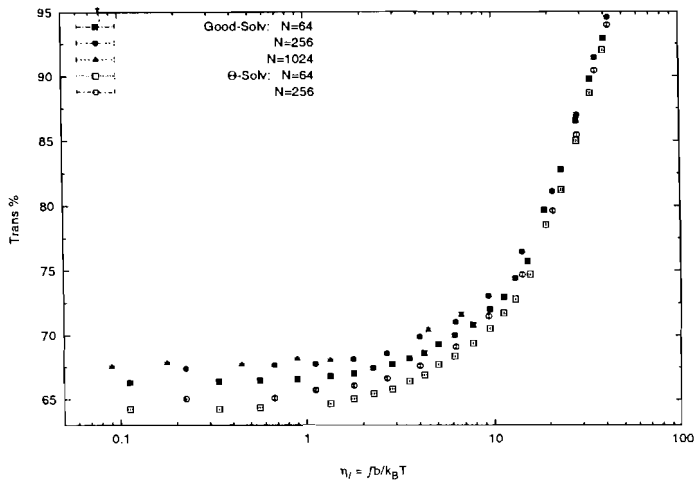

Figure 7.7: The trans population of polyethylene in good and Θ solvents.

The variation of these populations with the local reduced force is very much like that of the reduced extension $x = \langle R \rangle_f / L_c$, being solvent and chain size dependent for weak and moderate stretching, but tending asymptotically to a unique function irrespective of chain size and solvent quality once FE is entered.

Abe et al. [29], on investigating the rotational isomerisation of a polymer molecule on stretching, presented perturbative analysis of the apportionment of the bonds or the sequences of bonds amongst various rotational isomeric states of the molecule. They showed that the proportion ($\langle n_\varphi \rangle_r$) of bonds or sequences of bonds in a particular state, φ, grows as the square of the chain elongation specified by that state,

$$\langle n_\varphi \rangle_r = \langle n_\varphi \rangle + D_2 \left(\frac{r^2}{\langle r^2 \rangle_0} - 1 \right), \tag{7.22}$$

where r is the chain length prescribed by the conformation φ and D_2 is a constant of proportionality. Though this prediction is not evident from our results, the latter confirm the findings of Birshstein et al. [30] that the change in population is related to $f_e = (\partial U / \partial r)_{V,T}$, the change in intra-molecular energy on stretching as, a glance at the energy profile for a 64-segments PE reveals that the intra-molecular energy varies initially very little with chain deformation but once strong stretching sets in, it undergoes a steep drop just in the same manner as the gauche population (see Figures 7.7 and 7.8).

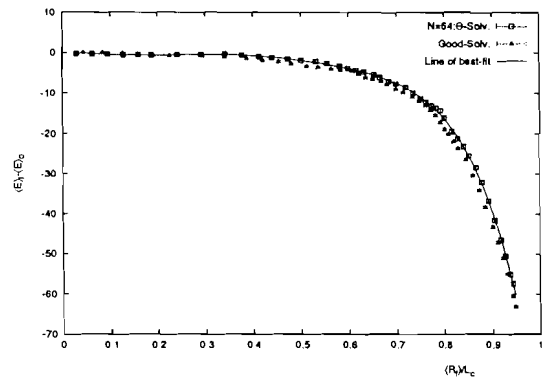

Figure 7.8: A plot of the difference between the internal energies of strained and unstrained 64-segment polyethylene chains in Θ and good solvent conditions as functions of the reduced mean end-to-end vector. The line is that of an ad hoc best fitting function on good solvent data to be used for the evaluation of f_e.

7.3.3 The entropic and enthalpic forces in PE

f_e, as defined in the last paragraph, introduces the notion of enthalpic forces. While the elasticity of rubber is predominantly of entropic origin (i.e. depending on the number of possible configurations of the molecule) and that of crystalline materials is of enthalpic nature, there is a competitive tendency between the two aspects in the elasticity of most polymers [5]. It will be interesting to attempt to disentangle these aspects, pointing out the relative importance of each. Most of the theories aimed at disentangling the enthalpic forces from entropic ones in polymers are done in the spirit of strain ensembles. Here, the polymer is subjected to a deformation and the mean fluctuating force necessary to sustain the strain is evaluated. By using thermodynamics arguments in this ensemble [1], the entropic component of the force can be deduced from the temperature variation of the total force. From the first law of thermodynamics, the internal energy change in any process is given by

$$dU = dQ + dW, \tag{7.23}$$

where dQ and dW are, respectively, the heat transfer to the system and the external work done on the system. If the system is at a temperature T and dS is the entropy change accompanying the process, the second law requires that if the process is reversible

$$dQ = TdS. \tag{7.24}$$

We can introduce the Helmholtz free energy

$$A = U - TS, \tag{7.25}$$

so that the free energy change in the reversible process is

$$dA = dW - SdT. \tag{7.26}$$

Let us suppose the case where the work is obtained by giving the polymer of unstrained length r a displacement dr resulting in a contractile internal force $f.$, then dW is given as

$$dW = f\,dr. \tag{7.27}$$

Thus in isothermal conditions

$$f = \left(\frac{\partial A}{\partial r}\right)_T. \tag{7.28}$$

Eqs.(7.26) and (7.27) lead to $dA = f\,dr - SdT$, so that

$$S = -\left(\frac{\partial A}{\partial T}\right)_r. \tag{7.29}$$

Exploiting Eqs.(7.25) and (7.28), the total force disintegrates into an enthalpic force $f_e = \left(\frac{\partial U}{\partial r}\right)_T$ and an entropic term $f_s = -T\left(\frac{\partial S}{\partial r}\right)_T$. Eq.(7.29) then permits us to write that $f_s = T\frac{\partial}{\partial r}\left(\frac{\partial A}{\partial T}\right)_r$ and since A is a thermodynamic function we permute the partial derivatives to obtain

$$f_s = -T\left(\frac{\partial S}{\partial r}\right)_T = T\left(\frac{\partial f}{\partial T}\right)_r. \tag{7.30}$$

The total force now reads

$$f = \left(\frac{\partial U}{\partial r}\right)_T + T\left(\frac{\partial f}{\partial T}\right)_r. \tag{7.31}$$

Eq.(7.31) is the cornerstone of early theories and experiments on thermo-elasticity [1, 5]. While some polymers have a positive enthalpic force, a wide range of polymers have negative enthalpic forces. This is due to the fact that the strained state of the latter class of polymers is less energetic. Natural rubber and polyethylene fall within this class.

Flory has shown that the enthalpic forces are related to the thermal expansivity of the polymer; that is, the ratio of enthalpic to total forces on straining is given by

$$f_e/f = T\left(d\ln\left\langle r^2\right\rangle_0/dT\right), \tag{7.32}$$

which from the definition of $\langle r^2\rangle_0$,

$$\left\langle r^2\right\rangle_0 = \frac{1}{Z(T)}\int d\underline{r}^N r^2 exp\left(-\frac{U(\underline{r}^N)}{k_BT}\right) \tag{7.33}$$

(with $Z(T) = \int d\underline{r}^N \exp\left(-\frac{U(\underline{r}^N)}{k_BT}\right)$), can be shown to depend on the intermolecular energy U as

$$\frac{f_e}{f} = \frac{1}{k_BT}\left[\frac{\langle Ur^2\rangle_0}{\langle r^2\rangle_0} - \langle U\rangle_0\right], \tag{7.34}$$

where the subscripts 0 indicate averaging on unperturbed chain. This equation demonstrates that freely jointed and gaussian chains (whose intra-molecular energies are independent of chain configuration) are purely entropic. Note that for PE, low energy trans conformations are characterised by large r^2 (due to its extended zig-zag form) while the higher energy gauche forms are shorter. The quantity Ur^2 will consistently never be large. This means that f_e/f will always be negative for PE.

Even though it is now well known from the previous chapter that the force-extension relationship of a stretched polymer depends on the choice of the working ensemble [31], we can, to first approximation, assume this relationship to be unique and ensemble independent. This permits us to approximate equation (7.30) as (see appendix C.1)

$$f_s \approx -T \left(\frac{\partial \langle R \rangle_f}{\partial T} \right)_f / \left(\partial \langle R \rangle_f / \partial f \right)_T, \tag{7.35}$$

from which f_e is obtained by simple deduction of f_s from the total imposed force. In our MC program we evaluated $\left(\frac{\partial \langle R \rangle_f}{\partial T}\right)_f$ using

$$\left(\frac{\partial \langle R \rangle_f}{\partial T} \right)_f = \frac{1}{k_B T^2} \left[\left\langle \delta r_{\|} \delta U(\underline{r}^N) \right\rangle_f - f \left\langle \delta r_{\|}^2 \right\rangle_f \right], \tag{7.36}$$

where U is the total intra-molecular interaction energy, $\delta U = U - \langle U \rangle_f$ and $\delta r_{\|} = r_f - \bar{r}_f$ with $\bar{r}_f = \langle R \rangle_f$ being the mean extension on stretching.

For both solvent conditions, at the simulation temperature of T=300K, the quantity $(\partial \langle R \rangle_f / \partial T)_f$ (not reported in this thesis), was found to be negative at all stretching forces demonstrating once more the negative thermal expansivity of PE. Remark that for a gaussian chain this quantity varies with temperature and mean chain length as

$$\left(\frac{\partial \langle R \rangle_f / R_0}{\partial T} \right)_f = -\frac{1}{T} \frac{\langle R \rangle_f}{R_0} \tag{7.37}$$

(with R_0 independent of temperature) and that of a freely jointed chain follows

$$\left(\frac{\partial \langle R \rangle_f / L_c}{\partial T} \right)_f = -\frac{\eta_\ell}{T} \left[1 - \mathcal{L}^2(\eta_\ell) - \frac{2}{\eta_\ell} \mathcal{L}(\eta_\ell) \right], \tag{7.38}$$

with η_ℓ the local reduced force and $\mathcal{L}$ is the Langevin function. Both models predict negative chain expansivities for all stretching.

f_e can also be estimated as $(\partial U / \partial r)_T$, by differentiating the intra-molecular energy with respect to the mean extension. As Figures 7.9 and 7.10 show, the different force components calculated using the two methods compare well for a 64-segments polyethylene in Θ and good solvent conditions.

The ratio of the enthalpic to total forces are illustrated on Figure 7.11 for the two solvent conditions. We observe that enthalpic forces are weak for weakly stretched PE in Θ-solvent but remain almost constant up to stretchings of about 60% of the contour length for good solvent conditions. The curves for the two solvent conditions seem not to merge when strongly stretched.

It is important to point out from figure 7.11 that under weak stretching enthalpic forces are vanishingly small for PE in Θ solvent while for good solvent conditions they are quite significant. Thus, as expected, the elastic properties of a weakly stretched PE in Θ solvent should be predominantly of entropic origin. This finding will be re-emphasised when other elasticity related properties like nuclear magnetic dipolar interactions will be considered.

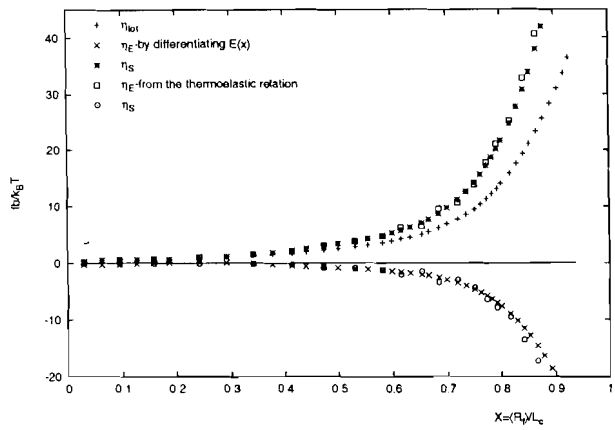

Figure 7.9: The entropic η_S and enthalpic η_E force components and the total force on a 64-segments PE at Θ-point. The results obtained using the two methods described in the text do agree well. η_E and η_S are obtained, firstly, by differentiating the best function fitting in in figure 7.8 with respect to the mean extension and secondly by using the thermoelastic equation (7.31).

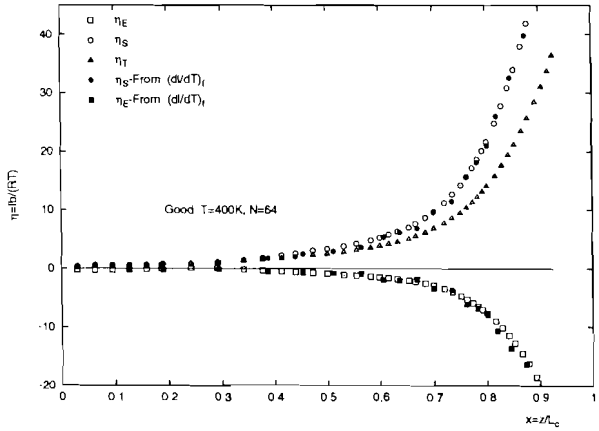

Figure 7.10: The entropic η_S and enthalpic η_E force components and the total force on a 64-segments PE in good solvent. The results obtained using the two methods described in the text do agree well.

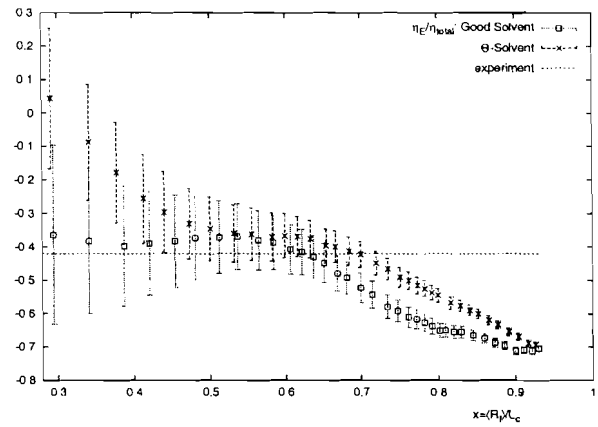

Figure 7.11: The ratio of the enthalpic force component to the total force for a 64-segments PE in good and Θ solvents. For intermediate extensions they agree with the experimental value of -0.42 [5].

7.4 Residual dipole-dipole interaction of a stretched polymer

7.4.1 Introduction

The approximated expression used to describe NMR properties in polymer gels and networks in the "not too strong" stretching case is [32]

$$\epsilon_{ij} = \Delta_G \langle r_{ij} \rangle^2 / L_{ij}^2, \tag{7.39}$$

where ϵ_{ij} is the residual dipole-dipole interaction of a series of nuclear spin pairs along the polymer strand, L_{ij} the contour length, $\langle r_{ij} \rangle$ the mean end-to-end vector of the strand between junctions i and j in the network and Δ_G the dipole-dipole interaction for a fully stretched strand. A more basic expression for ϵ_{ij} is given by Eq.(21) of chapter 3 in [21] where the residual dipole-dipole interaction is not specified in terms of the strand averaged extension $\langle r_{ij} \rangle$ but in terms of a corresponding stretching force $\pm \underline{f}$ applied to the single polymer strand ends.

If we denote by $\langle ... \rangle_f$ an ensemble average for a single polymer chain subject to a stretching force $\pm f$, the average dipolar residual interaction ϵ_{ij} for a particular pair of spins kk' is proportional (up to factors and spin operators irrelevant for our discussion) to $\left\langle \frac{3}{2}\cos^2\alpha_{kk'} - \frac{1}{2} \right\rangle_f$ where $\alpha_{kk'}$ is the angle between the vector joining the kk' spin pair and the magnetic field orientation. Such a statistical average can be the object of a second order perturbation calculation (in terms of f) yielding [32]

$$\langle P_2(\cos\alpha_{kk'}) \rangle_f \equiv \left\langle \frac{3}{2}\cos^2\alpha_{kk'} - \frac{1}{2} \right\rangle_f = \frac{1}{15}\left(\frac{3}{2}\cos^2\theta - \frac{1}{2}\right) \Lambda \left(\frac{fb}{k_B T}\right)^2 \left[\frac{3}{2}\cos^2\theta_{kk'} - \frac{1}{2}\right]. \tag{7.40}$$

In the last expression, θ is the angle between the stretching force orientation and the magnetic field, while $\theta_{kk'}$ is the angle between the spin pair vector and the skeleton bond vector to which the atomic pair kk' belongs. Note that in Eq.(7.40), the parameter of second-order

stiffness Λ [21] which contains the relevant ensemble average is, in fact, dependent upon the position along the chain back-bone and should therefore be written as

$$\Lambda_p = 15/4 \sum_{m,n} \left\langle \left(3\cos^2\theta_p - 1\right) \cos\theta_m \cos\theta_n \right\rangle_0 , \tag{7.41}$$

with an index p referring to the skeleton bond which is associated to the kk' spin pair. In Eq.(7.41), θ_p is the polar angle describing the orientation of the pth skeleton bond with respect to a fixed axis (the axis being arbitrary because of the isotropic nature of the average taken at zero force). To prove Eq.(7.40) we decompose the spin pair rotation with respect to the laboratory frame within which is the magnetic field lies (along the z axis of the frame) into three successive rotations in the following order: rotation of the spin pair about the skeletal bond vector at k $[\underline{\Omega}_{kk'} = (\theta_{kk'}, \phi_{kk'}, \psi_{kk'})]$, that describing the rotation of the skeletal bond with respect to the external tensile force or imposed end-to-end vector $[\underline{\Omega}_k = (\theta_k, \phi_k, \psi_k)]$ and that describing the force orientation with respect to the magnetic field $[\underline{\Omega} = (\theta, \phi, \psi)]$. We then remark that $P_2(\cos\alpha_{kk'})$ is related to the Wigner $\mathcal{D}$ function [33] which transforms, for a rotation that can be written as the sum of two rotations $[\underline{\Omega}_{kk'} = (\theta, \phi, \psi) \oplus (\theta_k, \phi_k, \psi_k)]$, as the spherical harmonics. (The rest of the proof is found in appendix C.2).

To first order in f one also has the elasticity law in Eq.(7.1) which, when combined with Eq.(7.40) gives

$$\langle P_2(\cos\alpha_{kk'})\rangle_f = \frac{3}{5}\left(\frac{3}{2}\cos^2\theta - \frac{1}{2}\right)\Lambda_p \left(\frac{\left\langle \underline{r}_{ij}\right\rangle^2 a^2}{\left\langle \underline{r}_{ij}^2\right\rangle_0^2}\right)\left[\frac{3}{2}\cos^2\theta_{kk'} - \frac{1}{2}\right]. \tag{7.42}$$

It can be shown that at a point with curvilinear coordinate s along the chain backbone of a long semi-flexible chain, $\Lambda(s)$ is given by

$$\Lambda(s) = \frac{5}{2} l_p^2 \left[2 - \exp\left(-s/l_p\right) - \exp\left[-\left(L_c - s\right)/l_p\right]\right], \tag{7.43}$$

which shows that Λ grows as the square of the chain stiffness. To get this expression we need the correlation functions

$$C_2^{\alpha,\gamma}(s_1, s_2) = \langle u_\alpha(s_1) u_\gamma(s_2)\rangle_{\underline{f}=\underline{0}} \text{ and } C_4^{\alpha,\gamma,\delta,\nabla}(s_1, s_2, s_3, s_4) = \langle u_\alpha(s_1) u_\gamma(s_2) u_\delta(s_3) u_\nabla(s_4)\rangle_{\underline{f}=\underline{0}},$$

where α, γ, δ and ∇ are, respectively, one of the three cartesian coordinates (x, y, z). To do this we shall exploit Eq.(7.18) for an n-uple correlation function from which

$$\begin{aligned}
\left(\frac{\partial^4 \beta\mathcal{F}[\underline{u}(s), \beta\underline{f}(s)]}{\partial\beta f_\alpha(s_1)\partial\beta f_\gamma(s_2)\partial\beta f_\delta(s_3)\partial\beta f_\nabla(s_4)}\right)_{\underline{f}=\underline{0}} &= -\left(\frac{\partial^3 \langle u_\alpha(s_1)\rangle_f}{\partial\beta f_\gamma(s_2)\partial\beta f_\delta(s_3)\partial\beta f_\nabla(s_4)}\right)_{\underline{f}=\underline{0}} \\
&= \langle u_\alpha(s_1) u_\gamma(s_2)\rangle_{\underline{f}=\underline{0}} \langle u_\delta(s_3) u_\nabla(s_4)\rangle_{\underline{f}=\underline{0}} \\
&\quad + \langle u_\alpha(s_1) u_\delta(s_3)\rangle_{\underline{f}=\underline{0}} \langle u_\gamma(s_2) u_\nabla(s_4)\rangle_{\underline{f}=\underline{0}} \\
&\quad + \langle u_\gamma(s_2) u_\delta(s_3)\rangle_{\underline{f}=\underline{0}} \langle u_\alpha(s_1) u_\nabla(s_4)\rangle_{\underline{f}=\underline{0}} \\
&\quad - \langle u_\alpha(s_1) u_\gamma(s_2) u_\delta(s_3) u_\nabla(s_4)\rangle_{\underline{f}=\underline{0}},
\end{aligned} \tag{7.44}$$

where we have used the fact that at $\underline{f} = \underline{0}$ the odd-uple correlations vanish and only even ones are non-zero. Remarking that the expression for $\mathcal{F}$ as obtained from Eq.(7.15), given in [27], is quadratic in $\underline{f}$, the left hand side of the above equation vanishes so that

$$\begin{aligned} C_4^{\alpha,\gamma,\delta,\nabla}(s_1,s_2,s_3,s_4) &= \langle u_\alpha(s_1)u_\gamma(s_2)u_\delta(s_3)u_\nabla(s_4)\rangle_{\underline{f}=\underline{0}} = \langle u_\alpha(s_1)u_\gamma(s_2)\rangle_{\underline{f}=\underline{0}} \\ &\times \langle u_\delta(s_3)u_\nabla(s_4)\rangle_{\underline{f}=\underline{0}} + \langle u_\alpha(s_1)u_\delta(s_3)\rangle_{\underline{f}=\underline{0}} \langle u_\gamma(s_2)u_\nabla(s_4)\rangle_{\underline{f}=\underline{0}} \\ &+ \langle u_\gamma(s_2)u_\delta(s_3)\rangle_{\underline{f}=\underline{0}} \langle u_\alpha(s_1)u_\nabla(s_4)\rangle_{\underline{f}=\underline{0}} . \end{aligned} \tag{7.45}$$

Note that in Eq.(7.41) $\cos\theta_m$ stands for the z component of the mth unit vector. The use of Eq.(7.45) together with Eq.(7.41) leads to

$$\Lambda(s) = \frac{45}{2}\left[\int_0^{L_c} dt\, \langle u_z(t)u_z(s)\rangle_{\underline{f}=\underline{0}}\right]^2 . \tag{7.46}$$

In the limit of very long chain the first and the last equalities in system (7.19) lead to $C_2^{z,z}(t,s) \approx 1/3 \exp\left(-\frac{|s-t|}{l_p}\right)$. $\Lambda(s)$ is then easily computed to give the required equation.

7.4.2 $\langle P_2(\cos\alpha_{kk'})\rangle_f$ for a FJC

The expression for $\langle P_2(\cos\alpha_{kk'})\rangle_f$ for a stretched FJC of Kuhn segment length a can be readily obtained. On considering the distribution of the bond vector of segment s as

$$\begin{aligned} W(\underline{u}_s, \underline{u}_f; \eta_\ell) &= \frac{\exp\left(\eta_\ell \underline{u}_s \cdot \underline{u}_f\right)}{\int d\underline{u}_s \exp\left(\eta_\ell \underline{u}_s \cdot \underline{u}_f\right)} \\ &= \left[I_{\frac{1}{2}}(\eta_\ell)\right]^{-1} \sum_{l=0}^{\infty} I_{l+\frac{1}{2}}(\eta_\ell) Y_{lm}(\underline{u}_s)) Y^\star_{lm}(\underline{u}_f,)^{[34]} \end{aligned} \tag{7.47}$$

where $\underline{u}_s$ and $\underline{u}_f$ are the orientations of the segment s and the external force $\underline{f}$, $\eta_\ell = \frac{fa}{k_BT}$; and

$$I_\nu(z) = \left(\frac{z}{2}\right)^\nu \sum_{k=0}^{\infty} \frac{\left(\frac{z}{2}\right)^{2k}}{k!\Gamma\left(k+\nu+1\right)}.$$

On using $W(\underline{u}_s, \underline{u}_f; \eta_\ell)$ to evaluate $\langle P_2(\cos\alpha_{kk'})\rangle_f$ we easily see from the orthogonality relation of the spherical harmonics that

$$\langle P_2(\cos\alpha_{kk'})\rangle_f \propto \left(3\cos^2\theta_f - 1\right) I_{\frac{5}{2}}/I_{\frac{1}{2}} \approx \frac{\Lambda}{15}\left(3\cos^2\theta_f - 1\right)\left(\frac{fa}{k_BT}\right)^2 \left[1 - \frac{2}{21}\left(\frac{fa}{k_BT}\right)^2 + \ldots\right], \tag{7.48}$$

where θ_f is the angle between the external force and the magnetic field. We would like to point out the appellation error encountered in [35] where the function $I_\nu(z)$ was termed the Bessel function of the second kind.

Although PE at Θ point can, in principle, be mapped to an equivalent FJC, it appears difficult to adapt the above formula to fit PE results. On deriving the formula, it is assumed

that the spin pairs are located at the ends of each Kuhn segment. In the case of PE, a Kuhn segment is made of more than 10 C-C bonds each contributing to the dipolar interaction of the segment. Nevertheless, the quadratic truncation of Eq.(7.48) should be able to explain the data for weakly stretched PE.

In this section, we test by Monte-Carlo (Configurational Biased Monte-Carlo coupled with reptation moves) the limit of validity of Eq.(7.40) and Eq.(7.42) and we estimate Λ_p including its dependence on p. This will be done for the two polymer models. In short, the EV model is a bead-rod chain model with excluded volume interactions: this model will be exploited mainly to focus on the influence of excluded volume effects. The PE model will be exploited mainly at theta point to test, on a realistic case, the effect of finite extensibility on residual interactions.

Let us stress that Eq.(7.42) is valid for Θ-conditions as long as $\eta_\ell < 1$ but in the presence of excluded volume, this equation is only valid for chains in the "weakly stretched regime".

The elastic laws (Eqs.(7.1) and (7.2)) are well established in the literature. They have been extensively reviewed in the present thesis. For this EV model, one has $\eta_a \simeq \eta_\ell$, as the bond length and the Kuhn segment length are identical.

As already mentioned, for the EV model the pair of spins which will be considered in the estimation of dipolar residual interactions is located along the skeleton bonds. This implies that in Eq.(7.40), one has $\theta_{kk'} = 0$. On the other hand, for PE one has $\theta_{kk'} = 90°$.

7.4.3 Results

In all what follows, all results for PE are for Θ-solvents while good solvent conditions are considered for the EV model. It should also be recalled that our EV model is closely related to the FJC model for which exact results are known, both for the elasticity law [2] and the residual dipolar interactions for stretched chains [35].

Equilibrium Calculations of Λ

We monitored, in the absence of the force, the evolution of Λ_p as a function of the position p along the chain backbone. Application of Eq.(7.41) leads to results shown in Figure 7.12 and Figure 7.13. We see that central segments in both cases do not have the same Λ as end segments. The end effect extends over 10 bonds for the EV model and over 20 for PE. We remark that in the presence of excluded volume, Λ is almost four times larger than for a FJC where it is unity.

7.4.4 Calculations of $P_2^{\parallel}(\eta)$ and $P_2^{\perp}(\eta)$

Forces of varying strengths were applied to the ends of the polymer for the two model systems and $\langle P_2(\alpha)\rangle_\eta = \frac{1}{2}\langle 3\cos^2\alpha - 1\rangle_\eta$ was calculated for each force, as an average over all the spin pairs along the chain (α is the angle between the spin pair joining vector and the magnetic field). In each case, calculations were done for both magnetic field parallel and perpendicular to the force. We recall that for the EV model, the spin pair was assumed to lie along the skeletal bond while for PE, the two spins are those associated to the nuclei of the hydrogen atoms attached to the methylene carbons. According to Eq.(7.40), the initial behaviour of $\langle P_2(\alpha)\rangle_\eta$ should go as

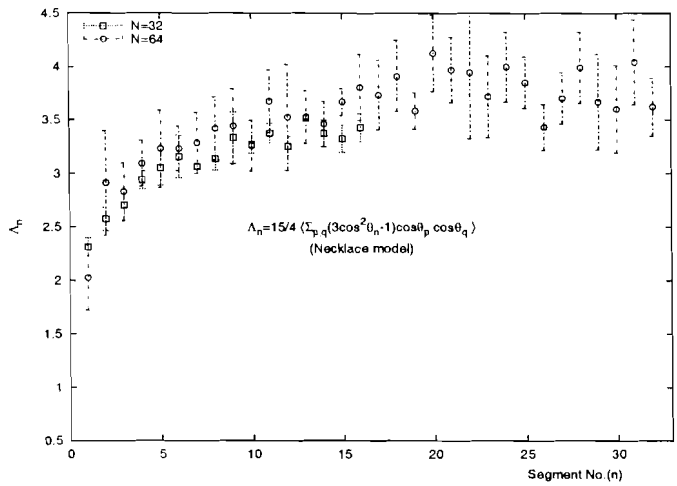

Figure 7.12: Segment position dependence of Λ for the EV bead-rod model: position 0 corresponds to chain end while the plateau corresponds to bulk segments.

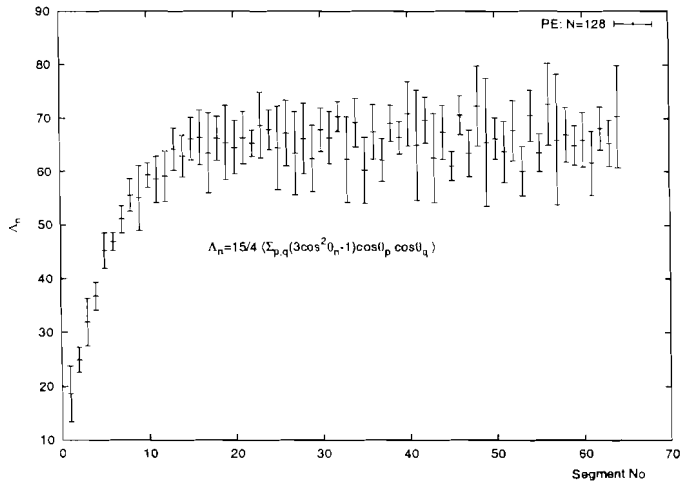

Figure 7.13: Segment position dependence of Λ for PE at Θ- point: position 0 corresponds to chain end while the plateau corresponds to bulk segments.

$$\left\langle P_2^{\parallel}(\alpha)\right\rangle_\eta^{EV} = \frac{\Lambda}{15}\eta_a^2, \quad \left\langle P_2^{\perp}(\alpha)\right\rangle_\eta^{EV} = -\frac{\Lambda}{30}\eta_a^2, \tag{7.49}$$

$$\left\langle P_2^{\parallel}(\alpha)\right\rangle_\eta^{PE} = -\frac{\Lambda}{30}\eta_a^2, \quad \left\langle P_2^{\perp}(\alpha)\right\rangle_\eta^{PE} = \frac{\Lambda}{60}\eta_a^2. \tag{7.50}$$

The MC results and the quadratic expressions expected at low stretching force (using the values of Λ computed with Eq.(7.41) are shown in Figures 7.14 and and 7.15 for EV and in Figure 7.16 for PE. We remark that $\langle P_2(\alpha)\rangle_f$ for both models is independent of chain size but depends on the chemical details of the chain.

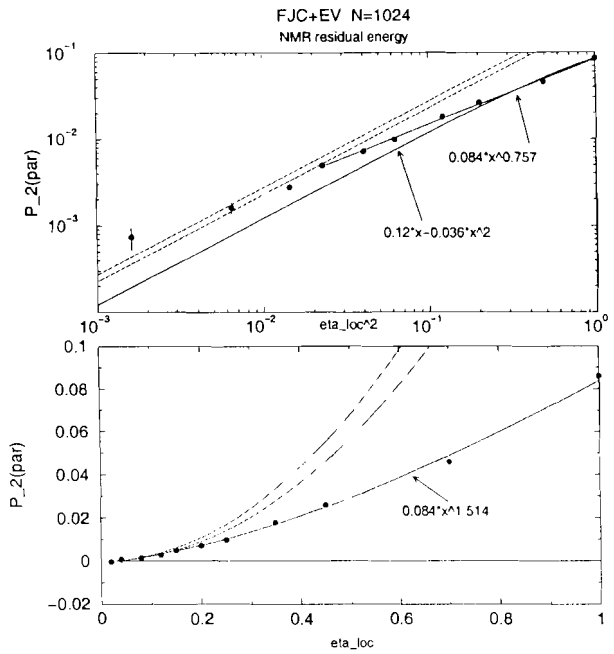

Figure 7.14: $\log - \log$ plot of $\left\langle P_2^{\parallel}(\cos\alpha)\right\rangle_f$ as a function of the square of the reduced force η_a^2 (upper) and linear plot of $\left\langle P_2^{\parallel}(\cos\alpha)\right\rangle_f$ as a function of the reduced force η_a (lower) for the EV model. The two parallel lines in the upper Figure indicate the limiting cases of the quadratic law (uncertainty on Λ). These are again indicated by the two parabola in the lower panel. The line of best fit for strong stretching ($\sim \eta_a^{1.5}$) is indicated.

7.4.5 Domain of validity of the f^2 law

For each model, we superposed in Figures 7.14, 7.15 and 7.16 the actual MC results and the expected quadratic forms. The latter are given explicitly in Eqs.(7.49) and (7.51). For PE, they can also be written as

$$\left\langle P_2^{\parallel}(\alpha)\right\rangle_\eta = -\frac{\Lambda a^2}{30b^2}\eta_\ell^2, \quad \left\langle P_2^{\perp}(\alpha)\right\rangle_\eta = \frac{\Lambda a^2}{60b^2}\eta_\ell^2. \tag{7.51}$$

The values of Λ are set to the observed plateau values in Figures 7.12 and 7.13 which are respectively, $\Lambda_{EV} \sim 3.8$ and $\Lambda_{PE} \sim 70$.

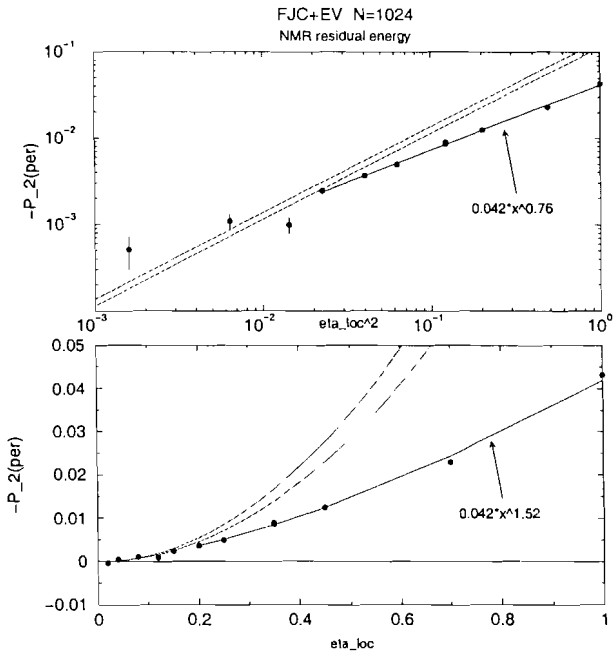

Figure 7.15: Same as in the last Figure but for minus $\left\langle P_2(\cos\alpha)^{\perp}\right\rangle_f$.

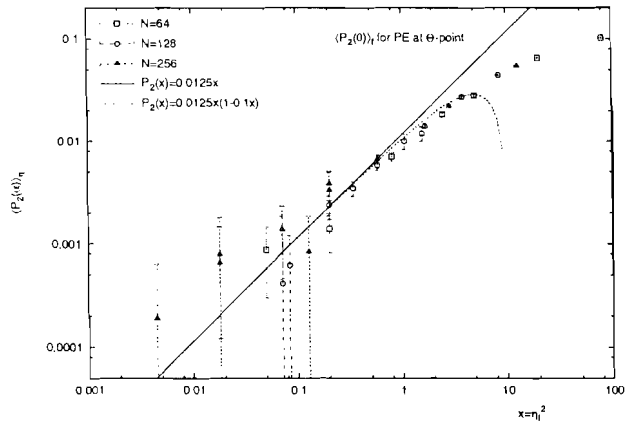

Figure 7.16: $\log - \log$ plot of $\left\langle P_2^{\perp}(\cos\alpha)\right\rangle_f$ as a function of η_ℓ^2 for PE at Θ-point.

For PE (see Figure 7.16), statistical error are large at small forces, nonetheless, it can be remarked that the quadratic regime is valid up to $\eta_\ell \approx 1$, a value which coincides with that of the upper limit of the extension-force linear regime of PE at Θ-point (see Figure 7.3). In particular, we note a good consistency between estimates of Λ deduced from unstretched chain expression (Eq.(7.41)) and from the force susceptibility expression (Eq.(7.51)).

For EV chain (see Figures 7.14 and 7.15), the limit of validity of the quadratic law is at best $\eta_\ell = 0.15$. Again, large statistical errors at weak stretching makes it difficult to say accurately the functional form. In the strong stretching regime, however, a power law $P_2 \sim \eta_\ell^y$, with $y \approx 1.5$, is observed. This is a crucial and unexpected result which has some implications in the link between P_2 and $\langle r_{ij} \rangle$ (see next section). In Figure 7.16, we have also shown the expected result for FJ chain up to the $4th$ order in η_ℓ as given by Eq.(7.48) [35] It seems that the correction to the quadratic form could explain the deviation of MC points for $0.8 < \eta_\ell < 3$.

7.4.6 Domain of validity of the r^2 law

We have plotted P_2 as a function of the reduced end-to-end vector $x = \langle r_{ij} \rangle / L_{ij}$ where L_{ij} is the contour length.

For PE at Θ-point, we remark in Figure 7.17, that the x^2 power law extends far in the strong stretching regime. On the basis of the assumption that Eqs.(7.49) and (7.51) are valid up to $\eta_\ell = 1$, it follows that the x^2 law should be valid up to $x = 1/3$, which seems to be indeed the case.

Figure 7.18 shows that the range of validity of the x^2 law is very short for the EV case. In the region of strong stretching ($\langle r_{ij} \rangle / R_0 > 1$, corresponding to $\eta_g > 3$, see Figure 7.2), a universal (i.e. independent of chain length) $x^{2.6}$ power law is found. The origin of such a behaviour can be traced by combining the apparent η_ℓ^y law for P_2 with the strong stretching excluded volume law $f \sim \langle r_{ij} \rangle^{\frac{\nu}{1-\nu}}$ to obtain,

$$P_2(\langle r_{ij} \rangle / L_c) \sim (\langle r_{ij} \rangle / L_c)^{\frac{y\nu}{1-\nu}} \left(\frac{L_c^\nu}{R_0} \right)^{\frac{y}{1-\nu}} . \tag{7.52}$$

Two points are evident from this result:

- Since $L_c \sim N$ and $R_0 \sim N^\nu$, P_2 is independent of number of monomers in the chain. It depends, thus, only on the relative extension with respect to the maximum extension.

- For excluded volume chains ($\nu = 0.6$), $y = 1.5$ should lead to a power law $x^{9/4}$, of which the exponent appears somewhat smaller than the observed value of 2.6. But if the errors associated to each parameter are considered, that is $y = 1.5 \pm 0.1$ and $\nu = 0.60 \pm 0.03$, then the exponent $\mu = \frac{y\nu}{1-\nu}$ should read 2.25 ± 0.45 which agrees with the calculated value within error bars.

It is important to point out that the function $P_2(x)$ for a chain composed of N monomers meets the power law $P_2(x) \sim x^\mu$ at $x \sim N^{\nu-1}$ since this law is a consequence of strong stretching which sets in as soon as $\langle r_{ij} \rangle \geq R_0$ i.e. for $x \geq R_0/L_{ij}$.

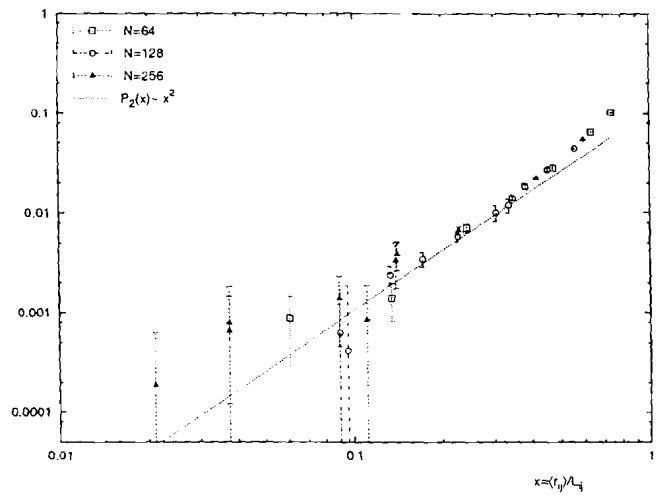

Figure 7.17: $P_2(x)$ as function of reduced extension $x = \langle r_{ij} \rangle / L_{ij}$ for PE at Θ-point.

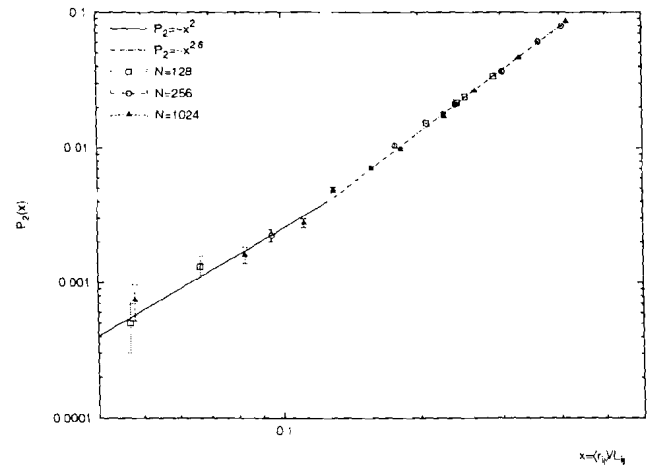

Figure 7.18: $P_2(x)$ as function of reduced extension $x = \langle r_{ij} \rangle / L_{ij}$ for the EV model.

7.5 Static structure factor

In this section we present the MC data for the single chain structure factor of a 512 segments PE in good and Θ solvent conditions. This structure factor is a measure (in the reciprocal space) of the spatial distribution of the scattering units within a coiled molecular system. To see this let us define the average density of a system of N scatterers around unit n. This is written as

$$g_n(\underline{r}) = \sum_m \delta\left(\underline{r} - (\underline{r}_m - \underline{r}_n)\right). \tag{7.53}$$

The pair correlation function $g(\underline{r})$ is the average over all N scattering units of $g_n(\underline{r})$.

$$g(\underline{r}) = \frac{1}{N}\sum_n g_n(\underline{r}) = \frac{1}{N}\sum_{n,m}\left\langle \delta\left(\underline{r} - (\underline{r}_m - \underline{r}_n)\right)\right\rangle. \tag{7.54}$$

Its Fourier transform reads

$$\tilde{g}(\underline{q}) = \frac{1}{N}\sum_{m,n}\left\langle \exp\left[i\underline{q}\cdot(\underline{r}_m - \underline{r}_n)\right]\right\rangle. \tag{7.55}$$

This quantity can be measured experimentally by various scattering methods (light scattering, small angle X-ray scattering (SAXS) and small angle neutron scattering (SANS)). Consider a ray capable of being scattered by the system of N scatterers mentioned above. If on entering the system its wave vector is $\underline{k}_0$ and on leaving, it is $\underline{k}$ then the change in wave vector is $\mid \underline{q} \mid = \mid \underline{k} - \underline{k}_0 \mid = \frac{4\pi}{\lambda_0}\sin(\frac{\theta}{2})$, where θ is the angle through which the beam is scattered. The intensity of the scattered ray is a measure of the quantity

$$S(\underline{q}) = \frac{1}{N}\sum_{m,n} a_m a_n^{\star}\left\langle \exp\left[i\underline{q}\cdot(\underline{r}_m - \underline{r}_n)\right]\right\rangle, \tag{7.56}$$

with a_m being the scattering amplitude of unit m (relative to that of the solvent). For a homopolymer $a_m = a$ is a constant. Consequently $\tilde{g}(\underline{q})$ is proportional to $S(\underline{q})$. In our simulations we shall let $\mid a \mid = 1$ so that at the limit of vanishing $\underline{q}$, $S(\underline{q})$ be equal to the number of scatterers in th system. In addition, for small q, $S(\underline{q})$ permits the knowledge of polymer size (for a single polymer in solution) or the mean polymer size for a melt of heteropolymers. To see this we perform the Taylor expansion of $S(\underline{q})$ up to quadratic term in $\underline{q}$ bearing in mind that due to isotropy $\langle \underline{r}_m - \underline{r}_n \rangle = 0$.

$$\begin{aligned}
S(\underline{q}) &= \frac{1}{N}\sum_{m,n}\left\langle 1 - \frac{1}{2}\left[\underline{q}\cdot(\underline{r}_m - \underline{r}_n)\right]^2 + \ldots\right\rangle \\
&= N - \underline{q}\underline{q} : \frac{1}{2N}\sum_{m,n}\left\langle (\underline{r}_m - \underline{r}_n)(\underline{r} - \underline{n}_n)\right\rangle + \ldots \\
&= N\left(1 - \frac{1}{2}\sum_{\alpha,\beta} q_\alpha q_\beta \frac{1}{N^2}\sum_{m,n}\left\langle (x_{m\alpha} - x_{n\alpha})(x_{m\beta} - x_{n\beta})\right\rangle\right) + \ldots \\
&= N\left(1 - \frac{q^2}{3}R_g^2 + \ldots\right),
\end{aligned} \tag{7.57}$$

where we have used $\langle (x_{m\alpha} - x_{n\alpha})(x_{m\beta} - x_{n\beta})\rangle = \frac{\delta_{\alpha\beta}}{3}(\underline{r}_m - \underline{r}_n)^2$ and the definition of the radius of gyration

$$R_g^2 = \frac{1}{N}\sum_m (\underline{r}_m - \underline{R}_G)^2 = \frac{1}{2N^2}\sum_{m,n}\left\langle (\underline{r}_m - \underline{R}_n)^2\right\rangle . \tag{7.58}$$

Therefore at small q polymer scattering is capable of furnishing informations on polymer properties like chain size and the osmotic compressibility of polymer solutions [37] as it has been shown that for a polymer solution, $\lim_{q\to 0} S(q) = Tc\frac{\partial c}{\partial \pi}$, where T is the temperature, c the polymer concentration and π the osmotic pressure.

At intermediate q values, the structure factor follows the universal curve $S(q) \propto q^{-1/\nu}$ where $\nu \approx 3/5$ is the Flory exponent for the excluded chain statistics or where $\nu = 0.5$ in the random walk chain statistics when chains are ideal. It should be noted that this scaling regime persists up to $q \approx \frac{1}{b}$ where b is the Kuhn segment length. Within the scaling regime various situations such as semi-dilute solutions, chains close to theta point or polymer stretching introduce a new length scale ξ across which the fractal dimension of the coil (which is $D = \frac{1}{\nu}$) undergoes a cross-over from random walks to self avoiding walks statistics. This new length scale is usually called the blob size whereby the blob is a portion of the chain within which space correlations decay differently from those seen on a coarse grained level englobing them. For the case of stretched chains (force $\pm f$ applied at chain ends) which is of interest to us, tensile blobs (Pincus blobs) were predicted by Pincus as a change of exponent in the power law regime of the structure factor, provided the blob size is in the right range, namely $R_g > \xi = k_B T/f > b$. This prediction was demonstrated by C. Pierleoni and J. P. Ryckaert using EV chain model of the hard sphere necklace [12]. Beyond the power law regime, the structure factor becomes specific to the precise chemistry of the chain. In this regime, the quality of solvent is expected to have very little influence. Figure 7.20 shows the structure factor of a 512-segment PE in good and theta solvents as obtained by CBMC simulations. We can see that the distinction between the two curves is manifest in the scaling regime but both functions clearly merge beyond $q = 0.2$ inverse angstroms ($\equiv \frac{2\pi}{30}$, where one enters the local regime). A value of 30Angstroms is about twice the the Kuhn segment length ($b = 14.9$Angstroms) that was obtained from MC simulations on polyethylene with some thousands of C atoms [24].

The structure factor of a stretched PE chain (see figure 7.19) is very similar to that of the simple EV chain of Pierleoni et al. [12] especially in the regime of small and intermediate q values. Some differences arise only in the chemical detail sensitive region of large q where all curves for different force intensities do not converge to a unique curve as is the case for the freely jointed necklace model. This high f regime should reflect (in a complicated way, though) local conformation changes; neutron spectroscopy, therefore, appears as a complementary way of probing the relative importance of the various polymer conformations. In a uni-axial system (here the axis coincides with the the direction of the force), the gyration tensor has three non vanishing components - one component in a direction parallel to the field $R_g^{\parallel}$ and two equal perpendicular components $R_g^{\perp}$. While the former describes how spread particles are along the axis of the forcing field, the latter demonstrate the perpendicular dispersion. Our explicit calculations of $R_g^{\parallel}$ and $R_g^{\perp}$ (not reported here) confirmed that $R_g^{\parallel}$ increases while $R_g^{\perp}$ decreases on stretching a polymer. The question one therefore poses is: considering the fact that a similar trend should be observed in the radius of gyration tensor of a stretched necklace chain, why do we not observe a similar trend in the structure factors, that is, why is it that in the large q

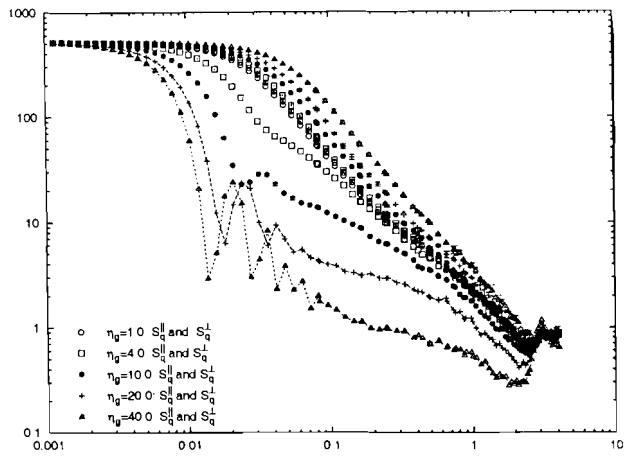

Figure 7.19: The static structure factor of a stretched 512 segment polyethylene in good and Θ solvents. Results for the scattering vector perpendicular to the external force are represented on the upper curves while those for scattering vectors parallel to the force are the lower curves.

regime all scattering curves for stretched PE do not converge to a unique curve as is the case for the hard sphere model. The answer seems to lie in the fact that while in a highly stretched PE $R_g^{\perp}(f)$ will never be zero due to bending angle constraints ($\lim_{f\to\infty} R_g^{\perp}(f) = \frac{1}{2}\ell_{cc}\sin(\frac{\gamma}{2})$, where ℓ_{cc} is the C-C bond length and γ is the C-C-C bending angle), in the freely jointed necklace chain, the highly stretched conformation will correspond to a complete linear array of scatterers ($\lim_{f\to\infty} R_g^{\perp}(f) = 0$). It will be interesting to investigate the effect, on the mean scatterer spread, of including finite bending and bonding energy terms in the Hamiltonian of a macromolecule.

In the next section, we briefly recall some of the theories widely used to interpret scattering experiment. We shall then show, for the first time, that polymer scattering is intimately related to single polymer elasticity. To do this we show that the knowledge of the extension-force relationship of a stretched linear polymer over all length scales permits, uniquely, the determination of the the scattering function in the whole reciprocal space.

7.5.1 Some theoretical background

The structure factor of a system of $N+1$ scattering centres subjected to an external stress $\underline{f}$ is written as:

$$S_{\underline{f}}(\underline{q}) \equiv \frac{1}{N+1}\sum_{l=0}^{N}\sum_{j=0}^{N}\left\langle \exp\left[i\underline{q}\cdot\left(\underline{r}_l - \underline{r}_j\right)\right]\right\rangle_{\underline{f}}, \tag{7.59}$$

where $\underline{q}$ is the scattering vector and $\underline{r}_j$ denotes the cartesian coordinates of the scattering unit j.

Assuming that the end-to-end vector of the chain segment between j and l obeys a gaussian distribution, $S(\underline{q})$ can be shown to follow the celebrated Debye function for stretched chains:

$$S_f(\underline{q}) = Re\left\{\frac{2(N+1)}{X^2}\left(e^{-X} - 1 + X\right)\right\}, \tag{7.60}$$

with

$$X = \begin{cases} \underline{q}_{\perp}^2 R_g^2 & \text{for } \underline{q} \perp \underline{f} \\ \underline{q}_{\parallel}^2 R_g^2 + i\frac{1}{3}\frac{fR_0^2}{k_B T} q_{\parallel} & \text{for } \underline{q} \parallel \underline{f}, \end{cases} \tag{7.61}$$

where R_0 and R_g are, respectively, the root-mean-square end-to-end distance and the radius of gyration of the unperturbed chain, k_B the Boltzmann constant, T the absolute temperature and f the intensity of the stretching force. It has been shown in the computer simulation of Pierleoni et al. [12] that the Debye function follows very closely the stretched EV chain structure factor up to the cross-over from the ideal chain statistics to the excluded volume statistic still prevailing within the tensile blobs.

In the present work we report the structure factor of a stretched and an unstretched polyethylene chain in good and Θ solvents. It is noticed that the Debye function fails to explain the numerical results for q values in the vicinity of and beyond $0.1\mathring{A}^{-1}$ for good solvent conditions. On the other hand in Θ solvent good agreement was observed beyond this q-value.

It was shown in [12] that when $S_f(\underline{q}_{\parallel})$ is plotted versus the effective scattering vector

$$\tilde{q} = \sqrt{q^2 + \frac{4}{\xi_T^2}\cos^2\theta}, \tag{7.62}$$

(where $\xi_T = \frac{k_B T}{f}$ is the tensile blob size and θ is the angle between the force and $\underline{q}$) which takes into account the change in metric due to stretching [13], the universal asymptotic behaviour at large q is recovered over a rather large domain. For moderate and large forces observed in the scaling curves of PE, the appearance of shoulders similar those pointed out in [12] at low q. As was explained, under strong stretching, a polymer molecule tends to behave as a rigid rod of length L with $N+1$ scatterers uniformly distributed on it. The scattering function for this rod is [15]

$$S(q) = \frac{2(N+1)}{(qL)^2}\left[1 - \cos(qL)\right]. \tag{7.63}$$

The shoulders mentioned above are a consequence of the rigidity of the polymer when stretched. In this case L corresponds to the mean end-to-end distance in the stretching direction.

In a beautiful work by Benoît et al. [16] aimed at calculating the structure factor of a stretched ideal chain, it was assumed that the end-to-end vector distribution for the strand made of $\mid i - j \mid$ bonds is gaussian with nonzero mean and stretch dependent width. They then obtained a Debye type equation (see Eq.(7.60)) that depends on the mean extension and fluctuations of the stretched chain [12] as

$$X_{\parallel} = \frac{1}{2} q_{\parallel}^2 \left\langle \delta R_{\parallel}^2 \right\rangle_f + i q_{\parallel} R_f. \tag{7.64}$$

Pierleoni et al. [12] demonstrated that for the necklace EV chain (largely explored in the previous and the present chapters) subjected to a force,

$$\begin{aligned} R_f &= \left\langle \underline{R} \cdot \frac{\underline{f}}{f} \right\rangle = R_O B \eta_g^{2/3}, \\ \left\langle \delta R_{\parallel}^2 \right\rangle_f &= R_o^2 C_{\parallel} \eta_g^{-1/3}, \\ \left\langle \delta R_{\perp}^2 \right\rangle_f &= R_o^2 B \eta_g^{-1/3}, \end{aligned} \tag{7.65}$$

where $B = \frac{3}{2}C_{\|} = 0.46$. When they combined system (7.65) and Eq.(7.64) with the corresponding Debye function, the resulting function was found to explain excellently the shape of the structure factor curve of the stretched EV chain.

We shall now proceed to develop a theory which is capable of describing the scattering of long linear polymers over a wide range of scattering angles and solvent quality. The elaboration of the theory is guided by an intuitive parallelism with the free energy of a stretched chain.

7.5.2 $S_f(q)$ from the extension-force relationship

Considering the unperturbed distribution $W_{lj}(\underline{r})$ of the strand between scattering units l and j of the molecule, we rewrite $S_{\underline{f}}(\underline{q})$ as

$$S_{\underline{f}}(\underline{q}) = \frac{1}{N+1}\sum_{l=0}^{N}\sum_{j=0}^{N}\frac{\int d\underline{r} W_{lj}(\underline{r}) \exp\left[\beta\left(\underline{f} + ik_BT\underline{q}\right)\cdot\underline{r}\right]}{\int d\underline{r} W_{lj}(\underline{r}) \exp\left(\beta\underline{f}\cdot\underline{r}\right)}, \tag{7.66}$$

which on defining the segment free energy $G_{lj}(\beta\underline{f})$ as

$$\exp\left(-\beta G_{lj}(\beta\underline{f})\right) \equiv \int d\underline{r} W_{lj}(\underline{r}) \exp\left(\beta\underline{f}\cdot\underline{r}\right), \tag{7.67}$$

becomes

$$S_{\underline{f}}(\underline{q}) = \frac{1}{N+1}\sum_{l=0}^{N}\sum_{j=0}^{N}\exp\left[-\beta\left(G_{lj}(\beta\underline{f}+i\underline{q}) - G_{lj}(\beta\underline{f})\right)\right]. \tag{7.68}$$

Since this free energy is related to the mean end-to-end extension via

$$\left\langle \underline{r}_{lj}\right\rangle_{\underline{f}} = \left(\frac{\partial}{\partial\beta\underline{f}}\right)\left[-\beta G_{lj}(\beta\underline{f})\right], \tag{7.69}$$

a complete knowledge of the extension-force law over all length scales renders possible the analysis of the structure factor over a wide range of the scattering vector.

7.5.3 Applications

1. The Gaussian chain Approximation: The structure factor of a gaussian chain is described by the Debye function. This means that the present theory must be able to recover this function. For the gaussian chain the extension-force relationship of a segment separated by $\mid i-j \mid$ bond vectors is given by

$$\langle r_{ij}\rangle_f = \frac{1}{3}R_{ij0}^2\beta f, \tag{7.70}$$

so that Eq.(7.69) leads to

$$\beta G_{ij}(\beta f) = -\frac{1}{6}R_{ij0}^2\beta^2 f^2 + \text{constant}. \tag{7.71}$$

On substituting this in Eq.(7.68) knowing that for a gausian chain $R^2_{ij0} = \mid i-j \mid b^2 = \frac{|i-j|}{N} R_0^2$, we obtain

$$S_{\underline{f}}(\underline{q} = \Re\left\{ \frac{1}{N} \sum_{lj} \exp\left[-\frac{\mid l-j \mid}{6N} \left\{ \left(\beta \underline{f} R_0 + i\underline{q} R_0\right)^2 - \left(\beta \underline{f} R_0\right)^2 \right\} \right] \right\}, \tag{7.72}$$

which gives the so-called generalised Debye function when the discrete sums are approximated by continuous ones as

$$S_{\underline{f}}(\underline{q} = \Re\left\{ \frac{2N}{\left(\frac{(qR_0)^2}{6} - i\frac{R_0^2}{3}\beta \underline{f} \cdot \underline{q}\right)^2} \left[\exp\left(-\frac{(qR_0)^2}{6} + i\frac{R_0^2}{3}\beta \underline{f} \cdot \underline{q}\right) - 1 + \frac{(qR_0)^2}{6} - i\frac{R_0^2}{3}\beta \underline{f} \cdot \underline{q} \right] \right\}. \tag{7.73}$$

$\Re$ denotes real part. Remark that though $X = \frac{(qR_0)^2}{6} - i\frac{R_0^2}{3}\beta \underline{f} \cdot \underline{q}$ is the complex conjugate of that given by the Debye theory, it does not influence the final result since only the real part, as indicated in Eq.(7.73), concerns us. On letting $f = 0$ we get the unperturbed Debye formula [16] $S(q) = \frac{2N}{X^2}\left(e^{-X} - 1 + X\right)$, where $X = R_0^2 q^2/6$.

2. The freely jointed chain: The extension-force relationship in this case is given by the Langevin function

$$\langle r_{ij} \rangle_f = \mid i-j \mid b \left[\coth\left(\beta f b\right) - \frac{1}{\beta f b} \right]. \tag{7.74}$$

The corresponding free energy is

$$\begin{aligned} \beta G_{ij}(\beta f) &= -\mid i-j \mid b \int d(\beta f) \left[\coth\left(\beta f b\right) - \frac{1}{\beta f b} \right] \\ &= -\frac{\mid i-j \mid}{N} N \ln \mid \frac{\sinh(\beta f b)}{\beta f b} \mid + \text{constant}. \end{aligned} \tag{7.75}$$

Then Eq.(7.68) leads to

$$S_{\underline{f}}(\underline{q}) = \Re\left\{ \frac{2N}{C^2}\left(e^C - 1 - C\right) \right\}, \tag{7.76}$$

where

$$C = N \ln \left[\frac{\sinh\left(\mid \beta \underline{f} + i\underline{q} \mid b\right)}{\sinh\left(\mid \beta \underline{f} \mid\right)} \frac{\mid \beta \underline{f} \mid b}{\mid \beta \underline{f} + i\underline{q} \mid b} \right],$$

with the vertical bars bounding the vectors indicating vector norms. For $f = 0$ we deduce the unperturbed chain structure factor

$$S_L(q) = \frac{2}{N\left[\ln \mid \frac{\sin(qb)}{qb} \mid\right]^2} \left\{ \left(\frac{\sin(qb)}{qb}\right)^N - 1 - N \ln \mid \frac{sin(qb)}{qb} \mid \right\}. \tag{7.77}$$

When this function is compared with that of Debye for small q values they coincide exactly for $R_g^2 = Nb^2/6$. Figure 7.20 shows $S_L(q)$ adapted to the Θ solvent PE (b and N are adapted by Eq.(7.20)). We remark the excellent agreement with MC results for small

and intermediate q values. Note that $S(q)$, as predicted by this theory, presents infinite branches at $qb = k\pi$ (for integral k) but above this q value $S(q)$ recovers its expected oscillatory character. Eq.(7.77), thus explains the structure factor of ideal chains over small and intermediate q range; and that of both ideal and excluded volume chains in the extra large q domain.

3. The scaling regime: The structure factor in this regime has often been explained by an asymptotic scaling law which barely explains the qualitative aspects (the $q^{-\frac{1}{\nu}}$ power law for large q). The present theory, rigorously exact for all q values, brings out clearly how $S(q)$, for a stretched chain, evolves in this regime.

   The starting point is again the mean end-to-end vector of the stretched segment known in the scaling regime to follow the law $\langle r_{ij}\rangle_f = AR_{ij0}\left(R_{ij0}\beta f\right)^{\frac{1}{\nu}-1}$ with $A = 0.46$, $\nu = 3/5$ and $\beta = 1/k_BT$. On integrating Eq.(7.69) we deduce that $\beta G_{ij}(\beta f) = -A\nu R_{ij0}^{\frac{1}{\nu}}\left(\beta f\right)^{\frac{1}{\nu}} +$ constant. If we assume that R_{ij0} follows $R_{ij0}^2 \sim \mid i-j \mid^{\nu}$ then $S_{\underline{f}}(\underline{q})$ reads

$$S_{\underline{f}}(\underline{q}) = \Re\left\{\frac{2N}{C^2}\left[e^C - 1 - C\right]\right\}, \tag{7.78}$$

where

$$C = A\nu\left\{\mid \underline{\eta} + iR_0\underline{q} \mid^{\frac{1}{\nu}} - \mid \underline{\eta} \mid^{\frac{1}{\nu}}\right\}, \tag{7.79}$$

with $\underline{\eta} = \beta R_0\underline{f}$. $S_{\underline{f}}(\underline{q})$ is explicitly written as

$$S_{\underline{\eta}}(\underline{q}) = \frac{2N}{\left(A\nu\right)^2 Z^2}\left\{\exp\left(-\nu AZ\cos\psi\right)\cos\left[2\psi + \nu AZ\sin\psi\right] - \cos(2\psi) + \nu AZ\cos\psi\right\} \tag{7.80}$$

where

$$\begin{aligned}
Z^2 &= X^{\frac{2}{\nu}} + \eta^{\frac{2}{\nu}} - 2X^{\frac{1}{\nu}}\eta^{\frac{1}{\nu}}\cos\left(\frac{\phi}{\nu}\right) \qquad Z \geq 0,\\
\tan\psi &= \frac{X^{\frac{1}{\nu}}\sin\left(\frac{\phi}{\nu}\right)}{X^{\frac{1}{\nu}}\cos\left(\frac{\phi}{\nu}\right) - \eta^{\frac{1}{\nu}}} \qquad -\frac{\pi}{2} \leq \psi \leq \frac{\pi}{2},\\
X^4 &= \left(\eta^2 - R_0^2q^2\right)^2 + 4R_0^2\left(\underline{\eta}\cdot\underline{q}\right)^2,\\
\tan\left(2\phi\right) &= \frac{2R_0\underline{\eta}\cdot\underline{q}}{\eta^2 - R_O^2q^2}.
\end{aligned} \tag{7.81}$$

Due to the complicated nature of $S_{\eta}(q)$ we only give here, the expression for $S_{\eta=0}(q)$ which reads

$$S_{\eta=0}(q) = \frac{2N}{\nu^2A^2\left(R_0q\right)^{\frac{2}{\nu}}}\left\{e^{-\nu A(R_0q)^{\frac{1}{\nu}}} - 1 + \nu A\left(R_0q\right)^{\frac{1}{\nu}}\right\}. \tag{7.82}$$

Remark that in the limit of large q

$$S_{\eta=0}(q) \to \frac{2N}{\nu A\left(R_0q\right)^{\frac{1}{\nu}}}, \tag{7.83}$$

which reproduces the usual asymptotic scaling prediction.

4. The extra strong stretching region: In this finite extensibility regime there is practically no theoretical expression for the extension-force relationship. It is believed that since in this regime most, if not all, monomers are well separated from each other, excluded volume forces are completely screened out. Thus, the molecule starts behaving as a freely jointed chain characterised by a finite stretch modulus S [39] such that the force extension relation is

$$\langle r_{ij}\rangle_f = |i-j|b\left[\coth\left(\frac{fb}{k_BT}\right) - \frac{k_BT}{fb}\right]\left(1+\frac{f}{S}\right). \tag{7.84}$$

Instead of using this idea, we assume (rightly) that in this regime $\langle r_{ij}\rangle_f \propto| i-j |f^{\alpha}$. By exploiting the extension-force simulation results in this region the constant of proportionality and α are obtained by best fitting. The corresponding free energy is substituted in Eq.(7.68) and $S_f(q)$ computed. Figure 7.20 again demonstrates agreement between the theory and simulation.

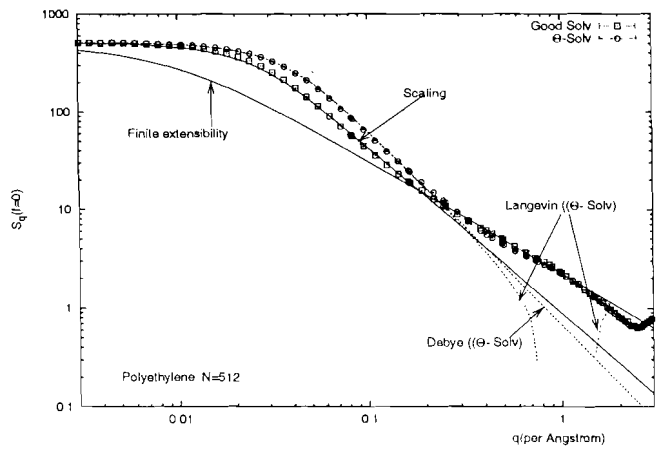

Figure 7.20: The static structure factor of an unperturbed 512 segments polyethylene in good and Θ solvents. Our different theoretical predictions are indicated as described in the text and demonstrated on the curves.

The above analyses have been enhanced by the linear dependence of the chain stress free energy on the number of bonds in segment irrespective of the segment size. This point has a strong physical backing than the linear assumption underlying the Debye function. While the Debye linear assumption is based on the second moment of the end-to-end vector (which is not always true), ours is based on a thermodynamic requirement that the free energy per particle of an N particles system be independent of N. The excellent agreements recorded between our more general theory and other theories based on limiting cases are strong indications that chain elasticity and neutron spectroscopy are complementary methods of investigating some polymer properties.

Bibliography

[1] L. R. G. Treloar, *The physics of rubber elasticity*, Clarendon Press, Oxford, 1975

[2] P.-J. Flory, *Statistical Mechanics of Chain Molecules*, Hanser Publishers, New York, 1989

[3] J. H. Weiner, *Statistical Mechanics of Elasticity*, John Wiley & Sons, Inc., New York, 1983

[4] R. H. Boyd and P. J. Phillips, *The Science of Polymer Molecules*, John Wiley & Sons, Inc., New York, 1983

[5] U. W. Gedde, *Polymer Physics (Chapman & Hall), London*, 1995

[6] X. Châtelier and J. F. Joanny, *Phys. Rev. E* **57** (6): 6923, 1998

[7] C. H. Wang and Q. R. Wang, *J. Chem. Phys* **106**(7): 2819, 1996

[8] P. G. de Gennes, *J. Chem. Phys.* **60**(1): 503, 1974

[9] J. M. West, L. E. Wedgewood and R. Wyron Bird, *J. Chem. Phys.* **90**(1): 587, 1988

[10] S. B. Smith, L. Finzi, and C. Bustamante, *Science* **256**: 1122, 1992

[11] C. Bustamante, J. F. Marko, E. D Siggia, and S. Smith. *Science* **265**: 1599, 1994

[12] C. Pierleoni and G. Arialdi and J.-P. Ryckaert, *J. Chem. Phys. Lett.* **79**:2990, 1997

[13] P. Pincus, *Macromolecules* 9(3): 386, 1976

[14] D. Y. Yoon and P. J. Flory. *Macromolecules* 9(2): 294, 1976

[15] A. Onuki, *J. Phys. Soc. Jpn.* **54**: 3656, 1985 *Macromolecules*, **9**(2): 294, 1976

[16] H. Benoît et al., *Macromolecules* 8(4): 451, 1975

[17] I. Webman J. Lebowitz and M. Kalos, *Phys. Rev. A* **23**: 316, 1981

[18] M. Wittkop, J. U. Sommer, S. Kreitmeier, and D. Göritz, *Phys. Rev. E* **49**: 5472, 1994

[19] J. des Cloizeaux and G. Jannink, *Polymers in solution*, (Clarendon Press, Oxford), 1990

[20] L. R. Dodd, T. D. Boone, and D. N. Theodorou, *Mol. Phys.*, **78**: 961, 1993

[21] J. P. Cohen-Addad, *Physical properties of polymeric gels*, John Wiley & Sons Ltd, 1996

[22] A. Ladd and D. Frenkel, *Macromolecules* **25**: 3435, 1992

[23] N. Fatkullin and R. Kimmich and H. W. Weber, *Phys. Rev. E*, **47**: 4600, 1992

[24] M. Destree, A. Lyulin and J.-P. Ryckaert, *Macromolecules* **29**(5): 1721, 1996

[25] D. Frenkel and B. Smit, *understanding Molecular Simulation*, Academic Press, 1996.

[26] M. N. Rosenbluth and A. W. Rosenbluth, *J. Chem. Phys.* **23**: 356, 1955

[27] B. Y. Ha and D. Thirumalai, *J. Chem. Phys.* **106**(10): 4243, 1996

[28] F. Marko and E. D. Sigia, *Macromolecules* **28**: 8759, 1995

[29] Y. Abe and P. J. Flory, *J. Chem. Phys.* **52**(6): 2814, 1970

[30] T. M. Birshstein and O. B. Ptitsyn, *Conformations of Macromolecules (interscience Publishers, Inc.), New York* , 1966.

[31] J. T. Titantah and C. Pierleoni and J.-P. Ryckaert, *Submitted to Phys. Rev. E*, 1998

[32] A. Guillermo and J.-P. Cohen-Addad, *Macromolecules* **24**: 3081, 1991

[33] H. Yamakawa, *Helical wormlike chains in polymer solutions*, Springer-Verlag, Berlin, 1997

[34] C. J. Jaochain, *Quantum Collision Theory*, North Holland Physics Publishing, Amsterdam, 1975

[35] J.-P. Cohen-Addad, *Physics of Finely Divided Matter*, Boccara and Daoud Ed., Springer-Verlag, 1985

[36] J.-P. Cohen-Addad, *J. Chem. Phys.* **60** (6): 2440, 1974

[37] M Daoud et al. *Macromolecules* **8** (6): 804, 1975

[38] Farnoux et al. *J. Phys.* **39**: 77, 1978

[39] S. B. Smith, Y. Cui, and C. Bustamante, *Science* **271**: 795 1996

Chapter 8

Effective potentials between two polymer segments in solution

Summary

The question of the choice of the effective potential between polymer segments in a solvent bath is examined. An attempt is made to search for a realistic solvent mediated effective potential that probes polymer properties over wide range of temperature or solvent quality. Using this realistic potential to evaluate the intermolecular force between two pentamers and the dependence of the radius of gyration tensor components of a single pentamer on its closeness to the second molecule, reveals good agreement with expensive calculations of same properties in explicit solvent.

8.1 Introduction

Calculations aimed at monitoring the properties of condensed media have often been done by modeling the costly solvent background by ad hoc effective potentials [1, 2, 3, 4]. Very little attention has been focused on the realities of the choices of these potentials. It is true that under certain conditions some simple models become well adapted. For example, at high temperatures, simple repulsive models for the interactions between polymer segments like the hard sphere model can be justified. Solvent quality plays a vital rule in the thermodynamic properties of polymer solutions since under different solvent conditions, polymer molecules behave differently. A meaningful study of polymer collapse transition must include an explicit consideration of solvent effects. In an article by A. Byrne and others [2] aimed at studying polymer collapse, effective potential between any two segments was assumed to be of the form $ar^{-12} - br^{-6}$ with a and b being adjustable parameters. Polymer collapse was monitored by adjusting b and exploring how the polymer clusters with time. A similar approach was introduced by M. Destrée and J.-P. Ryckaert [5] to search for the Θ condition for an atactic polypropylene. Harismiadis et al. [1], in their determination of the Θ-point of a polymer solution, employed the notion of the potential of mean force between two polymer segments [6]. The solvent effect on the segments was assumed to be an effective interaction of the Lennard-Jones type. In their simulations they dealt with reasonably high temperatures ($k_BT > \epsilon$). Nonetheless, they pointed out that as the

temperature decreases the range of the effective polymer intermolecular potential increases.

Very few polymer researchers [7, 8] have performed simulations in explicit solvent. By using the free energy perturbation (FEP) technique on a united atom model for methane and n-butane in water, Pellegrini [8] observed that these molecules present strong hydrophobic behaviours even at room temperature. Similar results were observed by D. van Belle [7].

In this chapter, we propose a model of implicit solvent effects which is established by a preliminary MC simulation aimed at obtaining effective monomer-monomer force in the presence of explicit solvent.

To search for a realistic solvent mediated effective monomer-monomer potential, the PMF ($\omega_\beta^{\epsilon_{sp}}(\xi)$) between two atoms (dimer) separated by a distance ξ in a mono-atomic solvent (chacterised by a solvent quality parameter ϵ_{sp}) are calculated using a Monte Carlo (MC) procedure. The force exerted between the constrained atoms is calculated. This force, $f_\beta^{\epsilon_{sp}}(\xi)$, is related to the effective potential $\omega_\beta^{\epsilon_{sp}}(\xi)$ via:

$$\omega_\beta^{\epsilon_{sp}}(\xi) = \int_\xi^\infty d\zeta \, f_\beta^{\epsilon_{sp}}(\zeta), \tag{8.1}$$

where $\beta = 1/k_BT$ and ϵ_{sp} is a solvent quality parameter. The force $f_\beta^{\epsilon_{sp}}(\zeta)$ is the ensemble average of half the force difference between the constrained atoms of the dimer projected on the dimer bond vector. To see how Eq.(8.1) comes about, we define the PMF on the dimer ($\omega_\beta^{\epsilon_{sp}}(\underline{r}_1, r_2)$) as

$$\exp\left[-\frac{\omega_\beta^{\epsilon_{sp}}(\underline{r}_1, \underline{r}_2)}{k_BT}\right] = C \int d\underline{r}_3 d\underline{r}_4 ... d\underline{r}_N \exp\left[-\frac{U^{\epsilon_{sp}}\left(r^N\right)}{k_BT}\right], \tag{8.2}$$

so that half the force difference between the monomers of the dimer reads:

$$\underline{f}_\beta^{\epsilon_{sp}}(\underline{r}_1, \underline{r}_2) = -\frac{1}{2}\frac{\int d\underline{r}_3 d\underline{r}_4 ... d\underline{r}_N \left(\frac{\partial U^{\epsilon_{sp}}}{\partial \underline{r}_1} - \frac{\partial U^{\epsilon_{sp}}}{\partial \underline{r}_2}\right) \exp\left[-\frac{U^{\epsilon_{sp}}\left(\underline{r}^N\right)}{k_BT}\right]}{\int d\underline{r}_3 d\underline{r}_4 ... d\underline{r}_N \exp\left[-\frac{U^{\epsilon_{sp}}(\underline{r}^N)}{k_BT}\right]} = -\frac{\partial}{\partial \underline{r}}\omega_\beta^{\epsilon_{sp}}(\underline{r}), \tag{8.3}$$

where $\underline{r} = \underline{r}_1 - \underline{r}_2$ and $\underline{r}^N = \{\underline{r}_1, \underline{r}_2, \underline{r}_3, \ldots, \underline{r}_N\}$. We have assumed that $\omega_\beta^{\epsilon_{sp}}$ depends only on the relative position vector $\underline{r}$. If we further assume isotropy, then $\omega_\beta^{\epsilon_{sp}}$ can be obtained by integrating the force profile (which vanishes for infinite distances), thus obtaining Eq.(8.1).

The solvent quality parameter, ϵ_{sp}, is introduced via interactions of the form

$$U_{sp}^{\epsilon_{sp}}(r) = \begin{cases} 4\,\epsilon_{sp}\left[\left(\left(\frac{\sigma}{r}\right)^{12} - \left(\frac{\sigma}{r}\right)^{6}\right) + 1\right] & r \le 2^{1/6}\sigma \\ 0 & r > 2^{1/6}\sigma, \end{cases} \tag{8.4}$$

where $U_{sp}^{\epsilon_{sp}}(r)$ is the solvent-solute interaction energy when the solvent quality is ϵ_{sp}. The solvent-solvent and solute-solute interactions are assumed to have identical forms as the above but with $\epsilon_{pp} = \epsilon_{ss} = \epsilon = 1$. For a given temperature and small ϵ_{sp} values ($\epsilon_{sp} < 1$), solvent molecules like to surround the solute. This situation will, therefore, correspond to good solvent conditions as it was shown by Grest and co-workers[3] who derived this potential. We have

thus in mind to consider chains made of monomers which are similar to solvent molecules, but with an adjustable parameter ϵ_{sp} which tunes the solvent quality.

Our implicit solvent model is based on our belief that the effective potential on the dimer should have a profile identical to that of any two monomers of the polymer so far as the overall thermodynamic conditions (temperature, pressure and density) are the same. This assumption is somehow limited; the potential profiles of bulk segments should differ slightly from those of the ends. Nonetheless, if the overall segment density increases, this difference vanishes. If an analytical expression for this profile (or its tabular representation) is known, it can be given as a realistic effective potential in a simulation of polymer solutions in which solvent effect is modeled implicitly. This will constitute one way of the second method of calculating the two polymer properties mentioned above.

If the solvent is an athermal one ($\epsilon_{sp} = 1$), the effective potential can be obtained directly from the pair distribution function $g(r)$ of the pure solvent since by definition:

$$g(r) = \exp\left(-\frac{1}{k_B T}\omega_\beta(r)\right). \tag{8.5}$$

Several procedures [9, 11, 12, 13] have been elaborated both theoretically and numerically to calculate the force between two molecules surrounded by a solvent bath. The numerical methods used include thermodynamic perturbation calculations [12], MC and constrained MD [9, 11]. Theoretical methods include solving the Ornstein-Zernike (OZ) equation [9, 14],

$$h(\underline{r}_1, \underline{r}_2) = c(\underline{r}_1, \underline{r}_2) + \rho \int d\underline{r}_3 c(\underline{r}_1, \underline{r}_3) h(\underline{r}_2, \underline{r}_3), \tag{8.6}$$

where $h(\underline{r}_1, \underline{r}_2) = g(\underline{r}_1, \underline{r}_2) - 1$ and $c(\underline{r}_1, \underline{r}_2) = \exp\left[-\beta U_{int}(\underline{r}_1, \underline{r}_2)\right] - 1$ are, respectively, the total and direct pair correlation functions between atom groups 1 and 2. ρ is the density of the system and U_{int} is the interaction energy.

To be able to elucidate the effect of using any ad hoc solvent mediated effective potential, one could calculate the same polymer properties using a simple effective potential of the form:

$$U(r) = 4\epsilon\left[\left(\frac{\sigma}{r}\right)^{12} - \lambda\left(\frac{\sigma}{r}\right)^{6}\right], \tag{8.7}$$

with λ believed to characterise the solvent effect. For $\lambda \to 0$, we expect to recover good solvent behaviours and $\lambda > 1$ should lead to precipitation of the polymer as the effective potential profile will exhibit strong attraction.

8.2 The effective potential on a dimer

Monte Carlo simulations were carried out on a system of 108 atoms at a density of $\rho = 0.80\sigma^{-3}$ and a temperature of $k_B T = 0.72\epsilon$ (here $\epsilon = 1$ corresponds to $119.8k_B$ and $\sigma = 1$ to 3.405 $\dot{A}$) to calculate the force on the dimer. Two atoms (solutes) are constrained in space at a distance of $\xi = 2.5\sigma$ at the centre of a cubic box of sides 5.2σ and 106 other atoms (solvent) are placed at the vertices of the face centred cubic box. The free ones are, then, displaced in constant volume (or pressure) and temperature conditions using the usual Metropolis criteria (see chapter 5).

The forces acting on the atoms of the dimer are calculated and their projections on the dimer bond vector are conserved for statistical averaging.

For various solvent qualities (various ϵ_{sp}), the force profiles on Figure 8.1 were obtained. These profiles, very similar to those obtained from X-ray and neutron scattering experiments on

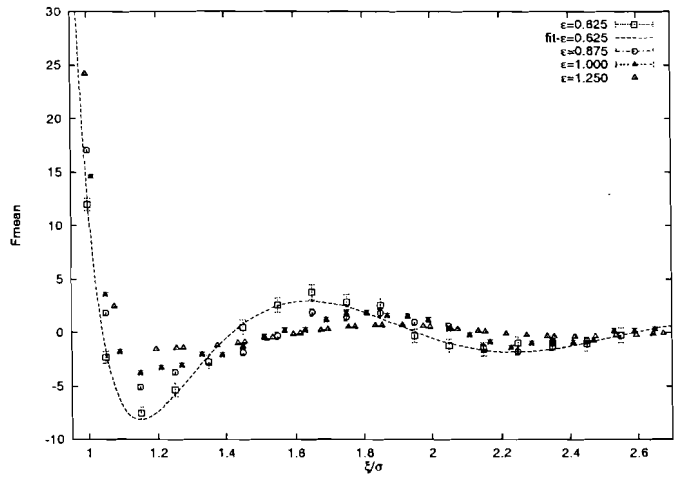

Figure 8.1: Effective forces on two solute molecules versus reduced distance ξ/σ for $k_BT = 0.7\epsilon$, $\rho = 0.8\sigma^{-3}$. Forces are expressed in units of ϵ/σ.

liquids [10], are combinations of the direct force and the solvent mediated term (see Figure 8.2). The latter, responsible for solvent effects, plays a vital role in the miscibility of macro-molecules with some solvents.

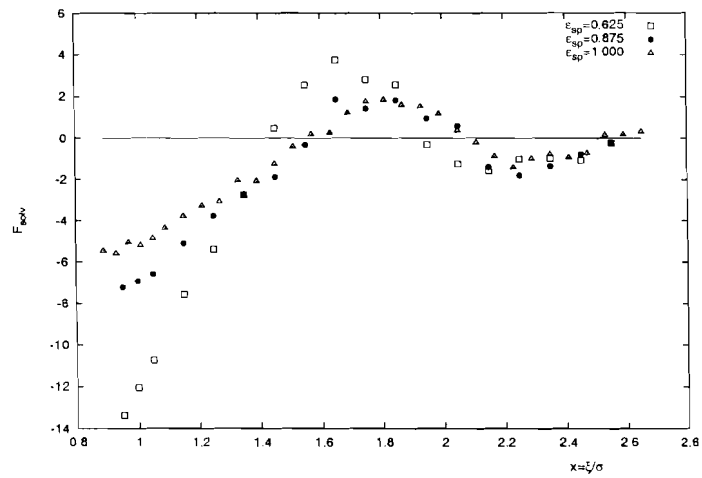

Figure 8.2: Solvent effective forces on two solute molecules versus reduced separation ξ/σ for $k_BT = 0.72\epsilon$, $\rho = 0.8\sigma^{-3}$. Forces are expressed in units of ϵ/σ.

As Figure 8.2 shows, the magnitude of the solvent mediated term grows as the solvent quality increases (decreasing ϵ_{sp}). For weak separations the solvent mediated force may be explained by the Asakura-Oosawa entropic or depletion force theory [9, 15]. On treating the mono-atomic fluid as an ideal gas of $N-2$ micro hard spheres each of radius r, Asakura and

Oosawa [15] considered the entropic force between a pair of macro hard spheres each of radius R immersed in the fluid. The free energy of the system is related to the volume V' available to all microspheres as

$$\mathcal{F}(V') = -Nk_BT \ln V' \quad \text{with} \quad V' = V - \frac{8\pi}{3}(R+r)^3 + v_{ov}(R,r,d) \tag{8.8}$$

since the particles are prohibited from the exclusion spheres of radius $R+r$. v_{ov} is the overlap volume of two exclusion spheres and d is the distance between the centres of the two macrospheres. By calculating the force as $f_{AO} = -\frac{\partial \mathcal{F}}{\partial d} = \frac{Nk_BT}{V'}\frac{\partial v_{ov}}{\partial d}$, they identified $\frac{\partial v_{ov}}{\partial d}$ as the projected area of the intersection of the two exclusion spheres to obtain

$$f_{AO} = -\rho k_BT\pi\left(R+r-\frac{d}{2}\right)\left(R+r+\frac{d}{2}\right) \tag{8.9}$$

for $d \leq 2R+2r$ and zero for larger separations. The effect of decreasing ϵ_{sp} is the increase of the radius $R+r$. This theory predicts a force of $-\rho k_BT\pi(R+r)^2$ at vanishing dimer length which again is consistent with simulation result on condition that $R+r$ increases as ϵ_{sp} diminishes. This last point merely brings out the fact that as ϵ_{sp} decreases there is a net decrease in the repulsion between micro and macrospheres leading to an accumulation of a large number of microspheres (of constant radii) around the macrosphere, thus inducing an attractive tendency between the macrospheres.

For subsequent use in implicit solvent molecular dynamic simulation of polymer solutions, an expression for the effective force was obtained by an ad hoc function fitting of the results of the simulation with the following functional form:

$$f_\beta^{\epsilon_{sp}}(\xi) = A\left(\frac{1}{\xi^{13}} - \frac{0.5}{\xi^7}\right) + \frac{B(\beta,\epsilon_{sp})}{\xi^{C(\beta,\epsilon_{sp})}} J_1(D(\beta,\epsilon_{sp})\,\xi), \tag{8.10}$$

where J_1 is the Bessel function of the first kind. A, B, C and D are medium parameter dependent constants. C, in particular, furnishes informations on the range of the effective potential. The line on Figure 8.1 indicates the ad hoc fit for $\epsilon_{sp} = 0.625$. Numerical integration of the force resulted in the effective potentials on Figure 8.3. This force and potential were tabulated for further use in a realistic implicit solvent molecular dynamic simulation of a polymer solution.

It is important to say a word about parameters intervening in Eq.(8.10) and their thermodynamic implications. Thermodynamic properties of a solution can be easily gathered from the free energy or the osmotic pressure variations. In a dilute solution the osmotic pressure is usually expressed as the Virial expansion

$$\frac{\pi}{k_BT} = \rho + B_2\rho^2 + B_3\rho^3 + \ldots, \tag{8.11}$$

where B_j is the jth Virial coefficient. When $B_2 = B_3 = 0$ the Van Hoff's law governs the thermodynamics of the solution. B_2 is known to be given by the two solute intermolecular effective potential $\omega(r)$ as

$$B_2 = 2\pi\int_0^\infty dr\, r^2\left(1 - \exp\left[-\frac{\omega(r)}{k_BT}\right]\right), \tag{8.12}$$

which converges when $\omega(r)$ decreases faster than r^{-3} (equivalently, when the mean force vanishes faster than r^{-4}). Since the Bessel function is bounded by $r^{-1/2}$ [18], a necessary condition on C for the convergence of B_2 is that it should be greater than 7/2- a condition that was largely satisfied ($C \approx 3.8$). The parameter D translates the oscillatory character of the effective potential. It is intimately related to the number of solvent molecules per unit volume. The density of $0.8\sigma^{-3}$ is high enough to induce the long range correlations depicted here by the weakly damped potential profile of Figure 8.3.

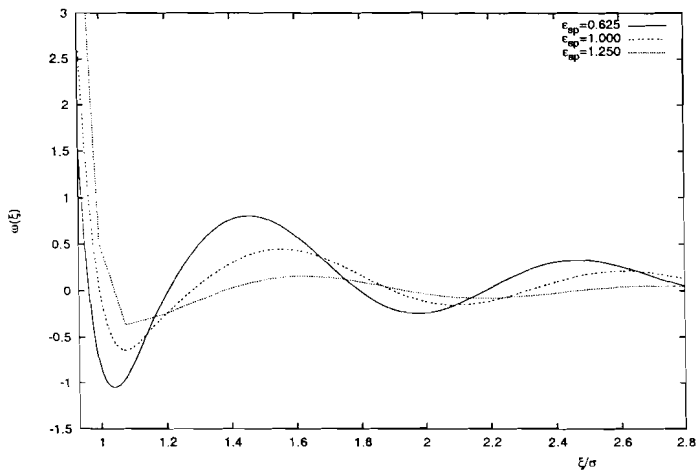

Figure 8.3: The PMF between two solute molecules versus the reduced separation $x = \xi/\sigma$ for $k_BT = 0.72\epsilon$ and $\rho = 0.8\sigma^{-3}$.

Remark that though the interparticle potentials between two isolated particles are usually of short range nature, depending on the thermodynamic state of a system composed of such particles, long range interparticle potentials may result. The present study clearly shows how, using very short range isolated particle potentials, relatively long range effects emerge as a result of high density or other state variable considerartions.

8.3 Solvent effects on the properties of a system of two interacting pentamers

In this section we investigate the effect of the choice of solvent mediated effective potential on polymer intermolecular forces. The effect, on polymer structure, of approaching two polymer molecules in a solvent is also examined by studying the variation of the radius of gyration tensor components.

For the polymer molecules, we assume free rotating bonds and model bond constraints by the anharmonic finitely extensible non elastic (FENE) potential [3],

$$U_{FENE}(r) = \begin{cases} -\frac{k_0}{2} R_0^2 \log\left(1 - \left(\frac{r}{R_0}\right)^2\right) & r \leq R_0 \\ \infty & r > R_0. \end{cases} \tag{8.13}$$

This way of modeling bonding is quite efficient and less time consuming compared to bond constraint (Shake) MD [16], but the price to pay is that the choice of k_0 must be such that a reasonably large time step should be chosen that renders the integration of the equations of motion stable. MD calculations are carried out to determine the 2-pentamer properties mentioned above in two ways.

8.3.1 Explicit solvent consideration

The presence of solvent is considered explicitly as follows: In a constant volume (a cubic box of sides 6.84σ) two pentamers are immersed in a bath of 246 mono-atomic solvent molecules at well defined distance of about 3σ apart. The solvent quality parameter is fixed at $\epsilon_{sp} = 1.0$ and the temperature at $k_BT = 0.72\epsilon$. Initially the solvent molecules are placed on the sites of a face centred cubic lattice. Short MC displacements of the solvent around the polymers are performed to dislodge the former from their unstable lattice sites. A Nose-Hoover [17, 19, 20, 21] equilibration MD run of 10^5 time-steps (with a time-step $\Delta t = 0.01$ in units of $\sigma\sqrt{m/\epsilon}$, where m is the mass of a monomer) is performed followed by a statistics collection MD simulation of 5×10^5 time-steps. The distance between the pentamers is decreased by simply giving the monomers of both polymers displacements until the pentamers' centres are at the required distance apart. MC displacements of the solvent are again performed to avoid instabilities that might have been created by the overlap of monomers with solvent molecules as a result of the polymer displacements. The process is repeated several times until the polymers are close enough. For each distance, the force between the two polymers and the radius of gyration tensor components of one of the polymers are calculated.

If we assume a cylindrical symmetry around an axis passing through the centres of mass of the pentamers, we can define three perpendicular axes (one along the vector joining the two centres and two perpendicular to it). The radius of gyration tensor in a referential system attached to these axes will be diagonal with two equal perpendicular components,

$$\underline{\underline{R_g}} = \begin{pmatrix} R_g^{\perp} & 0 & 0 \\ 0 & R_g^{\perp} & 0 \\ 0 & 0 & R_g^{\parallel} \end{pmatrix}. \tag{8.14}$$

$R_g^{\perp}$ and $R_g^{\parallel}$ are, respectively, the perpendicular and parallel components of the gyration tensor.

Figure 8.4 (filled squares) shows the variation of the inter-molecular force as a function of distance in the models of explicit solvent. Figures 8.5a,b,c show the variation of the radius of gyration tensor components for the same model.

8.3.2 The use of a realistic effective potential

In this method the solvent effect on monomer-monomer interaction is modeled by the special effective potential obtained in the monomer-monomer effective interaction obtained by MC calculation above. The "experiments" described in the last paragraph are repeated with the "dry" polymers and the same properties calculated above are again explored as shown on Figures 8.4 (open circles) and 8.5d,e,f. Qualitatively, the results reproduce very well those of the first method for the same thermodynamic conditions.

A close look at the intermolecular force profile reveals a finite non zero intermolecular force between the two pentamers at interpenetration. This big difference between the macromolecular intermolecular force and that of the mono-atomic system (Figure 8.1) can only be explained by the fact that there exist many polymer configurations for which the centres of mass of the two polymers coincide without segment overlaps.

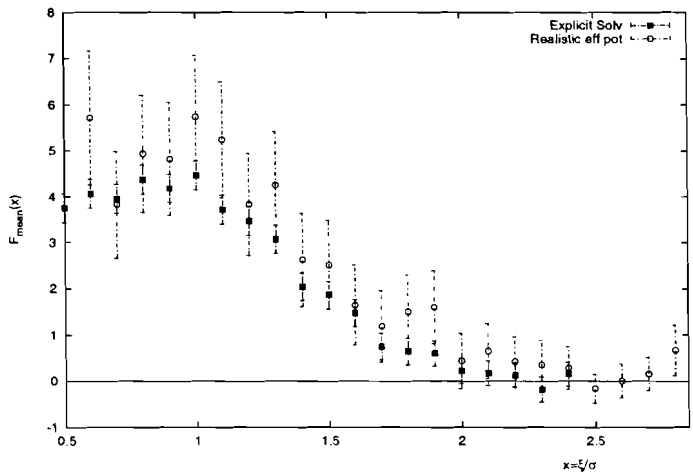

Figure 8.4: The intermolecular force between two pentamers versus centres of mass separation for $k_BT = 0.72\epsilon$ and $\rho = 0.8\sigma^{-3}$: filled squares - explicit solvent calculations and open circles - the use (in implicit solvent implementation) of the effective potential obtained by MC calculations.

We observe that the polymer structure depends on the relative separation between both polymer. When polymers are very far apart they assume spherical shapes (the components of the radius of gyration tensor become equal), but at intermediate distances ($\xi \leq 2\sigma$) they have distorted geometry, aligning themselves parallel to each other. We can assimilate polymer approach in a solvent to an increase of monomer concentration in a region of space.

The force profile shows that the interaction is repulsive when the pentamers are at intermediate and small separations. The magnitude of this force is seen to decrease when they completely inter-penetrate each other. This starts happening at separations $r \leq R_g$, with R_g being the radius of gyration of the free molecule.

In the next section we propose a theoretical explanation of the simulated effective force profile.

8.4 The smoothed density theory of intermolecular forces

Approximate theories for macromolecular intermolecular potentials based on the smoothed density model [6, 22, 23, 24, 25] exist that may be used to interpret, at least qualitatively, the shape of the intermolecular forces between macromolecules. This model is based on the idea that the intermolecular potential is related to the distribution of the segments of each polymer

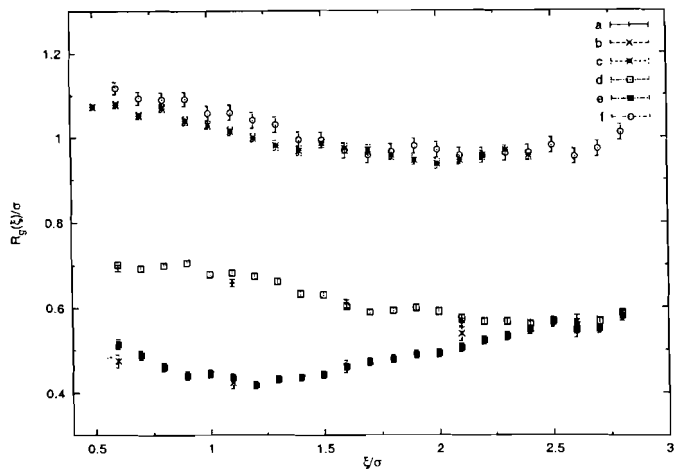

Figure 8.5: The radius of gyration tensor components as functions of centres of mass separation. Explicit solvent consideration: parallel component (a), perpendicular component (b) and the total R_g (c); implicit solvent implemented using the effective potential of Eq.(8.10): parallel component (d), perpendicular component (e) and the total R_g (f).

around their respective centres of mass through [22]

$$\frac{\omega_2(\underline{r})}{k_BT} = \alpha \sum_{i_1,i_2} \int P_{0i_1}(\underline{s}_{i_1}) P_{0i_2}(\underline{s}_{i_1} - \underline{r})\, d\underline{s}_{i_1}, \tag{8.15}$$

where $P_{0i_1}(\underline{s}_{i_1})$ is the probability that if the centre of mass of polymer 1 is at the origin of a referential system then the monomer i_1 is at $\underline{s}_{i_1}$. α is the binary cluster integral [6, 22] defined via the pair correlation function $g(\underline{r}_{ij})$ as

$$\alpha = \int d\underline{r}_{ij} \left(1 - g(\underline{r}_{ij})\right). \tag{8.16}$$

The derivation of Eq.(8.15) can be summarised as follows. Zimm [26] and Albrecht [27], using the Mc Millan-Mayer dilute solutions theory [23], formulated that the second Virial coefficient of a molecular solution can be written as

$$B_2^\star = -\frac{N}{2VM^2} \int\int d(1,2) \left[F_2(1,2) - F_1^0(1)F_1^0(2)\right], \tag{8.17}$$

where F_2 and F_1^0 are, respectively, the two solutes distribution function and the unperturbed one solute distribution function. (j) represents the internal and external degrees of freedom of solute j. N and M are, respectively, the number of units and the molecular mass of each solute molecule, and V is the volume of the solution. The two solute distribution function is related to the unperturbed single solute one through the two solute potential of mean force $\omega(\underline{r}_{i_1}, \underline{r}_{i_2})$ ($\underline{r}_{i_j}$ is the position vector of the i_jth mass unit of molecule j) as

$$F_2(1,2) = F_1^0(1)F_1^0(2) \exp\left(-\frac{1}{k_BT} \sum_{i_1,i_2} \omega(\underline{r}_{i_1}, \underline{r}_{i_2})\right). \tag{8.18}$$

On defining short range interaction matrix elements $\chi_{i_1,i_2} = -\alpha\delta(\underline{r}_{i_1,i_2})$ (which are non zero only at contact of segment i_1 and i_2) through $\exp\left[-\frac{1}{k_BT}\sum_{i_1,i_2}\omega(\underline{r}_{i_1},\underline{r}_{i_2})\right] = \prod_{i_1,i_2}(1+\chi_{i_1,i_2})$, $B_2^\star$ can be rewritten as

$$B_2^\star = -\frac{N}{2VM^2}\int\int d(1,2)F_1^0(1)F_1^0(2)\Big[\sum_{i_1,i_2}\chi_{i_1,i_2} + \sum_{i_1,i_2}\sum_{j_1,j_2}\chi_{j_1,j_2} + \ldots + \sum_{i_1,i_2}\sum_{j_1,j_2}\cdots\sum_{s_1,s_2}\chi_{i_1,i_2}\chi_{j_1,j_2}\cdots\chi_{s_1,s_2}\Big], \tag{8.19}$$

which for molecules with $N+1$ units contains $(N+1)^2$ terms grouped as sums of multiple contact points groups. The first group in the above equation, for example, is a one contact point group, the second a two contact points and so on. Each σ-contact group contains $[(N+1)^2]!\Big/([(N+1)^2-\sigma]!\sigma!)$ terms which can be approximated (for large N) as $N^{2\sigma}/\sigma!$. Remarking that $d(1,2)$ represents a volume element containing both internal and external degrees of freedom of all the units of molecules 1 and 2, we can define a distribution of internal degrees of freedom $\underline{s}_{i_1}$, $\underline{s}_{j_1}$, etc. of the unperturbed molecule 1 (with $\underline{s}_{i_1}$ being the displacement of unit i_1 from the centre of mass of molecule 1) as

$$P_0(\underline{s}_{i_1},\underline{s}_{j_1},\ldots) = \int F_1^0(1)d(1)_{int|_{d\underline{s}_{i_1},d\underline{s}_{j_1},\ldots}}, \tag{8.20}$$

where $|_{d\underline{s}_{i_1},d\underline{s}_{j_1},\ldots}$ indicates that integration is only on all external degrees of freedom associated with each unit of molecule 1. We assume that $P_0(\underline{s}_{i_1},\underline{s}_{j_1},\ldots)$ factorises into the product of the distributions of the individual units $\mathcal{P}_{0i_1}(\underline{s}_{i_1})$ around the centre of mass. Considering all these points and assuming that the centre of mass of molecule 1 is at the origin of the coordinate system and that of molecule 2 at $\underline{r}$, taking note of the correct restrictions on the summations, the equation for $B_2^\star$ boils down to

$$B_2^\star = \frac{N}{2VM^2}\int d\underline{r}\Big\{\frac{\alpha}{1!}\sum_{i_1,i_2}\int\mathcal{P}_{0i_1}(\underline{s}_{i_1})\mathcal{P}_{0i_2}(\underline{s}_{i_1}-\underline{r})d\underline{s}_{i_1} - \frac{\alpha^2}{2!}\Big[\sum_{i_1,i_2}\int\mathcal{P}_{0i_1}(\underline{s}_{i_1})\mathcal{P}_{0i_2}(\underline{s}_{i_1}-\underline{r})d\underline{s}_{i_1}\Big]^2 + \frac{\alpha^3}{3!}\Big[\sum_{i_1,i_2}\int\mathcal{P}_{0i_1}(\underline{s}_{i_1})\mathcal{P}_{0i_2}(\underline{s}_{i_1}-\underline{r})d\underline{s}_{i_1}\Big]^3 + \ldots\Big\} \tag{8.21}$$

which resembles very much the equation

$$B_2^\star = \frac{N}{2VM^2}\int d\underline{r}\left[1-\exp\left(-\frac{\omega_2(\underline{r})}{k_BT}\right)\right], \tag{8.22}$$

on condition that $\omega_2(\underline{r})/k_BT$ is given exactly as in Eq.(8.15). Though Eq.(8.15) is derived after gross approximations, it may be used as a first approximation for a qualitative study of macromolecular intermolecular intermolecular forces.

We now proceed to examine the effective potential profiles for two models of polymer segment distributions.

8.4.1 The Flory inter-penetrating uniform sphere theory

This theory, based on the probability distribution

$$P_0(r) = \begin{cases} \frac{3N}{4\pi R_F^3} & r \leq R_F \\ 0 & r > R_F, \end{cases} \tag{8.23}$$

(where R_F is the radius of the Flory uniform sphere and N is the number of monomers in the polymer) predicts that the intermolecular potential (proportional to the overlap volume of the two spheres) has the form:

$$\frac{\omega_2(r)}{k_BT} = \begin{cases} \frac{3\alpha_F N^2}{64R_F^6}(16R_F^3 - 12R_F^2 r + r^3) & r \leq 2R_F \\ 0 & r > 2R_F, \end{cases} \tag{8.24}$$

where α_F is the Flory excluded volume parameter defined through the cluster integral. Figure 8.6 compares the Flory prediction to our MD results. Within error bars there is agreement for $\xi > 2R_g \sim 2.0\sigma$ but theory fails to recover the small ξ range. The deviation from simulation results may be partly due to the size of the polymer - a 5 segment polymer is quite short to assume a spherical shape as required by the Flory theory. The discrepancy may be inherent of the theory which assumes that all the monomers are uniformly dispersed in a sphere.

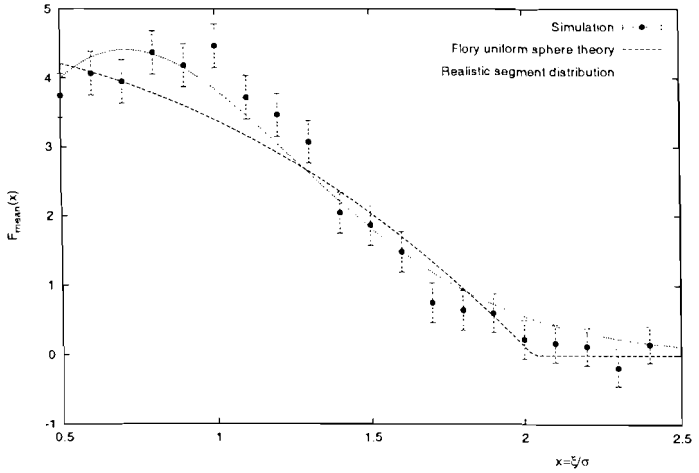

Figure 8.6: The effective polymer intermolecular force versus chains separations ξ (in σ): the explicit solvent simulation results on 5 C chains (points), the Flory uniform sphere theory (dashed line) and realistic segment distribution (tiny dashed line). The force units are k_BT/σ.

A realistic segment distribution implementation should be capable of lifting the above shortcomings. When we consider segment distribution of the form

$$P_{0i}(\underline{s}_i) = \left(\frac{3}{2\pi < s_i^2 >}\right)^{3/2} \exp\left[\frac{-3s_i^2}{2 < s_i^2 >}\right], \tag{8.25}$$

with $< s_i^2 >= \frac{R_N^2}{3}\left(1 - \frac{3i}{N^2}(N-i)\right)$ on equation (8.15), we obtain (see appendix D)

$$\frac{\omega_2(r)}{k_B T} = \frac{3\alpha N^2}{2R_N^2}\frac{1}{r}\left[\mathrm{erf}\left(\frac{3r}{R_N}\right) - \mathrm{erf}\left(\frac{3r}{R_N}\sqrt{\frac{2}{5}}\right)\right], \tag{8.26}$$

where R_N is the root mean square end-to-end distance of a free polymer and erf denotes the Error function defined as

$$\mathrm{erf}(x) = \frac{1}{\sqrt{\pi}}\int_0^x dy e^{-y^2}. \tag{8.27}$$

When we used the calculated root-mean-square end-to-end-distance into this formula we obtained a good agreement with the simulation result for $\alpha \sim 0.7\sigma^{-3}$ as Figure 8.6 shows.

Remark that the Flory result (Eq.(8.24)) reveals that $\frac{\omega_2(0)}{k_B T} \propto \frac{N^2}{R_F^3}$ while the prediction of the realistic segment distribution of Eq.(8.25) (given in Eq. (8.26)) shows that $\frac{\omega_2(0)}{k_B T} \propto \frac{N^2}{R_N^3}$. If the Flory radius is proportional to the polymer size (R_N), then both theories independently yield that $\omega_2(0)$ scales with N as $\omega_2(0) \sim N^{(2-3\nu)}$, where ν is the Flory excluded volume exponent ($\nu < 0.5$ for poor solvent conditions, $\nu = 0.5$ for Θ-solvents and $\nu = 3/5$ for good solvents). Thus, $\omega_2(0)$ will be an increasing function of N for all solvent conditions, which contradicts the findings of Vassilis et al. [1], who, using computer simulations, found that $\omega_2(0)$ decreases with increasing chain size. A possible reason for the descripancy between the present theoretical exploration and computer simulation results may be explained by the fact that the cluster integral parameter α (which gathers most of the solvent effects) is assumed to be independent of chain size especially at chains interpenetration - segments in a polymer matrix of large polymers may interact differently from those of short ones. In other words, the segment pair correlations function (by which α is defined) should be dependent upon chain sizes. For the effective potential to decrease with chain size α (which we note as α_N) should decrease faster than $N^{-(2-3\nu)}$. If we assume that α_N is proportional to monomer density it may scale as $N^{-(3\nu-1)}$, at least for low densities (since monomer density $\rho \approx \frac{N}{R_0^3} \sim N^{-(3\nu-1)}$) which decreases faster than $N^{-(2-3\nu)}$ for Θ and good solvent conditions (i.e. $\nu \geq 0.5$).

From the probabilistic definition of the potential of mean force (PMF) of Eq.(8.15) it is seen that the sign of the PMF is independent of the polymer separation (since this parity is given by that of the excluded volume parameter α) though it is known that at weak separations it is repulsive while at large separations, attractive behaviours may be observed.

We have investigated the effect of using any effective potential on two properties of interacting pentameres in a solvent. It is clear that the properties of polymer solutions depend strongly on the detailed nature of the the effective solvent interactions on the monomers especially under particular thermodynamic conditions. Care must therefore be taken during the choice of solvent mediated polymer segment effective potential. This point is very crucial when simulating polymer properties that are intermolecular force sensitive such as polymer stability in a solution.

Bibliography

[1] V. I. Harismiadis and I. Szleifer, *Mol. Phys.* **81**(4): 851, 1994

[2] A. Byrne, P. Kierman, D. Green and K. Davson, *J. Chem. Phys.* **102** (1): 573, 1995

[3] G. S. Grest, M. Lacasse, K. Kremer and A. M. Gupta, *J. chem. Phys.* **105** (23): 10583, 1996

[4] L. Lue and J. M. Pransnitz, *Macromolecules*, **30**: 6650, 1997

[5] M. Destrée and A. Lyulin and J.-P. Ryckaert, *Macromolecules* **29**: 1721, 1996

[6] T. L. Hill, *An introduction to Statistical Thermodynamics*, Addison-Weysley, 1960

[7] D. van Belle and S. J. Wodak, *J. Am. Chem. Soc.* **115**(47): 647, 1993

[8] M. Pellegrini and S. Doniach, *J. Chem. Phys.* **103**(7): 15, 1995

[9] R. Dickman, P. Attard and V. Simonian, *J. Chem. Phys.* **107** (1): 205, 1997

[10] J. N. Israelachvili, *Intermolecular and surface forces*, Academic Press Inc., 1991

[11] E. Paci, G. Ciccotti, M. Ferrario and R. Kapral, *Chem. Phys. Lett.* **176**(6): 581, 1991

[12] D. J. Tobias and C. L BrooksII, *Chem. Phys.Lett.*, **142**(6): 472, 1987

[13] P. Attard, *J. Chem. Phys.* **91**(5): 3083, 1989

[14] J. Ram, C. S. Ram, S. Yashwant, *Phys. Rev. E* **49**(6): 5117, 1994

[15] A. Assakura and F. Oosawa, *J. Polym. Sci.* **33**: 183, 1958

[16] G. Ciccotti and J.-P. Ryckaert, *Comput. Phys. Rep.* **4**: 345, 1986

[17] S. Nosé, *J. Chem. Phys.* **81**: 511, 1984.

[18] E. A. Hylleraas, *Mathematical and Theoretical Physics, Vol. 1, John Wiley & Sons*, 1969

[19] W. G. Hoover, *Phys. Rev. A* **81**: 1695, 1985.

[20] S. Nosé, *Mol. Phys.* **52** 255, 1984

[21] C. Pierleoni and J.-P. Ryckaert, *Comput. Phys. Rep.*, **4**: 345, 1986

[22] H. Yamakawa, *Modern theory of Polymer solutions*, Harper and Row, 1986

[23] W. G. Mc Millan and J. E. Mayer, *J. Chem. Phys.* **13**: 276, 1945

[24] P. J. Flory, *J. Chem. Phys.* **13**: 453, 1945

[25] P. J. Flory and W. R. Krigbaum, *J. Chem. Phys.* **18**: 1086, 1950

[26] B. H. Zimm, *J. Chem. Phys.* **13**: 453, 1945

[27] A. C. Albrecht, *J. Chem. Phys.* **27**: 1002, 1957

Conclusions and Perspectives of Part II

We have described the two computer simulation methods that are widely used for the calculation of static and dynamic properties of condensed media. Though quantum aspects usually encountered in molecular systems have not been considered here, the results of these classical computations have led to satisfactory conclusions.

The variant of the Configurational Biased Monte-Carlo (CBMC) method developed by us has enabled us to probe into some, up-to-now, unanswered or even unposed questions. The elasticity and its related properties of two model polymers (one physical and the other chemical) have been examined using the elaborated CBMC. The following points have been addressed:

1. The stress and strain elasticity ensembles:

   The distinction between fixed force and fixed end-to-end vector single chain ensembles was pointed out in chapter 6 in connection with the single polymer elasticity law at or above theta temperature. Actually, our approach has been more general: we have given some general tools to appreciate, for any type of observable O, the distinction between averages computed in the two stretched chain conjugated ensembles. We found that the correction term Δ_O takes the form of an infinite series, the nth term being the product of an average nth order fluctuation term in the fixed f ensemble and a nth order gradient respect to the end-to-end vector components which is computed at the average end-to-end vector value $< \mathbf{R} >_f$. This series always converges for gaussian chains (because of the fluctuation term only) while, for chains in good solvent represented by the RGT theory, it converges only in the high stretching regime.

   The elasticity law in the stress ensemble (fixed-f ensemble) $R_f = g(f)$ plays a central role in chapter 6. When convergence in the Δf expansion is sufficiently fast, this ensemble difference in the force can be estimated using the leading term $\Delta f^{(2)}$ given by Eq. (6.43). In this expression, fluctuations terms can be evaluated from $R_f = g(f)$ using Eqs. (6.13) and (6.14) while the gradient terms requiring the fixed-R elasticity law $f_R = h(R)$ can be approximated by $f = g^{-1}(R)$.

   In this way, we could establish the following main results. Quite generally, ideal chains lead to similar linear elasticity laws up to the FE regime where marginal differences $\propto \frac{1}{N}$, already discussed by Flory [1], are detected.

   Much stronger effects are noticed for chains in good solvent, with largest deviations between ensembles when the (average) end-to- end distance lies below R_0, the unstretched average value. This situation is however little experimentally relevant because confinement effects should be added to the description. For polymers in good solvent, stretched

over distances equal to or larger than R_0, one finds a relative difference on the force between ensembles which decreases from 25% down to 2% as the distance grows from R_0 to $3R_0$.

Stress-strain single chain laws are actually being probed by new experimental set-ups allowing micro-manipulations which either control the end-to-end vector or the stretching force. The experimental situation somewhat differs from the idealised ensemble description of textbooks which is adopted in the chapter 6. Elasticity measurements are often done dynamically at finite velocity, corrections must take into account the finite compliance of the micro-lever handling the polymer end when measuring the force, confinement effects may play a role. However, our analysis remains largely relevant and could further be modified to take some of the above effects into account.

To our knowledge, a direct experimental test of the single EV chain elasticity law in the Pincus blob regime remains to be done. What the present work suggests is that experimentalists might probe into this stretching regime different variants of the elasticity law depending upon the constraints introduced by specific set-ups ranging from fixed-f to fixed-R conditions. About the much studied biological macromolecules where specific intra-molecular forces resist to the stretching forces applied at chain ends, ensemble effects depending on the nature of the applied constraint should be considered in the molecular interpretation of elasticity data.

We note finally that the existence of specific EV single chain elasticity laws for different single stretched chain ensembles may have interesting implications for the elastic behaviour of swollen networks where the nature of the junction constraints is at the heart of network elasticity theories.

2. The force-extension relationship:

   In chapter 7 the three elastic regimes - linear, tensile blob and the finite extensibility regimes have been investigated. The various elastic laws in the different regimes have been expounded. We have not succeeded to map polyethylene (PE) at Θ point to an equivalent ideal chain model (especially the freely jointed chain model with zero stretch modulus) that incorporates finite extensibility aspects; but when we associate it to a freely jointed chain characterised by a stretch modulus (S) so that its force-extension relationship reads [2]

$$\frac{\langle R\rangle_f}{L_c} = \mathcal{L}(\eta_\ell)\left(1+\frac{f}{S}\right), \qquad \text{(CII.1)}$$

   we obtain good agreement with $S = (217.5 \pm 17.8)\,\frac{k_BT}{\ell}$ in the strong stretching regime. This aspect is accompanied by an increase of the chain rigidity demonstrated by the passage from a Kuhn length of $b = 14.9$Å to the characteristic length $b' = (19.1 \pm 0.3)$Å (see Figure C1).

   When the elasticity law is expressed in terms of the global reduced force $\eta_g = \beta f R_0$, then below a force value of $f^{\star\star} \equiv \frac{k_BT}{b}$, all $\langle R\rangle_f / R_0$ (for all chain sizes) curves lie on a unique one $\Phi(\eta_g)$, but beyond $f^{\star\star}$ the relevant reduced force becomes $\eta_l = \beta f b$ and all $\langle R\rangle_f / L_c$ (for all chain sizes) curves lie on a unique one $z(\eta_l)$. For Θ solvent conditions $\Phi(\eta_g)$ is the

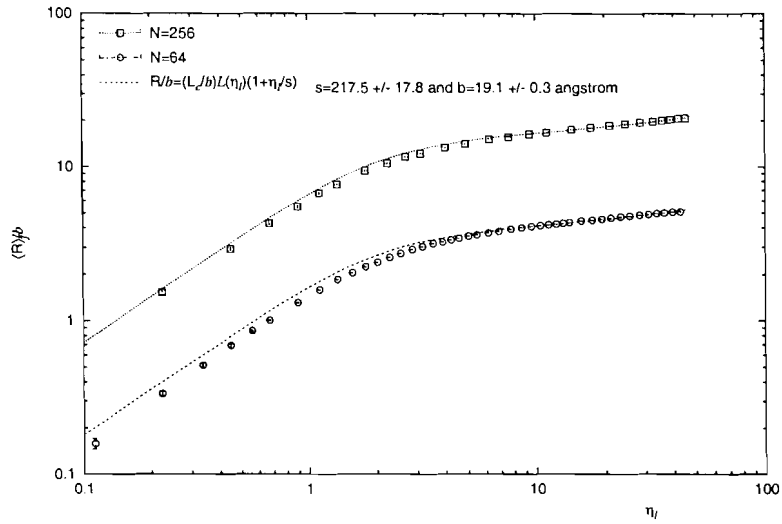

Figure C1: $\frac{\langle R\rangle f}{b}$ are shown as functions of the reduced force $\eta_\ell = \beta f R_0$ for 64 and 256 segments polyethylene in Θ solvent. The lines (——) represent the prediction of Eq.(CII.1).

linear law $\Phi(\eta_g) = \frac{1}{3}\eta_g$ while for good solvent conditions it starts as the linear law but switches continuously to the scaling function $\Phi(\eta_g) = 0.46\eta_g^{\frac{1}{\nu}-1}$.

For both polymer models $z(\eta_l)$ is neither the Langevin function nor the Ha and Thirumalai semi-flexible chain force-extension formula.

3. The internal molecular conformations and stretching:

   In good solvent conditions and for every force value, there is a relatively larger proportion of bond vectors in a trans conformation than in Θ solvent. This conformation mutation is found to be linked to the energy related elasticity.

4. The relative strength of the entropy/energy related elasticity:

   Our results confirm that while the elasticity of weakly stretched PE in Θ solvent is entropy driven, both entropy and enthalpy aspects coexist in competing proportions for the same polymer in good solvent conditions.

5. Polymer stretching or network swelling effects on NMR dipolar interaction:

   The effect of the stretched nature of a single polymer or the swollen nature of a polymer network on the nuclear magnetic resonance dipole-dipole interaction ($\langle P_2(\cos\alpha_{kk'})\rangle$) responsible for spectral line broadening and the splitting of resonance doublets [3] has been explored. Some new aspects that have hardly ever received any theoretical or experimental attention have been put to light. We have confirmed that for weakly stretched PE P_2 follows the usual $\langle R\rangle^2$ law but we have also found that for a strongly stretched chain in good solvent P_2 switches to the power law $P_2 \sim \langle R\rangle^{2.6}$, which is in conformity with the $P_2 \sim f^{1.5\pm0.1}$ scaling law in force. This is a crucial result, which to our knowledge, has never been pointed out.

   This study suggests that it is worth verifying experimentally this finding. This could be possible on polymer networks possessing magnetically active isotopes like ^{31}P, ^{13}C, ^{1}H,

etc.

6. The effect of stretching and solvent quality on the structure factor of PE:

   The static structure factor of a stretched PE is qualitatively similar to that of most widely described linear chain models in the region of small and intermediate scattering angles. But within the chemically sensitive length scale (of the order of the Kuhn segment length b), corresponding to scattering vector $q > q^{**} \equiv b^{-1}$, $S_q(f)$ does not converge to to a unique curve as those of the widely used physical models [4] that do not incorporate some chemical features like bond angle constraint and restricted torsional motions.

   Inspired by the similarity between the free energy $G_{ij}(f)$ of a stretched polymer strand and the structure factor of a stretched or unstretched chain (through a definition of a complex force $\tilde{\underline{f}} \equiv \underline{f} + ik_BT\underline{q}$), we have been able to exploit the already extended knowledge of of the dependence of $G_{ij}(f)$ on f and $|i-j|$ to derive new expressions for the structure factor of stretched chains. This expression which explain well our numerical results on PE, easily recover the Debye formula and the Pincus scaling prediction. A new expression

$$S(q) = \frac{2}{N\left[\ln\left|\frac{\sin(qb)}{qb}\right|\right]^2}\left\{\left(\frac{\sin(qb)}{qb}\right)^N - 1 - N\ln\left|\frac{\sin(qb)}{qb}\right|\right\}, \qquad \text{(CII.2)}$$

   corresponding to freely jointed chain molecules, has been derived which is found to explain well the calculated structure factor for small and intermediate scattering angles and extra large q that are farther from $\frac{\pi k}{b}$ (where k is an integer).

   The PE results presented in this thesis assume frozen C-C bond length and C-C-C bending angle. These two aspects play vital rules in chain flexibility, conformation distributions and most likely magnetic properties. It could be interesting to lift these restrictions and probe into their effects on the elasticity related properties.

7. Realistic effective potentials used on polymer solutions:

   In chapter 8 a Monte-Carlo (MC) program has been set up to calculate the intermolecular forces between two atomic solute molecules in an atomic solvent. On using a simple short range repulsive potential between solvent molecules, the usual force profile for dense liquids, showing a long range tail, has been obtained. An ad hoc function best-fitting the f-r profile has been used as a realistic solvent mediated potential on monomers of a polymer solution.

   Two interacting pentamer properties - the macromolecular intermolecular forces and the radius of gyration tensor components are calculated using two methods of solvent consideration:

   - in explicit solvent conditions and
   - in implicit solvent condition using a monomer-monomer effective potential derived from a previous MC study.

   Both methods yield very similar results. But suppose that instead of using the realistic potential between monomers we had used the simple repulsive interaction assumed

between the solvent molecules in the MC calculation, under what condition should the results compare well with those of the explicit solvent consideration?

The smoothed density theory has been found to explain qualitatively well the calculated intermolecular forces on condition that a physically acceptable monomer distribution be used in the theory.

Bibliography

[1] P. J. Flory, *Statistical Mechanics of Chain Molecules*

[2] S. B. Smith, Y. Cui, and C. Bustamante, *Science* **271**: 795 1996

[3] J.-P. Cohen-Addad, *Physics of Finely Divided Matter*, Boccara and Daoud Ed., Springer-Verlag, 1985

[4] C. Pierleoni and G. Arialdi and J.-P. Ryckaert, *J. Chem. Phys. Lett* **79**: 2990, 1997

Appendix C

C.1 Proof of $(\partial f/\partial T)_r = -(\partial r/\partial T)_f/(\partial r/\partial f)_T$

We can write that $r = r(f, T)$ with f intimately linked to T. This means that

$$dr = \left(\frac{\partial r}{\partial T}\right) dT + \left(\frac{\partial r}{\partial f}\right) df. \tag{C.1}$$

Then using $f = f(T)$ with r fixed, we have

$$dr = \left[\left(\frac{\partial r}{\partial T}\right)_f + \left(\frac{\partial r}{\partial f}\right)_T \left(\frac{\partial f}{\partial T}\right)_r\right] dT \tag{C.2}$$

The condition of fixed r ($dr = 0$) leads to the required equation.

C.2 Proof of the f^2 law for $\langle P_2(\alpha)\rangle_f$

$\underline{\Omega}_{kk'}$ can be decomposed into a sum of three rotations

$$\underline{\Omega}_{kk'} = (\theta, \phi, \psi) \oplus (\theta_k, \phi_k, \psi_k) \oplus (\theta_{kk'}, \phi_{kk'}, \psi_{kk'}) \tag{C.3}$$

$\mathcal{D}_l^{mn}(\underline{\Omega}_{kk'})$ transforms as

$$\begin{aligned} \mathcal{D}_l^{mn}(\underline{\Omega}_{kk'}) &= \frac{1}{c_l} \sum_t \mathcal{D}_l^{mt}(\theta, \phi, \psi) \mathcal{D}_l^{tn}[(\theta_k, \phi_k, \psi_k) \oplus (\theta_{kk'}, \phi_{kk'}, \psi_{kk'})] \\ &= \frac{1}{c_l^2} \sum_{t,s} \mathcal{D}_l^{mt}(\theta, \phi, \psi) \mathcal{D}_l^{ts}(\theta_k, \phi_k, \psi_k) \mathcal{D}_l^{sn}(\theta_{kk'}, \phi_{kk'}, \psi_{kk'}). \end{aligned} \tag{C.4}$$

During the evaluations of orientational observables, averaging will involve only bond orientations so that

$$\begin{aligned} \langle \mathcal{D}_l^{mn} \rangle_f &= \frac{1}{c_l} \sum_t \mathcal{D}_l^{mt}(\theta, \phi, \psi) \left\langle \mathcal{D}_l^{tn}[(\theta_k, \phi_k, \psi_k) \oplus (\theta_{kk'}, \phi_{kk'}, \psi_{kk'})] \right\rangle_f \\ &= \frac{1}{c_l^2} \sum_{t,s} \mathcal{D}_l^{mt}(\theta, \phi, \psi) \left\langle \mathcal{D}_l^{ts}(\theta_k, \phi_k, \psi_k) \right\rangle_f \mathcal{D}_l^{sn}(\theta_{kk'}, \phi_{kk'}, \psi_{kk'}), \end{aligned} \tag{C.5}$$

where $c_l = \left(\frac{2l+1}{4\pi}\right)^{1/2}$. Let us calculate the average under a weak stretching force of an orientational observable $\mathcal{A}_k$ associated with the segment k.

$$\langle \mathcal{A}_k \rangle_f = \frac{1}{Z_f} \int d\underline{\Omega}^N W_0(\underline{\Omega}^N) \exp\left(\beta \underline{f} \cdot \sum_l \underline{b}_l\right) \mathcal{A}_k, \tag{C.6}$$

where $\underline{b}_l$ is the bond vector of skeletal bond l (with bond length b), $W_0(\underline{\Omega}^N)$ the unperturbed bond vectors distribution and

$$Z_f = \int d\underline{\Omega}^N W_0(\underline{\Omega}^N) \exp\left(\beta \underline{f} \cdot \sum_l \underline{b}_l\right). \tag{C.7}$$

The Taylor expansion of the exponential term leads to

$$\langle \mathcal{A}_k \rangle_f = \langle \mathcal{A}_k \rangle_0 + \beta \underline{f} \cdot \sum_i \langle \mathcal{A}_k \underline{b}_i \rangle_0 + \frac{1}{2}\beta^2 \underline{f}\,\underline{f} : \sum_{ij} \left\langle \mathcal{A}_k \underline{b}_i\, \underline{b}_j \right\rangle_0 + \ldots. \tag{C.8}$$

For the quantity that interests us the first two terms vanish because of isotropy. Then we have for a uni-axial force:

$$\langle \mathcal{A}_k \rangle_f \approx \frac{1}{2}\beta^2 f^2 b^2 \sum_{ij} \langle \mathcal{A}_k \cos\theta_i \cos\theta_j \rangle_0 . \tag{C.9}$$

Concretely,

$$\langle \mathcal{D}_l^{mn} \rangle_f \approx \frac{\beta^2 f^2 b^2}{2c_l^2} \sum_{ts} \mathcal{D}_l^{mt}(\theta, \phi, \psi) \mathcal{D}_l^{sn}(\theta_{kk'}, \phi_{kk'}, \psi_{kk'}) \sum_{ij} \left\langle \mathcal{D}_l^{ts}(\theta_k, \phi_k, \psi_k) \cos\theta_i \cos\theta_j \right\rangle_0 . \tag{C.10}$$

It can be shown that due to isotropy

$$\left\langle \mathcal{D}_l^{ts}(\theta_k, \phi_k, \psi_k) \cos\theta_i \cos\theta_j \right\rangle_0 = \delta_{t0}\delta_{s0} \left\langle \mathcal{D}_l^{00}(\theta_k, \phi_k, \psi_k) \cos\theta_i \cos\theta_j \right\rangle_0 . \tag{C.11}$$

Knowing that $\mathcal{D}_l^{00}(\alpha_{kk'}, \phi_{kk'}, \psi_{kk'}) = c_l P_l(\cos\alpha_{kk'})$, (where $P_l(x)$ is the Legendre polynomial of order l) we then easily obtain

$$\langle P_2(\cos\alpha_{kk'}) \rangle_f = \frac{1}{2}\left(\frac{fb}{k_B T}\right)^2 P_2(\cos\theta) P_2(\cos\theta_{kk'}) \sum_{i=1}^{N}\sum_{j=1}^{N} \langle P_2(\cos\theta_k) \cos\theta_i \cos\theta_j \rangle_0 . \tag{C.12}$$

By defining Λ appropriately, we recover the required equation.

Appendix D

D.1 The smoothed density theory on realistic segment distribution

On using Eq.(8.25) in Eq.(8.15) we obtain

$$\frac{\omega_2(r)}{k_BT} = \alpha \sum_{i=1}^{N}\sum_{j=1}^{N} \left[\frac{3}{2\pi\left(\langle \underline{s}_i^2\rangle + \langle \underline{s}_j^2\rangle\right)}\right]^{3/2} \exp\left\{-\frac{3r^2}{2\left(\langle \underline{s}_i^2\rangle + \langle \underline{s}_j^2\rangle\right)}\right\} \tag{D.1}$$

The use of the expression of $\langle \underline{s}_i^2\rangle$ and approximating the above discrete sums by continuous ones on condition of large N while performing the variable changes $i \to xN$ and $j \to yN$ we get

$$\begin{aligned}\frac{\omega_2(r)}{k_BT} \approx\ & \alpha N^2 \left(\frac{9}{2\pi R_N^2}\right)^{3/2} \int_{x=0}^{1} dx \int_{y=0}^{1} dy \left[\frac{1}{3x^2-3x+3y^2-3y+2}\right]^{3/2} \\ & \times \exp\left(-\frac{9r^2/2R_N^2}{3x^2-3x+3y^2-3y+2}\right).\end{aligned} \tag{D.2}$$

Further changes of variables $x - \frac{1}{2} = \rho\cos\phi$ and $y - \frac{1}{2} = \rho\sin\phi$ lead to

$$\frac{\omega_2(r)}{k_BT} = 2\pi\alpha N^2 \left(\frac{3}{2\pi R_N^2}\right)^{3/2} \int_0^{\frac{1}{2}} d\rho\rho \left(\frac{1}{\rho^2+\frac{1}{6}}\right)^{3/2} \exp\left[-\frac{3r^2/2R_N^2}{\rho^2+\frac{1}{6}}\right], \tag{D.3}$$

which can be shown to be

$$\frac{\omega_2(r)}{k_BT} = \frac{3\alpha N^2}{2R_N^3}\frac{R_N}{r}\frac{1}{\sqrt{\pi}} \int_{\sqrt{\frac{2}{5}}\frac{3r}{R_N}}^{\frac{3r}{R_N}} du \exp(-u^2) \tag{D.4}$$

from which Eq.(8.26) follows straightforwardly.